

INTERNATIONAL DOCTORAL
SCHOOL OF THE USC

Ana
Garbayo Peón

PhD Thesis

Gauge-gravity duality with flavor branes

Santiago de Compostela, 2022

Doctoral Programme in Nuclear and Particles Physics

TESE DE DOUTORAMENTO

GAUGE-GRAVITY DUALITY WITH FLAVOR BRANES

ANA GARBAYO PEÓN

ESCOLA DE DOUTORAMENTO INTERNACIONAL DA UNIVERSIDADE DE SANTIAGO DE COMPOSTELA

PROGRAMA DE DOUTORAMENTO EN FÍSICA NUCLEAR E DE PARTÍCULAS

SANTIAGO DE COMPOSTELA

2022

USC
UNIVERSIDADE
DE SANTIAGO
DE COMPOSTELA

DECLARACIÓN DEL AUTOR/A DE LA TESIS

D./Dña. **Ana Garbayo Peón**

Título da tese: **Gauge-gravity duality with flavor branes**

Presento mi tesis, siguiendo el procedimiento adecuado al Reglamento y declaro que:

1) La tesis abarca los resultados de la elaboración de mi trabajo.
2) De ser el caso, en la tesis se hace referencia a las colaboraciones que tuvo este trabajo.
3) Confirmo que la tesis no incurre en ningún tipo de plagio de otros autores ni de trabajos presentados por mí para la obtención de otros títulos.
4) La tesis es la versión definitiva presentada para su defensa y coincide la versión impresa con la presentada en formato electrónico.

Y me comprometo a presentar el Compromiso Documental de Supervisión en el caso que el original no esté depositado en la Escuela.

En **Santiago de Compostela**, **21 de setembro de 2022**.

Firma electrónica

USC
UNIVERSIDADE
DE SANTIAGO
DE COMPOSTELA

AUTORIZACIÓN DEL DIRECTOR / TUTOR DE LA TESIS

Gauge-gravity duality with flavor branes

D. .Alfonso Vázquez Ramallo

INFORMA:

Que la presente tesis, se corresponde con el trabajo realizado por Dª. Ana Garbayo Peón , bajo mi dirección/tutorización, y autorizo su presentación, considerando que reúne los requisitos exigidos en el Reglamento de Estudios de Doctorado de la USC, y que como director de esta no incurre en las causas de abstención establecidas en la Ley 40/2015.

De acuerdo con lo indicado en el Reglamento de Estudios de Doctorado, declara también que la presente tesis doctoral es idónea para ser defendida en base a la modalidad de Monográfica con reproducción de publicaciones, en los que la participación del doctorando/a fue decisiva para su elaboración y las publicaciones se ajustan al Plan de Investigación.

En Santiago de Compostela, 21 de septiembre de 2022

USC
UNIVERSIDADE
DE SANTIAGO
DE COMPOSTELA

Aos meus pais

USC
UNIVERSIDADE
DE SANTIAGO
DE COMPOSTELA

Agradecementos

Esta tese pecha a miña etapa como doutoranda, e supón tamén a miña desvinculación da física, polo menos da máis teórica, que me leva acompañando nos últimos anos. Ademais, remátase aquí (polo menos no curto e medio prazo) o meu paso pola universidade que, en distintas posicións, dura xa nove anos. Moitas persoas formaron parte deste proceso.

Gustaríame comezar por dar as gracias a Alfonso Vázquez Ramallo. Primeiro, por ser un dos mellores docentes cos que conta a facultade de física, que non só ten un amplísimo coñecemento de temas moi diversos, senón que invirte o tempo e o coidado necesarios para explicalos as veces que faga falla, das formas que faga falla. Segundo, por darme a oportunidade de volver a Santiago e facer con el a tese. Terceiro, polo trato ao longo destes catro anos, a axuda coa que sempre puiden contar, moitas veces sen necesidade de pedila.

En segundo lugar, non podo deixar de mencionar a Javier Mas. Penso que en moitísimas ocasións fun tan alumna súa como de Alfonso. Grazas pola infinita paciencia coa que os programas puideron comezar a andar, e pola ilusión coa que afrontas cada proxecto.

Moitos máis dentro do IGFAE fixeron do meu paso polo centro unha experiencia que sempre lembrarei con cariño. Dende aqueles cos que tiven docencia, aos que sempre lles agradecerei a axuda nunha profesión tan bonita, ata todas e tódolos traballadores do centro que facilitan o noso día a día: Alfonso, Elena, Ricardo, Marcos....

I would also like to thank Niko Jokela. The pandemic made it hard to organise my stay at Helsinki, but you were always available and welcoming, both before my arrival and during the time I spent there. Online or in-person, I truly appreciate all the physics you have taught me. Tamén dende Helsinki, grazas a Jose Manuel Penín polas discusións ao longo do último ano.

De entre tódolas persoas marabillosas que a física me permitiu coñecer, moitas pertencen a este período. Aos compañeiros de despacho, tanto do vello coma do novo, téñovos que agradecer facer do traballo un lugar moito máis atractivo. En particular, gustaríame mencionar a Alberto, a David (dende primeiro de carreira e ata o segundo mestrado), a Alex e a Pedro. E non me esquezo de Adolfo, que non estaba no IGFAE pero estivo en Laponia, nin tampouco de Javi.

Moitísimas grazas tamén a tódalas amigas, dende as que están preto ata as que están lonxe. Por escoitar, por aconsellar, por soportar, por discutir e sobre todo por estar sempre aí. En especial, as compañeiras de piso, coas que compartín o día a día incluso nese ano no que estivemos máis encerrados do que podíamos prever. Tamén a Jenny, regalo que me fixo Santiago, e a Anastasia, dende París.

USC DE SANTIAGO

Por último, e nunca menos importante, á familia.

Quixo a casualidade que puidese coincidir neste período en Santiago con Ana. Nunca deixará de fascinarme como consigues atopar tempo para estar con todos, cando ás veces non o tes nin para respirar. Además, en poquitos días la Tati cumple noventa años. No hay palabras para expresar la ilusión que me hace que puedas ver esta tesis terminada. Aunque se te haya hecho largo, como si pretendiese defenderla *la semaine des quatre jeudis*, aquí estamos. Pese a no ser ni la primera ni probablemente la última de tus nietos en doctorarse, sé que descontando a mis padres tú vas a disfrutarlo como nadie (para algo soy la más pequeña).

Finalmente, esta tese está dedicada aos meus pais. Polo amor e polo apoio incondicionais, nesta e en tódalas etapas pasadas e futuras da miña vida. Non podería facer a metade das cousa que fago sen saber que estades aí.

USC
UNIVERSIDADE
DE SANTIAGO
DE COMPOSTELA

USC
UNIVERSIDADE
DE SANTIAGO
DE COMPOSTELA

USC
UNIVERSIDADE
DE SANTIAGO
DE COMPOSTELA

Contents

Resumo (*in galician*) **i**

About this thesis **vii**
Objectives and methodology . . . vii
Outline . . . viii
List of reproduced publications . . . ix

1 Introduction and motivation **1**
1.1 From points to strings . . . 1
1.1.1 The bosonic string . . . 2
1.1.2 Supersymmetry . . . 2
1.1.3 Superstrings . . . 4
1.1.4 D-branes . . . 7
1.2 The AdS/CFT correspondence . . . 8
1.2.1 D3-branes . . . 9
1.2.2 Strong-weak coupling relation . . . 10
1.2.3 Field operator map. Reduction on the $\mathbb{S}^5$ . . . 11
1.2.4 Thermodynamics . . . 13
1.2.5 Summary: the dictionary . . . 13
1.3 Flavored systems in the AdS/CFT correspondence . . . 14
1.3.1 't Hooft limit: quenched approximation . . . 15
1.3.2 Veneziano limit: unquenching the flavors . . . 16
1.3.3 The D3/D5 system . . . 17
1.4 Applications . . . 17
1.5 Floquet theory . . . 19
1.5.1 High frequency expansion of the effective Floquet Hamiltonian . . . 20
1.5.2 Floquet engineering . . . 22

I Holographic Floquet states in low dimensions **25**

2 Overview and holographic setup **27**
2.1 D3/D5 system in the quenched approximation . . . 30

Appendices for chapter 2 . . . 37
2.A Coordinates and D5-brane action . . . 37
2.A.1 Lagrangian, IR and UV conditions . . . 39
2.A.2 Effective horizon and effective temperature . . . 41
2.B Some details on the parametrization in the $T = 0$ case . . . 42
2.B.1 Boundary conditions . . . 44
2.B.2 Types of embeddings . . . 45
2.B.3 Effective metric . . . 46

3 Numerical computations **49**
3.1 Phase space . . . 49
3.1.1 Floquet suppression points . . . 55
3.2 Conductivities . . . 57
3.2.1 Non-linear conductivity . . . 57
3.2.2 Photovoltaic Optical Conductivity . . . 60
Appendices for chapter 3 . . . 69
3.A Linearised Minkowski embeddings and Meson Spectrum . . . 69
3.B Phase space structure for the D3/D7 system . . . 70
3.C Derivation of the optical conductivities . . . 72
3.C.1 More on optical conductivities . . . 75

4 Analytic results **79**
4.1 Massless limit . . . 79
4.1.1 Black hole embeddings in the massless limit . . . 79
4.1.2 Optical conductivities in the masless limit . . . 81
4.2 High frequency limit for vanishing temperature . . . 82
Appendices for chapter 4 . . . 85
4.A Black hole embeddings in the small mass limit . . . 85
4.B Derivation of the optical conductivities in the massless limit . . . 89
4.C Embeddings in the linearised approximation at $T = 0$ . . . 91
4.C.1 Minkowski embeddings . . . 91
4.C.2 Black hole embeddings . . . 92
4.C.3 Critical embeddings . . . 96

5 Some final remarks **99**

II Black holes in the backreacted flavored D3/D5 system **103**

6 Overview and holographic setup **105**
6.1 D3/D5 system in the unquenched approximation . . . 107
Appendices for chapter 6 . . . 113
6.A Equations of motion . . . 113

USC DE SANTIAGO

7 Flavored anisotropic black holes **119**
7.1 Black holes without charges . . . 119
7.2 Charged black holes . . . 120
7.3 Thermodynamics . . . 122
Appendices for chapter 7 . . . 131
7.A Solution at vanishing chemical potential . . . 131
7.B Solution with non-zero chemical potential . . . 134
7.C Grand canonical potential from the euclidean action . . . 138

8 Applications **139**
8.1 Hydrodynamics at zero chemical potential . . . 139
8.2 Quark-antiquark potentials . . . 140
8.2.1 Intra-layer potential . . . 141
8.2.2 Inter-layer potential . . . 143
8.2.3 Physical interpretation . . . 145
8.3 Entanglement entropy . . . 146
8.3.1 Parallel slab . . . 146
8.3.2 Transverse slab . . . 151
8.3.3 Mutual information and correlations among flavors . . . 153
Appendices for chapter 8 . . . 155
8.A Dimensional reduction . . . 155
8.A.1 Hydrodynamics in the shear channel . . . 156

9 Some final remarks **161**

Conclusions **165**

Bibliography **181**

USC
UNIVERSIDADE
DE SANTIAGO
DE COMPOSTELA

USC
UNIVERSIDADE
DE SANTIAGO
DE COMPOSTELA

Resumo (*in galician*)

Dúas teorías revolucionaron a física durante o século vinte. Dunha banda, a mecánica cuántica propuxo unha descrición da natureza ás escalas máis pequenas e, actualmente, tres das catro interaccións fundamentais poden ser entendidas grazas a ela, un éxito apoiado polos resultados experimentais a precisións moi altas. Doutra banda, a formulación da teoría xeral da relatividade abriu a porta á predición da existencia de buratos negros e ondas gravitacionais, así como a propor modelos cosmolóxicos que toman en conta a expansión do universo, entre outros moitos exemplos.

Sen desmerecer a potencia da relatividade xeral, unha comprensión profunda das leis da natureza parece requirir a formulación da gravidade dende un punto de vista cuántico, de tal modo que sexa posible establecer certa continuidade entre aquilo que acontece a escalas pequenas e o que se observa a escalas maiores. Porén, as técnicas habituais ás que se podería recorrer para construír unha teoría cuántica da gravidade presentan diversos problemas, o que fai necesaria a busca de vías alternativas.

A teoría de cordas, nacida nos anos sesenta co obxectivo de explicar a interacción forte, aínda que posteriormente relegada deste propósito pola formulación da cromodinámica cuántica (QCD), ten a virtude de ser unha teoría cuántica na que a relatividade xeral, tal e como foi formulada por Einstein, aparece de xeito natural. Isto a convirte nunha prometedora candidata á descrición cuántica da gravidade.

Un exemplo concreto da relevancia da teoría de cordas é a dualidade holográfica, tamén coñecida como correspondencia AdS/CFT e proposta por Juan Maldacena no ano 1997 [1]. O termo *dualidade* emprégase para facer referencia a dúas teorías que, se ben poidan parecer diametralmente opostas dende un punto de vista puramente físico, resultan matematicamente idénticas. En consecuencia, a identificación dunha dualidade supón o feito de ter dúas perspectivas sobre un mesmo problema, o cal abre a porta a aplicar camiños diversos para estudalo e, quizais, resolvelo.

No caso concreto da dualidade holográfica, a relación establécese entre teorías cuánticas de campos nun espazo plano e unha teoría de cordas. En particular, a correspondencia parte do feito de que unha teoría de cordas no límite próximo ao horizonte da xeometría dun conxunto de D-branas apiladas é equivalente á teoría efectiva a baixa enerxía das devanditas branas. Para máis detalles técnicos sobre a correspondencia, pódense consultar [2–7].

As siglas AdS do seu nome fan referencia ao espazo Anti-de-Sitter, mentres que con CFT alúdese a teorías de campo conformes. A teoría gravitatoria defínese, entón, en $AdS \times X$, onde X representa un espazo compacto e, pola súa banda, a teoría de campos defínese na fronteira

do espazo AdS. O feito de considerala unha dualidade *holográfica* responde precisamente a que a descrición gravitatoria estea feita nun espazo-tempo que conta, polo menos, cunha dimensión non compacta adicional respecto á teoría cuántica de campos, poñendo de manifesto deste xeito o principio holográfico tal e como foi proposto por 't Hooft e interpretado no eido da teoría de cordas por Susskind [8].

Na actualidade, o alcance da correspondencia é moi amplo. Primeiro, permite relacionar unha teoría candidata á descrición da gravidade cuántica cunha teoría cuántica de campos sen graos de liberdade gravitatorios, o cal implica a posibilidade de abordar cuestións enmarcadas no mundo cuántico en termos de modelos puramente clásicos. Ademais, das relacións entre os acoplamentos de ambas teorías dedúcese que, cando a teoría de campos se atopa no réxime de acoplamento forte, a curvatura na teoría gravitatoria é pequena. Polo tanto, problemas que non son accesibles no lado CFT da correspondencia pódense plantexar en AdS mediante técnicas perturbativas. As vantaxes que isto comporta son evidentes, dada a enorme dificultade que adoita entrañar o estudo de calquera teoría cando os acoplamentos son fortes, tanto mediante técnicas analíticas como numéricas.

Para poder construír modelos que persigan describir interaccións como aquelas propias de QCD é preciso que estes conteñan materia transformando na representación fundamental, como fan os quarks. Porén, na formulación orixinal da correspondencia a teoría de campos só inclúe graos de liberdade transformando na representación adxunta do grupo gauge. O procedemento para conseguir ambos tipos de materia e polo tanto modificar a teoría de campos (o lado CFT da dualidade) pasa, necesariamente, por unha modificación da parte AdS da correspondencia. Isto lévase a cabo mediante a inclusión de novas branas na teoría orixinal, ás que se denomina branas de sabor (*flavor*), en contraposición coas branas de color. Esta metodoloxá foi inicialmente proposto en [9], e amplamente empregado nos anos sucesivos.

Para levalo a cabo, pódense considerar dous escenarios. No primeiro, as branas adicionais non inflúen na xeometría preexistente, polo que se denomina aproximación de branas de proba. Isto equivalería a desprezar os diagramas de lazos dos quarks; para máis detalles, pódese consultar [10]. No segundo, é preciso ter en conta a influencia das branas de sabor na xeometría, a denominada *backreaction*, que se verá modificada. Este cambio na xeometría preexistente é o que permite incluír os efectos dinámicos dos quarks, que son necesarios á hora de propoñer modelos que traten de explicar fenómenos como pode ser o plasma de quarks e gluóns.

O obxectivo desta tese, dividida en dúas partes, é o estudo dun sistema de D3 e D5 branas intersecadas, sendo as D3 branas de color, e as D5 branas de sabor. En ambas partes considerarase que as branas están distribuídas de tal xeito que comparten dúas das tres direccións espaciais, mentres que a terceira é paralela ás branas de color e transversal ás branas de sabor. Para proceder coa análise do sistema, na primeira parte (parte I) empregarase o límite de branas de proba, mentres que na segunda (parte II) considerarase a backreaction das branas de sabor. Ademais, encenderase un campo gauge no *world-volume* distinto en cada unha das partes, dependendo dos efectos que se persegue estudar. Previamente, no capítulo 1 descríbense os aspectos básicos da teoría de cordas e introdúcese a dualidade holográfica, así como algunhas das súas aplicacións, con exemplos concretos que poden axudar

USC DE SANTIAGO

a contextualizar os análises posteriores.

A primeira parte, *Estados holográficos de Floquet en dimensións pequenas*, persegue abondar no estudo de sistemas baixo a influencia dunha forza periódica. A enxeñaría de Floquet parte do teorema de Floquet [11], que é un análogo do teorema de Bloch no que, no canto de considerarse unha periodicidade espacial, o Hamiltoniano dos sistemas de estudo é temporalmente periódico [12–17]. Fundamentalmente, a súa fin é o control de sistemas cuánticos empregando campos externos periódicos no tempo. Entre os moitos exemplos que se atopan facilmente na literatura, pódense destacar a superconductividade inducida por luz [18, 19], os illantes topolóxicos de Floquet [20–26] ou os semimetais artificiais Weyl [27–29].

Na liña dos estudos levados a cabo en [30] e [31] para o sistema D3/D7, analizarase unha teoría gauge en (2+1)-dimensións, no réxime de acoplamento forte e baixo a influencia dun campo eléctrico rotante, co fin de estudar a existencia de estados estacionarios de Floquet fóra do equilibrio (NESS polas súas siglas en inglés, *Floquet non-equilibrium steady states*) e estendendo a devandita análise a sistemas a temperatura finita.

O capítulo 2 describe o sistema, o ansatz e as notacións empregados. Existen diversos xeitos de parametrizar a métrica, que resultan máis ou menos prácticos segundo a aplicación que se persegue mediante eles. Aínda que no propio capítulo só se considere unha delas, outras opcións aparecen descritas nos apéndices, que conteñen ademais multitude de detalles técnicos omitidos no texto central para maior claridade. Compre salientar que a resolución analítica das ecuacións en certos límites require facer uso de parametrizacións contidas nos devanditos apéndices.

Vese que o feito de incluír unha temperatura distinta de cero no sistema implica a necesidade de considerar dous horizontes distintos na xeometría. Un deles é o habitual horizonte de sucesos, mentres que o outro trátase dun horizonte efectivo que está relacionado coa presenza do campo externo. En consecuencia, faise necesario tomar en consideración dúas temperaturas distintas: a temperatura de Hawking T_{H} e unha temperatura efectiva T_{eff}, onde a primeira sempre resulta ser menor que a segunda (véxase Fig. 2.2).

As posibles configuracións da brana defínense segundo se esta cruza ou non o horizonte efectivo, ao que tamén se lle denomina pseudohorizonte. Enuméranse a continuación:

- Pódesense atopar configuracións de tipo Minkowski, nas que a brana acada a orixe de AdS_4. Resultan ser duais ás fases illantes da teoría gauge.

- Pódesense atopar configuracións de tipo burato negro, nas que a brana atravesa o pseudohorizonte. Estas son duais á fase condutora.

- Por último, na interface entre ambas atópanse as configuracións de tipo crítico.

O sistema pode atoparse, polo tanto, en dúas fases distintas, illante ou condutora. Para levar a cabo a análise de diversos aspectos deste sistema, ambas deben ser estudadas por medio de técnicas ás veces analíticas e ás veces numéricas. Un aspecto moi relevante deste ansatz é que a acción e, consecuentemente, as ecuacións do movemento resultan independentes do tempo. Isto tradúcese nunha notable simplificación do sistema de ecuacións a resolver.

USC DE SANTIAGO

Pola súa banda, o capítulo 3 contén os principais resultados que poden ser obtidos a partir de cálculos numéricos. En primeiro lugar discútese a estrutura do espazo fase. De xeito análogo ao sistema D3/D7, existe unha serie de frecuencias nas que se produce unha resonancia do campo externo cos mesóns da teoría gauge, o que da lugar a aparición de resonancias de Floquet a campo cero (véxase Fig. 3.1). En xeral, as configuracións próximas á liña crítica que separa as dúas fases condutora e illante amosan características que as diferencian claramente das demais. É importante mencionar que, ao contrario do que se poida pensar en base ás figuras, o paso da rexión Minkowski á rexión de burato negro non é brusca, senón que no entorno das liñas críticas existe unha certa multivaluación, que fai posible atopar configuracións tipo Minkowski por riba da mesma, así como configuracións tipo burato negro debaixo.

A grandes trazos, a presenza de temperatura vai na mesma liña que o aumento no módulo do campo eléctrico. No caso da estrutura dos lóbulos, pódese observar como a altura dos mesmos vai diminuíndo progresivamente ata chegar a un valor máximo do radio do horizonte a partir do cal desaparece a fase illante. Este límite, en unidades de masa dos quarks, atópase en $r_{\mathrm{h}}/m \geq 0{,}8897$. No caso do sistema D3/D7 é lixeiramente superior, entorno a $r_{\mathrm{h}}/m \geq 1{,}09$.

En canto ás masas dos mesóns do modelo D3/D5 supersimétrico, pódese observar como decrecen progresivamente conforme vai aumentando o cociente r_{h}/m. Unha vez acadado o límite $r_{\mathrm{h}}/m \geq 0{,}8897$ desaparecen, fenómeno asociado ao de fusión (*melting*) dos mesóns [32].

É relevante salientar a existencia dunha serie de puntos que serán denominados *de supresión de Floquet*, no entorno dos cales a situación e esencialmente análoga á que se dá preto dos condensados de Floquet intercambiando j e E. Compre destacar que esta dualidade non é exclusiva do sistema de D3/D5, senón que tamén pode atoparse no caso D3/D7, en ambos tanto ao considerárense configuracións a temperatura finita como nula.

Posteriormente, procédese ao análise das condutividades do sistema. A sección 3.2.1 está adicada ao estudo pormenorizado da corrente xerada en resposta ao campo eléctrico externo. Pódese ver como o ángulo formado entre ambas crea un interesante patrón dependente de Ω. Ademais, é posible interpretar a existencia de dous tipos distintos de corrente. Dunha banda, habería unha corrente de polarización e, doutra, unha debida ao fluxo de carga. A primeira delas é a única existente nas configuracións tipo Minkowski, mentres que nas de tipo burato negro daríase unha mestura de ambas. Deste xeito, os estados de supresión de Floquet pódense identificar con puntos nos que a polarizabilidade do baleiro cambia de positiva a negativa. Doutra banda, nos límites particulares de campo forte ou alta temperatura a corrente de polarización desaparece e $j(t) \sim j_{con}(t) = \sigma E(t)$, con σ constante, concordando con [33].

A sección 3.2.2, pola súa banda, céntrase no estudo da corrente fotovoltaica, que constitúe a resposta do Floquet NESS á un campo eléctrico AC adicional, que se emprega a modo de sonda das propiedades condutivas modificadas do medio. Ao estudar o caso masivo chégase a un tensor de condutividade cunha estrutura moi rica, especialmente ao fixar a frecuencia do campo externo ao valor da primeira resonancia.

O capítulo 4 analiza solucións analíticas e exactas que poden ser obtidas en dous réximes particulares. O primeiro deles é o límite sen masa ou de masa pequena. Nel a única configuración posible é a de tipo burato negro e, tanto a temperatura finita como nula, é factible atopar unha solución analítica ás ecuacións do movemento. Ademais, pódense obter

as condutividades de xeito exacto, chegándose a un valor que de novo concorda con [33] e permite verificar a tendencia das condutividades calculadas numericamente no mesmo límite. O segundo caso analítico é o correspondente a altas frecuencias do campo externo, aínda que só ao considerarse temperatura nula. Neste límite analízanse as tres posibles configuracións.

A primeira parte pecha co capítulo 5, que persegue presentar un resumo dos principais resultados do mesmo, así como sinalar posibles continuacións.

Na segunda parte, *Buratos negros no sistema D3/D5 con backreaction e sabor*, preséntase un dual holográfico a densidade bariónica finita e cunha fonte de anisotropía.

Na literatura abundan os exemplos de duais anisotrópicos estudados mediante a correspondencia [34–81]. Este tipo de modelo ten relevancia no eido da materia condensada no que, por exemplo, sistemas con electróns fortemente correlacionados exhiben fases nemáticas [82]. Doutra banda, o desenvolvemento dunha fase anisotrópica en QCD a alta densidade bariónica podería conducir a estrelas de neutróns máis compactas, o que ten relación directa coa termodinámica de buratos negros [83, 84].

Nesta tese obtéñense xeometrías que permiten resolver as ecuacións do movemento do sistema, no que se considera que as D5 branas están distribuídas de xeito uniforme ao longo do seu espazo transverso, no que se coñece como técnica do *smearing*, que ten a virtude de simplificar notablemente o sistema de ecuacións diferenciais que se derivan da acción. Este método foi introducido en [85], e pódense atopar moitos detalles sobre o mesmo en [86]. A idea principal consiste en distribuír as branas de sabor de xeito uniforme ao longo da súa dirección transversal, co que se logra deslocalizar as fontes e non ter dependencia nas devanditas coordenadas transversais. O feito de considerar que a terceira coordenada espacial e paralela ás D3 branas pero perpendicular ás D5 branas, como foi indicado anteriormente, permite introducir de xeito natural a desexada anisotropía neste sistema.

No capítulo 6 establécese o ansatz empregado para os diferentes campos que conforman a teoría tipo IIB de supergravidade. Ademais, derívanse as ecuacións de Einstein e constrúese unha acción efectiva que permite chegar ao mesmo sistema de ecuacións diferencias.

As solucións obtidas recóllense no capítulo 7. Trátanse de buratos negros con carga, correspondentes a teorías de campos nas que se considera unha temperatura finita e a presenza de pontencial químico. Debido á complexidade das ecuacións do movemento que se derivan da acción efectiva do sistema, na resolución empregouse unha expansión perturbativa en dous parámetros, relacionados coa densidade de sabores n_{f} e de barións n_{b} (véxase (7.3.15)), nun procedemento similar ao exposto en [87, 88]. Consecuentemente, só é válida no caso no que ambos parámetros sexan pequenos (véxase (9.2)). Compre destacar a existencia de solucións exactas no caso no que non se inclúe a densidade de barións, introducidas primeiro en [76] e amplamente estudadas en [77–81]. Nelas, o límite $N_{\mathrm{f}} \to 0$ é singular, mentres que a solución aquí proposta analiza precisamente o caso no que o número de sabores é pequeno.

No réxime de validez da solución, puidéronse estudar as propiedades termodinámicas do sistema, expostas na sección 7.3. En primeiro lugar obtéñense a temperatura e a entropía do mesmo, así como a densidade de enerxía a partir da enerxía de ADM. A densidade de enerxía libre do sistema pode ser calculada a través de dous procedementos: ben usando as relacións termodinámicas usuais, a partir da densidade de entropía e enerxía, ou ben a partir da acción euclídea. Posteriormente, e coa fin de caracterizar a anisotropía do sistema, introdúcese un

USC DE SANTIAGO

potencial de brana que permite ter en conta a variación do número de D5 branas. Finalmente, obtéñense as presións, velocidades do son do sistema e o tensor de enerxía-momento. Compre salientar que os resultados acadados para a entropía, a densidade de enerxía e as presións do sistema amosan a presenza de grados de liberdade extra ao longo da intersección que contribúen a elas ao longo desta, pero non á presión na dirección transversa.

O capítulo 8 presenta a obtención de diversos observables, como coeficientes de transporte, potenciales quark-antiquark e entropía de entrelazamento. En particular, preténdese determinar o efecto das deformacións introducidas nos devanditos observables.

A hidrodinámica só foi estudada no caso sen densidade de carga, debido a que para levalo a cabo foi necesario empregar a teoría reducida en 4 dimensións, coñecida no caso con potencial químico nulo, pero non no sistema no que este está encendido. Observouse que o coeficiente de transporte a segunda orde no canal de cizalla (*shear channel*) ao longo da intersección crece co número de D5 branas. Na entropía de entrelazamento pódese observar un aumento conforme o fai a densidade de defectos. Cabe tamén destacar que o aumento de entropía de entrelazamento co tamaño da rexión entrelazada é proporcional á entropía térmica nun certo límite, resultado equivalente ao considerar rexións transversas ou paralelas á intersección. No relativo aos potenciais quark-antiquark, os graos de liberdade nas intersección teñen unha clara repercusión no apantallamento das cargas de color, especialmente na dirección transversa. Pola contra, a densidade de carga ten unha maior influencia nas direccións paralelas aos defectos.

O capítulo 9 ofrece un resumo dos resultados e algunhas ideas de posibles extensións do traballo e de aplicacións do mesmo. Ademais, tódolos capítulos compleméntanse con apéndices aos que foron relegados a meirande parte dos cálculos, coa fin de clarificar o máximo posible a lectura dos principais aspectos de cada un.

Finalmente, aínda que os capítulos 5 e 9 proporcionen de xeito detallado os resultados e discusión de cada unha das partes, a tese remata cun capítulo de Conclusions a modo de breve resumo das análises previas.

USC
UNIVERSIDADE
DE SANTIAGO
DE COMPOSTELA

About this thesis

Objectives and methodology

The holographic duality, also known as AdS/CFT correspondence, allows to formulate a quantum field theory in terms of a classical theory when taking an appropriate limit. In particular cases, it relates strongly coupled theories to weakly coupled ones. This implies the possibility of performing very involved computations with simpler and sometimes analytic techniques.

Since it was originally proposed by Maldacena in 1997 [1], the correspondence has been generalised in order to study a wide range of problems. One prominent example among the variety of extensions of the duality is the addition of flavor degrees of freedom as a result of the inclusion of supplementary D-branes on the initial system.

The main goal of this thesis is the application of the correspondence in two particular situations where fields transforming in the fundamental representation of the gauge group are taken into account. In the first part, we will try to gain some insight into periodically driven systems and, in particular, into Floquet type of non-equilibrium steady states. In order to do so, we will study the behavior of a strongly-coupled $(2+1)$-dimensional gauge theory under the influence of a external rotating electric field, by means of a system of intersecting D3 and D5 branes. This analysis will be performed in the quenched approximation, where the D5 branes can be considered as probes in the D3 background.

The second part will be devoted to the construction of a holographic dual that realises anistropy, as well as a finite baryon density. This kind of model could then be applied to physical systems exhibiting similar characteristics. In this case, we will be dealing again with intersecting D3 and D5 branes, but now in the unquenched approximation, in which the backreaction of the D5 flavor branes into the original geometry has to be considered.

Concerning the methodology, we will sometimes be able to present results that have been analytically solved through various mathematical techniques. However, many of the computations needed to be performed numerically. Besides, some analytic problems turn out to be quite challenging, if solved by hand. In both cases, the well-known Wolfram's Mathematica software has been used.

USC
UNIVERSIDADE
DE SANTIAGO
DE COMPOSTELA

Outline

This thesis is structured as follows. We will start with an introductory chapter (see chapter 1), where we review some of the basic aspects of string theory, which will allow us to present the holographic duality. We then move on to discuss the techniques behind the inclusion of flavor degrees of freedom into the original formulation of the correspondence and, in particular, we will focus on the system of intersecting D3 and D5 branes, which is used later on. We finish the introduction with some notes on the most relevant applications of the holographic duality.

Parts I and II deal with two of these applications. Part I, *Holographic Floquet states in low dimensions*, will be devoted to the analysis of a periodically driven system. We will be studying the D3/D5 system in the quenched approximation. This will allow us to describe a strongly-coupled $(2 + 1)$-dimensional gauge theory under the influence of a external rotating electric field. In chapter 2 we present the holographic setup and ansatz. Then, we have divided the numerical and analytic results in two different chapters. Chapter 3 deals with the numerical computations, which mainly covers the phase space structure and conductivities; these two distinguished topics have been split into separate sections. On the other hand, chapter 4 is focused on some particular limits where we have been able to find analytic results. These are the massless (and small mass) limit, for both finite and vanishing background temperature, and the high frequency limit, although only when we consider zero background temperature. Part I concludes with chapter 5, aiming at summarizing the main results and conclusions extracted from them, as well as giving some ideas of possible extensions of this work.

In part II, *Black holes in the backreacted flavored D3/D5 system*, we study the D3/D5 system in the unquenched approximation and we construct a holographic dual realizing finite baryon density and anisotropy. In chapter 6 we describe our holographic setup. Chapter 7 is devoted to possible solutions to the equations of motion derived from the action, which we found in terms of two expansion parameters. These are related to the density of the smeared flavors in the direction transverse to the defect, n_{f}, and the baryon density, n_{b}. Besides, we analyzed the thermodynamic properties of this system.

Chapter 8 reviews some applications of our solutions, namely the computation of hydrodynamic coefficients in the shear channel, the quark-antiquark potentials and the entanglement entropy. Moreover, chapter 9 discusses the main results obtained in previous chapters and presents possible extensions.

Furthermore, both part I and II include several appendices, where the reader can find all technicalities omitted in the main text for clarity.

Finally, although chapters 5 and 9 contain a more detailed discussion of the results and possible extensions of each part, we summarised them in the final chapter Conclusions.

USC
UNIVERSIDADE
DE SANTIAGO
DE COMPOSTELA

List of reproduced publications

Along this thesis, three publications have been reproduced. All relevant information about them is collected in what follows, as well as the exact part (I or II) where they have been used.

Holographic Floquet states in low dimensions, *Journal of High Energy Physics* **2020** (2020) 13 [89]	
Authors	Ana Garbayo[1,2], Javier Mas[1,2] and Alfonso V. Ramallo[1,2] [1] Departamento de Física de Partículas and [2] Instituto Galego de Física de Altas Enerxías (IGFAE) Universidade de Santiago de Compostela, E-15782 Santiago de Compostela, Spain
Included at	Part I: Holographic Floquet states in low dimensions
PhD student contribution	Collaboration in numerical and analytic computations, discussions and writing of the article
Further information	**Journal:** Journal of High Energy Physics **Publisher:** Springer **ISSN:** 1029-8479 **Year of publication:** 2020 **DOI:** `https://doi.org/10.1007/JHEP10(2020)013` **Impact factor***: 5.81 **Rank in Physics, Particles & Fields***: 5/29 (Q1) Article distributed under the terms of the Creative Commons Attribution License (CC-BY 4.0). *Data corresponding to 2020, from JCR.

USC
UNIVERSIDADE
DE SANTIAGO
DE COMPOSTELA

Holographic Floquet states in low dimensions (II), *arXiv e-prints* (2022) [90]	
Authors	Martí Berenguer[1,2], Ana Garbayo[1,2], Javier Mas[1,2] and Alfonso V. Ramallo[1,2] [1] Departamento de Física de Partículas and [2] Instituto Galego de Física de Altas Enerxías (IGFAE) Universidade de Santiago de Compostela, E-15782 Santiago de Compostela, Spain
Included at	Part I: Holographic Floquet states in low dimensions
PhD student contribution	Collaboration in numerical and analytic computations, discussions and writing of the article
Further information	**Year of publication:** 2022 **DOI:** `https://arxiv.org/abs/2209.03884` Article distributed under the terms of the Creative Commons Attribution License (CC-BY 4.0).

USC
UNIVERSIDADE DE SANTIAGO DE COMPOSTELA

Flavored anisotropic black holes, *Journal of High Energy Physics* **2022** (2022) 61 [91]	
Authors	Ana Garbayo[1,2], Carlos Hoyos[3,4], Niko Jokela[5,6], José Manuela Penín[5,6] and Alfonso V. Ramallo[1,2] [1] Departamento de Física de Partículas and [2] Instituto Galego de Física de Altas Enerxías (IGFAE) Universidade de Santiago de Compostela, E-15782 Santiago de Compostela, Spain [3] Department of Physics and [4] Instituto de Ciencias y Tecnologías Espaciales de Asturias (ICTEA) Universidad de Oviedo, E-33007/33004 Oviedo, Spain [5] Department of Physics and [6] Helsinki Institute of Physics University of Helsinki, P.O.Box 64, FIN-00014 Helsinki, Finland
Included at	Part II: Black holes in the backreacted flavored D3/D5 system
PhD student contribution	Collaboration in numerical and analytic computations, discussions and writing of the article
Further information	**Journal:** Journal of High Energy Physics **Publisher:** Springer **ISSN:** 1029-8479 **Year of publication:** 2022 **DOI:** `https://doi.org/10.1007/JHEP10(2022)061` **Impact factor***: 6.379 **Rank in Physics, Particles & Fields***: 6/29 (Q1) Article distributed under the terms of the Creative Commons Attribution License (CC-BY 4.0). *Data corresponding to 2021, from JCR.

USC UNIVERSIDADE DE SANTIAGO DE COMPOSTELA

USC
UNIVERSIDADE
DE SANTIAGO
DE COMPOSTELA

1 Introduction and motivation

1.1 From points to strings

String theory was born in the sixties as a theory aiming to describe nuclear forces. In this picture, particles are specific oscillation modes of the strings. Although the development of QCD in the seventies relegated it as the preferred candidate for explaining the strong interaction, string theory was used later on in an ambitious project: finding a quantum theory of gravity.

General relativity and quantum mechanics were two crucial developments in physics during the past century. Understanding gravity in terms of space-time geometry has led to the prediction of the existence of black holes or gravitational waves, and to cosmological models describing the expansion of the universe, among many other examples. From its side, quantum mechanics allows to study the properties of nature at its tinniest scales, providing models that describe three out of the four fundamental interactions with amazingly high experimental accuracy; only gravity is missing. The most direct approaches in order to reconcile quantum mechanics and general relativity in the framework of quantum field theory present problems related to the appearance of ultraviolet divergences, which cannot be removed by means of the usual renormalization techniques. However, a complete understanding of the fundamental laws of nature seems to require the formulation of a quantum theory of gravity.

String theory is a quantum theory in which general relativity, as it was formulated by Einstein, naturally appears at the distances and energies where we expect to find it. For this reason, it became an appealing candidate to give a quantum description of gravitational interactions. Moreover, it turns out to be very helpful when studying quantum gauge theories. One example of this is the AdS/CFT correspondence, whose ideas have been applied in a wide range of domains, such as condensed matter physics, because they give a tool to tackle strongly coupled systems, as we will see latter on. For this reason, even if string theory is not able to provide a *true* description of nature, it has proved to be a very useful framework to explore a variety of problems.

On what follows, we review some basics of string theory. Many great books exist on the subject, where more details can be found; for example [92–97].

USC DE SANTIAGO

1.1.1 The bosonic string

The starting point of string theory is extending the usual physics of point particles to one-dimensional objects, strings. Instead of moving along a line, these objects will cover a (1+1)-dimensional surface in space-time, that we will refer to as worldsheet, parametrised by two coordinates: a time-like coordinate τ and a space-like coordinate σ. When σ is periodic, then the string is said to be closed, while if it covers a finite interval it is termed open.

The Nambu-Goto action is the simplest reparametrization invariant action for the strings, and it is given by

$$S_{\text{NG}} = -T \int d\sigma\, d\tau \sqrt{-\det\left(\partial_\alpha X^\mu\, \partial_\beta X^\nu\, \eta_{\mu\nu}\right)}\ . \tag{1.1.1}$$

The functions $X^\mu(\tau, \sigma)$, with $\mu = 0, ...D-1$, are the embedding of the wordlsheet into the target space. The constant T in front of the action is identified with the string tension, given by

$$T = \frac{1}{2\,\pi\,\alpha'}\ , \tag{1.1.2}$$

with $l_s = \sqrt{\alpha'}$ being the string length. In spite of being Poincaré and reparametrisation invariant, the action (1.1.1) poses different problems when trying to quantise the theory, mostly due to the squared root. For this reason, the Polyakov action, which leads to the same equations of motion for X, has to be introduced. It incorporates a new field g, which is nothing but a dynamical metric on the worldsheet, and has the advantage of including Weyl invariance. In the so-called conformal gauge, the action reads

$$S = -\frac{1}{4\,\pi\,\alpha'} \int d\sigma\, d\tau\ \left(\partial_\tau X^\mu\, \partial_\tau X^\nu - \partial_\sigma X^\mu\, \partial_\sigma X^\nu\right)\, \eta_{\mu\nu}\ . \tag{1.1.3}$$

However, when studying the spectrum of the bosonic string, two major problems appear. First, it does not contain fermions. This is of course a critical matter if one wishes to find a theory able to describe the particle spectrum found in nature, that has to include the quarks and leptons of the Standard Model. The second issue is related to the presence of tachyons, states of negative mass squared that lead to an instability of the vacuum.

The need to formulate string theory without tachyons and with fermions makes the range of consistent and non-anomalous theories very restricted. The way to implement it is via supersymmetry, a symmetry that relates bosons to fermions and, as we will see, will allow us to obtain the desired particle spectrum, with fermions and without tachyons. On top of this, it is worth mentioning that, while consistency of the bosonic string theory requires $D = 26$, once we have included supersymmetry the critical dimension goes down until $D = 10$.

1.1.2 Supersymmetry

Even though supersymmetry ended up being a key part of all potentially realistic string theories, the motivations behind it cover a much wider range. Actually, supersymmetric

theories aim to solve a variety of open problems in physics beyond the Standard Model, from the strong CP problem to the need of a dark matter candidate. Moreover, it tries to assess more fundamental questions, such as the hierarchy problem. For a nice review of supersymmetry, check [98].

When including supersymmetry in a given theory, since one has to relate bosonic fields to the fermionic ones and viceversa, the number of fields necessarily increases. Although this might look like turning the original problem into a much more complicated one, it actually gets simplified. The fact is that the appearance of new symmetries renders possible to perform computations that would have been out of reach otherwise.

As it has already been stated, we are after a supersymmetry transformation that turns a bosonic state into a fermionic state, and viceversa. The simplest picture of such a transformation is of the form

$$Q\,|\text{boson}\rangle \propto |\text{fermion}\rangle \qquad , \qquad Q\,|\text{fermion}\rangle \propto |\text{boson}\rangle \ . \tag{1.1.4}$$

In order to implement this, the basic idea is to extend the Poicanré algebra with this new generator Q. Thus, let us take the well-known generators for the Poincaré group, the hermitian operators $M^{\mu\nu}$ (rotations and Lorentz boosts) and P^σ (translations), with algebra

$$[P^\mu, P^\nu] = 0 \qquad , \qquad [M^{\mu\nu}, P^\sigma] = i\,\left(P^\mu\,\eta^{\nu\sigma} - P^\nu \eta^{\mu\sigma}\right) \ ,$$

$$[M^{\mu\nu}, M^{\rho\sigma}] = i\,\left(M^{\mu\sigma}\eta^{\nu\rho} + M^{\nu\rho}\eta^{\mu\sigma} - M^{\mu\rho}\eta^{\nu\sigma} - M^{\nu\sigma}\eta^{\mu\rho}\right) \ . \tag{1.1.5}$$

P^μ and $M^{\mu\nu}$ will be the bosonic generators in supersymmetry. Now, the Coleman-Mandula theorem [99] tells us that Q in (1.1.4) needs to be a fermionic generator; we will note the fermionic generators as Q^A_α, $\bar{Q}^A_{\dot\alpha}$, where $A = 1, ..., N$ and N is the number of Q's. For now, let us take $N = 1$ for simplicity. To the commutation relations (1.1.5) from the Poincaré algebra, we need to add[1]

$$[Q_a, M^{\mu\nu}] = (\sigma^{\mu\nu})_a^{\ \beta}\, Q_\beta \qquad , \qquad [Q_a, P^\mu] = 0 \qquad , \qquad \{Q_a, Q_\beta\} = 0 \ ,$$

$$\{Q_a, \bar{Q}_{\dot\beta}\} = 2(\sigma^\mu)_{\alpha\dot\beta}\, P_\mu \ . \tag{1.1.6}$$

The Coleman-Mandula theorem also states that, for internal symmetry generators T, the commutator $[Q_\alpha, T_i]$ usually vanishes. However, this is not the case when considering the $U(1)$ automorphisms of the supersymmetry algebra, known as R symmetry

$$[Q_\alpha, R] = Q_\alpha \qquad , \qquad [\bar{Q}_{\dot\alpha}, R] = -\bar{Q}_{\dot\alpha} \ . \tag{1.1.7}$$

Moreover, when recovering extended supersymmetry ($N > 1$), the algebra is the same as the one given for $N = 1$, except for the following anticommutators

$$\{Q^A_a, Q^B_\beta\} = \epsilon_{\alpha\beta}\, Z^{AB} \qquad , \qquad \{\bar{Q}^A_{\dot\alpha}, \bar{Q}^B_{\dot\beta}\} = \epsilon_{\dot\alpha\dot\beta}\,(Z^\dagger)^{AB} \ ,$$

$$\{Q^A_a, \bar{Q}_{\dot\beta B}\} = 2(\sigma^\mu)_{\alpha\dot\beta}\, P_\mu \delta^A_B \ . \tag{1.1.8}$$

[1] ψ_α notes, left-handed Weyl spinors, and $\bar\chi_{\dot a}$ right-handed Weyl spinors.

USC UNIVERSIDADE DE SANTIAGO

In this last expression, antisymmetric central charges $Z^{AB} = -Z^{BA}$ have been included. They commute with all generators, and their existence is a key difference between simple and extended supersymmetry.

Particles are then organised in supermultiplets, formed by both fermionic and bosonic states, usually referred to as superpartners. These superpartners have equal masses, electric charges, weak isospin and color degrees of freedom but can, of course, have different spin. On the other hand, the number of bosons (n_{B}) and fermions (n_{F}) has to be the same within one multiplet. For example, the simplest one, which is called chiral multiplet, will be that containing a Weyl fermion (two spin-$\frac{1}{2}$ helicity states, $n_{\mathrm{F}} = 2$) and two real or one complex scalar (each real scalar having $n_{\mathrm{B}} = 1$).

It is worth mentioning that all $N > 1$ supersymmetries are non-chiral and, as a consequence, $N = 1$ supersymmetry has key importance when looking for extensions of the Standard Model. For instance, all Standard Model fermions would be included in chiral multiplets. Needless to say, no superpartner of the Standard Model zoo has been detected so far, which means that, if existing, supersymmetry must be a broken symmetry.

However, in order to introduce superstring theory, we will be considering extended supersymmetry. The maximum number of supersymmetries is believed to be $N = 8$, and there are no renormalisable field theories with $N > 4$.

When considering massive representations in $N > 1$ supersymmetry with non-vanishing central charges, states of minimal mass are the so-called BPS states. These are stable states. In extended supergravity theories, extremal black holes are BPS states and, in string theory, non-perturbative objects known as D-branes (see 1.1.4) are also BPS states.

1.1.3 Superstrings

Here we will briefly discuss the Ramond-Neveu-Schwarz (RNS) formalism, which imposes supersymmetry in the worldsheet. Basically, as it was heuristically introduced in (1.1.4), the idea will be to pair the X^μ bosonic fields to ψ^μ fermionic partners, which are Majorana spinors with two real components, $\psi^\mu = \begin{pmatrix} \psi^\mu_- \\ \psi^\mu_+ \end{pmatrix}$, so that (1.1.3) becomes

$$S = -\frac{1}{4\,\pi\,\alpha'} \int \, d\sigma\, d\tau\, \eta^{\alpha\beta} \left(\partial_\alpha X^\mu\, \partial_\beta X^\nu + i\, \bar{\psi}^\mu\, \gamma_\alpha\, \partial_\beta \psi^\nu \right) g_{\mu\nu}(X) \ . \tag{1.1.9}$$

Let us now analyze the string spectrum. In the open string case, assuming $\sigma \in [0, \pi]$ and $\psi^\mu_+(\sigma = 0) = \psi^\mu_-(\sigma = 0)$, one can impose two different boundary conditions according to the choice of sign at the other end of the string:

- **Ramond boundary condition (R)**: $\psi^\mu_+(\sigma = \pi) = \psi^\mu_-(\sigma = \pi)$. This gives rise to space-time fermions.
- **Neveu-Schwartz condition (NS)**: $\psi^\mu_+(\sigma = \pi) = -\psi^\mu_-(\sigma = \pi)$. This gives rise to space-time bosons.

USC DE SANTIAGO

Similarly, on the closed string case, one can chose to impose periodic or antiperiodic boundary conditions on the fermionic fields, $\psi_\pm(\sigma) = \pm\psi_\pm(\sigma + \pi)$. The positive sign corresponds to periodic boundary conditions, that we will refer to as Ramond boundary conditions, while the minus signs accounts for the antiperiodic ones, the Neveu-Schwartz conditions. Moreover, it is possible to choose (anti)periodic boundary conditions on the left and right moving sectors, or to make one of them periodic while imposing antiperiodicity on the remaining one. As a consequence, we can define four different sectors: states belonging to NSNS or RR sectors will be bosons, while those in RNS or NSR sectors are fermions.

At this point, we will again encounter similar problems as those discussed for the bosonic string case, since the NS open string sector ground state is a tachyon. First of all, this is unsatisfactory because we were precisely trying to get rid of such a state. However, this entails a second issue: the theory is not supersymmetric, for no fermion in the spectrum has the same mass as this tachyon.

The way to avoid this is the GSO projection, named after Gliozzi, Scherk and Olive [100]. After implementation, the NS sector tachyon disappears. Let us see what happens to the massless closed string spectrum. After GSO projection, we are left with two options for the R sector: either both left and right moving ground states are chosen to have the same chirality, or the opposite. This choice will lead to two distinct theories: type IIB and type IIA supergravity, respectively.

In both type II theories, the massless spectrum contains two Majorana-Weyl gravitinos, so that they form $N = 2$ supergravity multiplets, which in 10 dimensions implies 32 supercharges. We can distinguish:

- **NSNS**: A scalar (the dilaton, ϕ), an antisymmetric two-form gauge field (B_2) and a symmetric traceless rank-two tensor (a graviton, $g_{\mu\nu}$).
- **NSR or RNS**: A spin-$\frac{3}{2}$ gravitino and a spin-$\frac{1}{2}$ dilatino for each sector. If we are speaking about type IIA (IIB), then the gravitinos have opposite (same) chirality.
- **RR**: In type IIA, a vector gauge field (C_1) and a three-form gauge field (C_3), while in type IIB we find a scalar gauge field (C_0), a two-form gauge field (C_2) and a four-form gauge field (C_4), with the additional condition of having a self-dual field strength.

It is worth mentioning that other superstring theories exist, mainly heterotic strings and type I, which are connected to type II theories through different dualities.

Low energy efective action of type IIB supergravity

When we take the $\alpha' \to 0$ limit, which from (1.1.2) corresponds to large string tension, the masses become very large and, in Minkowski space background, this corresponds to the low energy limit. Thus, the massive modes would become too heavy to be observed, and one can approximate string theory by a supergravity theory considering only the interactions of the massless modes. In this way, a low energy effective action is constructed from the massless closed string states listed in the previous section.

USC DE SANTIAGO

Although type IIA supergravity can be constructed by means of dimensional reduction of 11-dimensional supergravity, this cannot be done in the case of type IIB, that has to be built up using supersymmetry and gauge invariance. One of the main difficulties comes from the presence of the dual five-form field strength, that renders the task of formulating the action in a manifestly covariant form more complicated. When one writes an action as

$$\int |F_5|^2 \, d^{10}x \ , \tag{1.1.10}$$

it does not incorporate self-duality, and we end up describing twice the number of propagating degrees of freedom. This issue can be solved by introducing an auxiliary scalar field and a gauge symmetry, following the Pasti, Sorokin and Tonin (PST) approach. However, another option is to write a action that, after imposing the self-duality condition, leads to the correct equations of motion. This action is not going to be supersymmetric since, before incroporating the self-duality condition, one has more bosonic than fermionic degrees of freedom.

The bosonic part of such an action is of the form

$$S_{\rm IIB} = S_{\rm NS} + S_{\rm R} + S_{\rm CS} \ , \tag{1.1.11}$$

where

$$\begin{aligned} S_{\rm NS} &= \frac{1}{2\kappa_{10}^2} \int d^{10}x \, \sqrt{-g} \left[R - \frac{1}{2} \left(\partial \phi \right)^2 - \frac{e^{-\phi}}{2 \cdot 3!} H_3^2 \right] \ , \\ S_{\rm R} &= \frac{1}{2\kappa_{10}^2} \int d^{10}x \, \sqrt{-g} \left[- \frac{e^{2\phi}}{2} F_1^2 - \frac{e^{\phi}}{2 \cdot 3!} F_3^2 - \frac{1}{4 \cdot 5!} F_5^2 \right] \ , \\ S_{\rm CS} &= - \frac{1}{4\kappa_{10}^2} \int C_4 \wedge H_3 \wedge F_3 \ . \end{aligned} \tag{1.1.12}$$

With the additional condition

$$F_5 = \star \, F_5 \ . \tag{1.1.13}$$

When writing the various forms in the action we are using the notation

$$\int d^{10}x \, \sqrt{-g} \, |F_{(p)}|^2 = \frac{1}{p!} \int d^{10}X \, \sqrt{-g} \, g_{\mu_1 \nu_1} \dots g_{\mu_p \nu_p} \bar{F}^{\mu_1 \dots \mu_p} \, F^{\nu_1 \dots \nu_p} \ , \tag{1.1.14}$$

and the forms satisfy

$$F_p = d \, C_{p-1} - C_{p-3} \wedge H_3 \qquad , \qquad H_3 = d \, B_2 \ . \tag{1.1.15}$$

As expected, we encounter NSNS bosons, particularly the metric, the two-form B_2 with field strength H_3 and the dilaton ϕ, while the form fields $C_{0,2,4}$ belong to the RR sector.

USC DE SANTIAGO

1.1.4 D-branes

Apart from one-dimensional strings, string theory contains other kind of objects. In particular, its non-perturbative sector is made of extended objects, the solitons. The Dp-branes are one of those, covering p spatial directions, plus time. One can view them as hypersurfaces where open strings can end or as massive objects curving the spacetime, charged under the antisymmetric tensor field $A_{\mu_1,\dots\mu_{p+1}}$.

The appropriate perspective depends on the value of the string coupling g_s, that is what determines the strength of the interaction between open and closed strings. We will analyze both cases in what follows.

Open string perspective: low-energy effective action

Let us consider open strings whose boundary conditions are specified by the D-branes in which they end, coupled to the gauge field A living on their worldvolume. The Dp-brane action is the result of the sum of two contributions, the Dirac-Born-Infeld action S_{DBI} and a Wess-Zumino term S_{WZ}

$$S = S_{\rm DBI} + S_{\rm WZ} \ . \tag{1.1.16}$$

The DBI action takes into account two kinds of massless open string excitations: on the one hand, we have those due to rigid motions and deformations of the brane, represented by $9-p$ real scalar fields ϕ^i, and on the other hand internal excitations that consist of a gauge field A^μ (plus their fermionic superpartners). The DBI action is given by

$$S_{\rm DBI} = -T_{\rm D_p} \int d^{p+1}\xi \, e^{-\phi} \sqrt{-\det\left(\hat{g}_{ab} + \mathcal{F}\right)} \ , \tag{1.1.17}$$

where ξ^a denote the coordinates for the worldvolume of the brane, $\mathcal{F} = \hat{B}_{ab} + 2\pi\alpha' F_{ab}$ and the hatted quantities are the pullback of the NS-NS fields $g_{\mu\nu}$ and $B_{\mu\nu}$. It is also worth mentioning that the constant T_{D_p}, the Dp-brane tension, is given by

$$T_{\rm D_p} = \frac{1}{(2\pi)^p \, g_{\rm s} \, l_s^{p+1}} \ . \tag{1.1.18}$$

The non-perturbative nature of the Dp-branes can be easily checked by the fact that this multiplicative constant scales as $T_p \sim g_s^{-1}$.

Moreover, the Wess-Zumino term encodes the interation of the RR fields C_{q+1} with B

$$S_{\rm WZ} = \frac{T_{\rm D_p}}{g_{\rm s}} \int \sum_p \hat{C}_{q+1} \wedge e^{\mathcal{F}} \ . \tag{1.1.19}$$

As it has been stated, the Dp-branes contain a gauge theory in their worldvolume. In the case of a stack of N Dp-branes, the gauge group is $U(N)$, and they realise a $SU(N)$ gauge theory in $p+1$ dimensions. One particularly important case is that of D3-branes, since the $SU(N)$ gauge theory is identified with super Yang-Mills with $\mathcal{N} = 4$.

Closed string perspective: D-branes in supergravity

The addition of D-branes to a type IIA or IIB vacuum configuration leads to a theory with closed strings in the bulk plus open strings ending on the branes. Since a n-form gauge field can couple electrically to a p-brane with $p = n - 1$ and magnetically if $p = 7 - n$, according to their massless spectrum, type IIA contains stable branes with even p, while in the case of type IIB, p should be odd.

Furthermore, some of the symmetries will be broken. In Minkowski space vacuum of a type II theory, the $SO(1,9)$ Lorentz symmetry will be broken to $SO(1,p) \times SO(9-p)$. Besides, in the presence of D-branes the maximum number of unbroken supersymmetries is 16, which means that at least half of the 32 supersymmetries present on type II superstring are broken.

The following ansatz solves the equations of motion of type IIB supergravity

$$\begin{aligned} ds^2 &= H_p(r)^{-\frac{1}{2}}\, \eta_{\mu\nu}\, dx^\mu\, dx^\nu + H_p(r)^{\frac{1}{2}}\, dy^i\, dy^i \ , \\ e^\phi &= g_{\rm s}\, H_p(r)^{\frac{3-p}{4}} \ , \\ C_{(p+1)} &= \Big(H_p(r)^{-1} - 1\Big)\, dx^0 \wedge dx^1 \wedge ... \wedge dx^p + ... \ , \\ B_{\mu\nu} &= 0 \ , \end{aligned} \tag{1.1.20}$$

where the wrap factor $H(r)$ and the constant L_p are given by

$$H_p(r) = 1 + \left(\frac{L_p}{r}\right)^{7-p} \qquad , \qquad L_p^{7-p} = (4\pi)^{\frac{5-p}{2}}\, \Gamma\left(\frac{7-p}{2}\right)\, g_{\rm s}\, N\, (\alpha')^{\frac{7-p}{2}} \ . \tag{1.1.21}$$

It turns out that one can distinguish two regions. In the case in which r is large in comparison to L_p, $r \gg L_p$, then $H(r) \sim 1$ and, as a consequence, the metric (1.1.20) is that of a flat spacetime. On the contrary, when we consider $r \ll L_p$ and $H(r) \sim (L_p/r)^{7-p}$, we are in the near-horizon region.

We should also mention the existence of non-BPS branes with the following solution

$$\begin{aligned} ds^2 &= H_p(r)^{-\frac{1}{2}}\, \Big(-f(r)\, dt^2 + dx^i\, dx^i\Big) + H_p(r)^{\frac{1}{2}}\, \left(\frac{dr^2}{f(r)} + r^2\, d\Omega_{8-p}\right) \ , \\ f(r) &= 1 - \left(\frac{r_{\rm h}}{r}\right)^{7-p} \ , \\ H_p(r) &= 1 + \left(\frac{L_p}{r}\right)^{7-p} \ . \end{aligned} \tag{1.1.22}$$

The function $f(r)$ in (1.1.22) is a blackening factor, which implies that this metric represents a black hole. which has an event horizon at $r = r_{\rm h}$.

1.2 The AdS/CFT correspondence

A duality relates two theories that are mathematically identical, even if they seem to be very different from a physical point of view.

The AdS/CFT correspondence was proposed by Juan Maldacena in 1997 [1], providing a link between string theory and quantum field theory on flat space time. The basic idea behind this duality is that string theory in the near horizon geometry of a stack of D-branes is equivalent to the low energy effective theory of the corresponding branes. The acronym AdS stands for Anti-de-Sitter space, while CFT refers to conformal field theory, a quantum field theory which is invariant under the group of conformal transformations.

The gravity theory has to be defined on $AdS \times X$, where X is a compact space. Then, the field theory is defined on the AdS space boundary. Thus, in this sense the correspondence realises the holographic principle, first proposed by 't Hooft and interpreted in the domain of string theory by Susskind [8], that states that all the information in a quantum gravity theory can be encoded in an effective theory at the boundary of its volume. As a result of the duality, we end up with a possible theory of quantum gravity that is mapped to a quantum field theory with no gravitational degrees of freedom, that would not appear to be an appropriate candidate for a theory of quantum gravity otherwise. All technical details about the correspondence can be found in [2–7].

As we will see later on, the specific relations between the couplings at both sides of the correspondence implies that, when the field theory is in a strongly coupled regime, the gravity theory exhibits a small curvature. Therefore, problems that are classically tractable on the AdS side allow us to gain insight into the non-perturbative regime of the CFT side, where the computations would be significantly involved, many times out of reach.

In what follows, we will mostly restrict ourselves to the duality between $\mathcal{N} = 4$ super Yang-Mills theory in $3 + 1$ dimensions, and IIB superstring theory in $AdS_5 \times S^5$, where S^5 is the five-sphere, having the same radius L as the 5-dimensional space AdS_5. This is the example that arises when one considers a stack o N D3-branes.

1.2.1 D3-branes

In order to motive the correspondence, it is useful to look at the open and close string perspective of D3-branes.

Let us begin with the open string perspective, which corresponds to the case in which $g_s \ll 1$ and the effective coupling $g_s N$ also fulfills the condition $g_s N \ll 1$. If we consider type IIB superstring theory in (9+1)-Minkowski space time, and then embed N coincident D3 branes, we have to take into account open strings, those that begin and end on the branes, as well as closed strings. The open strings will be excitations of a $3+1$ dimensional hyperplane, while closed strings will correspond to excitations of the $9 + 1$ dimensional spacetime.

In this regime the action of the D3-brane will be given by

$$S = S_{\text{closed}} + S_{\text{open}} + S_{\text{int}} \ , \tag{1.2.1}$$

where S_{closed} and S_{open} encode the closed and open string modes respectively, and S_{int} the interactions between them. Now, if one further takes the limit $\alpha' \to 0$, S_{int} vanishes, which means the open and closed string modes decouple. On the other hand, S_{open} reduces to the bosonic part of $\mathcal{N} = 4$ super Yang-Mills (provided $2\pi\, g_s = g^2_{\text{YM}}$) and S_{closed} is the action of free supergravity in (9+1)-dimensional Minkowski spacetime.

USC DE SANTIAGO

Let us now turn to the closed string perspective and, thus, consider the case $g_s N \to \infty$. Now the presence of the D3 branes modifies the space time, and closed strings of type IIB superstring theory propagate.

As we have already seen, we can distinguish to different regions from the supergravity solution of the D3-branes that we can obtain by setting $p = 3$ in (1.1.20): a near-horizon region and an asymptotically flat region. It turns out that in the asymptotically flat region the dynamics are described by type IIB supergravity in ten-dimensional flat spacetime, while in the near horizon region the accurate theory is IIB supergravity on $AdS_5 \times S^5$. Moreover, when taking the $\alpha' \to 0$ limit, as we did for the open string perspective, both types of closed strings decouple.

Thus, in the low energy limit of both perspectives two theories decouple. They are:

- **Open string perspective:** $\mathcal{N} = 4$ super Yang-Mills theory and type IIB supergravity on flat spacetime.

- **Closed string perspective:** type IIB supergravity on $AdS_5 \times S^5$ and type IIB supergravity on flat spacetime.

Finally, since type IIB supergravity on flat spacetime appears in the two perspectives, the remaining two theories should also be identified.

If this conjecture is true, the symmetries on both sides should be the same. Actually, one can check that the complete symmetry is given by the superalgebra $PSU(2,2|4)$, that has a bosonic subgroup $SU(2,2) \times SU(4)$. The bosonic subalgebra of a superalgebra $SU(m|n)$ is $SU(m) \times SU(n) \times U(1)$, and the letter P indicates that the $U(1)$ factor is absent. On top of this, it contains 32 fermionic generators.

On the one hand, $\mathcal{N} = 4$ super Yang-Mills has 16 Poincaré supercharges, since it is $\mathcal{N} = 4$ supersymmetric, and another 16 superconformal supercharges. This is translated into the supergroup $PSU(2,2|4)$. On the other hand, $AdS_5 \times S^5$ has $SO(4,2)$ and $SO(6)$ isometries, which are the isometry groups of AdS_5 and S^5, respectively, whose covering groups are $SU(2,2)$ and $SU(4)$, and coincide with the bosonic subgroup of $PSU(2,2|4)$. This background realises all 32 supersymmetries of the type IIB superstring theory as vacuum symmetries.

1.2.2 Strong-weak coupling relation

As previously stated, perturbative computations on one side of the duality allow us to gain information on the non-perturbative regime of the other side. As a consequence, we need to know how the different parameters relate to each other. Besides, some specific limits will have to be considered.

We have already given the relation between the string and the Yang-Mills coupling constants

$$g^2_{\mathrm{YM}} = 2\pi\, g_s \ . \tag{1.2.2}$$

USC UNIVERSIDADE DE SANTIAGO DE COMPOSTELA

Which, setting $p = 3$ in (1.1.21), leads to an expression of the AdS radius L and the string length l_s in terms of N, $g_{\rm YM}$ or the 't Hooft coupling $\lambda = N\, g^2_{\rm YM}$ as

$$\left(\frac{L}{l_s}\right)^4 = 2\, g^2_{\rm YM}\, N \qquad , \qquad \frac{l^2_{\rm s}}{L^2} = \frac{1}{\sqrt{2\,\lambda}}\ . \tag{1.2.3}$$

On the other hand, the ten-dimensional Newton constant may be related to the string or Yang Mills coupling as

$$G = \frac{(2\pi)^7\, g^2_{\rm s}\, (\alpha')^4}{16\,\pi} = 2\,\pi^4\, g^4_{\rm YM} l^8_{\rm s}\ , \tag{1.2.4}$$

which can be recast in terms of the Plank length $l_{\rm P}$, since $G = l^8_{\rm P}$

$$\left(\frac{l_{\rm P}}{L}\right)^8 = \frac{\pi^4}{2\, N^2}\ . \tag{1.2.5}$$

On the gravity side, weak coupling corresponds to taking $g_{\rm s} \ll 1$ while the ratio $L/l_{\rm s}$ is kept constant. On the conformal side, according to (1.2.3), this amounts to taking $g_{\rm YM} \ll 1$ while $g^2_{\rm YM}\, N$ (or λ) remains finite. Making $N \to \infty$ while keeping λ fixed is known as the 't Hooft limit.

However, in order to avoid stringy corrections we further need to require $l_{\rm s}/L \ll 1$, which according to (1.2.3) implies large 't Hooft coupling, and so $\lambda \gg 1$. Note this is actually convenient, since we are interested in the strongly coupled regime of the field theory side. Besides, we would also like to avoid quantum corrections, and thus impose $l_{\rm P}/L \ll 1$. This corresponds to the small curvature limit. Finally, from (1.2.5), this last condition is equivalent to having $N \gg 1$. This limit is referred as the weak of the AdS/CFT correpondence, in which we have

$$N \gg 1 \qquad , \qquad \lambda \gg 1\ . \tag{1.2.6}$$

1.2.3 Field operator map. Reduction on the $\mathbb{S}^5$

The field operator map allows to relate generating functionals on both sides of the correspondence. This is specially interesting because physical observables in CFT are correlation functions of gauge-invariant operators. Once we have a prescription relating bulk fields ϕ to operators $\mathcal{O}$ on the boundary, we would like to be able to identify such correlation functions to computable quantities in AdS. Let ϕ_0 be the boundary value of a field ϕ in AdS. Then we would have

$$Z_{\rm QFT}[\phi_0] = < e^{\int \phi_0\, \mathcal{O}} >_{\rm QFT} = Z_{\rm AdS}[\phi \to \phi_0]\ , \tag{1.2.7}$$

where $Z_{\rm AdS}[\phi \to \phi_0]$ is the partition function evaluated over all functions having ϕ_0 at the boundary

$$Z_{\rm AdS}[\phi \to \phi_0] = \sum_{\phi \to \phi_0} e^{S_{\rm gravity}} \approx e^{S^{\rm on-shell}_{\rm gravity}[\phi \to \phi_0]}\ . \tag{1.2.8}$$

USC UNIVERSIDADE DE SANTIAGO DE COMPOSTELA

This last approximation is only valid when classical gravity dominates. Finally, it is worth noting that, since the on-shell action will be usually divergent, one has to substitute it with the renormalised one.

The fact that symmetries match on both sides of the correspondence implies that we will be able to map operators in $N = 4$ Super Yang-Mills in certain representations of $PSU(2,2|4)$ to states in $AdS_5 \times S^5$ in the same representation. In particular, we will see how operators can be mapped to supergravity fields.

Let ϕ be a field in $AdS_5 \times S^5$. This field can be decomposed to a tower of fields ϕ_l in AdS_5 and, in order to do so, we should expand it in terms of the harmonics $Y_l(\Omega)$ on the five-sphere

$$\phi(x, \Omega_5) = \sum_l \phi_l(x)\, Y_l(\Omega_5) \ , \tag{1.2.9}$$

where x denotes the AdS coordinates, and Ω_5 refer to coordinates on $\mathbb{S}^5$.

We will consider the case in which ϕ is a massless scalar field, that obeys the Klein Gordon equation (in ten dimensions) $\nabla^2\phi = 0$, with $\nabla^2 = \nabla^2_{\text{AdS}} + \nabla^2_{\mathbb{S}^5}$. Thus, for the reduced fields

$$\nabla^2_{\text{AdS}}\, \phi_l = m_l^2\, \phi_l \qquad , \qquad m_l^2 = \frac{l(l+4)}{L^2} \ , \tag{1.2.10}$$

so that, starting from a massless scalar field, we have obtained a tower of massive fields ϕ_l, whose masses are given by m_l in (1.2.10).

Now, since fields in AdS act as sources of the operators on the CFT side of the correspondence, we would like to know how these scalar fields behave near the boundary $z = 0$, where $z = L/r$. When solving the equation of ϕ close to the bounday that follows from the action of a scalar field in AdS_{d+1}, we arrive at

$$\phi(z, x) \approx A(x)\, z^{d-\Delta} + B(x)\, z^{\Delta} \qquad , \qquad z \to 0 \ , \tag{1.2.11}$$

where

$$\Delta = \frac{d}{2} + \sqrt{\frac{d^2}{4} + m^2\, L^2} \ . \tag{1.2.12}$$

In the last expression Δ is real as long as $m^2 \geq -\left(d/2L\right)^2$, which is the so-called Breitenlohner-Freedman (BF) bound that we will assume satisfied in what follows. As a consequence, $d - \Delta \leq \Delta$, and the term going as z^{Δ} in (1.2.11) can be neglected. By removing the divergence of the boundary value of ϕ, we can readily read the QFT source $\varphi(x)$

$$\varphi(x) = \lim_{z \to 0} z^{\Delta - d} \phi(z, x) \ . \tag{1.2.13}$$

From the relation between φ and ϕ, $d - \Delta$ must be the mass scaling dimension of the source φ. On the other hand, Δ is identified with the mass scaling dimension of the dual operator $\mathcal{O}$. Note that, when fulfilling the BF bound, the scaling dimension is real. For example, let us consider a massless scalar ($l = 0$) in four dimensions. Then, (1.2.12) leads to $\Delta = 4$, and thus $\mathcal{O}$ should be a scalar operator of dimension 4. Now, if we consider a general l, using (1.2.10), the scaling dimension will give $\Delta = 4 + l$.

USC DE SANTIAGO

1.2.4 Thermodynamics

It is well-known from general relativity that black holes behave as thermodynamic objects, whose temperature and entropy can be computed. The entropy is given by the Bekenstein-Hawking formula

$$S_{\rm BH} = \frac{1}{4\,G_{10}} A \ , \tag{1.2.14}$$

where A is the horizon area.

As for non-extremal black holes, D-branes are expected to have thermodynamic properties. Actually, in order to construct the gravity dual of quantum field theory at finite temperature, it will be necessary to consider a black hole in asymptotically AdS space. The metric (1.1.22) of a non-extremal D3-brane has an event horizon at $r = r_{\rm h}$, similar to the one we would encounter on a black hole. To determine its temperature, one has to introduce the Euclidean time coordinate $\tau = i\,t$ and adjust the periodicity of τ in such a way that there is no conical singularity at the horizon. It gives

$$T = \frac{r_{\rm h}}{\pi} \ . \tag{1.2.15}$$

This allows us to identify the brane as the dual of strongly coupled $\mathcal{N} = 4$ Super Yang Mills plasma at finite temperature T. The next obvious step is to obtain the entropy, that will be given by (1.2.14)

$$S_{\rm BH} = \frac{\pi^2}{2}\, N^2\, T^3\, {\rm Vol}(\mathbb{R}^3) \ . \tag{1.2.16}$$

However, this result will not agree with the one carried out in the $\mathcal{N} = 4$ gauge theory. This is due to the fact that, on the gravity side of the correspondence, we are considering $N \gg 1$ and $\lambda \gg 1$, while the CFT computation would have to be done for $\lambda \ll 1$. Specifically, we would arrive at

$$S_{\rm CFT} = \frac{2}{3}\pi^2\, N^2\, T^3\, {\rm Vol}(\mathbb{R}^3) \ . \tag{1.2.17}$$

So that there is a $4/3$ difference between both results. A natural way of solving this disagreement is to introduce a function $c(\lambda)$, in such a way that $c(\lambda \to 0) = 1$ and $c(\lambda \to \infty) = 3/4$

$$S = c(\lambda)\, \frac{2}{3}\pi^2\, N^2\, T^3\, {\rm Vol}(\mathbb{R}^3) \ . \tag{1.2.18}$$

Other thermodynamic quantities, such as the free energy or the energy density, can be derived following the usual thermodynamic relations.

1.2.5 Summary: the dictionary

We will close this section by emphasizing those key parts of the D3-brane correspondence, that can nevertheless be extended to other types of Dp-branes. We considered a stack of N coincident D3 branes, and saw that type IIB supertring theory in $AdS_5 \times \mathbb{S}^5$ could be identified with $\mathcal{N} = 4$ super Yang Mills with gauge group $SU(N)$. Then:

USC DE SANTIAGO

- The value of N, which is an integer, corresponds to the rank of the gauge group. Additionally, it also coincides with the flux of F_5 through the $\mathbb{S}^5$. This is related to the fact that N D3 branes will carry N units of D3-brane charge.

- The complete symmetry is given by $PSU(2,2|4)$.

- Many relations can be obtained among the constants on both sides of the correspondence. In particular, between the Yang-Mills coupling constant and the string coupling, and between the AdS radius and the 't Hooft coupling.

- Operators on the CFT side can be mapped to supergravity fields on the AdS part of the correspondence.

1.3 Flavored systems in the AdS/CFT correspondence

So far the field theory under consideration has been $\mathcal{N}=4$ super Yang-Mills, that contains matter in the adjoint representation of the gauge group. However, if one wishes to be able to construct a model that could be used to account for interactions such as those in QCD, fields transforming in the fundamental representation, as quarks do, should be included. As a consequence, it is necessary to try to modify the correspondence with the presence of fundamentals that, besides, will lead to the appearance of new symmetries and to subsequently changes on the spectrum.

Taking into account what we know from the AdS/CFT duality, it is obvious that if we want to have flavors on the field theory side some new object should be included on the original string background. Actually, this can be accomplished by adding more D-branes to the initial setup, that, for obvious reasons, we will refer to as *flavor branes*. This was first described in [9] and has been widely implemented afterwards. We will comment here the basic idea behind this process.

Let $N_{\rm f}$ be the number of flavor branes. Then, the gauge field propagating on them will encode a $U(N_{\rm f})$ gauge symmetry in the bulk, dual to a global $U(N_{\rm f})$ in the field theory side, and meson fields will propagate on them.

For continuation with the discussion on previous sections, we will consider a system of $N_{\rm c}$ *color* D3-branes in flat space-time. When adding a stack of $N_{\rm f}$ flavor Dp-branes to this background, the first obvious implication is that open strings will no longer solely begin and end on the D3-branes, but we will have to take into account those starting and/or ending on these new p-branes. Namely, we may encounter 3-3, 3-p, p-3 or p-p strings.

Since we will be dealing with type IIB supergravity we can already limit the possible dimensions of the flavor branes. Firstly, we know that for the branes to be stable in type IIB, p has to be odd and, thus, its maximum value should be 7: $p \leq 7$. Moreover, we need to make sure that the p-p strings decouple in the Maldacena limit; we will do so by comparing the coupling of the D3 and Dp branes. We have

$$\lambda_{\rm D3} = 2\,\pi\, g_{\rm s}\, N_{\rm c} \qquad , \qquad \lambda_{Dp} = (2\,\pi)^{p-2}\,(\alpha')^{(p-3)/2}\, g_{\rm s}\, N_{\rm f}\ . \tag{1.3.1}$$

USC UNIVERSIDADE DE SANTIAGO DE COMPOSTELA

Thus

$$\frac{\lambda_{\mathrm{Dp}}}{\lambda_{\mathrm{D3}}} = (2\,\pi)^{p-1}\,(\alpha')^{(p-3)/2}\,\frac{N_{\mathrm{f}}}{N_{\mathrm{c}}}\ . \tag{1.3.2}$$

As a consequence, in the Maldacena limit ($\alpha' \to 0$) the ratio (1.3.2) vanishes for $p > 3$, and is finite for $p = 3$. However, when $p < 3$ it diverges, so we should limit the lowest flavor brane dimension in $p = 3$. Then, we will restrict ourselves to $p = 3, 5$ and 7.

On top of this, the flavor branes are required to fulfill additional conditions, related to how they are extended in spacetime. One should remember that D-branes can be regarded as the hypersurfaces where open strings may begin and end. When studying open strings, one can chose to impose either Neumann or Dirichlet boundary conditions on their endpoints. D-branes are extended along the directions where Neumann boundary conditions are imposed, while they are transverse to the directions where Dirichlet boundary conditions have been used. In chapters 2 and 6 we will be denoting with "×" directions with Neumann boundary conditions, and with "_" those with Dirichlet boundary conditions. With this in mind, we require:

1. The Dp branes have to be stretched in the timelike direction, as well as into at least one direction transverse to the D3 brane.

2. The intersection has to be supersymmetric if we want it to be stable. This condition is satisfied when the number of Neumann-Dirichlet boundary conditions is 0, 4 or 8. Neumann-Dirichlet boundary conditions refer to the directions where the D3 and the Dp brane have different boundary conditions (a direction in which the D3 brane is streched but not the Dp, or viceversa).

Now we have set some of the basics, let us see how to proceed with the addition of the flavor branes. When discussing D-branes in string theory we had to distinguish to perspectives, depending on the effect they had on the surrounding spacetime. Similarly, we will encounter two distinct ways of dealing with the flavor branes, whose central ideas are stated in what follows.

In both cases we will assume a large number of color branes, $N_{\mathrm{c}} \to \infty$, while $g^2_{\mathrm{YM}}\,N_{\mathrm{c}}$ remains fixed. Then, one can consider two different limits: either we chose N_{f} to be fixed and thus $N_{\mathrm{f}}/N_{\mathrm{c}} \to 0$, or $N_{\mathrm{f}} \to \infty$ while $N_{\mathrm{f}}/N_{\mathrm{c}}$ is fixed. This corresponds to the so-called 't Hooft [101] and Veneziano [102] limits, respectively.

1.3.1 't Hooft limit: quenched approximation

In the 't Hooft picture, the fact of including additional D-branes does not deform the pre-existent background, and we can treat them as probes. It is also referred to as the quenched approximation, a term used in the lattice literature. Applying this approximation amounts to considering infinitely massive quarks, so that we can ignore their dynamical effects (they don't run in loops). In spite of looking as a quite harsh approximation, since many physical phenomena are known to be intimately related to the quantum effects of quarks, it allows to

USC DE SANTIAGO

explore many interesting features, such as chiral symmetry breaking or the exact computation of the messon spectrum; a review on the topic can be found in [10].

Let us present the flavor brane action for the 't Hooft picture. The color branes background determines an induced metric $\hat{g}_{ab}$ on the flavor branes, which is what will finally give us the mass spectrum and the interactions of the fluctuations of the Dp-branes, the mesons. Additionally, another field $\mathcal{F}_{ab}$ will also be induced by the background. The dynamics of the flavor Dp branes will be described by the Dirac-Born-Infeld-Wess-Zumino action

$$S_{\text{DBI-WZ}} = -T_{\text{Dp}} \int d^{p+1}x\, e^{\frac{p-3}{4}\phi} \sqrt{\det\left(\hat{g}_{ab} + 2\,\pi\,\alpha'\, e^{-\frac{\phi}{2}} \mathcal{F}_{ab}\right)} + T_{\text{Dp}} \int C \wedge e^{\mathcal{F}} \ , \qquad (1.3.3)$$

The quenched approximation will be used in the first part of this thesis (see I) to study the behavior of a strongly-coupled $(2+1)$-dimensional gauge theory under the influence of a external rotating electric field.

1.3.2 Veneziano limit: unquenching the flavors

In the Veneziano limit or unquenched approximation, the additional D-branes do deform the background, so that one has to take into account their backreaction on the original geometry. In contrast with the previous approximation, this picture includes the dynamical effects of quarks, that are needed when trying to tackle a variety of problems, as can be the construction of toy-models for quark-gluon plasma.

Thus, appart from the Dirac-Born-Infeld-Wess-Zumino action, one has to consider the deformation of the background after introducing the flavor branes. The total action results from adding both contributions

$$S = S_{\text{IIA/IIB}} + S_{\text{DBI-WZ}} \qquad (1.3.4)$$

Needless to say that, in general, trying to find a solution from the action that arises from considering a stack of N_{c} color branes and N_{f} flavor branes is quite complicated. The main difficulties come from the fact that the flavor branes are localised in spacetime, which results on challenging differential equations with localised sources.

One procedure that has successfully been applied to overcome this issue is the so-called smearing technique; it was first introduced in [85], and is thoroughly explained in [86]. The key idea is to distribute the flavor branes uniformly along their perpendicular space, which would look like if we were adding one brane at each point of this transverse space. By doing so we delocalise the sources and get rid of the dependence on the transverse coordinates, which will at least ease some of the difficulties of the original calculation. On field theory grounds, this implies that we are not breaking any global symmetry when adding the fundamentals.

As a counterpart, it is worth noting that this approach restricts significantly the possible dual theories. However, it has been used in a variety of systems [87, 103–108], and we will implement it in later chapters (see part II) when studying a backreacted brane intersection.

USC UNIVERSIDADE DE SANTIAGO

1.3.3 The D3/D5 system

Let us now focus on the particular case of the D3/D5 system, that will be the one studied in both parts I and II of this thesis. We will start by describing the setup, and finally we will establish how the correspondence is modified by the emergence of flavors.

An interesting model was first proposed in [109] when they were trying to construct localised gravity in AdS_4, and later studied in [110]. It consisted of D3-branes stretched along the 0126 directions, and D5 branes along 012345, thus intersecting along three dimensions (0, 1 and 2). Note that, as previously stated, the flavor D5-branes are extended along the time-like direction 0, and on more than one direction transverse to the D3-branes (namely, four). Besides, the number of Neumann-Dirichlet boundary conditions is equal to 4 (on the directions 3456).

With respect to the symmetries, the initial D3 system would have had $SO(3,1)$ Lorentz symmetry on 0126 directions, while $SO(6)$ would be acting on the remaining ones. Afterwards, the addition of the D5 flavor branes will modify this situation: it reduces $SO(3,1)$ to $SO(2,1)$ and causes the breaking of $SO(6)$ to $SO(3) \times SO(3) \sim SU(2)_{\rm H} \times SU(2)_{\rm V}$ on 345 and 789.

Furthermore, we have already seen that strings beginning and/or ending on the D5 branes should be added to those doing so on the D3 branes. Firstly, we will encounter 3-3 (5-5) strings that lead to 16 supercharge vector multiples on the D3 (D5) branes and split into a vector multiplet and hypermultiplet under the preserved eight supercharges. On the other hand, 3-5 strings, that will be localised in the intersection, lead to a three-dimensional hypermultiplet transforming under the fundamental representation of each branes, as required. Additionally, closed strings will give rise to IIB supergravity.

Now, in this set-up the duality works as follows. As for the original statement followed by Maldacena, we will impose $g_{\rm s} \ll 1$ and $N_{\rm c} \gg 1$ while $g_{\rm s}\, N_{\rm c} \propto \lambda$ remains fixed, and we will later apply the Maldacena limit $\alpha' \to 0$

- If $\lambda \ll 1$, the branes are described as flat hypersurfaces. After taking $\alpha' \to 0$, the modes on the heavy D5 branes decouple. Thus, in most of the spacetime we are left with $\mathcal{N} = 4$ super Yang Mills, a (3+1)-dimensional field theory, plus a (2+1)-dimensional defect in which a localised interacting fundamental hypermultiplet lies.
- If $\lambda \gg 1$ and $\alpha' \to 0$ we end up with the usual D3-brane $AdS_5 \times S^5$ near horizon geometry plus a probed D5 brane embedded on this geometry.

As a consequence, the gravity side is described by closed strings and 5-5 strings, while 3-3 and 3-5 strings take care of the field theory side. As for the original correspondence, we regard the two systems as being dual of each other.

1.4 Applications

USC DE SANTIAGO

In this section we will review some important applications of the duality, related to the study of strongly coupled systems. We have already referred in various occasions to the possibility of

using the AdS/CFT correspondence in order to model quantum chromodynamics. Although we have commented on the matter of including flavors in the theory, there are other important characteristics of the strong interactions that one has to make sure to reproduce when aiming to find a realistic model for them.

First of all, QCD should be understood at finite temperature and density. In particular, gaining knowledge of its phase diagram is of major interest: it happens to be highly complex, again because of the strong coupling nature of the strong interaction at the relevant energy range. A work on the subject is [111]. Besides, QCD manifests color confinement, since quarks in this theory are forced to form colorless combinations. This can be realised by means of particular geometries, that can be proved to lead to a confinement theory by calculating Wilson loops with holography [112, 113].

Finally, QCD is not supersymmetric and shows chiral symmetry breaking. In order to break supersymmetry completely and obtain a geometrical picture of chiral symmetry breaking, one can embed probe branes, as we considered when trying to include in our theory fields transforming in the fundamental representation. One way of doing so consists on adding a D7-brane probe to the original D3-brane geometry on the presence of a non vanishing magnitic field [114].

On the other hand, many theoretical challenges can be found within the study of fluid dynamics, in particular those related to the description of strongly coupled fluids, highly difficult to describe by means of standard methods. Thus, we would like to use the duality to tackle problems in the hydrodynamics domain. The limit of the AdS/CFT correspondence that relates the physics of a fluid to gravity is also known as the fluid/gravity correspondence; a nice review can be found in [115].

This new perspective of hydrodynamics will lead to new insights in problems otherwise out of reach. They can be characterised by some transport coefficients and, actually, the fluid/gravity duality has predicted some universal values of such coefficients for strongly coupled fluids, a prominent example being the shear viscosity to entropy ratio [116].

An interesting application of the correspondence in studying fluid dynamics that we should emphasise leads again to QCD. Heavy ion collisions have led to the discovery of a new state of matter behaving like an ideal, strongly coupled and relativistic fluid, the quark gluon plasma. Again, the description of such an state requires strongly coupled QCD.

Moreover, many problems in condensed matter can also be explored by means of the holographic duality. For example, systems with strongly correlated electrons display nematic phases [82]; these kind of anisotropic states, in which at least one spatial direction is distinguished from the rest while remaining homogeneous can be naturally realised with the correspondence. It is worth mentioning that, if an anisotropic phase was developed in QCD at large baryon density, this could lead to more compact neutron stars, leading to interesting connections with black hole thermodynamics [83,84]. Indeed, many gravity backgrounds dual to anisotropic field theories have been studied in the literature. Among them, we can mention initial anisotropic states of the quark-gluon plasma formed in heavy ion collisions [34, 35], states with axionic/dilatonic sources [36–51], electromagnetic fields [52–69], p-wave superfluids [70–75], and multilayered systems [76–81]. In part II we will present a holographic dual that realises a source of anisotropy, as well as a finite density (see chapter 6).

USC DE SANTIAGO

Another interesting application in the condensed matter realm is Floquet engineering, whose goal is to control quantum systems by using time-periodic external fields. The artificial setup involves mainly irradiating the system with a circularly polarised laser, or shaking it around. With appropriate periodic drivings, new phases of quantum materials have been created and non-equilibrium phenomena have emerged. Examples include light-induced superconductivity [18, 19] and Floquet topological insulators [20–26]. Moving on to (3+1) dimensions, artificial Weyl semimetals have also been reported [27–29].

Floquet engineering follows from Floquet theorem [11], and we will refer to it in part I of this thesis. Below, we briefly review some of its aspects, but more detailed explanations and technicalities may be found in [12–17].

1.5 Floquet theory

Bloch's theorem, well-known in quantum mechanics, allows to study systems under a periodic potential by making use of translational invariance in space. One of the most physically interesting applications concerns the description of electronic properties of crystals.

Once we have a prescription for analyzing spatially periodic but temporally static problems, it is also interesting to look for the opposite situation and try to tackle the time dependent case. Floquet's method, which is a temporal analogous to Bloch's theorem, aims at studying those kind of systems. It enables to find solutions to the time dependent Schrödinger equation, when the Hamiltonian is time-periodic. It can be stated as follows

Theorem 1 (Floquet's theorem.) *Let $H(t)$ be a Hamiltonian periodic with period T. Then a solution to the Schrödinger equation*

$$i\hbar\frac{\partial}{\partial t}\left|\psi,t\right\rangle = H(t)\left|\psi,t\right\rangle \ , \tag{1.5.1}$$

can be written as

$$\left|\psi,t\right\rangle = e^{-i\,\varepsilon\,t/\hbar}\left|\phi,t\right\rangle \ , \tag{1.5.2}$$

where ε is real and $\left|\phi,t+T\right\rangle = \left|\phi,t\right\rangle$.

Solutions of the type (1.5.2) are referred to as Floquet solutions, while $\left|\phi,t\right\rangle$ are denoted Floquet modes. Floquet modes follow the equation

$$H_{\mathrm{F}}(t)\ \left|\Phi_\alpha,t\right\rangle = \varepsilon_\alpha\ \left|\Phi_\alpha,t\right\rangle \qquad , \qquad H_{\mathrm{F}}(t) = H(t) - i\,\hbar\,\frac{\partial}{\partial t}\ , \tag{1.5.3}$$

where we have defined the *time-dependent* Floquet Hamiltonian $H_{\mathrm{F}}(t)$. It is clear from (1.5.3) that ε plays the role of an energy and, for this reason, it is referred to as quasienergy.

The stroboscopic evolution is defined as the evolution of the system within one period T of the Hamiltonian. From the time-evolution operator in such an interval of time one

can define the *time independent* stroboscopic Floquet Hamiltonian $H_{\rm F}[t_0]$ as the operator satisfying

$$U(t_0+T,t_0) = e^{-i\,T\,H_{\rm F}[t_0]}\ . \tag{1.5.4}$$

Note that, although it does not depend on t, the stroboscopic Hamiltonian $H_{\rm F}[t_0]$ does depend on the choice of the initial time of the cycle t_0, which defines the beginning of the stroboscopic driving frame and is, in fact, a gauge choice. The relation between $H_{\rm F}[t_0]$ and $H_{\rm F}(t)$ can be easily found in terms of the so-called fast motion operator $P(t,t_0)$ or the stroboscopic kick operator $K_{\rm F}[t_0](t)$, defined as

$$P(t_2,t_0) = U(t_2,t_0)\,e^{i\,(t_2-t_0)\,H_{\rm F}[t_0]} = e^{-i\,K_{\rm F}[t_0](t_2)}\ , \tag{1.5.5}$$

giving

$$H_{\rm F}[t_0] = P^\dagger(t_2,t_0)\,H(t_2)\,P(t_2,t_0) - i\,P^\dagger(t_2,t_0)\,\partial_{t_2}\left(P(t_2,t_0)\right)\ . \tag{1.5.6}$$

This last expression can be understood as a statement of the existence of a periodic operator $P(t,t_0)$ such that the RHS of this equation is time-independent.

Since the choice of t_0 is the Floquet gauge choice and different stroboscopic Floquet Hamiltonians are gauge equivalent, one can define some fixed Floquet Hamiltonian $\hat{H}_{\rm F}$, which is related to $H[t_0]$ via an unitary operator, the so-called kick operator, denoted by $\hat{K}(t_0)$

$$\hat{H}_{\rm F} = e^{i\,\hat{K}(t_0)}H_{\rm F}[t_0]e^{-i\,\hat{K}(t_0)} \qquad , \qquad H_{\rm F}[t_0] = e^{-i\,\hat{K}(t_0)}\,\hat{H}_{\rm F}\,e^{i\,\hat{K}(t_0)}\ , \tag{1.5.7}$$

where, by construction, the kick operator carries t_0 dependence. One can relate this kick operator to the stroboscopic kick operator,

$$e^{-i\,\hat{K}(t)}\,e^{i\,\hat{K}(t_0)} = e^{-i\,K_{\rm F}[t_0](t)}\ . \tag{1.5.8}$$

In general, the exact form of the time-evolution operator or Floquet Hamiltonian in these time dependent systems is not known, and one needs to make use of approximations [117–123]. One option is trying to compute them in the high-frequency limit by making use of expansions, such as the Magnus expansion [124] or the high frequency expansion of the effective Floquet Hamiltonian. We briefly review the latter below.

1.5.1 High frequency expansion of the effective Floquet Hamiltonian

Let us consider the problem

$$i\,\partial_t\,|\psi(t)\rangle = H(t)\ |\psi(t)\rangle \quad , \quad H(t) = H_0 + V(t) \quad , \quad V(t+T) = V(t)\ , \tag{1.5.9}$$

and let us perform the following unitary transformation of the state vector

$$|\psi(t)\rangle \to |\phi(t)\rangle = e^{i\,K(t)}\,|\psi(t)\rangle\ . \tag{1.5.10}$$

USC UNIVERSIDADE DE SANTIAGO DE COMPOSTELA

The transformed state $|\phi(t)\rangle$ evolves as

$$i\,\partial_t\,|\phi(t)\rangle = H_{\text{eff}}\;|\phi(t)\rangle \qquad , \qquad H_{\text{eff}} = e^{i\,K(t)}\,H(t)\,e^{-i\,K(t)} + i\,\partial_t e^{i\,K(t)}\,e^{-i\,K(t)}\;, \quad (1.5.11)$$

where H_{eff} is an effective Hamiltonian. We are going to choose $K(t)$ in such a way that H_{eff} is time independent, so that the time evolution operator becomes

$$U(t_2,t_1) = e^{-i\,K(t_2)}e^{-i\,(t_2-t_1)\,H_{\text{eff}}}\,e^{i\,K(t_1)}\;. \quad (1.5.12)$$

Besides, let us assume H_{eff} and $K(t)$ can be expanded in power series of the inverse frequency of the driving, $\Omega^{-1} = T/2\pi$, as

$$H_{\text{eff}} = \sum_{n=0}^{\infty}\frac{1}{\Omega^n}H_{\text{eff}}^{(n)} \qquad , \qquad K(t) = \sum_{n=1}^{\infty}\frac{1}{\Omega^n}K^{(n)}(t)\;. \quad (1.5.13)$$

On the other hand, the periodic potential $V(t)$ will be expanded as

$$V(t) = \sum_{j=1}^{\infty}\left(V^{(j)}e^{i\,j\,\Omega\,t} + V^{(-j)}e^{-i\,j\,\Omega\,t}\right)\;. \quad (1.5.14)$$

Thus, the time dependent Hamiltonian in (1.5.9) reads

$$H(t) = H_0 + \sum_{j=1}^{\infty}\left(V^{(j)}e^{i\,j\,\Omega\,t} + V^{(-j)}e^{-i\,j\,\Omega\,t}\right)\;, \quad (1.5.15)$$

and H_0 is the Fourier zero mode of $H(t)$, while, for $j \neq 0$

$$H_j = V^{(j)} \qquad , \qquad j = \pm 1, \pm 2, ... \quad (1.5.16)$$

Then, the different terms $H_{\text{eff}}^{(n)}$ in (1.5.13) can be obtained by expanding H_{eff} in (1.5.11) order by order. As previously stated, the key idea is to choose the $K^{(n)}(t)$ terms in such a way that they absorb all the time dependence in (1.5.11) and, therefore, H_{eff} is time independent. Following this procedure, the first two terms of the high frequency expansion of the effective Hamiltonian read

$$H_{\text{eff}}^{(0)} = H_0 \qquad , \qquad H_{\text{eff}}^{(1)} = \sum_{j=1}^{\infty}\frac{1}{j}[H_j, H_{-j}]\;. \quad (1.5.17)$$

Let us see how to apply this approach in a simple problem.

A simple example: Floquet Weyl semimetal

We are going to study the case of a free Dirac particle in the presence of a rotating electric field of the form

$$A_x = -\frac{E}{\Omega}\,\sin\Omega\,t \qquad , \qquad A_y = \frac{E}{\Omega}\,\cos\Omega\,t \qquad , \qquad A_z = 0\;. \quad (1.5.18)$$

USC UNIVERSIDADE DE SANTIAGO DE COMPOSTELA

The time dependent Hamiltonian may be written as

$$H(t) = H_0 + H_{bg} \ , \tag{1.5.19}$$

with

$$H_0 = \gamma^0 \, \vec{\gamma} \, \vec{p} + \gamma^0 \, m \qquad , \qquad H_{bg} = -e \, \gamma^0 \, \vec{\gamma} \, \vec{A} \ . \tag{1.5.20}$$

The γ matrices in the previous expression satisfy the anticommutation relation $\{\gamma^\nu, \gamma^\mu\} = 2\,\eta^{\nu\mu}$. Let us recast the background Hamiltonian as

$$H_{bg} = e^{i\,\Omega\,t} H_+ + e^{-i\,\Omega\,t} H_- \qquad , \qquad H_\pm = \mp i \, \frac{e\,E}{2\,\Omega} \, \gamma^0 \ (\gamma^x \mp i\,\gamma^y) = \mp i \, \frac{e\,E}{\Omega} \, \gamma^0 \, \gamma^\mp \ , \tag{1.5.21}$$

where we have defined $\gamma^\pm = \frac{1}{2} \ (\gamma^x \pm i\,\gamma^y)$. Note that, from (1.5.15) and (1.5.16), we can relate the $H_\pm$ coefficients in (1.5.21) to those $H_{\pm j}$ in the first order term $H^{(1)}_{\text{eff}}$ of the high frequency expansion of the effective Hamiltonian (1.5.17)

$$H_\pm = H_{j=\pm 1} \ . \tag{1.5.22}$$

Thus, according to (1.5.17) the effective Hamiltonian reads

$$H_{\text{eff}} = H_0 + \frac{1}{\Omega} \, [H_+, H_-] = H_0 + \frac{e^2\,E^2}{4\,\Omega^3} \, [2\,\gamma^0\,\gamma^-, 2\,\gamma^0\,\gamma^+] = H_0 + \frac{e^2\,E^2}{\Omega^3} \, \gamma^0\,\gamma^5\,\gamma^z \ , \tag{1.5.23}$$

where γ^5 has been introduced. This Hamiltonian can be diagonalized in order to obtain the pseudoenergies

$$\lambda = \pm \sqrt{p_x^2 + p_y^2 + \Delta^2} \qquad , \qquad \Delta = \frac{e^2\,E^2}{\Omega^3} \pm \sqrt{m^2 + p_z^2} \ . \tag{1.5.24}$$

Which shows the Dirac point is split into two Weyl points [125].

1.5.2 Floquet engineering

Floquet engineering is based on Floquet's formalism. Actually, it is possible to establish an equivalence between different Hamiltonians describing a moving lattice by means of unitary transformations

$$H_a(t) = \frac{p^2}{2\,m} + V(x) - F(t)\,x \qquad \leftrightarrow \qquad H_b(t) = \frac{p^2}{2\,m} + V(x - x_0(t)) \ , \tag{1.5.25}$$

which means we can move from a problem with shaking to a system under an external force. In (1.5.25), the change of reference frame to absorb the shaking generates the external force $F(t)$.

USC DE SANTIAGO DE COMPOSTELA

For instance, irradiation of a laser can be modeled by a time periodic perturbation that makes the Hamiltonian describing the system inherit a time periodicity, which was the starting point for introducing Floquet theorem. These ideas can be applied to a variety of systems, such as cold atoms in optical traps [118, 126] and electronic systems. In the particular case of cold atom experiments in shaken optical lattices, interesting phenomena such as dynamical localization and stabilization and artificial gauge fields have been realised. In this way, Floquet engineering provides a tool to control different parameters of optical lattices, such as varying the position in time.

Below we review an example of dynamical localization in a vibrating lattice, in which one can see how transport disappears for specific values of the driving frequency. More details may be found in [127].

Modulated optical lattice

Let us start from a Hamiltonian of the form of $H_a(t)$ in (1.5.25) and study its 1D-lattice version. In the tight binding limit, the non-modulated part is described by the Hubbard Hamiltonian, and only jumps between nearest neighbors are taken into account

$$\frac{p^2}{2\,m} + V(x) \qquad \rightarrow \qquad -J \sum_j a^\dagger_{j+1}\, a_j + \text{h.c.}\ , \tag{1.5.26}$$

For simplicity, we define

$$H_0 = -J \sum_j a^\dagger_{j+1}\, a_j + \text{h.c.}\ , \tag{1.5.27}$$

which is the lattice version of the one-particle Hamiltonian in the tight-binding approximation. The operator $a^\dagger_j$ in (1.5.27) creates a particle at the site $j\,a$, with a being the lattice spacing, while J represents the hopping-matrix element. On the other hand, the term containing the external force in (1.5.25) becomes

$$-F(t)\,x \qquad \rightarrow \qquad \omega\,\xi(t)\,V\ , \tag{1.5.28}$$

where

$$V = \sum_j j\, a^\dagger_j\, a_j \qquad , \qquad \xi(t) = \xi_0\, \cos\omega\, t\ . \tag{1.5.29}$$

V is the lattice version of the position operator and, apart from constants, $\xi(t)$ encodes the external force, that has been chosen to be periodic. In our notation the Hamiltonian becomes

$$H(t) = H_0 + \omega\,\xi(t)\,V\ . \tag{1.5.30}$$

Thus, $H(t)$ represents a particle in a spatial potential driven by a time periodic force. Let us define the operator T as

$$T = \sum_j a^\dagger_{j+1}\, a_j \qquad \rightarrow \qquad H_0 = -J\,T + \text{h.c.} = -J\,\left(T + T^\dagger\right)\ , \tag{1.5.31}$$

USC UNIVERSIDADE DE SANTIAGO DE COMPOSTELA

Moreover, we also define the operator H_1 as

$$H_1 = i\,J\,\left(T - T^\dagger\right)\ . \tag{1.5.32}$$

These operators satisfy the following commutation relations

$$[H_0, H_1] = 0 \qquad , \qquad [T, T^\dagger] = 0 \qquad , \qquad [T, V] = -T\ ,$$

$$[H_0, V] = -i\,H_1 \qquad , \qquad [H_1, V] = i\,H_0\ . \tag{1.5.33}$$

The commutation relations in (1.5.33) imply that, for real γ, we have

$$e^{i\,\gamma\,V}\,H_0\,e^{-i\,\gamma\,V} = H_0\,\cos\gamma - H_1\,\sin\gamma\ . \tag{1.5.34}$$

Now, one can consider the unitary transformation $|\psi\rangle = R\,|\psi\rangle$, with $R = e^{-i\,\xi_0\,\sin(\omega\,t)\,V}$, which absorbs the driving term $\omega\,\xi(t)\,V$ in the Hamiltonian. The transformed Hamiltonian $\tilde{H}$ becomes

$$\tilde{H} = R^\dagger\,H\,R - i\,R^\dagger\,\partial_t R = H_0\,\cos\alpha(t) - H_1\,\sin\alpha(t)\ , \tag{1.5.35}$$

where we have defined the phase $\alpha(t) = \xi_0\,\sin(\omega\,t)$. One could as well write $\tilde{H}$ in terms of the operators $a^\dagger$ and a, namely

$$\tilde{H} = -J\,\left(e^{i\,\alpha(t)}\sum_j a^\dagger_{j+1}a_j + e^{-i\,\alpha(t)}\sum_j a^\dagger_j a_{j+1}\right)\ . \tag{1.5.36}$$

Note the time dependence has been transferred to the phases of the hopping terms. This means that, as with Peierls substitution [128], the driving generates an artificial gauge field.

Since $[\tilde{H}(t_1), \tilde{H}(t_2)] = 0$, the stroboscopic time evolution operator $U(T,0) = U(T)$ for $\tilde{H}$ can be written as

$$U(T) = e^{-i\,\int_0^T \tilde{H}(t)\,dt}\ . \tag{1.5.37}$$

The previous integral introduces the Bessel function $\mathcal{J}_0(x)$

$$\int_0^T \tilde{H}(t)\,dt = T\,\mathcal{J}_0\left(\xi_0\right)\,H_0\ . \tag{1.5.38}$$

Thus, the effective Hamiltonian may be defined as

$$U(T) = e^{-i\,T\,\mathcal{J}_0(\xi_0)\,H_0} = e^{-i\,T\,H_{\text{eff}}} \qquad \rightarrow \qquad H_{\text{eff}} = \mathcal{J}_0\left(\xi_0\right)\,H_0\ . \tag{1.5.39}$$

Which amounts to a redefinition of the hopping parameter $J_{\text{eff}}\left(\xi_0\right) = J\,\mathcal{J}_0\left(\xi_0\right)$. The fact that shaking the lattice is equivalent to a redefinition of J means one can suppress the hopping by choosing ξ_0 as one of the zeros of the Bessel function, which would induce dynamical localization. This was experimentally demonstrated in [129].

Part I

Holographic Floquet states in low dimensions

USC
UNIVERSIDADE
DE SANTIAGO
DE COMPOSTELA

USC
UNIVERSIDADE
DE SANTIAGO
DE COMPOSTELA

2 Overview and holographic setup

Periodically driven systems form a separate chapter in the book of non equilibrium dynamics. Much progress has been achieved both at theoretical and experimental level in the path to control their effective long time dynamics [12–17, 126]. This has opened the way to engineer Hamiltonians that embody non trivial phenomena and new phases of quantum materials. Of particular interest is the case of solutions where energy injection and dissipation balance, thereby reaching a Floquet type of *non-equilibrium steady state* (NESS). In a series of previous works, the existence of a Floquet NESS has been studied in the context of the AdS/CFT correspondence in the case of a D3/D7 system [30] [31].

In [30], the authors studied the massless D3-D7 flavor system and computed the artificially induced Hall conductivity, while in [31] they extend part of the analysis to massive flavors where an interesting phase space shows up.

In this chapter we aim to study the behavior of a strongly-coupled $(2+1)$-dimensional gauge theory under the influence of a external electric field $\vec{\mathcal{E}}$ rotating in the xy plane as

$$\mathcal{E}_x \,+\, i\,\mathcal{E}_y \,=\, E\,e^{i\Omega t}\ . \tag{2.1}$$

The $(2+1)$-dimensional theory in place is realised as a codimension-one defect in $\mathcal{N}=4$ supersymmetric $SU(N_c)$ Yang-Mills theory in four dimensions and it can be obtained by means of the intersection of D3- and D5-branes along $2+1$ dimensions discussed in chapter 1 (see section 1.3.3).

We will work in the quenched probe approximation. In our holographic setup the flavor degrees of freedom are modeled as the excitations of a probe D5-brane embedded in the $AdS_5 \times \mathbb{S}^5$ ten-dimensional background. The probe brane extends along an $AdS_4 \times \mathbb{S}^2$ submanifold of the ten-dimensional background. The holographic duality in the D5-brane worldvolume relates the fields at the boundary of AdS_4 to those of the dual (2+1)-dimensional gauge theory, as it has already been explained in chapter 1.

In particular, to model the rotating field (2.1) we have to switch on an electric gauge field on the worldvolume attaining the value (2.1) as we approach the AdS_4 boundary (the subleading term near the boundary determines the current j). The D5-brane with this worldvolume gauge field has a non-trivial profile which can be found by solving the equations

of motion of the probe brane. The leading value of the profile function at the boundary determines mass of the quarks, while the subleading term is related to the quark condensate.

When an external electric field acts on a medium, a vacuum polarization due to virtual charged particles (quarks) is produced. As a consequence, an oscillating polarization current is induced. If the external field is weak enough, the medium will remain in an insulator gapped phase in which the induced current is always perpendicular to the applied field. There is no Joule heating and the system is dissipation-less. When the external field is large enough the vacuum is unstable against the creation of quark-antiquark pairs (Schwinger effect). In the conductive phase the current becomes dissipative, and the driving induces a Joule heating.

For an external oscillating electric field as in (2.1) the critical value $E_{\rm c}$ at which the insulator-conductor transition takes place depends on the frequency Ω, *i.e.*, $E_{\rm c} = E_{\rm c}(\Omega)$ [130]. Remarkably, for some values $\Omega = \Omega_{\rm c}$ of the frequency, the transition occurs for vanishing external electric field, *i.e.*, $E_{\rm c}(\Omega_{\rm c}) = 0$. At this point of the phase space the rotating current j is not zero, in spite of the fact that the external driving field vanishes. Physically, for these frequencies the driving field enters in resonance with the vector meson excitations of the gauge theory. Actually, this resonating states with zero electric field and non-zero current also occur in the insulating phase in a finite range of frequencies $\Omega_{\rm c} < \Omega \leq \Omega_{\rm m}$. Following [31], where this behaviour was first found in the D3-D7 model, we will call a configuration with $E = 0$ and $j \neq 0$ a zero field *Floquet condensate of vector mesons*, or simply a *vector meson Floquet condensate*. Such stable rotating state is a fixed point of time evolution, namely a non-thermal fixed point [131]. Conversely, we will find a set of frequencies for which $j = 0$ and $E \neq 0$, defining what we chose to term *Floquet suppression points*.

We first consider the zero temperature case, and then add a background temperature to the adjoint degrees of freedom which, therefore, are now deconfined. The nonzero temperature breaks supersymmetry and adds charge carriers to the ones previously formed by Schwinger pair production. These are naturally melted mesons that are present at finite temperature for low enough quark mass. Therefore, the phenomenology is expected to yield a continuous deformation of the case at zero temperature. The take home message is that the addition of a background temperature acts in the same direction as an increase in the module of the electric field. Hence, many delicate phenomena related to the vicinity to critical embeddings get screened away.

It is known that the fluctuations of the flavor brane degrees of freedom feel another temperature, $T_{\rm eff}$, through an effective metric named *open string metric*. That this is a *bona fide* temperature has been the subject of careful studies that examined, for example, the universality of the fluctuation dissipation relations [132]. In most common cases the effective temperature is larger than the bulk temperature of the gluon plasma $T_{\rm eff} > T$. Some exceptional cases have been reported where the inequality is reversed [133]. We don't find such exceptional situation after scanning throughout our phase space.

As a consequence, we can borrow the terminology of the non-zero temperature case and classify the configurations of the brane depending on whether or not it crosses the effective horizon:

USC UNIVERSIDADE DE SANTIAGO

- In the so-called *Minkowski embeddings* the brane reaches the origin of AdS_4 without

developing the effective horizon. These Minkowski configurations are dual to the insulating phase of the defect gauge theory.

- On the contrary, *black hole embeddings*, where the induced horizon forms at a finite radial distance from the D3-brane system, correspond to the conductive phase. The flavor mesons are deconfined and a current can set up in response to an external electric field.

- At the interface between these two cases we find the *critical embeddings*, in which the probe develops the effective horizon right at its IR endpoint.

In this work we study both types of embeddings in order to determine the stable non-equilibrium phases of the theory. In this task we will employ both numerical and analytic techniques. The crucial ingredient that allows for the system to be solved numerically is the fact that, in the rotating frame, the action becomes time independent and, therefore, all differential equations turn out to be of the ordinary type. This is a remarkable ansatz where the technique developed in [52] can still be applied to obtain the fully non-linear one point functions just from demanding reality of the action. In the literature, this extremely useful IR fixing mechanism has been applied to several static configurations. For time dependent sources very little is known. In spatial dimension $d_{\rm s} = 2$, and for massless charge carriers, the current response is linear and instantaneous $j(t) = \sigma E(t)$ [33]. Our results are consistent with this observation in the limit of small mass flavors.

The rest of part I is organised as follows. In what remains of this chapter, we shall set up the stage and the notation although most of the details are relegated to appendix 2.A. On the other hand, appendix 2.B gives some details about the zero temperature limit, which will be helpful in the coming chapters.

In chapter 3 we review the results obtained by means of numerical computations. The numerical integration of the equations of motion and the structure of the phase diagram of the theory is presented in section 3.1, while section 3.2 summarises what was found for the conductivities . In particular, section 3.2.1 is devoted to a detailed study of the macroscopic rotating current generated in response to the rotating electric field. Namely, the relative angle between them shows an interesting pattern as a function of the driving frequency Ω. Section 3.2.2 is devoted to the study of the so called photovoltaic current, the response of the Floquet NESS to an additional AC electric field that probes the modified conduction properties of the medium as a result of the rotating electric field applied. Further details on the analysis of the phase space and the computation of the optical conductivities are relegated to appendices 3.A, 3.B and 3.C.

Besides, exact analytic solutions to the equations of motion can be found in two particular limits, studied in chapter 4. One of them is the massless (and small mass) limit, which we present in section 4.1 both for finite and vanishing temperature. In appendix 4.A, we find approximate analytic solutions of the equations of motion when the mass is small. The exact conductivities for the massless case are obtained in appendix 4.B. The other analytic limit corresponds to large driving frequency and it is discussed in 4.2, but only in the zero

USC DE SANTIAGO

temperature system. The different embeddings when the equations of motion are linearised are studied in appendix 4.C.

Finally, in chapter 5 we summarise our results and discuss some possible extensions of our work.

2.1 D3/D5 system in the quenched approximation

In order to analyze the Floquet states in the strong coupling regime, we will engineer a holographic brane setup in which two sets of branes intersect along $2+1$ dimensions. More concretely we will consider the intersection of two stacks of D3- and D5-branes according to the following array

$$\begin{array}{rccccccccc} & 1 & 2 & 3 & 4 & 5 & 6 & 7 & 8 & 9 \\ D3: & \times & \times & \times & _ & _ & _ & _ & _ & _ \\ D5: & \times & \times & _ & \times & \times & \times & _ & _ & _ \end{array} \tag{2.1.1}$$

In (2.1.1) the D3- and D5-branes share the spatial directions 1 and 2, whereas the direction 3 is parallel to the D3-brane and orthogonal to the D5-brane. The field theory dual to the brane setup (2.1.1) is well-known [9, 110, 134, 135]. It consists of a supersymmetric theory with $N_{\rm f}$ matter hypermultiplets (flavors) living on the $(2+1)$-dimensional defect and coupled to the ambient $\mathcal{N}=4$ theory realised by the stack of $N_{\rm c}$ color D3-branes. We will adopt the approximation in which the D5-branes are probes in the geometry generated by the D3-branes, so $N_{\rm f} \ll N_{\rm c}$. The latter is the standard holographic dual of four-dimensional $\mathcal{N}=4$ super Yang-Mills, namely $AdS_5 \times \mathbb{S}^5$ with flux.

In this section we will set up the stage and review the main results obtained in this study for the D3/D5 systems. Further details on the coordinates choice and on the equations of motion can be found in appendices 2.A and 2.B. We chose to parametrise the D5 brane embeddings with an angular coordinate function $\psi(u) \in [0,1]$ where $\psi(u)=0$ corresponds to massless embeddings and the boundary of AdS sits at $u=\infty$. The induced metric takes the form

$$ds^2 \;=\; g_{tt}dt^2 + g_{ii}(dx^2+dy^2) + g_{uu}du^2 + g_{\Omega\Omega}d\Omega_2^2 \,, \tag{2.1.2}$$

where $d\Omega_2^2$ is the metric of a unit two-sphere and

$$g_{tt} = -\frac{u^2}{L^2}\frac{g^2(u)}{h(u)} \;\;,\;\; g_{ii} = \frac{u^2}{L^2}h(u) \;\;,\;\; g_{uu} = L^2\left(\frac{1}{u^2}+\frac{\psi'^2}{1-\psi^2}\right) \;\;,\;\; g_{\Omega\Omega} = L^2(1-\psi^2)\,,$$

with

$$g(u) = 1-\frac{u_{\rm h}^4}{u^4} \;\;,\;\;\; h(u) = 1+\frac{u_{\rm h}^4}{u^4} \tag{2.1.3}$$

This black hole metric has a Hawking temperature

$$T = \frac{\sqrt{2}\,u_{\rm h}}{\pi L^2} = \frac{r_{\rm h}}{\pi L^2}\,. \tag{2.1.4}$$

USC UNIVERSIDADE DE SANTIAGO DE COMPOSTELA

where we have written T both in terms of the isotropic coordinate u and the radial coordinate r related by (2.A.6). At the horizon there is merely a factor $r_{\rm h} = \sqrt{2}\, u_{\rm h}$ among them (in what follows we will take $L = 1$). In the remaining we will parametrise background temperatures in terms of $r_{\rm h}/m$.

We want to study the response of these systems to an external driving by a circularly polarised electric field

$$\vec{\mathcal{E}}(t) = \begin{pmatrix} \mathcal{E}_x(t) \\ \mathcal{E}_y(t) \end{pmatrix} = \begin{pmatrix} \cos\Omega t & -\sin\Omega t \\ \sin\Omega t & \cos\Omega t \end{pmatrix} \begin{pmatrix} E_x \\ E_y \end{pmatrix} \equiv O(t)\vec{E} \ , \tag{2.1.5}$$

with $\vec{E} = \vec{\mathcal{E}}(t=0)$. To properly account for the rotation it is convenient to complexify this field $\mathcal{E}(t) = \mathcal{E}_x(t) + i\mathcal{E}_y(t)$

$$\mathcal{E}(t) = E\, e^{i\Omega t} = -i\,\Omega\, A\, e^{i\Omega t} \ , \tag{2.1.6}$$

where A is the boundary value of a world-volume gauge field one-form

$$2\pi\,\alpha'\,\mathcal{A}(t,u) \;=\; a_x(t,u)\,dx \;+\; a_y(t,u)\,dy \ , \tag{2.1.7}$$

The Born Infeld action reduces to

$$\frac{I_{\rm D5}}{\mathcal{N}} = -\int du g_{\Omega\Omega}\sqrt{g_{ii}^2|g_{tt}|g_{uu} - \left(\mathrm{Im}(\bar{a}'\dot{a})\right)^2 + g_{ii}(|g_{tt}||a'|^2 - g_{uu}|\dot{a}|^2)} \ , \tag{2.1.8}$$

with $\mathcal{N} \equiv 4\pi N_{\rm f} T_{\rm D5}\mathrm{vol}(\mathbb{R}^{1,2})$. The complexification in 2.1.6 motivates to do it also at the level of the bulk fields

$$a(t,u) \;=\; a_x(t,u) + i a_y(t,u) = c(t,u)e^{i\Omega t} \ , \tag{2.1.9}$$

leading to the following form of the action [1]

$$\frac{I_{D5}}{\mathcal{N}} = -\int du\, g_{\Omega\Omega}\Big[g_{ii}^2|g_{tt}|g_{uu} - \left(\mathrm{Im}(\bar{c}'\dot{c}) + \Omega\mathrm{Re}(\bar{c}'c)\right)^2 + \\ + g_{ii}(|g_{tt}||c'|^2 - g_{uu}(|\dot{c}|^2 + \Omega^2|c|^2 + 2\Omega\mathrm{Im}(\dot{c}\bar{c})))\Big]^{\frac{1}{2}} \ .$$

A particular ansatz is to assume that $c(t,u) = c(u)$. Hence $\dot{c} = 0$ and the only remnant of the rotating dynamics is the presence of the parameter Ω.

To exhibit the presence of a conserved quantity it is convenient to switch to a polar image with $c(u) = b(u)e^{i\chi(u)}$. Then

$$\frac{I_{\rm D5}}{\mathcal{N}} = -\int du\sqrt{(1-\psi^2)\left[(u^4g^2 - \Omega^2b^2)\left((1-\psi^2)b'^2 + h(1-\psi^2+u^2\psi'^2)\right) + (1-\psi^2)u^4g^2b^2\chi'^2\right]} \ ,$$

[1] Notice that, unlike the case of a constant background electric field $A_x = -Et + ...$ [52] , in this case there is no explicit dependence on the UV value of the source in the action. This is a notorious difference that is at the heart of many differences among the two cases. For example the fact that the critical radius is not only dependent on the value of $|E|$ in our case.

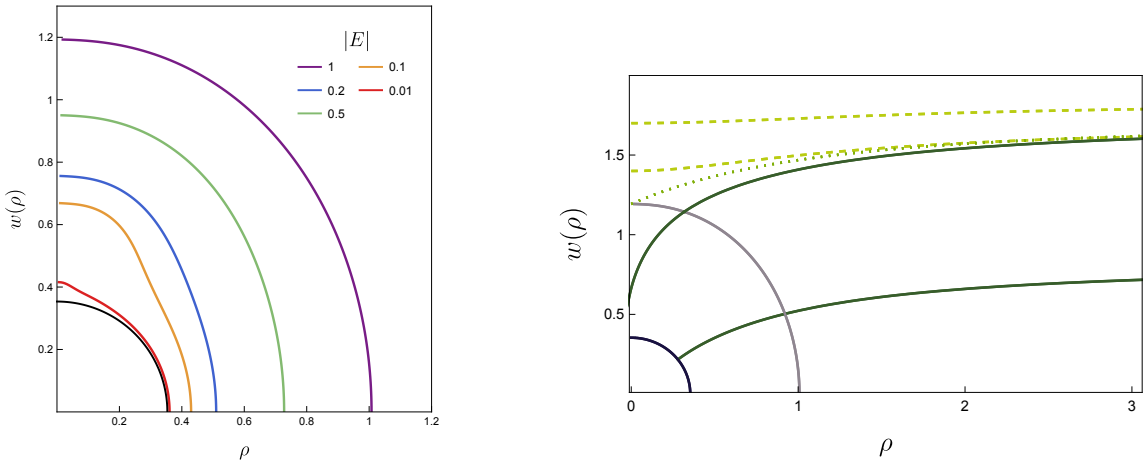


Figure 2.1: *Left plot:* shapes of the singular shells as a function of the applied electric field. The axes are $\rho = u\sqrt{1-\psi^2}$ and $w = u\,\psi$ with $\psi = \sin\theta$. The curves are the points $\rho^2 + w^2 = u_c(E, \psi_0)$ with $\psi_0 = \sin\theta_0$ the embedding angle at the singular shell. Outside the limit $E \to 0$ the shell shape is non spherical. Hence, unlike the case of a constant electric field, in the rotating situation we have a non trivial dependence of u_c on the mass m of the D5-brane at fixed $|E|$. *Right plot:* profiles of different embeddings for $\Omega = |E| = 1$. The solid lines represent black hole embeddings. They can be either regular (thermal), ending on the horizon, or singular, ending in a conical singularity. The dotted line represents a critical embedding. The dashed lines represent Minkowski embeddings. The black hole and pseudo-horizon are shown by the black (inner) and gray (outer) lines.

and the searched for conserved quantity is the one associated to the shift symmetry of χ

$$q \equiv \Omega \frac{\partial \mathcal{L}}{\partial \chi'} \,. \tag{2.1.10}$$

As has become the usual case when there is an electric field switched on [52], demanding reality of the Routhian (partial Legendre transform with respect to χ)

$$\frac{\tilde{I}_{D5}}{\mathcal{N}} = -\int \frac{du}{\Omega\, b\, g\, u^2} \sqrt{(\Omega^2 b^2 - u^4 g^2)\left(q^2 - u^4\Omega^2 b^2 g^2 (1-\psi^2)^2\right)\left(b'^2 + h + \frac{u^2 h\, \psi'^2}{1-\psi^2}\right)} \,, \tag{2.1.11}$$

imposes that the first two terms under the square root must vanish at the same point $u = u_c$, which locates the so called *singular shell*. At once, this condition fixes both the value of u_c and that of the conserved quantity q

$$b_0 = \frac{u_c^4 - u_h^4}{\Omega u_c^2} \qquad , \qquad q = \frac{(u_c^4 - u_h^4)^2}{u_c^4}(1-\psi_0^2) \,, \tag{2.1.12}$$

where $b_0 = b(u_c)$, $\psi_0 = \psi(u_c)$. As $b_0 \geq 0$ we see that $u_c \geq u_h$ and the singular shell sits always at a larger radius than the black hole horizon. Moreover, here it is the IR data b_0

what controls the position of $u_c(u_h, b_0)$. This is unlike the case of constant E [52]. Hence the shape of the critical surface at constant $|E|$ is non spherical, as can be seen in Fig. 2.1.

There are three types of embeddings in place now. First of all, we find the *Minkowski* embeddings, which do not intersect the singular shell. They end up closing smoothly at a value of $u = u_0$ while $\psi = 1$. With *black hole* (BH) embeddings we will generically denote solutions that intersect the singular shell. This accounts for the fact that for a world-volume observer the singular shell acts as an event horizon, inducing thermal effects through Schwinger pair production. For this reason, we will term interchangeably singular shell and effective horizon.

Black hole embeddings can be further subdivided into two classes, *thermal* and *conical*. The first ones hit the bulk black hole horizon, while the second ones close up at $\psi = 1$ with a conical singularity, most likely a reflection of the sink of energy pumped by the electric field in a conducting albeit non-dissipative system. These conical black hole embeddings are the remnant of the ones that are found at zero temperature. For a constant electric field they were analyzed in [136, 137].

As a technical remark, notice that, in order to solve numerically for the black hole embeddings, boundary conditions must be placed at the singular shell. The first derivatives are then not free but commanded by regularity (see eqs. (2.A.21)(2.A.22) and (2.A.23)). In contrast, we could place boundary conditions at the background horizon for the embedding function ψ and the module b, but not for the phase χ since this function diverges logarithmically as $\log(u - u_h)$ (see Eq. (2.A.26)). Starting from the effective horizon, then, one can integrate either outwards or inwards and this is how the thermal and/or conical embeddings are completed.

As mentioned before, and explained in Appendix 2.A, the critical radius u_c signals the position of an event horizon in the induced open string metric which governs the dynamics of the worlsheet fluctuations. Associated with it, we find an effective temperature

$$T_{\rm eff} = \frac{2u_c\, h(u_c) \,-\, \Omega b'(u_c)}{2\pi\, b(u_c)\, \chi'(u_c)}\,. \tag{2.1.13}$$

As in the vast majority of the situations encountered in the literature, here we also find that $T_{\rm eff} > T$ as far as we have been able to scan, as shown in Fig. 2.2.

As usual, the UV asymptotic analysis establishes the holographic dictionary. Near the UV boundary $u \to \infty$, the fields $\psi(u)$, $b(u)$, $\chi(u)$ behave as

$$\psi(u) \;=\; \frac{m}{u} + \frac{\mathcal{C}}{u^2} + \dots \tag{2.1.14}$$

$$c(u) \;=\; A + \frac{j}{u} + \dots \,=\, b(u) e^{i\chi(u)}\,, \tag{2.1.15}$$

with $A = iE/\Omega$. From where we can read off the 1-point functions $\mathcal{C}$ and j for the chiral condensate and the electric current respectively.

The relation between E, j, m and $\mathcal{C}$ and the electric field $\mathcal{E}_{\rm YM}(t)$, the electric current

USC DE SANTIAGO

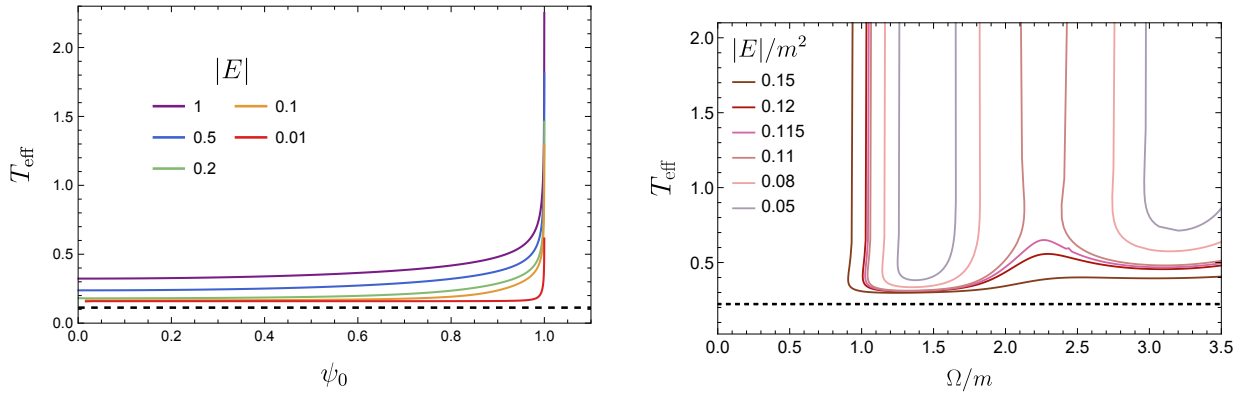


Figure 2.2: Left plot: effective temperature for different BH embeddings labelled by the insertion angle at the effective horizon $\psi_0 = \psi(u_{\rm c})$. Right plot: effective temperature as we vary Ω/m at fixed $|E|/m^2$. In both cases, the divergence in $T_{\rm eff}$ arises as the curves come close to the critical embeddings. In both plots, the lowest dashed line in black signals the background temperature.

$\mathcal{J}_{\rm YM}(t)$, quark mass $m_{\rm q}$ and quark condensate $\langle O_{\rm m}\rangle$ in the boundary theory are

$$\mathcal{E}_{\rm YM}(t) \,=\, \sqrt{\frac{\lambda}{2\pi^2}}\, e^{i\Omega\, t}\, E\ , \qquad\qquad \mathcal{J}_{\rm YM}(t) \,=\, \frac{N_{\rm f}\, N_{\rm c}}{\pi^2}\, e^{i\Omega\, t}\, j\ , \tag{2.1.16}$$

$$m_{\rm q} \,=\, \sqrt{\frac{\lambda}{2\pi^2}}\, m\ , \qquad\qquad \langle O_{\rm m}\rangle \,=\, -\frac{N_{\rm f}\, N_{\rm c}}{\pi^2}\, \mathcal{C}\ , \tag{2.1.17}$$

where $\lambda = g^2_{\rm YM}\, N_{\rm c}$ is the 't Hooft coupling of the $\mathcal{N} = 4$ theory. The consistency of the holographic dictionary for our model has been checked in appendix B of [90], that is, that the 1-point functions $\mathcal{C}$ and $\vec{j}$ are obtained from the functional variation of the on-shell action with respect to the sources m and $\vec{A}$. Using this asymptotics, the integration constant in (2.1.12) acquires the meaning of a Joule heating

$$q \,=\, \frac{\Omega\, u^4\, g^2}{\mathcal{L}}\, {\rm Im}(\bar{c}\, c') \,=\vec{j}\cdot\vec{E}\,. \tag{2.1.18}$$

Only black hole embeddings have a non zero value for this quantity. The stationarity of the background metric upon this energy injection can only be understood as a transient effect due to the imbalance $N_{\rm f}/N_{\rm c} \sim 0$ that is present in the probe limit. In the presence of a black hole in the bulk, the long time effect of a non-negligible backreaction would be a slow increase in the horizon radius.

An important remark for later use is the fact that both the worldvolume electric field and the black hole horizon add up their effects of bending the brane in the IR towards the origin $r \to 0$. This will mean that as we increase the temperature we will find black hole embeddings with milder electric fields.

The following is a scaling symmetry of the Lagrangian $\mathcal{L} \to \alpha^2\mathcal{L}$ and the boundary

conditions

$$
\begin{aligned}
&t \to t/\alpha\,, \qquad u \to \alpha\, u\,, \qquad w \to \alpha\, w\,, \qquad b \to \alpha b\,, \qquad \chi \to \chi\,,\\
&\Omega \to \alpha\,\Omega\,, \qquad E \to \alpha^2\, E\,, \qquad j \to \alpha^2\, j\,, \quad \psi \to \psi\,,\\
&m \to \alpha\, m\,, \qquad \mathcal{C} \to \alpha^2\, \mathcal{C}\,, \qquad q \to \alpha^4\, q\,, \quad T \to \alpha T\,, \quad T_{\text{eff}} \to \alpha T_{\text{eff}}\,.
\end{aligned}
\tag{2.1.19}
$$

By choosing $\alpha = 1/m$ in (2.1.19) we can make $m = 1$ and deal with the remaining quantities in units of (the appropriate powers of) m.

USC
UNIVERSIDADE
DE SANTIAGO
DE COMPOSTELA

USC
UNIVERSIDADE
DE SANTIAGO
DE COMPOSTELA

Appendices for chapter 2

2.A Coordinates and D5-brane action

There are several ways of parametrising the metric and chosing the embedding function. We present here three possibilities, that will turn out to be more convenient when dealing with different analysis and computations in what follows.

The ten-dimensional black hole metric generated by a stack of D3-branes is

$$ds_{10}^2 = \left(\frac{r}{L}\right)^2\Big(- f(r)\ dt^2 + dx_3^2\Big) + \left(\frac{L}{r}\right)^2\Big(\frac{dr^2}{f(r)} + r^2\ d\Omega_5^2\Big)\ , \tag{2.A.1}$$

where L is the anti-de Sitter radius, $d\Omega_5^2$ is the line element of a unit five-sphere and $f(r)$ is a blackening function given by

$$f(r) = 1 - \left(\frac{r_{\rm h}}{r}\right)^4\ , \tag{2.A.2}$$

where the horizon radius $r_{\rm h}$ is related to the black hole temperature as

$$T = \frac{r_{\rm h}}{\pi L^2}\ . \tag{2.A.3}$$

Let us now rewrite the line element (2.A.1) in a coordinate system more convenient for our purposes. First of all, we split $d\Omega_5^2$ as

$$d\Omega_5^2\ =\ d\theta^2\ +\ \cos^2\theta\, d\Omega_2^2\ +\ \sin^2\theta\, d\hat{\Omega}_2^2\ , \tag{2.A.4}$$

So that (2.A.1) becomes

$$ds^2 = \left(\frac{r}{L}\right)^2\Big(-f(r)\ dt^2+dx_3^2\Big)+\left(\frac{L}{r}\right)^2\left(\frac{dr^2}{f(r)} + r^2\left(d\theta^2 + \cos^2\theta d\Omega_2^2 + \sin^2\theta d\hat{\Omega}_2^2\right)\right)\ . \tag{2.A.5}$$

Moreover, let us introduce the so-called *isotropic coordinate* u

$$u^2 = \frac{r^2}{2}\left(1 + \sqrt{1 - \frac{r_{\rm h}^4}{r^4}}\right)\ , \tag{2.A.6}$$

with the horizon sitting at $u_{\rm h} = r_{\rm h}/\sqrt{2}$. We also define

$$\psi = \sin\theta\ . \tag{2.A.7}$$

USC UNIVERSIDADE DE SANTIAGO DE COMPOSTELA

Then, the metric (2.A.1) becomes

$$ds_{10}^2 = \frac{u^2}{L^2}\left(-\frac{g(u)^2}{h(u)}dt^2 + h(u)dx_3^2\right) + \frac{L^2}{u^2}du^2 + L^2\left(\frac{d\psi^2}{1-\psi^2} + (1-\psi^2)d\Omega_2^2 + \psi^2 d\hat{\Omega}_2^2\right) , \tag{2.A.8}$$

where $g(u)$ and $h(u)$ are the functions

$$g(u) = 1 - \frac{u_{\rm h}^4}{u^4}, \qquad h(u) = 1 + \frac{u_{\rm h}^4}{u^4} . \tag{2.A.9}$$

We can also work with coordinates (ρ, w), defined as

$$\rho = u\cos\theta, \qquad w = u\sin\theta, \qquad d\rho^2 + dw^2 = du^2 + u^2 d\theta^2 , \tag{2.A.10}$$

and in terms of these coordinates (2.A.1) would read

$$ds^2 = \frac{u^2}{L^2}\left(-\frac{g^2(u)}{h(u)}dt^2 + h(u)dx_3^2\right) + \frac{L^2}{u^2}\left(d\rho^2 + dw^2 + \rho^2 d\Omega_2^2 + w^2 d\hat{\Omega}_2^2\right) , \tag{2.A.11}$$

where $u^2 = \rho^2 + w^2$.

Now, different choices of the embedding function will lead us to different induced metrics. In all of them, we will take the angles in the second 2-sphere in (2.A.5), (2.A.8) and (2.A.11) to be constant, and then:

1. Choose the ansatz $\theta = \theta(r)$ in (2.A.5)

$$ds^2 = \left(\frac{r}{L}\right)^2\left(-f(r)\,dt^2 + dx_2^2\right) + L^2\left(\frac{1}{r^2 f(r)} + \theta'^2\right)dr^2 + L^2\cos^2\theta d\Omega_2^2 . \tag{2.A.12}$$

2. Choose the ansatz $\psi = \psi(u)$ in (2.A.8)

$$ds^2 = \frac{u^2}{L^2}\left(-\frac{g^2(u)}{h(u)}dt^2 + h(u)dx_2^2\right) + L^2\left(\frac{1}{u^2} + \frac{\psi'^2}{1-\psi^2}\right)du^2 + L^2(1-\psi^2)d\Omega_2^2 . \tag{2.A.13}$$

3. Choose the ansatz $w = w(\rho)$ in (2.A.11)

$$ds^2 = \frac{u^2}{L^2}\left(-\frac{g^2(u)}{h(u)}dt^2 + h(u)dx_2^2\right) + \frac{L^2}{u^2}\left(\left(1+w'^2\right)d\rho^2 + \rho^2 d\Omega_2^2\right) . \tag{2.A.14}$$

USC UNIVERSIDADE DE SANTIAGO DE COMPOSTELA

2.A.1 Lagrangian, IR and UV conditions

The action of the probe brane is given by the DBI action

$$I_{\rm D5} = -N_{\rm f} T_5 \int d^6\xi \sqrt{-\det\left(g_6 + 2\pi\alpha' \mathcal{F}\right)} \,, \tag{2.A.15}$$

where T_5 is the tension of the D5-brane, g_6 is the six-dimensional induced metric on the worldvolume of the D5-brane and $\mathcal{F} = d\mathcal{A}$ is the worldvolume gauge field strength.

Let us embed the D5-brane in such a way that one of the cartesian coordinates is constant and the brane sits at fixed point of the second two-sphere with $\psi = \psi(u)$. The induced metric is then given by (2.A.13).

Let us write down explicitly the action of the probe D5-brane. For simplicity in what follows we will take $L = 1$. When $\mathcal{F} = d\mathcal{A}$ and the one-form $\mathcal{A}$ is given by the ansatz (2.1.7), the DBI action can be written as

$$\frac{I_{\rm D5}}{\mathcal{N}} = -\int du\, \mathcal{L} \,, \tag{2.A.16}$$

where $\mathcal{N} \equiv 4\pi N_{\rm f} T_{\rm D5} {\rm vol}(\mathbb{R}^{1,2})$ and the Lagrangian density $\mathcal{L}$ is given by

$$\mathcal{L} = \sqrt{(1-\psi^2)\left[(u^4 g^2 - \Omega^2 b^2)\left((1-\psi^2)b'^2 + h(1-\psi^2+u^2\psi'^2)\right) + (1-\psi^2)u^4 g^2 b^2 \chi'^2\right]} \,. \tag{2.A.17}$$

In (2.A.17) the phase $\chi(u)$ only appears through its derivative $\chi'(u)$. So a conserved quantity, q, can be defined as

$$q \equiv \Omega \frac{\partial \mathcal{L}}{\partial \chi'} = \chi' \frac{u^4 \left(1 - \frac{u_{\rm h}^4}{u^4}\right)^2 \Omega\, b^2 (1-\psi^2)^2}{\mathcal{L}(\psi, \psi', b, b', \chi')} = \frac{(u_{\rm c}^4 - u_{\rm h}^4)^2}{u_{\rm c}^4}(1-\psi_0^2) \tag{2.A.18}$$

where the last equality is the one obtained by imposing reality of the Routhian action (2.1.11) at the singular shell. Therefore, χ is a cyclic variable that can be written in terms of the other functions as

$$\chi' = \frac{q}{u^2\, b\, g(u)} \sqrt{h(u) + b'^2 + \frac{u^2 h(u)\, \psi'^2}{1-\psi^2}} \frac{\sqrt{\Omega^2 b^2 - u^4 g(u)^2}}{\sqrt{q^2 - u^4 \Omega^2 b^2 g(u)^2 (1-\psi^2)^2}} \,, \tag{2.A.19}$$

where q is the constant of motion defined in (2.1.10). Near the UV boundary, the fields $\psi(u)$, $b(u)$, $\chi(u)$ behave as

$$\begin{aligned} \psi(u) &= \frac{m}{u} + \frac{\mathcal{C}}{u^2} + \mathcal{O}(u^{-4}) \,, \\ b(u) e^{i\chi(u)} &= \frac{iE}{\Omega} + \frac{j}{u} + \mathcal{O}(u^{-2}) \,. \end{aligned} \tag{2.A.20}$$

USC UNIVERSIDADE DE SANTIAGO DE COMPOSTELA

At the singular shell, the fields $\psi(u)$, $b(u)$, $\chi(u)$ can be written as

$$\begin{aligned}\psi(u) &= \psi_0 + \psi_1(u-u_{\rm c}) + ... \ ,\\ b(u) &= b_0 + b_1(u-u_{\rm c}) + .. \ ,\\ \chi(u) &= \chi_0 + \chi_1(u-u_{\rm c}) + ...,\end{aligned} \tag{2.A.21}$$

where $\psi_0 = \psi(u=u_{\rm c})$, $b_0 = b(u=u_{\rm c})$, $\chi_0 = \chi(u=u_{\rm c})$ (χ_0 can be set to 0). The coefficients χ_1, ψ_1 and b_1 are fixed by the equations of motion, and read

$$\begin{aligned}\chi_1 &= \frac{\Omega}{g(u_{\rm c})\,u_{\rm c}^3}\sqrt{\sqrt{C(1+C)}\left[2\Omega^2C^2+\frac{1}{2}\left(\Omega^2+4\,h(u_{\rm c})\,u_{\rm c}^2\right)\right]-\frac{1}{2}C\left[(3+4C)\Omega^2+4\,h(u_{\rm c})\,u_{\rm c}^2\right]}\ ,\\ \psi_1 &= \frac{1}{2\,h(u_{\rm c})\,u_{\rm c}^2}\left(B\,C-\sqrt{A(1+C)}\right)\ ,\\ b_1 &= -\frac{\Omega}{u_{\rm c}}\left(\frac{1}{2}+C-\sqrt{C(1+C)}\right)\ ,\end{aligned} \tag{2.A.22}$$

where the constants A, B, C are given by

$$\begin{aligned}A =&\ (1-\psi_0^2)\,h(u_{\rm c})\left[\Omega^2+4\,h(u_{\rm c})\,u_{\rm c}^2\right]\ ,\\ B =&\ 2\,\psi_0\,g(u_{\rm c})\,u_{\rm c}\ ,\\ C =&\ \frac{A}{B^2}\ .\end{aligned} \tag{2.A.23}$$

The Minkowski embeddings close off smoothly above the horizon at some $u_0 > u_{\rm c}$. At u_0 we can write

$$\begin{aligned}\psi(u) &= 1-\frac{3(u_0^4+u_{\rm h}^4)(u_0^8+u_{\rm h}^8-u_0^4(2u_{\rm h}^4+\Omega^2b_0^2))}{u_0(u_0^4-u_{\rm h}^4)(3(u_0^8+u_{\rm h}^8)+u_0^4(2u_{\rm h}^4-\Omega^2b_0^2))}(u-u_0)+\cdots\ ,\\ b(u) &= b_0-\frac{b_0u_0\Omega^2(u_0^4+u_{\rm h}^4)^2}{(u_0^4-u_{\rm h}^4)(3(u_0^8+u_{\rm h}^8)+u_0^4(2u_{\rm h}^4-\Omega^2b_0^2))}(u-u_0)+\cdots\ ,\end{aligned} \tag{2.A.24}$$

where now $b_0 = b(u=u_0)$. BH embeddings and Minkowski embeddings are separated by the critical solution, for which $u_0 \to u_{\rm c}$. It can be expanded as

$$\begin{aligned}\psi(u) &= 1-\frac{4(u_{\rm c}^4+u_{\rm h}^4)+\Omega^2u_{\rm c}^2}{2u_{\rm c}^2(u_{\rm c}^4+u_{\rm h}^4))}(u-u_{\rm c})^2+\cdots\ ,\\ b(u) &= \frac{u_{\rm c}^4-u_{\rm h}^4}{\Omega u_{\rm c}^2}-\frac{\Omega}{2u_{\rm c}}(u-u_{\rm c})+\cdots\ .\end{aligned} \tag{2.A.25}$$

Finally, suppose we would like to fix boundary conditions at the background black hole horizon. Setting

$$\begin{aligned}\psi(u) &= \psi_0^{\rm BH}+\psi_1^{\rm BH}(u-u_{\rm h})+...\\ b(u) &= b_0^{\rm BH}+b_1^{\rm BH}(u-u_{\rm h})+...\end{aligned}$$

USC UNIVERSIDADE DE SANTIAGO DE COMPOSTELA

we can insert this expansion into (2.A.19) and find

$$\chi'(u) = \frac{\Omega}{4u_{\rm h}}\sqrt{2+(b_1^{\rm BH})^2+\frac{2u_{\rm h}^2(\psi_1^{\rm BH})^2}{1-(\psi_0^{\rm BH})^2}}\,\frac{1}{u-u_{\rm h}}+\mathcal{O}(u-u_{\rm h})^0\ , \tag{2.A.26}$$

which exhibits a logarithmic divergence of $\chi(u)$ close to the background black hole horizon.

2.A.2 Effective horizon and effective temperature

Let h_{ab} be the induced six-dimensional metric and $\mathcal{F}_{ab}$ the worldvolume gauge field. The effective open string metric γ_{ab} is defined as [138]

$$\gamma_{ab} \,=\, h_{ab} \,+\, (2\pi\alpha')^2\,\mathcal{F}_{ac}\,\mathcal{F}_{bd}\,h^{cd}\ . \tag{2.A.27}$$

In order to write the form of this metric for our ansatz when the embedding is parameterised as a function $\psi = \psi(u)$, let us define the function $F(u)$ as

$$F(u) \,\equiv\, \left(u^2\,g^2\,-\,\frac{\Omega^2\,|c|^2}{u^2}\right)\frac{1}{h}\ , \tag{2.A.28}$$

and the complex one-forms $e_\pm$ as

$$e_\pm \,=\, e^{\mp i\Omega t}(dx\pm i dy)\ . \tag{2.A.29}$$

Then, we have

$$\begin{aligned}\gamma_{ab}\,d\xi^a\,d\xi^b = -F(u)\,dt^2+\left[\frac{1}{u^2}+\frac{\psi'^2}{1-\psi^2}+\frac{|c\,'|^2}{u^2\,h}\right]du^2+\frac{2}{u\,h}\,{\rm Im}\Big(c\,\bar{c}'\Big)dtdu+\\ +\frac{1}{4}\Big[\frac{1}{u^2}+\frac{\psi'^2}{1-\psi^2}\Big]^{-1}(e_-c'+e_+\bar{c}')^2+\frac{\Omega^2}{4}\frac{h}{u^2\,g^2}(e_-c+e_+\bar{c})^2+\frac{h^2\,F(u)}{g^2}e_+e_-\ ,\end{aligned} \tag{2.A.30}$$

where $c = b\,e^{i\chi}$ is the complexified field potential in the rotating frame. In order to diagonalise the (t,u) part of the metric (2.A.30), let us define new coordinates (τ,u_*) as

$$d\tau \,=\, dt\,-\,A(u)\,du\ , \qquad\qquad du_* \,=\, B(u)\,du\ , \tag{2.A.31}$$

where $A(u)$ and $B(u)$ are given by

$$A(u) \,=\, \frac{\Omega\,b^2\,\chi'}{u^2\,h\,F}\ , \qquad\qquad B(u) \,=\, \frac{\mathcal{L}}{u^2\,h\,(1-\psi^2)\,F}\ , \tag{2.A.32}$$

and $\mathcal{L}$ is the Lagrangian density (2.A.17). In these new coordinates the effective open string metric takes the form

$$\begin{aligned}\gamma_{ab}\,d\xi^a\,d\xi^b \,=\, F(u)\,(-d\tau^2+du_*^2)\,+\,\frac{1}{4}\Big[\frac{1}{u^2}\,+\,\frac{\psi'^2}{1-\psi^2}\Big]^{-1}(e_-c'+e_+\bar{c}')^2\,+\\ +\frac{\Omega^2}{4}\frac{h}{u^2\,g^2}\,(e_-c+e_+\bar{c})^2\,+\,\frac{h^2\,F(u)}{g^2}e_+e_-\ .\end{aligned} \tag{2.A.33}$$

USC UNIVERSIDADE DE SANTIAGO DE COMPOSTELA

The function $F(u)$ vanishes at $u = u_c$ (where $|c| = (u_c^4 - u_h^4)/(\Omega\, u_c^2) = b_0$). Thus, $u = u_c$ is an event horizon for the effective metric. The corresponding Hawking temperature can be obtained from the surface curvature at $u = u_c$, namely

$$T_{\rm eff} \;=\; -\frac{\gamma'_{tt}}{4\pi\,\gamma_{tu}}\bigg|_{u=u_c} \;. \tag{2.A.34}$$

From the values of γ_{tt} and γ_{tu} found above, we can readily demonstrate that

$$T_{\rm eff} \;=\; \frac{2u_c\,h(u_c) \;-\; \Omega b_1}{2\pi\, b_0\,\chi_1} \;=\; \frac{\Omega}{2\pi\,\chi_1\,u_c\,g(u_c)}\Big[2\,h(u_c) \;-\; \frac{\Omega\, b_1}{u_c}\Big]\;, \tag{2.A.35}$$

where b_0, b_1 and χ_1 are the coefficients defined in (2.A.21) for black hole embeddings.

2.B Some details on the parametrization in the $T = 0$ case

For latter convenience, let us give some more details on the parametrization used when studying this system at zero temperature. In particular, we will choose the cartesian embedding function w, and start from the induced metric on the D5-brane woldvolume presented in (2.A.14) when $T = 0$. Besides, we will suppose w is not only a function of ρ but can also depend on time ($w(t,\rho)$)

$$\begin{aligned} ds_6^2 \;=\; -\Big(\rho^2+w^2\Big)\left(1 \;-\; \frac{\dot w^2}{\Big(\rho^2+w^2\Big)^2}\right) dt^2 \;+\; (\rho^2+w^2)(dx^2+dy^2) \;+ \\ +\frac{1}{\rho^2+w^2}\left((1+w'^2)d\rho^2 \;+\; 2\,\dot w\,w'\,dtd\rho \;+\; \rho^2\,d\Omega_2^2\right)\,, \end{aligned} \tag{2.B.1}$$

where the dot denotes derivative with respect to t and the prime with respect to the holographic coordinate ρ. Using the same notation as in section 2.1 for the driving and the gauge field, the DBI action becomes

$$\begin{aligned} S \sim -\int dt\,d\rho\;\frac{\rho^2}{\rho^2+w^2}\;\Bigg[(1+w'^2)\Big((\rho^2+w^2)^2 \;-\; |\dot a|^2\Big) \;-\; \dot w^2\Big(1+|a'|^2\Big) \;+ \\ +|a'|^2\,(\rho^2+w^2)^2 \;+\; 2\,\dot w\,w'(\,\mathrm{Re}(\dot a\,a'^*) \;-\; \Big(\mathrm{Im}(\dot a\,a'^*)\Big)^2\Bigg]^{\frac12}\,. \end{aligned} \tag{2.B.2}$$

Or in (b,χ) variables

$$\begin{aligned} S \sim -\int dt\,d\rho\;\frac{\rho^2}{\rho^2+w^2}\;\Bigg[(1+w'^2)\Big((\rho^2+w^2)^2 \;-\; \dot b^2 \;-\; (\Omega+\dot\chi)^2\,b^2\Big) \;- \\ -\dot w^2\Big(1+b'^2 \;+\; b^2\,\chi'^2\Big) \;+\; (\rho^2+w^2)^2\Big(b'^2 \;+\; b^2\,\chi'^2\Big) \;+ \\ +2\,\dot w\,w'\left(\dot b\,b' \;+\; (\Omega+\dot\chi)\,\chi'\,b^2\right) \;-\; b^2\Big(\dot b\,\chi' \;-\; (\Omega+\dot\chi)\,b'\Big)\Bigg]^{\frac12}\,. \end{aligned} \tag{2.B.3}$$

USC UNIVERSIDADE DE SANTIAGO DE COMPOSTELA

Since the action does not depend on t explicitly, taking the functions b, χ and w as independent of the time is a consistent ansatz[2]

$$b = b(\rho) , \qquad \chi = \chi(\rho) , \qquad w = w(\rho) . \tag{2.B.4}$$

By removing the terms with the time derivative from the action, we can rewrite it in a much more simplified fashion as $S \sim \int d\rho\, \mathcal{L}$, where now

$$\mathcal{L} = \frac{\rho^2}{\rho^2+w^2}\sqrt{\Big((\rho^2+w^2)^2 - \Omega^2 b^2\Big)\Big(1+b'^2+w'^2\Big) + (\rho^2+w^2)^2\, b^2\, \chi'^2} . \tag{2.B.5}$$

We first notice that χ is a cyclic variable which means that q, defined as

$$q = \Omega \frac{\partial \mathcal{L}}{\partial \chi'} = \Omega \frac{\rho^4}{\mathcal{L}} b^2 \chi' , \tag{2.B.6}$$

is independent of ρ. The Euler-Lagrange equations derived from $\mathcal{L}$ are

$$\begin{aligned}
&\rho(\rho^2+w^2)\Big[(\rho^2+w^2)^2 - \Omega^2 b^2\Big] b'' = \\
&\quad = -(1+b'^2+w'^2)\Big[2(\rho^2+w^2)^3 b' + \Omega^2 b\Big(\rho(\rho^2+w^2) - 2w^2 b\, b'\Big)\Big] + \\
&\qquad + b(\rho^2+w^2)^3(\rho - 2bb')\,\chi'^2 , \\
&\rho(\rho^2+w^2)\Big[(\rho^2+w^2)^2 - \Omega^2 b^2\Big] w'' = \\
&\quad -2\,(1+b'^2+w'^2)\Big[(\rho^2+w^2)^3 w' - \Omega^2 b^2 w\,(\rho + w\,w')\Big] - 2\,b^2\,(\rho^2+w^2)^3\, w'\,\chi'^2 , \\
&b\rho(\rho^2+w^2)\Big[(\rho^2+w^2)^2 - \Omega^2 b^2\Big]\chi'' = -2\chi'\Big[(\rho^2+w^2)^3\Big(b^3\chi'^2 + \rho\, b' + b(1+b'^2+w'^2)\Big) - \\
&\qquad -\Omega^2 b^3\Big(2\rho^2 + 2\rho\, w\, w' + w^2(1+b'^2+w'^2)\Big)\Big] .
\end{aligned} \tag{2.B.7}$$

The last equation in (2.B.7) is redundant, since we can use the first integral (2.B.6) to obtain the value of χ' in terms of the other functions

$$\chi'^2 = \frac{q^2\Big[(\rho^2+w^2)^2 - \Omega^2 b^2\Big]}{(\rho^2+w^2)^2\, b^2\Big[\Omega^2\rho^4 b^2 - q^2\Big]}\,(1+b'^2+w'^2) . \tag{2.B.8}$$

We can next use this last equation to eliminate χ' in the first two equations in (2.B.7). The resulting equations for w and b depend on q (alternatively one could Legendre transform and obtain the corresponding Routhian).

[2]This of course does not preclude the existence of time dependent solutions. For example, at special points in phase space, instabilities may trigger first order phase transitions that can occur between Black Hole and Minkowski embeddings

2.B.1 Boundary conditions

Let us now study the equations of motion of the gauge field at the UV $\rho \to \infty$ in terms of the complex combination $c(\rho) = b(\rho)\, e^{i\chi(\rho)}$. The Lagrangian density $\mathcal{L}$ gives

$$\mathcal{L} \sim \frac{\rho^2}{\rho^2+w^2}\left[(1+w'^2)\left[(\rho^2+w^2)^2 - \Omega^2\,|c|^2\right] + (\rho^2+w^2)^2\,|c'|^2 - \Omega^2\left[\mathrm{Re}\,(c\,c'^*)\right]^2\right]^{\frac{1}{2}}, \quad (2.B.9)$$

and the equation of motion for $c(\rho)$ derived from $\mathcal{L}$ is

$$\partial_\rho\left[\frac{\rho^4}{(\rho^2+w^2)^2\,\mathcal{L}}\left((\rho^2+w^2)^2\,c' - \Omega^2\,\mathrm{Re}\,(c\,c'^*)\,c\right)\right] + \quad (2.B.10)$$
$$+\,\Omega^2\,\frac{\rho^4}{(\rho^2+w^2)^2\,\mathcal{L}}\left((1+w'^2)\,c + \mathrm{Re}\,(c\,c'^*)\,c'\right) = 0\,.$$

Near the UV at $\rho \to \infty$ we can show that $\mathcal{L} \approx \rho^2$ and the equation of motion reduces to $\partial_\rho(\rho^2\,c') = 0$, whose general solution is of the form $c(\rho) = a_1 + a_2/\rho$. Proceeding similarly for the embedding function and redefining the constants, we can write asymptotically

$$c(\rho) = b(\rho)\,e^{i\chi(\rho)} = \frac{i\,E}{\Omega} + \frac{j}{\rho} + \cdots,$$
$$w(\rho) \sim m + \frac{\mathcal{C}}{\rho} + \cdots. \quad (2.B.11)$$

Which corresponds to what was found in (2.1.14) and (2.1.15). The integration constant q defined in (2.B.6) can be written in terms of the field c and c^*

$$q = i\,\frac{\Omega\,\rho^4}{2\,\mathcal{L}}\left(c\,c'^* - c^*\,c'\right), \quad (2.B.12)$$

and can be easily related to UV data. As $w(\rho) \sim m + \mathcal{C}/\rho$ when $\rho \to \infty$, it follows that $\mathcal{L} \approx \rho^2$ for large ρ. Moreover, from (2.B.11) $c' \sim -j/\rho^2$ and, therefore

$$q = \mathrm{Re}(E\,j^*) = j_x\,E_x + j_y\,E_y\,, \quad (2.B.13)$$

which endows q with the physical interpretation of the Joule heating. If we assume that the driving effectively heats the system we should expect that $q \geq 0$, and from (2.B.6) this implies $\Omega\,\chi' \geq 0$. We can see that this result is consistent with the ingoing boundary condition at the pseudohorizon, which can be argued as follows. The wavefront of the complexified gauge potential $a(t,\rho)$ in (2.1.9) is the surface $\chi(\rho) + \Omega\,t = $ constant (we are in the case in which χ does not depend on t). By performing a generic variation of this condition, it follows that

$$\delta\,\rho = -\frac{\Omega}{\chi'}\,\delta\,t\,. \quad (2.B.14)$$

Requiring that our gauge potential represents an infalling wave at the pseudo-horizon implies $\delta\rho < 0$ for $\delta t > 0$ which, following (2.B.14), only occurs when $\Omega\,\chi' \geq 0$ and, therefore, $q \geq 0$.

2.B.2 Types of embeddings

The equations of motion written in (2.B.7) are potentially singular when

$$b_0 \,=\, \frac{w_0^2+\rho_{\rm c}^2}{\Omega}\ , \tag{2.B.15}$$

where $b_0 = b(\rho=\rho_{\rm c})$ and $w_0 = w(\rho=\rho_{\rm c})$. The pseudohorizon is located at $\rho=\rho_{\rm c}$ where the condition (2.B.15) holds. Indeed, we will show below that $\rho=\rho_{\rm c}$ is the event horizon of the induced open string metric on the D5-brane. We can have black hole embeddings (which cross the horizon), Minkowski embeddings (which do not intersect the pseudohorizon and reach the point $\rho=0$) and critical embeddings (for which the brane reaches the $\rho_{\rm c}$ at $\rho_{\rm c}=0$). In order to avoid the singularity at $\rho=\rho_{\rm c}$ the first derivatives of the functions $w(\rho)$, $b(\rho)$ and $\chi(\rho)$ have to be adjusted properly for black hole and critical embeddings.

Black hole embeddings

Expanding the functions $w(\rho)$, $b(\rho)$ and $\chi(\rho)$ around $\rho=\rho_{\rm c}$ as

$$\begin{aligned} w(\rho) \,&=\, w_0 \,+\, w_1\,(\rho-\rho_{\rm c}) \,+\, \cdots\ , \\ b(\rho) \,&=\, b_0 \,+\, b_1\,(\rho-\rho_{\rm c}) \,+\, \cdots\ , \\ \chi(\rho) \,&=\, \chi_0 \,+\, \chi_1\,(\rho-\rho_{\rm c}) \,+\, \cdots\ , \end{aligned} \tag{2.B.16}$$

we obtain coefficients w_1, b_1 and χ_1 imposing that the right-hand side of the equations (2.B.7) vanishes at the pseudohorizon $\rho=\rho_{\rm c}$ in order to avoid the potential singularity at this point. We get

$$\begin{aligned} \chi_1^2 \,&=\, \frac{\rho_{\rm c}\,(\Omega+2\rho_{\rm c}\,b_1)\,(1+b_1^2+w_1^2)}{\Omega\,b_0^2\,(\rho_{\rm c}-2b_0\,b_1)}\ , \\ b_1 \,&=\, \frac{\Omega}{2w_0}\,\frac{\rho_{\rm c}\,w_0 \,-\, (2\rho_{\rm c}^2+w_0^2)\,w_1}{\rho_{\rm c}^2+w_0^2}\ , \\ w_1 \,&=\, \frac{1}{w_0\,D}\Big[-4\rho_{\rm c}\,(\rho_{\rm c}^2+w_0^2)^2 \,-\, \Omega^2\,\rho_{\rm c}^3 \,+\, (\rho_{\rm c}^2+w_0^2)\,s\Big]\ . \end{aligned} \tag{2.B.17}$$

With

$$\begin{aligned} s \,&\equiv\, \sqrt{\Big[4(\rho_{\rm c}^2+w_0^2)+\Omega^2\Big]\,\Big[4(\rho_{\rm c}^2+w_0^2)^2+\Omega^2\rho_{\rm c}^2\Big]}\ , \\ D \,&\equiv\, 4(\rho_{\rm c}^2+w_0^2)^2 \,+\, \Omega^2\,(2\rho_{\rm c}^2+w_0^2)\ . \end{aligned} \tag{2.B.18}$$

Notice that χ_1 appears in the expression of the on-shell Lagrangian density $\mathcal{L}_0$ evaluated at the pseudohorizon $\rho=\rho_{\rm c}$

$$\mathcal{L}_0(\rho_{\rm c}) \,=\, \rho_{\rm c}^2\,b_0\,\chi_1\ . \tag{2.B.19}$$

USC DE SANTIAGO DE COMPOSTELA

We can use this expression to obtain the Joule heating q in (2.B.6). Indeed as q is constant, we can evaluate it at the pseudohorizon, with the result

$$q \,=\, \Omega\, \rho_{\rm c}^2\, b_0 \ , \tag{2.B.20}$$

which only depends on b_0. Using (2.B.15), we get

$$q \,=\, \rho_{\rm c}^2 \Big(w_0^2 + \rho_{\rm c}^2 \Big) \ . \tag{2.B.21}$$

Minkowski embeddings

In this case there is no $\rho_{\rm c}$ that solves (2.B.15) and the brane reaches the origin $\rho = 0$. We can therefore evaluate the Joule heating constant q by taking $\rho = 0$ in (2.B.8) and, since the right-hand side of this equation contains a ρ^4 factor we get $q = 0$. Thus, for these embeddings there is no net energy flux on the boundary theory. Moreover, from (2.B.8) one readily concludes that the phase function $\chi(\rho)$ is in fact a constant. Expanding $b(\rho)$ and $w(\rho)$ around $\rho = 0$

$$\begin{aligned} b(\rho) \,&=\, b_0 \,-\, \frac{b_0\, \Omega^2}{6\Big(w_0^4 - \Omega^2\, b_0^2 \Big)}\, \rho^2 \,+\, \cdots \ , \\ w(\rho) \,&=\, w_0 \,+\, \frac{b_0^2\, \Omega^2}{3\, w_0 \Big(w_0^4 \,-\, \Omega^2\, b_0^2 \Big)}\, \rho^2 \,+\, \cdots \ . \end{aligned} \tag{2.B.22}$$

Critical embeddings

When the effective horizon reaches the origin, $\rho_{\rm c} = 0$, the embedding is critical. The value of the b field at the horizon is $b_0 = w_0^2/\Omega$, $\chi(\rho)$ is also here constant and we can expand $b(\rho)$ and $w(\rho)$ around $\rho = 0$, with the result

$$\begin{aligned} b(\rho) \,&=\, \frac{w_0^2}{\Omega} \,-\, \frac{\Omega}{2\sqrt{\Omega^2 + 4\, w_0^2}}\, \rho \,+\, \cdots \\ w(\rho) \,&=\, w_0 \,+\, \frac{w_0}{\sqrt{\Omega^2 + 4 w_0^2}}\, \rho \,+\, \cdots \ . \end{aligned} \tag{2.B.23}$$

2.B.3 Effective metric

The effective open string metric (2.A.27) in this ansatz is

$$\begin{aligned} \gamma_{ab}\, d\xi^a\, d\xi^b = -F(\rho)\, dt^2 + \frac{1 + w'^2 + |c'|^2}{\rho^2 + w^2}\, d\rho^2 - \frac{2\Omega\, {\rm Im}(c\, c'^*)}{\rho^2 + w^2}\, dt\, d\rho + \, F(\rho)\, e_+\, e_- \, + \\ + \frac{\rho^2 + w^2}{4(1 + w'^2)} \Big(e_-\, c' + e_+\, c'^* \Big)^2 \,+\, \frac{\Omega^2}{4(\rho^2 + w^2)} \Big(e_-\, c + e_+\, c^* \Big)^2 + \frac{\rho^2}{\rho^2 + w^2} d\Omega_2^2 \ , \end{aligned} \tag{2.B.24}$$

USC UNIVERSIDADE DE SANTIAGO DE COMPOSTELA

with $F(\rho)$ given by the following function

$$F(\rho) \equiv \frac{(\rho^2+w^2)^2-\Omega^2\,|c|^2}{\rho^2+w^2}\ , \tag{2.B.25}$$

and $e_\pm$ are complex 1-forms defined in (2.A.29). The (t,ρ) part of the metric gets diagonalised by means of the following change of coordinates

$$d\tau \,=\, dt \,-\, A(\rho)\,d\rho\ , \qquad\qquad d\rho_* \,=\, B(\rho)\,d\rho\ , \tag{2.B.26}$$

where $A(\rho)$ and $B(\rho)$ are the following functions

$$A(\rho) \,=\, -\frac{\Omega\,\mathrm{Im}\Big(c\,c'^{\,*}\Big)}{(\rho^2+w^2)^2-\Omega^2\,|c|^2}\ , \qquad\qquad B(\rho) \,=\, \frac{(\rho^2+w^2)\,\mathcal{L}_0}{\rho^2\Big[(\rho^2+w^2)^2-\Omega^2\,|c|^2\Big]}\ . \tag{2.B.27}$$

The new coordinate ρ_* is just the Eddington-Finkelstein tortoise coordinate. In these coordinates, the transformations in (2.1.19) act as a rescaling $(\tau,\rho_*)\to\lambda^{-1}(\tau,\rho_*)$, and the effective metric takes the form

$$\begin{aligned}\gamma_{ab}\,d\xi^a\,d\xi^b = F(\rho)\,(\,-d\tau^2+d\rho_*^2\,)\,+\,F(\rho)\,e_+\,e_-\,+\,\frac{\rho^2+w^2}{4(1+w'^{\,2})}\Big(e_-\,c'+e_+\,c'^{\,*}\Big)^2\,+\\ +\frac{\Omega^2}{4(\rho^2+w^2)}\Big(e_-\,c+e_+\,c^*\Big)^2+\frac{\rho^2}{\rho^2+w^2}d\Omega_2^2\ ,\end{aligned} \tag{2.B.28}$$

The function $F(\rho)$ vanishes at $\rho=\rho_{\rm c}$ and, therefore, this function acts as a blackening factor for the effective metric (2.B.28), with $\rho=\rho_{\rm c}$ playing the role of an event horizon. The effective Hawking temperature $T_{\rm eff}$ is given by

$$T_{\rm eff} \,=\, \left.\frac{2(\rho_{\rm c}+w\,w')-\Omega\,b'}{2\pi\,\chi'\,b}\right|_{\rho=\rho_{\rm c}} \,=\, \frac{2(\rho_{\rm c}+w_0w_1)\,-\,\Omega\,b_1}{2\pi\chi_1\,b_0}\ . \tag{2.B.29}$$

USC
UNIVERSIDADE
DE SANTIAGO
DE COMPOSTELA

USC
UNIVERSIDADE
DE SANTIAGO
DE COMPOSTELA

3 Numerical computations

In chapter 2 we obtained a time independent action for the system, from which it is immediate to derive a system of ordinary differential equations. Besides, we have addressed the different types of embedding according to the IR boundary conditions required by regularity of the solutions. Once integration has been performed, the phase diagram is constructed out of the UV boundary data that contains information about the sources and the responses.

In the present chapter we review some of the properties of the system that need to be studied by means of numerical methods, mainly the phase space structure and conductivities. Further details are relegated to the appendices.

As usual, the integration proceeds from the IR to the UV. Indeed, enforcing the regularity conditions found in chapter 2 (see appendix 2.A) as initial conditions at the pseudohorizon $u = u_c$ for black hole embeddings or at $u = u_0 > u_c$ for Minkowski embeddings and integrating out up to the boundary yields a unique solution. For a given frequency Ω and horizon radius r_h, from the UV behavior of the solutions when $u \to \infty$ one can extract E, j, m and $\mathcal{C}$. Due to the scaling symmetry (2.1.19) these quantities are not independent. It is natural to measure all quantities in terms of the quark mass m. Accordingly, we will present our results for Ω/m, r_h/m, $|E|/m^2$, j/m^2 and $\mathcal{C}/m^2$.

3.1 Phase space

The standard lore in flavor branes is that Minkowski (black hole) embeddings are dual to insulating (conducting) phases of the quantum system. In the case of a rotating electric field, we must be more careful. Actually, two types of currents emerge. Black hole embeddings carry dissipating currents because of the presence of fundamental carriers. The external driving has to supply energy in order to maintain the stationary rotating current. For Minkowski embeddings j is a polarization current. In analogy with the case of D3/D7 [31], we interpret this polarization as a coherent alignement of the vector meson vacuum fluctuations parallel to the electric field. The polarization current is the time derivative of the polarization and rotates at right angles with the electric field, signalling zero Joule heating, hence not dissipating any energy. This conservative aspect allows for the possibility to have non-zero

USC DE SANTIAGO

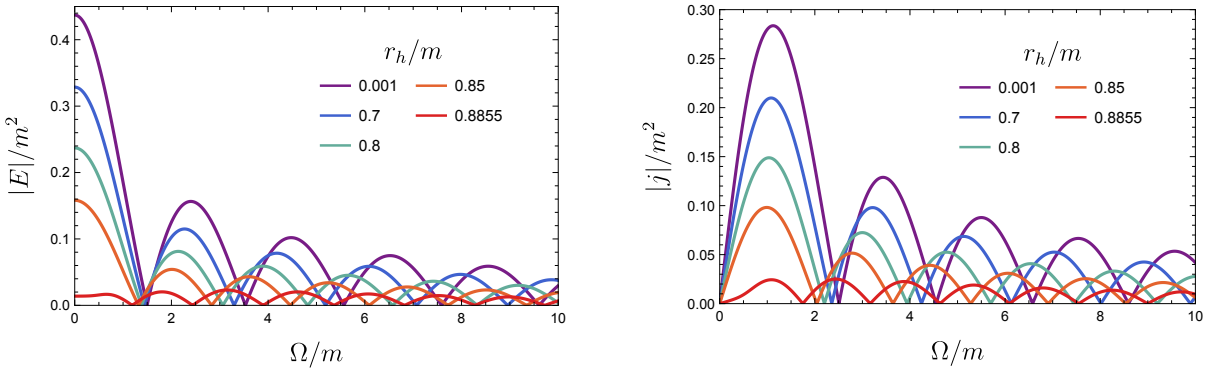


Figure 3.1: Electric field and current of the critical embeddings versus driving frequency, for different values of $r_{\rm h}$ in D3/D5. The frequencies for which $|E|$ vanishes are the critical frequencies $\Omega_{\rm c}$ of the vector meson Floquet condensates. The regions of black hole embeddings between lobes, above such critical points, are termed *wedges* in the text. In the right plot we show the value of the current along the curve of critical embeddings. We observe points with $|j| = 0$ somewhere close to the maxima of the lobes in the left plot. We will term these points *Floquet suppression points*, and will study them in detail in section 3.1.1.

persistent current even in the limit of vanishing driving field. As we will see, there exists a dual possibility, namely, the dynamical cancellation of the polarizability of the vacuum at discrete frequencies.

In Fig. 3.1 we show how the background temperature affects the splitting of the phase space into the two types of embeddings. For a given temperature, points on the corresponding curve represent critical embeddings, pictured in dotted green on the right plot in Fig. 2.1. Roughly speaking, points above such curves correspond to black hole embeddings, whereas those below are Minkowski. However, close to the lines, the situation can be multivalued and we can find both types of embeddings in the near vicinity. The lobed structure was already present at zero temperature in the D3/D7 system [31].

We can observe that the effect of increasing the temperature is a depletion of the height of the lobes with rising $r_{\rm h}$, until they fully dissappear beyond some temperature. Let us pause to describe the origin of this damping effect. We choose to measure dimensionful quantities in units of the quark mass. In particular, the curves above are drawn each one for a fixed value of $r_{\rm h}/m$. Remember that both the electric field and the temperature tend to bend the probe brane towards the origin in the IR. Let us fix a mass $m = 1$ for concreteness. Then, for a small value of $r_{\rm h}$ we can still switch on and fine tune the electric field to make the embedding bend enough so as to touch the critical surface. As $r_{\rm h}$ grows, this supplemental field needed becomes less and less, which accounts for the drop in the lobe structure to be seen on the plots in Fig. 3.1. Finally, there is a maximum value for $r_{\rm h}/m = 0.8897$ beyond which all the embeddings are of black hole type for any value of $|E|$ and Ω.

We notice in Fig. 3.1 that $|E|/m^2$ has a series of maxima whose values decrease as Ω/m increases. Moreover, for some discrete values $\Omega_{\rm c}/m$ of the frequency the electric field vanishes and the corresponding rotating current is non-zero. Thus, for these frequencies we have a

vector meson Floquet condensate of the type mentioned in the introduction. Actually, these $E = 0$ Floquet states exist also for Minkowski embeddings in a finite range of frequency $\Omega_c < \Omega \leq \Omega_{\rm meson}$, where $\Omega_{\rm meson}$ is the mass of a vector meson in the defect theory. This mass spectra was computed in [139] in the zero temperature case and is given by a tower of values depending on a principal quantum number n

$$\Omega_{\rm meson}/m \,=\, 2\sqrt{\left(n+\frac{1}{2}\right)\left(n+\frac{3}{2}\right)}\,, \qquad\qquad n \,=\, 0,1,2,\cdots\,. \tag{3.1.1}$$

In chapter 4 (see appendix 4.C) we obtain these frequencies by means of a linear analysis of the equations of motion (in the $T = 0$ limit). The first four values of the critical resonant frequencies and of the meson masses are

$$\Omega_c/m \,=\, 1.4965\,,\, 3.5308\,,\, 5.5676\,,\, 7.5851\,\cdots \tag{3.1.2}$$

$$\Omega_{\rm meson}/m \,=\, 1.7320\,,\, 3.8730\,,\, 5.9161\,,\, 7.9372\,,\cdots\,. \tag{3.1.3}$$

Figure 3.2 unfolds the fine structure in the vicinity of the vector meson Floquet condensates. The left (right) plots show the values of the current $|j|/m^2$ (the condensate $\mathcal{C}$) as a function of the applied electric field $|E|/m^2$ for different values of the rotating speed Ω. From top to bottom, the temperature increases parametrised by $r_{\rm h}/m = \sqrt{2}u_{\rm h}/m$. The upper case, with $r_{\rm h}/m = 0.5$ is almost indistinguishable from the case with $r_{\rm h}/m = 0 = T$. Points on the continuous (dashed) lines are for black hole (Minkowski) embeddings. From the lower left corner all curves start at the Minkowski solution with $|j| = |E| = 0$ (no singular shell). For a small value of Ω the behaviour is as shown in the blue curves with $\Omega = 1.2$. As the electric field increases a non-dissipative polarization current builds up along the dashed portion of the blue curves. At some point the curve becomes multivalued, the prelude of a presumably discontinuous phase transition to a black hole configuration (a point on the continuous curve segment upwards) where a dissipative conduction current is allowed. The nature and exact ocurrence of this transition is beyond the reach of equilibrium thermodynamics where free energy evaluation is enough. Rising the frequency Ω all the curves get displaced towards their left and, at some value Ω_c, that depends on $r_{\rm h}/m$, contacts the axis $|E| = 0$ at a nonzero value for both $|j| > 0$ (and also $\mathcal{C} \neq 0$) (green curves). Precise computation reveals the contact point to correspond to a critical embedding. Further increase in Ω makes this contact point slide down the vertical axis, now inside the Minkowski branch. Eventually, it reaches zero, merging again with the trivial Minkowski embedding with $|E| = |j| = 0$. All the embeddings having $|j| \neq 0$ with $|E| = 0$ build the manifold of *vector meson Floquet condensates* [31].

When $r_{\rm h}/m$ reaches 0.84 we start seeing an interference between the two horizons as they come close together. The effect is a multivaluedness in the curve of black hole embeddings that precludes the monotonic growth of $|j|$ and $\mathcal{C}$ with $|E|$ that is seen at lower temperatures. In all cases, in the large field regime, the Ohmic behaviour $|j| = \sigma|E|$ with constant σ is reached. However, in the small interval $r_{\rm h}/m \in (0.84, 0.8897)$, this regime is not approached monotonocally, and we find a multivaluedness of $|j|$ and $\mathcal{C}$ as functions of $|E|$. This looks similar to the multivaluedness encountered in [140] within the superconducting phase. We, however, encounter this multivaluedness in the conducting phase (the normal phase there).

USC DE SANTIAGO

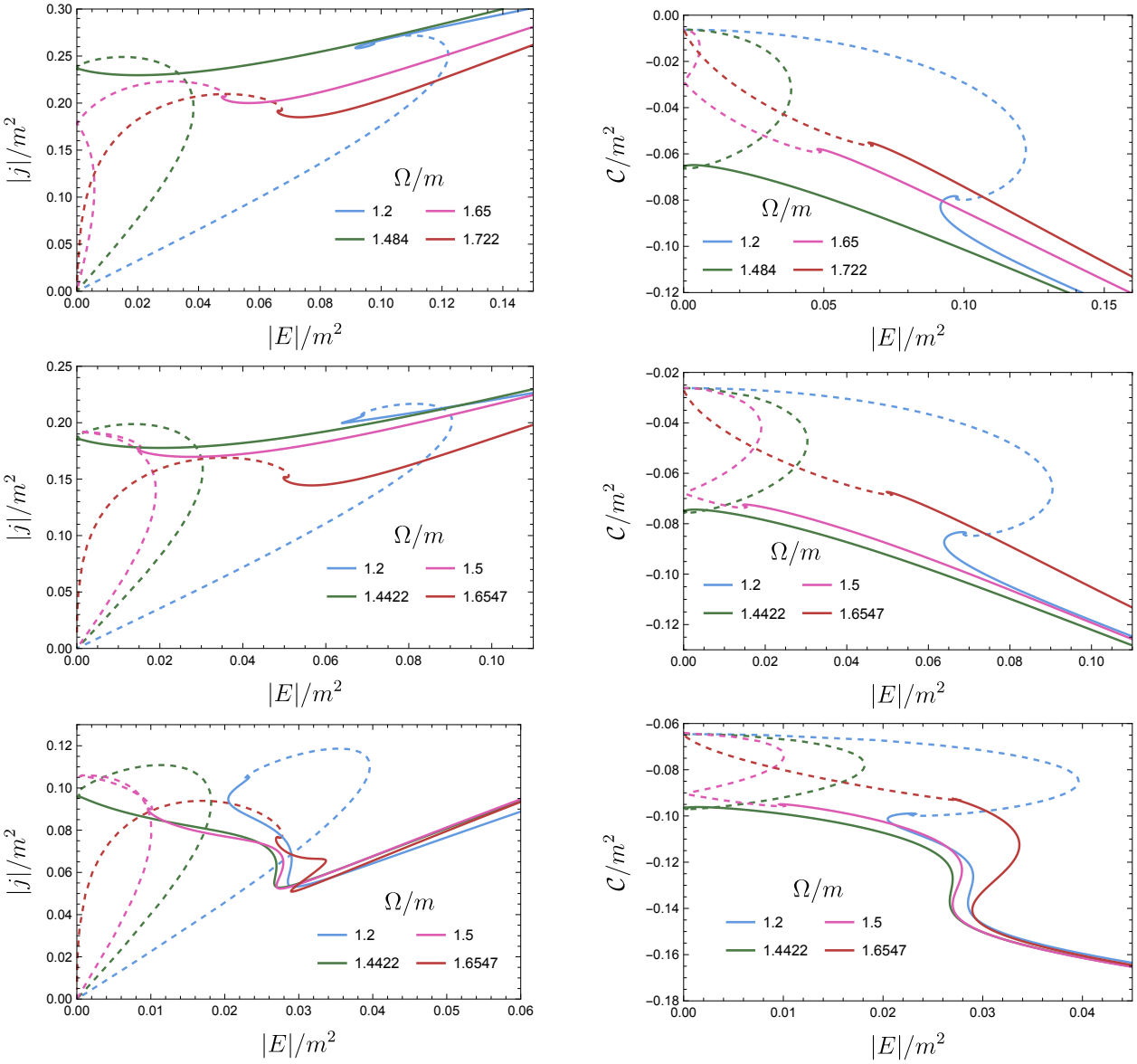


Figure 3.2: The dashed curves represent the insulator (Minkowski) phase and the solid curves the conductive (BH) phase. Electric current $|j|/m^2$ and condensate $\mathcal{C}/m^2$ versus electric field for $r_{\rm h}/m = 0.5$, 0.7 and 0.84, from top to bottom. The driving frequency is fixed to some $\Omega/m < \Omega_{\rm c}/m$ (blue), $\Omega/m = \Omega_{\rm c}/m$ (green), $\Omega_{\rm c}/m < \Omega/m < \Omega_{\rm m}/m$ (pink) and $\Omega/m = \Omega_{\rm m}/m$ (red). We show that E can only vanish for $j \neq 0$ for Minkowski embeddings with $\Omega_{\rm c} \leq \Omega \leq \Omega_{\rm meson}$.

In Fig. 3.3, we see the interference effect between the two nearby horizons is so effective that a trivial configuration with $|j| = |E| = 0$ is again attained, but now inside the branch of black hole embeddings.

In Fig. 3.4 we have promoted the list of frequencies in each of the plots in Fig. 3.2 to a

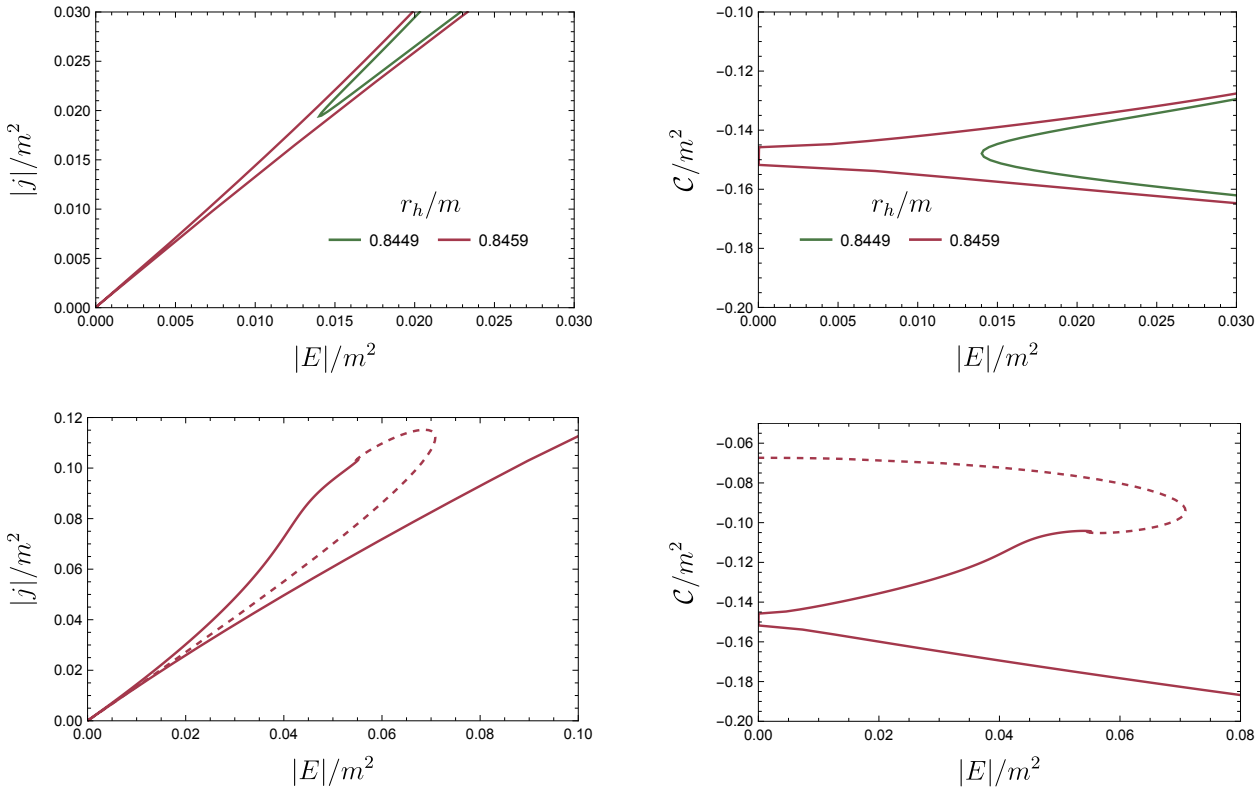


Figure 3.3: Electric current and condensate versus electric field for $\Omega/m = 1$. The continuous lines represent BH embeddings, while the dashed ones are the Minkowski embeddings. The upper plots show that for $r_{\rm h}/m$ around 0.845, we start getting $E/m^2 = 0$ for BH embeddings. The lower plots are the full curves for the $r_{\rm h}/m = 0.8459$ case. Notice that the electric field increases again, to recover the limit $|j| = \sigma|E|$.

third Ω axis, where the associated curves are sections of a 3D surface. On the bottom plane $|E| = 0$ the surfaces intersect in a curve which is the full manifold of vector meson Floquet condensates. The curve interpolates between two endpoints. On one end, $|j| = 0$, and we find the frequencies corresponding exactly to the vector meson masses i.e. the fluctuations in the probe brane worldvolume gauge field [10]. We have checked this in Appendix 3.A (see Fig. 3.16 for the first three meson masses). The other end, with $|j| > 0$, corresponds to a critical embedding. Turning on $r_{\rm h}$ causes an overall shift of this curve towards lower values of Ω, which can be inferred from the movement of the extreme points as shown on the lower right plot in Fig. 3.4.

In figure 3.5 we plot the Joule heating q as a function of the electric field (left) and driving frequency (right), both in the $T = 0$ limit. From the right plot we can see how it vanishes when entering the Minkowski embeddings.

On general grounds, the influence of the temperature on the results at $r_{\rm h} = 0$ is small until we approach the maximum temperature $r_{\rm h}/m = 0.8897$, hence, when the lobes in Figs. 3.1 are very small. Regarding the upper plots in Fig. 3.4, observe how the manifold of black

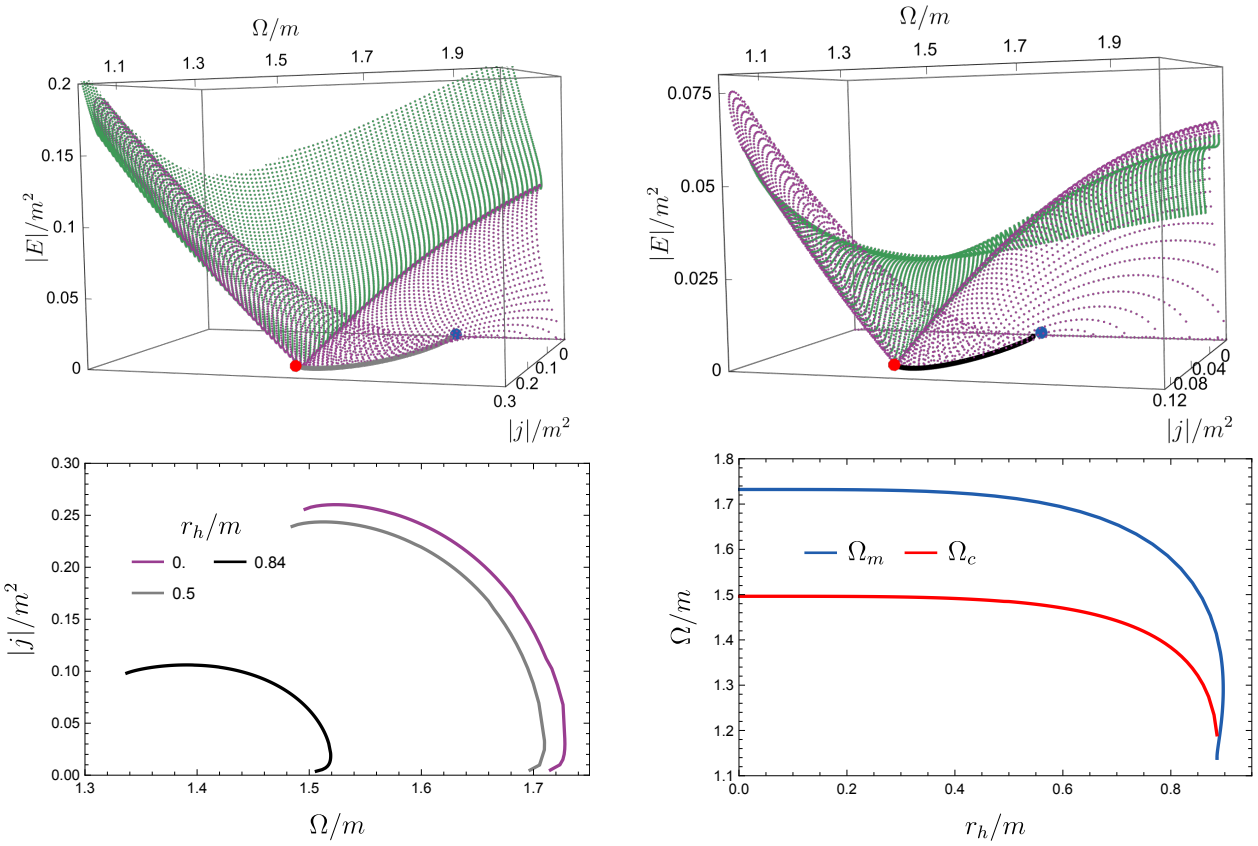


Figure 3.4: *Top:* 3D development of the lobed curves in Fig. 3.1 in the vicinity of the first critical point, with an extra Ω axis, for $r_{\rm h}/m = 0.5$ (left) and $r_{\rm h}/m = 0.84$ (right). Magenta (green) surfaces belong to the Minkowski (BH) phase. Beware the difference in vertical scales. The purple or blue dots are Minkowski embeddings and the green or red ones BH embeddings. The gray thick lines represent the $|E| = 0$ vector meson Floquet condensates. *Lower left:* vertical view of the upper left plot where the gray lines in the upper left plot have been graphed for three different temperatures. *Lower right:* movement of the two extreme points in the curve as a function of $r_{\rm h}$. They are the critical embedding and the first meson mass frequency respectively. We see that the effect of the background temperature is mild (less than 10%) until the value $r_{\rm h}/m \sim 0.8$ is reached.

hole embeddings folds down for the right plot $r_{\rm h}/m = 0.84$ in contrast with the monotonic growth on the left one, at $r_{\rm h}/m = 0.5$. This is precisely the multivaluedness remarked for higher temperatures inside the branch of BH embeddings.

To finish this section, let us comment on the possibility of accurately locating the first order phase transitions where the phase space curves become multivalued. The usual prescription of comparing the free energies is valid in thermodynamical equilibrium. The usual holographic prescription that proposes the euclidean gravitational action for such a construction is not working properly in the present context of a non-equilibrium steady state (see [140]

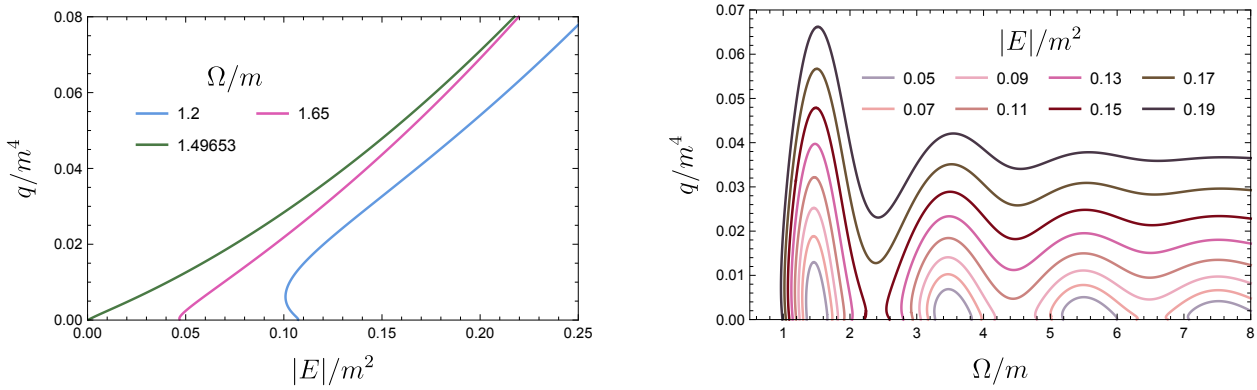


Figure 3.5: *Left*: Joule heating q as a function of the electric field E for black hole embeddings, with driving frequency fixed to some $\Omega/m < \Omega_c/m$ (blue), $\Omega/m = \Omega_c/m$ (green) and $\Omega_c/m < \Omega/m < \Omega_m/m$ (pink). *Right*: Joule heating q as a function of the frequency Ω for black hole embeddings and several values of the electric field. In both cases the temperature has been set to zero.

for similar concerns and [141] for a review on the topic). A more sophisticated approach using techniques taylored for non equilibrium open systems applied to the holographic context is an interesting project to carry out also here. Eventually, an exact dynamical simulation with a slowly varying $|E|/m^2$ should be the right thing to do.

3.1.1 Floquet suppression points

In Fig. 3.1, on the right plot, we already mentioned the presence of points within the line of critical embeddings where the current vanishes $|j| = 0$ even in the presence of nonzero electric field. They roughly coincide with the points where the electric field becomes maximal within the same family. We will term these points *Floquet suppression points* and the corresponding states *Floquet-suppressed states*. As we will show, the existence of these points extends to the Minkowski embeddings and, in a sense to be explained in the next section, also to the black hole embeddings. Focusing on critical and Minkowksi embeddings, we have already mentioned that the current has its origin in the polarizability, $\tilde{\pi}$, of the vacuum, $\mathcal{P} = \tilde{\pi}\mathcal{E}$, with $\mathcal{P} = \langle\bar{\psi}(\gamma_x + i\gamma_y)\psi\rangle$ [31]. Hence $\mathcal{J} = \dot{\mathcal{P}} = i\Omega\tilde{\pi}\mathcal{E}$ and a vanishing value of $\mathcal{J} = 0$ implies $\tilde{\pi} = 0$, i.e. the polarizability is *dynamically* suppressed.

This suppression of the vacuum polarizability for certain frequencies is similar to well known (and searched for) dynamical effects in other examples of Floquet engineering. For example, in periodically driven lattices, hopping between neighbouring sites, although present in the bare Hamiltonian, can be completely suppressed by tuning the ratio of frequency to amplitude, leading to induced dynamical localization (see [12, 15, 16] for references).

Figure 3.2 is built by scanning frequencies $\Omega \in (1.2, 1.7)$, i.e., around the point of the first vector meson Floquet condensate. In Fig. 3.6 we show, on the upper left plot, the similar curves setting instead $\Omega \in (2.3, 2.7)$, that is, in a small interval around the first Floquet suppression point. The result exhibits a remarkable similarity, but with $|j|/m^2$ and $|E|/m^2$

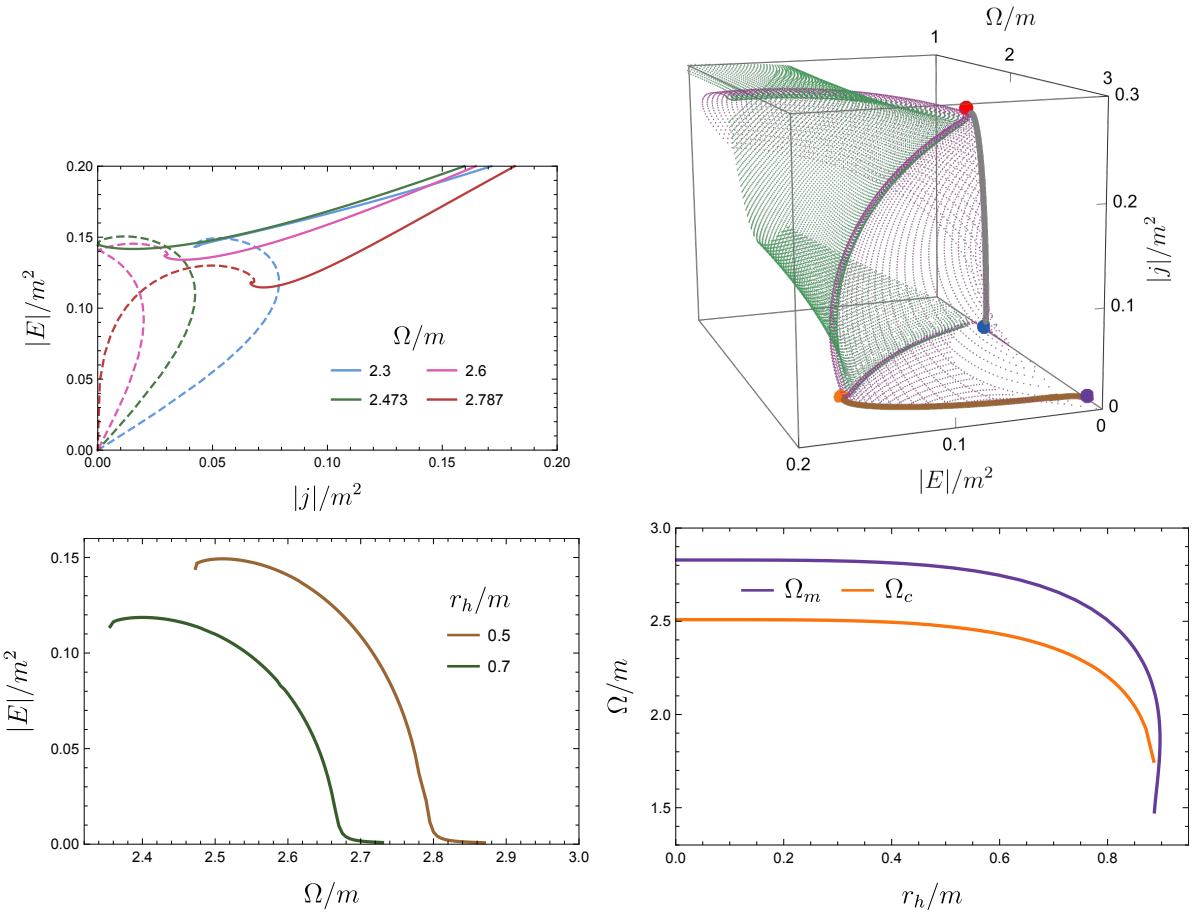


Figure 3.6: *Top:* On the left, plots of $|j|/m^2$ vs. $|E|/m^2$ where we exchanged the axes to make apparent the striking similarity with the plots in Fig. 3.2. On the right, 3D plot where the range of Ω has been extended to cover the first vector meson Floquet condensate (grey curve at $|E| = 0$) as well as the first Floquet suppressed condensate (brown curve at $|j| = 0$). *Bottom.* The left plot shows view of the $|j| = 0$ plane of the upper plots. The suppressing effect of the temperature is apparent. The right plot is the downshift in Ω of the two extreme points (orange and violet) in the plot above this, as a function of $r_{\rm h}/m$.

axes exchanged. Indeed the symmetry is not exact, as can be seen by comparing the curves in the lower left plots in Figs. 3.4 and 3.6. These are respectively the curves of vector meson Floquet condensates and Floquet suppression points. End points on the lower axis can be obtained in both cases by studying the linearised fluctuations of the world-volume gauge field subject to the boundary conditions $|E| = 0$ and $|j| = 0$ respectively. At zero temperature

this calculation can be performed analytically giving (see appendix 4.C.3 in chapter 4)

$$\begin{aligned} |E| = 0 \quad &\rightarrow \quad \Omega_n = 2\sqrt{\left(n+\frac{1}{2}\right)\left(n+\frac{3}{2}\right)} = 1.732, 3.873, ... \\ |j| = 0 \quad &\rightarrow \quad \Omega_k = 2\sqrt{k\ (k+1)} = 2.828, 4.899, ... \end{aligned} \tag{3.1.4}$$

Upon rising the temperature, $r_{\rm h} > 0$, these quantities get shifted downwards, as shown on the lower right plots in Figs. 3.4 and 3.6. The (almost) symmetry between vector meson Floquet condensates and Floquet suppression points is highlighted on the top right plot of Fig. 3.6, where both manifolds have been included within the same 3D development.

It is worth mentioning that the existence of these Floquet suppression points is not restricted to the D3/D5 system, hence is not apparently linked to the dimensionality. For completeness we devote Appendix 3.B to the twin version of this section in the context of a D3/D7 scenario. Apart from the discrepancy in the precise numerical values, the global picture is the same. For example, in Fig. 3.17 we reproduce the lobe structure for the D3/D7 system, which is analogous to the one found in Fig. 3.1 for D3/D5. Also the $(|j|/m^3, |E|/m^2)$ curves in Fig. 3.18 are very similar counterparts of the ones in Figs. 3.2 and 3.6.

3.2 Conductivities

3.2.1 Non-linear conductivity

The relation between the current vector and the electric field vector defines a *rotating current (RC) conductivity* [1]

$$j = \tilde{\sigma}_{\rm RC} E \tag{3.2.1}$$

where $\tilde{\sigma}_{\rm RC}(\Omega, |E|)$ is a complex number which is, itself, a non-linear function of $|E|$ (by rotational symmetry) and Ω. Writting

$$\tilde{\sigma}_{\rm RC} = \gamma e^{i\delta}$$

the modulus γ is the non-linear conductivity whose value is plotted in Fig. 3.7. The phase δ encodes the angle between the instantaneous vectors $\vec{j} = (j_x, j_y)$ and $\vec{E} = (E_x, E_y)$. This is why we will refer to δ as the angle, even if we use complex instead of vector notation. For a given $|E|$ this relative angle controls the Joule heating (2.1.18)

$$q = \gamma |E|^2 \cos\delta \, .$$

Its microscopic origin is unclear although we will make an attempt to put forward a consistent picture after we have collected all the bits and pieces.

[1] Notice that in the rotating frame we write $\tilde{\sigma}_{\rm RC}$ as we are dealing here with a single Fourier component Ω of the rotational time dependence. In general, in the lab frame, we would write instead $\mathcal{J}(t) = \int d\tau \sigma_{\rm RC}(\tau)\mathcal{E}(t-\tau)$. Also the use of complex instead of vector notation is implicit.

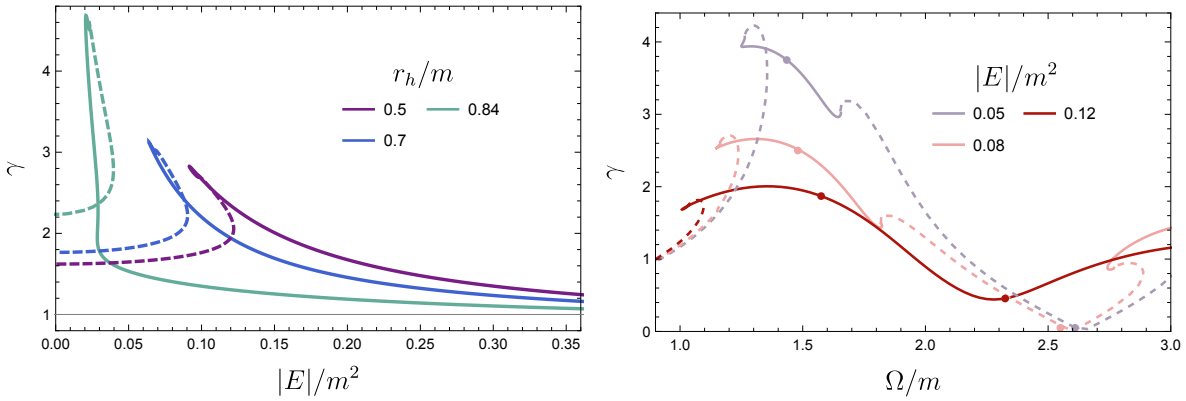


Figure 3.7: Modulus of the non-linear conductivity $\gamma = |\tilde{\sigma}_{\rm RC}|$ as a function of $|E|/m^2$ for fixed $\Omega/m = 1.2$ (*left plot*) or as a function of Ω/m for fixed values of $|E|/m^2$ (*right plot*). For large $|E|/m^2$ the curves asymptote to the value $\gamma = 1$.

For Minkowski embeddings $\vec{j}$ and $\vec{E}$ are perpendicular and $q = 0$. This is consistent with the picture of the polarization of the meson condensate into dipoles aligned with the electric field. It leaves two possibilities for $\delta = \pm\pi/2$. In ref. [31] only the positive sign was considered, as it is natural to think that the polarization and the electric field are parallel vectors. We will show here that the existence of both signs is a natural consequence of the presence of Floquet suppression points.

In Fig. 3.8 we observe the behaviour of the relative angle δ as we scan embeddings along the horizontal lines of constant $|E|$ while increasing Ω, as shown in the right plot. As usual, BH (Minkowski) embeddings belong to solid (dashed) segments. On the left plot, using the same color coding, we can see the value of the angle, δ, as we move along these sets of solutions. Notice the jumps $\delta = \pi/2 \to -\pi/2$ that occur within the dashed segment, i.e. for Minkowski embeddings. They seem to reflect a discontinuous transition but this is not the case. Indeed, looking at the right plot in Fig. 3.7 we see that, precisely at those points, we find a vanishing value for the module of the polarization current $\gamma = 0 \Rightarrow |j| = 0$. The corresponding Ω frequencies have been signalled with a dot on the right plot in Fig. 3.8. Joining all such Floquet suppression points yields the green dashed curve which is, precisely, the same curve represented in the lower left plot of Fig. 3.6, also in (solid) green.

In summary, the transition $\delta = \pi/2 \to -\pi/2$ occurs through a Floquet-suppressed state where the polarizability $\tilde{\pi}$ vanishes and transits smoothly from positive to negative. This is remarkable as it states that, for ample intervals in the range of driving frequencies Ω, the meson condensate is polarised *antiparallel* to the applied electric field!

Looking back to the left plot in Fig. 3.8 we notice that the opposite transition $\delta = -\pi/2 \to +\pi/2$ is *not* discontinuous. It occurs through a sequence of black hole embeddings that interpolate between those values along a curve that crosses smoothly the axis $\delta = 0$ with finite slope. A look at the right plot in Fig. 3.7 reveals that, in contrast, at those points γ stays strictly positive.

Putting all the information together the interpretation we find most plausible is as follows:

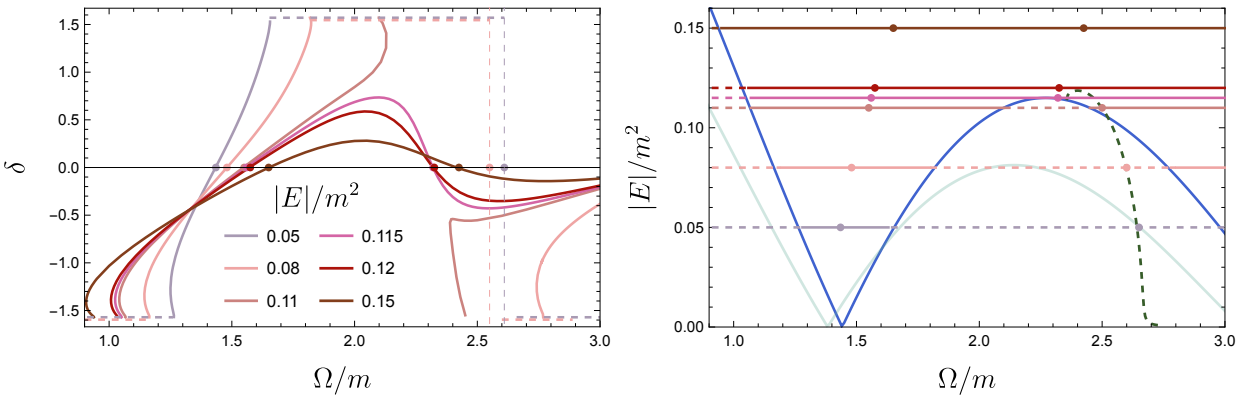


Figure 3.8: Continuous lines are black hole embeddings, whereas dashed lines are Minkowski (with a slight vertical offset for clarity). *Left:* relative angle δ for different embeddings at various fixed values of the electric field and with $r_{\rm h}/m = 0.7$ for varying Ω/m. *Right:* this is a zoom of the first lobe region in figure 3.1, where the color code for constant $|E|/m^2$ lines corresponds to the ones on the left plot. The dots indicate the frequencies where the angle δ either becomes zero in the BH segments, or flips sign in the Minkowski segments. In this later case, joining all the points gives the dashed green curve. The fact that this curve of Minkowski embeddings exits the lower lobe is related to the spiralling multivaluedness of the phase space curves in the vicinity of the critical embeddings. We have added another (dimmed green) lobed curve with higher temperature $r_{\rm h}/m = 0.8$ to show that the effect of rising the temperature is similar to that produced by increasing the electric field $|E|/m^2$.

in general, the total current will be an admixture $j = j_{\rm con} + j_{\rm pol}$ of conduction (dissipative) and a polarization (conservative) currents [142, 143]. The precise contribution of each component is controlled by the driving frequency Ω and by $|E|$. The conduction component $j_{\rm con}$, embodied by deconfined charged carriers, is parallel to the applied electric field. The polarizarion component $j_{\rm pol}$, as explained above, is perpendicular. The vector sum of these two components gives j and E a relative phase angle δ.

Changing Ω at fixed $|E|/m^2$, like on the left plot in Fig. 3.8, we find that $j_{\rm pol}$ vanishes at given frequencies Ω, thereby flipping $\delta = \pm\pi/2 \to \mp\pi/2$. In the gapped (Minkowski phase) only this component of the current is present. In the gapless (BH) phase, both components generically contribute. We interpret the points where $\delta = 0$ as precisely signalling that, there also, $j_{\rm pol} = 0$. Thereby the total current becomes parallel to the electric field. This is the reason why the transition in δ is continuous in the BH phase (solid segments). If this picture makes sense, the conclusion is that *we also have Floquet suppression points within the BH phase*. It is just that in the BH phase this vanishing is masked by the conduction component $j = j_{\rm con} + 0$. In summary, all the dots in Fig. 3.7 and 3.8 correspond to Floquet suppressed states. As we approach the boundaries of these segments, the conduction component disappears $j_{\rm con} \to 0$, and the polarization component survives making $j = j_{\rm pol}$ and E mutually perpendicular again.

For large enough $|E|/m^2$ we always stay within the phase of BH embeddings, and the

(solid) curves smoothly relax down to the asymptotic regime where $\delta = 0$. We interpret this as the vanishing of the $j_{\rm pol}$ component in this limit. This is the same effect we get for large temperature $T/m \gg 1$ as both are indistinguishable from the limit of small mass $m \to 0$.

In the following chapter (section 4.1) we prove exactly this fact, $\tilde{\sigma}_{\rm RC} = 1$, for massless flavors. This implies that, in this case, the response is both instantaneous and linear. We make contact and fully agree here with the results in [33]. In a sense, the claim there is stronger as it applies to *any* time dependence of a linearly polarised electric field $\mathcal{E}_x(t)$ at the boundary. Here, on one side, we go to a rotational polarization ansatz and, moreover, in Appendix 4.A we prove this result to hold also at linearised order in a small mass δm. Linearity of the response entails that it should also extend to arbitrary two dimensional time dependent electric fields $\vec{\mathcal{E}}(t)$ at linear order in small masses.

3.2.2 Photovoltaic Optical Conductivity

One of the main uses of the Floquet driving is the artificial engineering of materials exhibiting transport phenomena with topological character. In this sense, the obtention of a Hall conductivity without a magnetic field is an important hallmark. In the present context, this has been termed photovoltaic Hall effect [20] where it's origin has been shown to be topological, like the Thouless pumping. The time-reversal symmetry breaking and hence, the nontrivial band topology, is induced by the circularly polarised light. This proposal has been the subject of both theoretical and experimental studies during the last decade [26, 144–147]. In [30] the photovoltaic Hall conductivity for massless carriers was obtained in the D3-D7 model, and speculated to behave consistently with the picture of a strongly coupled version of a (3+1) Weyl semimetal. Our findings show similarities and departures from their results. For example, the massless case will be shown to be trivial. However, in the massive case, we will indeed find an intricate Hall effect.

Following the proposal in [148] we proceed to study the response of our system to a small additional electric field on the boundary pointing in a fixed direction. From this response we will be able to extract the AC and DC conductivities. We will closely mimic the strategy in [30] whose main steps will be reviewed and extended here for completeness, as our case involves three coupled field perturbations. Details on the computation are relegated to appendix 3.C.

In what follows, we present the results obtained for both the AC and DC conductivities in the zero temperature limit. We finish this section with some comments on the effects of having non-vanishing temperature.

AC conductivities in the $T = 0$ limit

The results for the photovoltaic optical Hall conductivity, σ_{xy}, as well as for the photovoltaic optical absorption spectrum, σ_{xx}, can be seen in Fig. 3.9. We have plotted everything in units of the carrier mass m.[2] The driving laser has been set to the first resonant frequency

[2]Numerically we have performed the integration for 2 different sets of values of (E, Ω, m) in order to verify the scaling symmetry of Eq. (2.1.19)

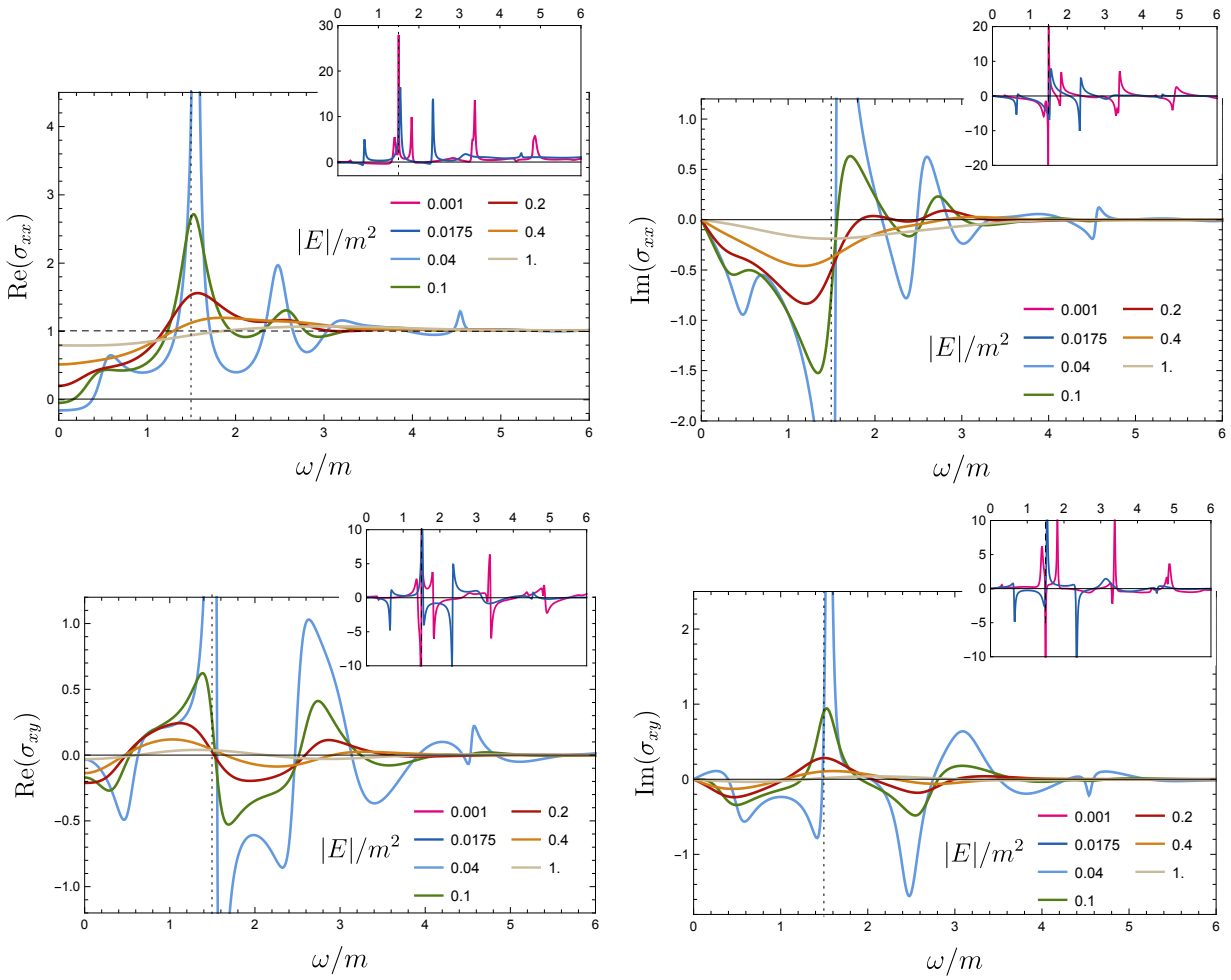


Figure 3.9: AC conductivities for fixed value of $\Omega/m = 1.496$ and different values of $|E|/m^2$. They correspond to the vertically aligned dots in Fig. 3.11 with the same color code. In the insets, the curves at low values of $|E|/m^2 \to 0$ deep into the critical wedge, where they develop peak resonances. The value $\omega/m = \Omega/m = 1.496$ is signalled with a dashed vertical line.

$\Omega/m = 1.496$ for a discrete set of values of $|E|/m^2$ (see the coloured dots along the vertical dashed line in Fig. 3.11).

The behaviour in all components of $\boldsymbol{\sigma}$ shows oscillations whose amplitude grows for decreasing $|E|/m^2$. All conductivities oscillate around 0 except for $\mathrm{Re}(\sigma_{xx})$ which does it around a saturation value 1.

The departure in (2+1) dimensions, from the analog (3+1) dimensional holographic system is significant (see Fig. 7 and 8 in [30]). In both cases, in the large frequency limit, the conductivity becomes proportional to the identity matrix $\boldsymbol{\sigma}(\omega \to \infty) = c\,\mathbb{I}$. In the D3/D7 case, c is a complex linearly growing function of ω, whereas in our case c is a constant (equal to 1 in our normalization in this section, see later however). This asymptotic behaviour is

also attained in the limit of high $|E|/m^2 \gg 1$, as controlled by the massless limit $m \to 0$ which is analytically solvable. Not only the amplitude of the maxima, but also their movement is different. In the D3/D7 case their positions shift to lower frequency for decreasing external field. Here we see that they tend to approach the critical $\omega = 1.496$.

As $|E|/m^2$ becomes smaller, strong oscillations develop, with the most prominent one sharpening around the resonance value for the optical and driving frequencies $\omega = \Omega$ (signalled with a dotted vertical line in all the plots). This feature bears resemblance with the one obtained in [148] (Fig 1b), although the behaviour of the peak amplitude with the intensity is the opposite.

In the limit $|E|/m^2 \to 0$ these oscillations become very sharp peaks as shown in the insets in Figs.3.9. As we move down towards $E/m^2 \to 0$ the shape and positions of these peaks change rapidly. This can be appreaciated in the insets, where the curves for $E/m^2 = 0.0175$ and 0.001 look decorrelated. This last magenta curve shows a subseries of peaks at frequencies $\omega = 1.496, 3.38, 4.87, ...$ which have some overlap with the vector meson Floquet condensate spectrum $\omega = 1.496, 3.53, 5.56, ...$ at shifted values.

The fact that $\boldsymbol{\sigma}$ is dimensionless in (2+1) dimensions eases the comparison with results in the literature. For the Hall component, $\sigma_{xy}(\omega)$ there is a striking similarity with the plot in Figs. 8 of [149], where also the resonance peak is visible as well as secondary peaks. Importantly, in the limit $E \to 0$ the photoelectric Hall conductivity does not vanish. This signals spontaneous time reversal symmetry breaking and might be a consequence of the underlying vector meson Floquet condensate state.[3]

The enhancement of the oscillations and peak formation observed in Fig.3.9 is a universal feature as we approach the line of critical embeddings. We have followed the movement of the peaks for a sequence of configurations very closely above the critical line, for background frequencies in the range $\Omega/m \in (1.3, 2.32)$ (see Fig. 3.1). The resulting curves are plotted in Fig. 3.10. A remarkable fact is the presence of one peak whose position barely changes and is confined to the interval $\omega/m \in (1.4965, 1.73)$, i.e. among the vector meson Floquet condensate frequency and the meson mass resonance (see Fig. 3.1 and eqs. (3.1.2)(3.1.3)). Very slightly above the critical line there are two sidewise peaks which appear within a short interval in E/m^2. They all can be seen also in Fig. 3.10. The remarkable fact about these lateral peaks is that they shift position with the driving in such a way that their mean value coincides with the background frequency Ω, while their splitting is almost constant $\Delta\omega/m \sim 1.7$. This curious result is very neatly seen on embeddings to the right of the vector meson Floquet condensate, i.e. in the segment $\Omega/m \in (1.496, 2.32)$ and, very much damped, nearby to its left. The blue curve at $\Omega/m = 1.496$ is the same one that can be observed in the insets of Fig. 3.9, which has $E/m^2 = 0.0175$. At this frequency $\Omega = \Omega_c$, there are embedding solutions down to $E = 0$ and this gives the magenta curves in those insets at values of $E/m^2 = 0.001$ and even lower.

We also computed the heterodyning conductivities $\boldsymbol{\sigma}^{\pm}(\omega)$. They bear the same features as for the normal conductivity, and the reader can found further information in Appendix 3.C.1. Roughly stated, the curves for these exotic conductivities share, each of them, half of

[3]We thank T. Oka for this observation.

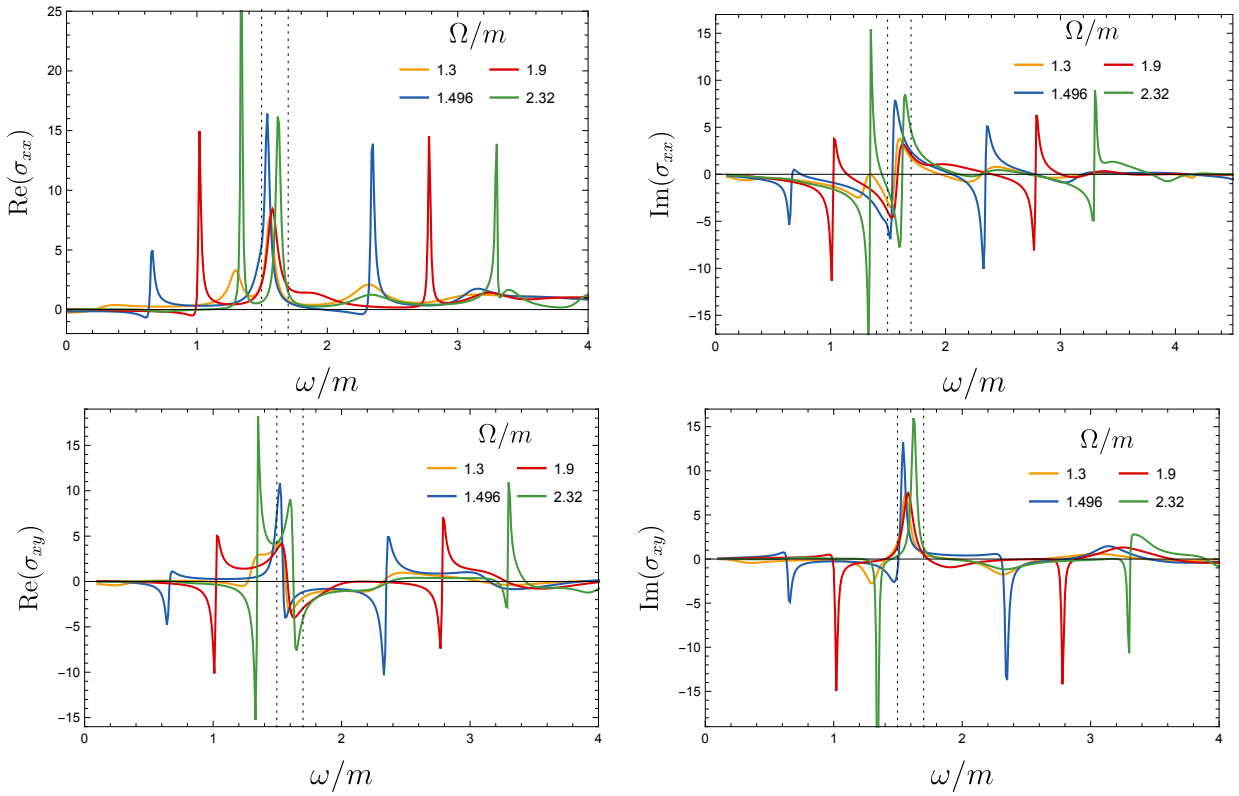


Figure 3.10: Peaks in the AC conductivities closely above along the critical line. The exact position of these curves in phase space can be seen in Fig. 3.11 as coloured circles. The vertical dashed lines signal the vector meson Floquet condensate and the meson mass frequencies respectively. The central peaks bunch in this region whereas the two lateral peaks move with ω while keeping their separation almost constant, $\Delta\omega/m \sim 1.7$.

the peaks visible in $\boldsymbol{\sigma}(\omega)$.

DC conductivities in the $T = 0$ limit

The zero frequency limit $\omega \to 0$ is formally singular (c.f.(3.C.17)). However the numerical value of the AC conductivity is well behaved and stable down to values of ω/Ω well below 10^{-3}. Hence we will use this value to define our DC conductivity. The authors of [30] performed a numerical analysis in the time domain and showed consistent agreement between the two prescriptions. From the plots in Figs. 3.9, it is apparent that the imaginary parts vanish in the limit $\omega \to 0$. Hence the DC conductivities are real, as follows from the relation $\boldsymbol{\sigma}(-\omega) = \boldsymbol{\sigma}(\omega)^*$.

Figs.3.12 and 3.13 summarise our numerical results. In Fig. 3.12 we exhibit $\boldsymbol{\sigma}(\omega = 0)$ for varying Ω/m along lines of constant $|E|/m^2$. For high enough E/m^2 the limit $\Omega \to 0$ stays in the conducting phase and the direct conductivity σ_{xx} has the correct static limit obtained in [52] where it becomes a constant that only depends on m, and saturates to a maximum

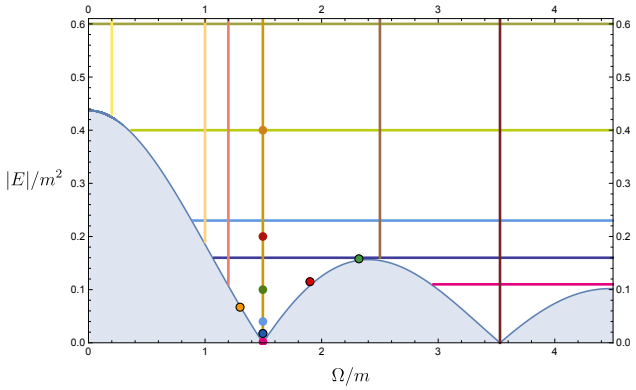


Figure 3.11: The dots and circles signal the points where the AC conductivities in Figs. 3.9 and 3.10 have been plotted respectively. Also shown are the lines with either Ω/m or $|E|/m^2$ fixed, used to plot the DC conductivities in Figures 3.12 and 3.13. In all cases, the same color code has been used.

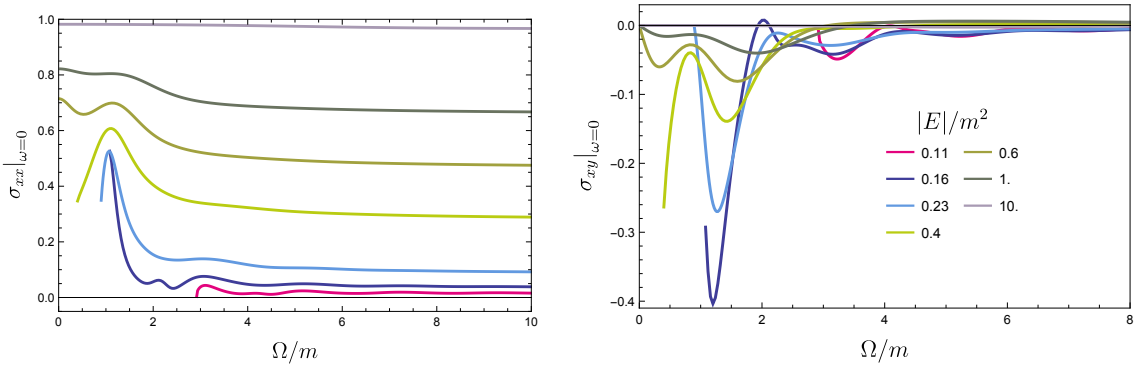


Figure 3.12: DC Conductivities as a function of Ω/m for various values of $|E|/m^2$.

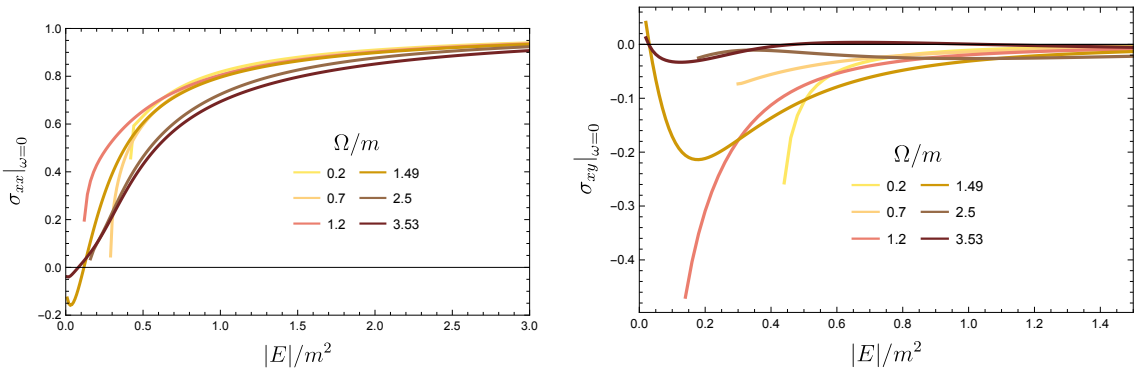


Figure 3.13: DC Conductivities as a function of $|E|/m^2$ for various values of Ω/m.

value equal to one (see section 4.1 for the correct normalization and appendix 4.B for the detailed derivation).

In Fig. 3.13 we plot $\boldsymbol{\sigma}(\omega = 0)$, varying $|E|/m^2$ along lines of constant Ω/m. Our results should be compared with the condensed matter calculation in [20] (see the discussion after Fig.2). For the Hall conductivity we see qualitative agreement in that, in absolute value, $|\sigma_{xy}|$ first increases with $|E|/m^2$ and then decreases. For high $\Omega/m(\sim 3.53)$ we find values where this conductivity has zeros, this being a remarkable feature. For σ_{xx} we find a monotonic growth that reaches a limiting value for high $|E|/m^2$. In contrast, authors of [20] (see Fig.2b) obtained an intermediate valley which they proposed to be a reflection of the gap opening at the Dirac points. If so, our model is too crude to capture this feature.

The comparison with the (3+1) case is complicated because the authors of [30] only considered the massless case, which in our setup turns out to be analytic and trivial. Indeed, taking $(|E|/m^2, \Omega/m) \to \infty$ the Hall conductivity vanishes whereas the DC conductivity asymptotes to a constant value. One important difference is the sign of σ_{xy} which in our case comes out negative, hence opposite to the one in the (3+1) dimensional setup. This is so, despite the fact that we have been careful in keeping all the conventions the same, and the sign in σ_{xx} is positive as well.[4]

The region in phase space where a significant photoelectric Hall conductivity is obtained is rather small. It happens for values of the parameters in the region of $\Omega/m \leq 2$ and also small $|E|/m^2 \leq 0.6$. This corresponds roughly to the close vicinity of the first dome to the left of the critical value $\Omega_{\rm c} = 1.496$ in Fig. 3.11.

Finite temperature effects

The finite temperature results are contained in the plots shown in Fig. 3.14. The curves represent the absortion spectrum $\sigma_{xx}(\omega)$ and the Hall conductivity $\sigma_{xy}(\omega)$. The background rotating electric field has been fixed to $|E|/m^2 = 0.1$. Its frequency has been set to the first critical frequency $\Omega_{\rm c}(r_{\rm h})$ which decreases with the temperature as seen in the lower right plot of Fig. 3.4. The band in which these values lie for the chosen temperatures has been signalled by a vertical band in pink. The curves for σ_{xx} and σ_{xy} show a smooth deformation of the ones in Fig. 3.9 for the same value of $|E|/m^2$.

Succintly stated, the temperature in the gluon bath, in general destroys the AC Hall optical conductivity, and hence, also the DC Hall conductivity. Again, the effect of the temperature is similar to the one caused by the increase in electric field. Namely, the conductivity peaks get roughened and lowered. In a sense, both agents, the temperature and the electric field act in parallel by enhancing the amount of deconfined charge carriers in the medium.

The effect becomes more pronounced beyond some temperature $r_{\rm h}/m \sim 0.5$, as shown in the lower plots of Fig. 3.14. In the large temperature limit, $r_{\rm h} \to \infty$, all conductivities, both AC and DC tend towards $\sigma_{xx} = 1\,,\, \sigma_{xy} = 0$. This result is the same we obtained for the rotating current conductivity $\tilde{\sigma}_{\rm RC}$ in the massless limit. Since in this case the electric field is linearly polarised, rather than circularly, we see this as a further evidence in favor of the fact that the response will be Ohmic and instantaneous for an arbitrary time dependence of

[4] yet, notice a change of sign for very low values of $|E|/m^2$ approaching the Floquet condensates. It would be interesting to know if the configuration is unstable in this region and would decay to Minkowski embeddings.

USC SANTIAGO COMPOSTELA

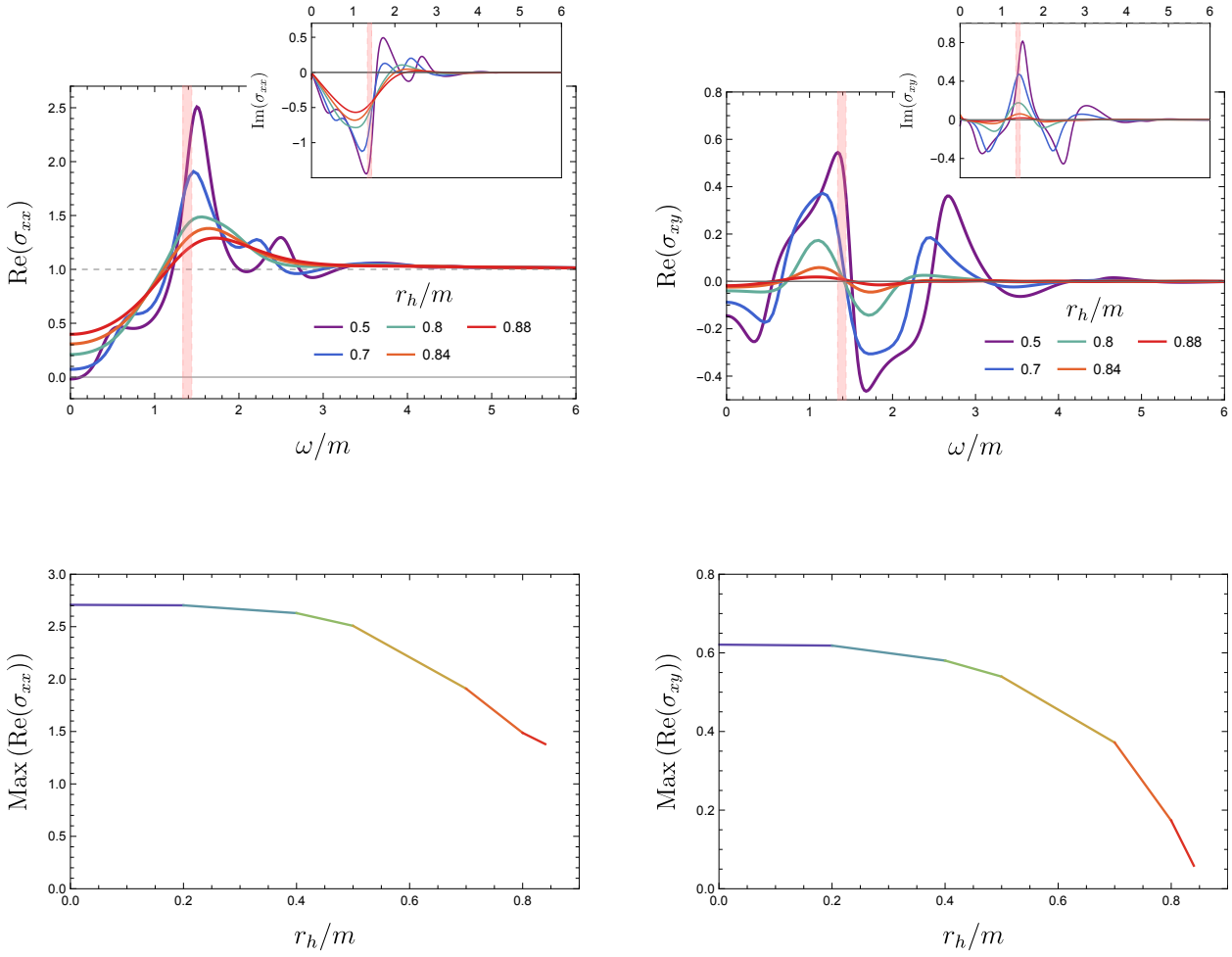


Figure 3.14: *Top:* AC conductivities for four values of $r_{\rm h}$ at their corresponding $\Omega_{\rm c}(r_{\rm h})$, for $E/m^2 = 0.1$. The pink band marks the range where the four values of $\Omega_{\rm c}(r_{\rm h})$ belong. The main peak is close to this region. *Bottom:* Variation with the temperature of the maximum value of the real part of σ_{xx} and σ_{xy} for $E/m^2 = 0.1$

the electric field in the plane $j(t) = \sigma E(t)$.

A peculiar observation is that the frequencies ω of highest peaks in the absortion spectrum $\mathrm{Re}(\sigma_{xx})$ slightly deviate above the one of the driving $\omega \gtrapprox \Omega$ (within the vertical band in pink). This was also observed in Fig. 3.9 where the drift is seen to be enhanced with increasing $|E|$. We could not offer any explanation to this. Here we can see that there is a very similar shift in the driving frequencies Ω of the Floquet suppression points inside the BH phase (solid segments) in Fig. 3.8 with increasing $|E|$ towards the right. We have tried to make sense of this qualitative coincidence but could not find an exact numerical agreement.

USC
UNIVERSIDADE
DE SANTIAGO
DE COMPOSTELA

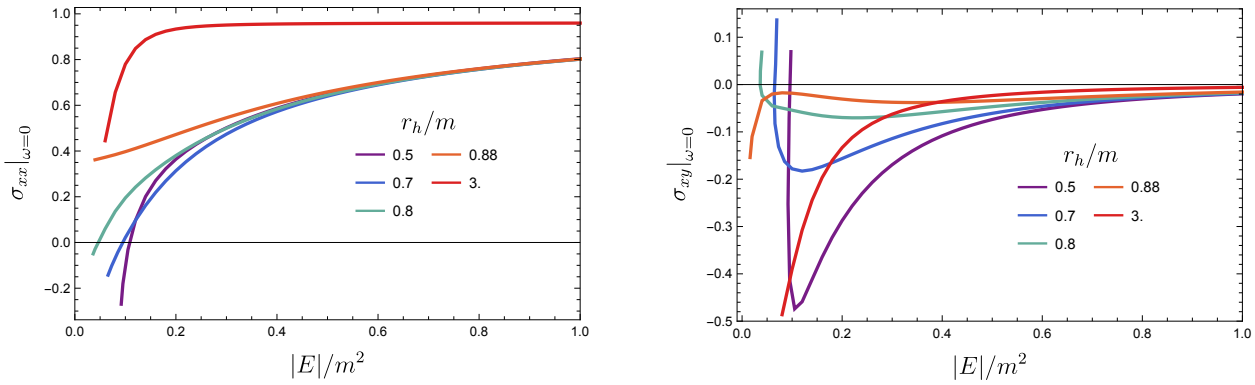


Figure 3.15: DC conductivities as functions of $|E|/m^2$ for different values of $r_{\rm h}/m$ at $\Omega/m = 1$. At high temperatures the conductivity tensor tends towards the identity $\sigma_{xx} = 1$ and $\sigma_{xy} = 0$.

USC
UNIVERSIDADE
DE SANTIAGO
DE COMPOSTELA

USC
UNIVERSIDADE
DE SANTIAGO
DE COMPOSTELA

Appendices for chapter 3

3.A Linearised Minkowski embeddings and Meson Spectrum

To study Minkowski embeddings is rather convenient to use cartesian coordinates (ρ, w), defined in (2.A.10). In these coordinates the embeddings are parameterised by functions $w = w(\rho)$, and the induced metric is given by (2.A.14). The effective Lagrangian reads

$$\mathcal{L} \sim \frac{\rho^2}{(\rho^2+w^2)^3}\Big[\left(\rho^2+w^2\right)^2\left(u_{\rm h}^4-\left(\rho^2+w^2\right)^2\right)^2|c'|^2-\Omega^2\left(\rho^2+w^2\right)^4{\rm Re}\{c\bar{c}'\}^2+$$
$$+\left(\left(\rho^2+w^2\right)^2+u_{\rm h}^4\right)\left(w'^2+1\right)\left(\left(u_{\rm h}^4-\left(\rho^2+w^2\right)^2\right)^2-\Omega^2\left(\rho^2+w^2\right)^2|c|^2\right)\Big]^{1/2}\,, \quad (3.A.1)$$

where $u_{\rm h} = r_{\rm h}/\sqrt{2}$ and now the primes denote derivatives with respect to ρ. Let us consider the case in which the gauge field $c(\rho)$ vanishes, and let $\tilde{w} = \tilde{w}(\rho)$ denote the Minkowski embedding function in such case. It can be obtained by solving the equation of motion of the Lagrange density $\tilde{\mathcal{L}} = \mathcal{L}(c=0)$

$$\tilde{\mathcal{L}} \sim \frac{\rho^2\left(u_{\rm h}^4-(\rho^2+\tilde{w})^2\right)}{(\rho^2+\tilde{w}^2)^3}\sqrt{\left[(\rho^2+\tilde{w}^2)^2+u_{\rm h}^2\right]\left[\tilde{w}'^2+1\right]}\,. \quad (3.A.2)$$

Let us next suppose that we perturb around the $c=0$ solution by making $c \to \delta c$ and $w \to \tilde{w} + \delta w$ in the equations of motion derived from the Lagrangian density (3.A.1)). It is easy to see that, at first order in the variations, the equation for δc reads

$$\partial_\rho\left(\frac{\rho^2\left(u_{\rm h}^4-(\rho^2+\tilde{w}^2)^2\right)}{(\rho^2+\tilde{w}^2)\sqrt{\left((\rho^2+\tilde{w}^2)^2+u_{\rm h}^4\right)(\tilde{w}'^2+1)}}\delta c'\right)+$$
$$+\frac{\rho^2\Omega^2\sqrt{\left((\rho^2+\tilde{w}^2)^2+u_{\rm h}^4\right)}}{(\rho^2+\tilde{w}^2)\left(u_{\rm h}^4-(\rho^2+\tilde{w}^2)^2\right)\sqrt{\tilde{w}'^2+1}}\delta c = 0\,. \quad (3.A.3)$$

To obtain the resonant frequencies of the mesonic Floquet condensates we integrate (3.A.3) and find the solutions that are regular at $\rho = 0$ and such that $E = 0$. This last condition is

USC DE SANTIAGO

only possible when the frequency Ω/m takes values in a discrete set (which depends on the horizon radius $r_{\rm h}$). For $r_{\rm h}/m = 0$, *i.e.*, at zero temperature, this sequence of frequencies can be obtained analytically and is given by (3.1.4) (details on its computation will be given in chapter 4, see equation (4.C.11))

$$\left.\frac{\Omega}{m}\right|_{T=0} = 2\sqrt{\left(n+\frac{1}{2}\right)\left(n+\frac{3}{2}\right)}\,, \qquad (n=0,1,2,\cdots)\,, \tag{3.A.4}$$

which are just the masses of the vector mesons of the supersymmetric D3-D5 model [139]. For $r_{\rm h}/m \neq 0$ the masses of these mesonic states decrease as $r_{\rm h}/m$ grows. At some value of $r_{\rm h}/m$ they cease to exist (see figure 3.16), as the mere Minkowski embeddings themselves do (see section 3.1). This behavior is dual to the meson melting phenomenon, as discussed in [32].

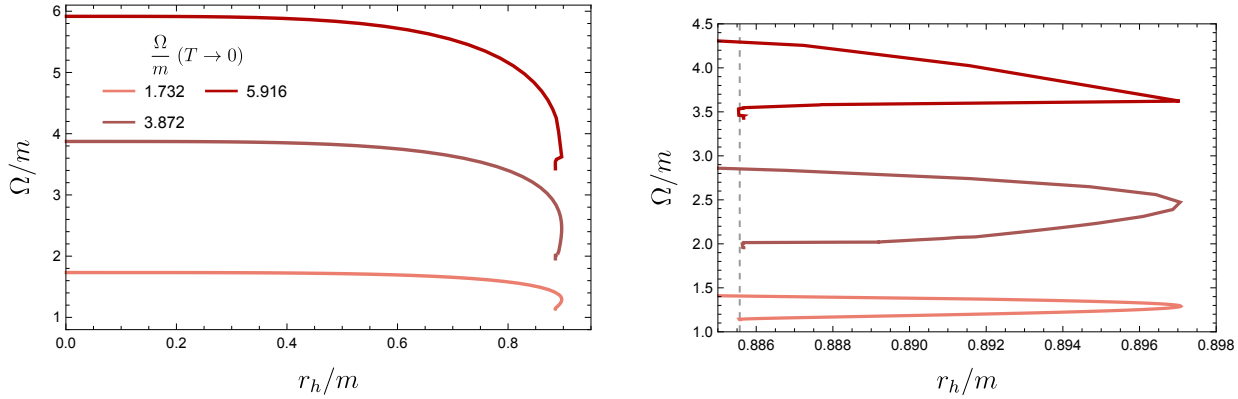


Figure 3.16: The first three meson frequency Ω/m variation with $r_{\rm h}/m$. The right figure shows the endpoint of the curves. All of them are bivaluated between $r_{\rm h}/m = 0.8855$ and $r_{\rm h} = 0.8897$.

3.B Phase space structure for the D3/D7 system

It is worth mentioning that the existence of the Floquet suppression points is not restricted to the D3/D5 system. In Fig. 3.17 we reproduce the lobe structure for the D3/D7 system, which is analogous to the one found in Fig. 3.1 for D3/D5. The $r_{\rm h} \to 0$ limit for the electric field plot coincides, of course, with the one studied in [31].

We find again a set of points where the induced current vanishes while the electric field is close to its maximum value within the lobe. This seems to indicate the presence of a range of frequencies for which, in Minkowski embeddings, $|j| = 0$ with $|E| \neq 0$, ranging from the critical frequency of the current $\Omega_{\rm c,j}$ (c stands for critical) up to son maximum value $\Omega_{\rm m,j}$ (m stands for meson).

The analytic computation of $\Omega_{\rm m,j}$ in the $T = 0$ limit of the D3/D7 system is more complicated than the one corresponding to the D3/D5 intersection but it can, however, be obtained numerically. We have found that the Floquet suppression points first appear for

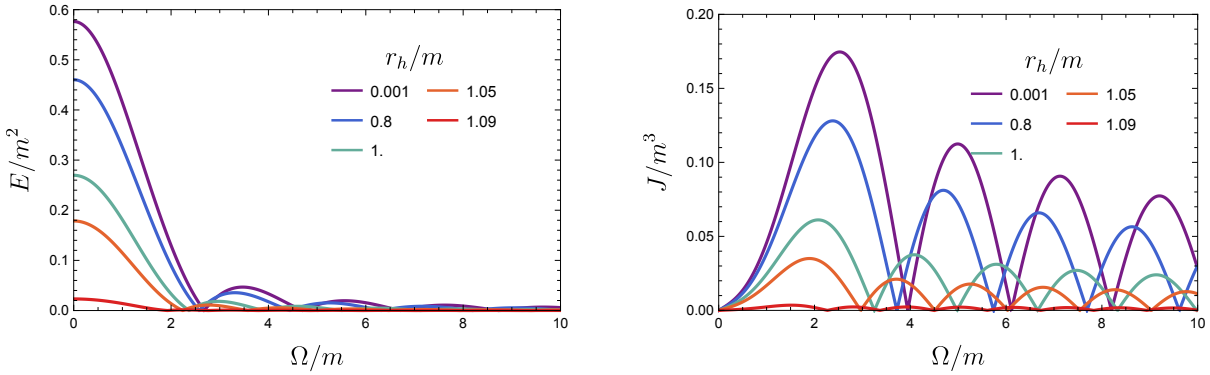


Figure 3.17: Electric field and current of the critical embeddings versus driving frequency, for different values of $r_{\rm h}$ in the D3/D7 system. The structure is mainly the same as the one found for the D3/D5 case. Here the maximum temperature for the Minkowski embeddings is slightly higher, while the height of the lobes is suppressed faster as one increases the driving frequency.

$\Omega/m \in (3.950, 4.159)$, and we have plotted in Fig. 3.18 the modulus of the current and the electric field for frequencies close or within that range. As anticipated, the similarity with the structure studied in [31] is quite obvious, and thus we conclude that a 3D diagram as that of Fig. 3.6 is also found when studying D3/D7 branes.

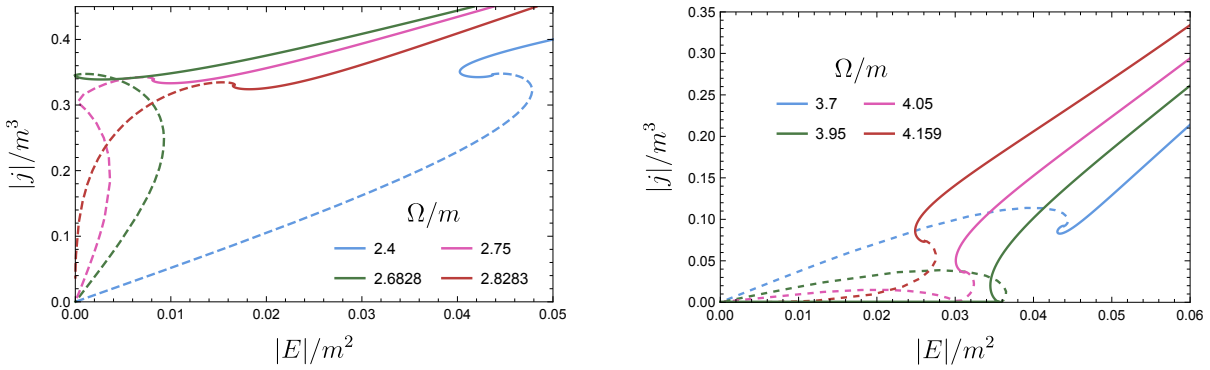


Figure 3.18: Electric current $|j|/m^3$ versus electric field $|E|/m^2$ for $r_{\rm h}/m = 0.001$. The solid curves represent the insulator (Minkowski) phase and the dashed curves the conductive (BH) phase. The driving frequency is fixed to some $\Omega/m < \Omega_{\rm c}/m$ (blue), $\Omega/m = \Omega_{\rm c}/m$ (green), $\Omega_{\rm c}/m < \Omega/m < \Omega_{\rm m}/m$ (pink) and $\Omega/m = \Omega_{\rm m}/m$ (red). The curves on the left, with $\Omega \sim 2.68$ scan the region close to the Floquet vector meson condensates and were obtained in [31]. On the right, for $\Omega \sim 3.95$ we do the same around the first Floquet suppression point.

USC
UNIVERSIDADE
DE SANTIAGO
DE COMPOSTELA

3.C Derivation of the optical conductivities

For this analysis it is most convenient to stick to the vector cartesian basis used in (2.1.5). On top of this background field, the idea is to place another fixed direction electric field

$$\vec{\mathcal{E}}(t) = O(t)\vec{E} + \vec{\epsilon}(t)\,, \tag{3.C.1}$$

with $|\vec{\epsilon}| \ll |\vec{E}|$, and a harmonic (AC) time dependence

$$\vec{\epsilon}(t) = \vec{\epsilon}\, e^{-i\omega\, t}\ . \tag{3.C.2}$$

Our task is to extract the response of the system out of the non equilibrium steady state (NESS) solutions spelled out in the previous sections. In particular, the currents will also suffer a perturbation $\vec{\mathcal{J}}(t) \to O(t)\vec{j} + \delta\vec{j}(t)$ and one of our targets will be to extract the *effective* conductivity response matrix $\boldsymbol{\sigma}$, such that $\delta\vec{j}(t) = \boldsymbol{\sigma}\cdot\vec{\epsilon}(t)$.

From (3.C.1) we expect a perturbation of the bulk gauge field, which we also write now in cartesian components, $\vec{a}(t,r) \to \vec{a}(t,r) + \delta\vec{a}(t,r)$. The idea is now to refine the ansatz, taking into account the new driving data (3.C.1) and (3.C.2). First of all, let us reconsider the boundary conditions of the unperturbed gauge field, $\vec{a}(t,r)$ (2.1.6). The near boundary expansion will be

$$\begin{aligned}\vec{a}(t,r) &= -\int^t \vec{\mathcal{E}}(t)dt + \frac{\vec{\mathcal{J}}}{r} + ... \\ &= -\frac{1}{\Omega}\, O(t)\, \boldsymbol{\varepsilon}\, \vec{E} + \frac{\vec{\mathcal{J}}}{r} + ...\end{aligned} \tag{3.C.3}$$

where $\boldsymbol{\varepsilon}$ stands for the 2×2 antisymmetric matrix

$$\boldsymbol{\varepsilon} = \begin{pmatrix} 0 & 1 \\ -1 & 0 \end{pmatrix}\ . \tag{3.C.4}$$

The leading term matches the vector potential of the rotating electric field through $\vec{\mathcal{E}}(t) = -\partial_t\, \vec{a}(t, r=\infty)$. This easily follows from the relation $\partial_t\, O\, \boldsymbol{\varepsilon} = -\Omega\, O$. The boundary condition (3.C.3) suggests the following ansatz for the bulk solution

$$\vec{a}\,(t,r) \,=\, O(t)\,\vec{c}\,(r)\ . \tag{3.C.5}$$

which is equivalent to (2.1.9) with $c = c(r)$. Near the boundary

$$\vec{c}(r) \approx \vec{c}_0 \,+\, \frac{\vec{c}_1}{r} \,+\, ... \tag{3.C.6}$$

with[5]

$$\vec{c}_0 \,=\, -\frac{1}{\Omega}\boldsymbol{\varepsilon}\,\vec{E} \quad , \quad \vec{\mathcal{J}}(t) \,=\, O(t)\,\vec{c}_1\ . \tag{3.C.7}$$

[5]This replaces (2.B.11) with $j = c_{1x} + ic_{1y}$

USC UNIVERSIDADE DE SANTIAGO

Considering the perturbations, now the bulk gauge potential $\vec{a}+\delta\vec{a}$ has to match the full electric field (3.C.1) at the boundary, $-\partial_t(\vec{a}+\delta a)=\vec{\mathcal{E}}(t)$

$$\vec{a}(t,r=\infty)\,+\delta\vec{a}(t,r=\infty)\,=\,-\frac{1}{\Omega}\,O(t)\,\boldsymbol{\varepsilon}\,\vec{E}\,-\,\frac{i}{\omega}\,\vec{\epsilon}\,e^{-i\omega\,t}\,. \tag{3.C.8}$$

Induced by this new boundary conditions, the ansatz will assume that the static field, $c(r)$, develops a time dependent perturbation

$$\vec{a}\,(t,r)\,+\delta\vec{a}\,(t,r)=\,O(t)\left(\vec{c}\,(r)+\delta\vec{c}\,(t,r)\right)\,. \tag{3.C.9}$$

When the flavor branes are massive, these fluctuations couple to a perturbation of the brane embedding functions $\theta(r)\to\theta(r)+\delta\theta(t,r)$. In this case we will be dealing with a 3 component vector of fluctuations $\delta\vec{\xi}(t,r)=(\delta c_x,\delta c_y,\delta\theta)$. The perturbed equations of motion, linear in $\delta\vec{\xi}$, will assume the following form, in terms of the (τ,r_*) coordinates (see Eq. (4.1.4))

$$\left(\partial_\tau^2\,-\,\partial_{r_*}^2\,+\,\mathbf{A}(r)\,\partial_\tau\,+\,\mathbf{B}(r)\,\partial_{r_*}\,+\,\mathbf{C}(r)\right)\delta\vec{\xi}\,=\,0\,. \tag{3.C.10}$$

Here, $\mathbf{A}$, $\mathbf{B}$ and $\mathbf{C}$ are 3×3 matrices depending on the radial coordinate $r(r_*)$ and, parametrically, on the rotating frequency Ω.

At the pseudo-horizon $r=r_{\rm c}\,(r_*\to-\infty)$ one finds

$$\mathbf{A}(r=r_{\rm c})\,=\,-\mathbf{B}(r=r_{\rm c})\,\equiv\,\mathbf{A}_{\rm c}\qquad\qquad\mathbf{C}(r=r_{\rm c})\,=\,0\,. \tag{3.C.11}$$

Thus, in this limit, $r_*\to-\infty$, the fluctuation equations become

$$\left(\partial_\tau^2\,-\,\partial_{r_*}^2\right)\delta\vec{\xi}\,+\,\mathbf{A}_{\rm c}\,(\partial_\tau\,-\,\partial_{r_*})\delta\vec{\xi}\,=\,0\,, \tag{3.C.12}$$

whose general solution takes the form

$$\delta\vec{\xi}\,=\,\vec{f}(\tau+r_*)\,+\,e^{-\mathbf{A}_{\rm c}\,r_*}\,\vec{g}(\tau-r_*)\,, \tag{3.C.13}$$

with $\vec{f}$ and $\vec{g}$ arbitrary vector functions. Imposing that $\vec{g}\,=\,0$ selects the ingoing wave boundary condition at the pseudohorizon.

Let us now work out the boundary conditions for the fluctuations. First, we want to keep the mass of the flavor brane fixed. After inserting (3.C.9) into (3.C.8) and multiplying by $\mathcal{O}^{-1}$, the boundary conditions for $\delta\vec{\xi}(t,\infty)$ turn out to be

$$\delta\vec{c}(t,r=\infty)\,=\,-\frac{i}{\omega}\,O(-t)\,e^{-i\omega\,t}\,\vec{\epsilon}\quad,\quad\delta\theta(t,r=\infty)=0\,. \tag{3.C.14}$$

Following [30], we expand the matrix $\mathcal{O}(t)$, defined in (2.1.5) as

$$O(t)=\mathbf{M}_+e^{i\Omega t}+\mathbf{M}_-e^{-i\Omega t}\,, \tag{3.C.15}$$

where $\mathbf{M}_\pm$ are orthogonal projectors given by

$$\mathbf{M}_\pm=\frac{1}{2}\begin{pmatrix}1&\pm i\\ \mp i&1\end{pmatrix}\,. \tag{3.C.16}$$

USC UNIVERSIDADE DE SANTIAGO DE COMPOSTELA

Finally, defininig $\omega_\pm = \omega \pm \Omega$, the boundary UV condition of $\delta\vec{c}$ can be written as

$$\delta\vec{c}(t, r=\infty) = -\frac{i}{\omega}\left(\mathbf{M}_+ e^{-i\omega_+ t} + \mathbf{M}_- e^{-i\omega_- t}\right)\vec{\epsilon}\,. \tag{3.C.17}$$

It is natural to assume that from these boundary conditions the bulk fluctuations $\delta\vec{c}(t,r)$ will oscillate with frequencies

$$\delta\vec{c}(t,r) = \vec{\beta}_+(r)\, e^{-i\omega_+ t} + \vec{\beta}_-(r)\, e^{-i\omega_- t}\,. \tag{3.C.18}$$

As a consequence of the coupling in the linearised equations, we will assume likewise that the embedding fluctuations will resonate with the same frecuencies

$$\delta\theta(t,r) = \gamma_+(r) e^{-i\omega_+ t} + \gamma_-(r) e^{-i\omega_- t}\,. \tag{3.C.19}$$

In summary, setting $\delta\vec{\xi}(t,r) = \vec{\xi}_\pm(r) e^{-i\omega_\pm t}$, the 3 component vectors $\vec{\xi}_\pm(r) = (\beta_{\pm,x}, \beta_{\pm,y}, \gamma_\pm)$ will satisfy the linearised ordinary differential system

$$\left[\frac{d^2}{dr_*^2} - \mathbf{B}(r)\frac{d}{dr_*} + \omega_\pm^2 + i\omega_\pm \mathbf{A}(r) - \mathbf{C}(r)\right]\vec{\xi}_\pm = 0\,. \tag{3.C.20}$$

Let us write the boundary expansions for the fields in the form

$$\delta\vec{c}(t,r) \approx \delta\vec{c}^{(0)}(t) + \frac{\delta\vec{c}^{(1)}(t)}{r} + \ldots \quad , \quad \vec{\beta}_\pm(r) = \vec{\beta}_\pm^{(0)} + \frac{\vec{\beta}_\pm^{(1)}}{r} + \ldots \tag{3.C.21}$$

Plugging the expansions in (3.C.18) we get

$$\delta\vec{c}^{(0)}(t) = \vec{\beta}_+^{(0)}\, e^{-i\omega_+ t} + \vec{\beta}_-^{(0)}\, e^{-i\omega_- t} \quad , \quad \delta\vec{c}^{(1)}(t) = \vec{\beta}_+^{(1)}\, e^{-i\omega_+ t} + \vec{\beta}_-^{(1)}\, e^{-i\omega_- t}\,. \tag{3.C.22}$$

Comparing the first of these equations with (3.C.17) we conclude that

$$\vec{\beta}_\pm^{(0)} = -\frac{i}{\omega}\mathbf{M}_\pm\,\vec{\epsilon}\,. \tag{3.C.23}$$

The subleading vectors $\vec{\beta}_\pm^{(1)}$ determine the variation of the current $\delta\vec{\mathcal{J}}(t) = O(t)\,\delta\vec{c}^{(1)}(t)$. Using (3.C.7), (3.C.15) and (3.C.17)

$$\delta\vec{\mathcal{J}}(t) = e^{-i\omega t}\left(\mathbf{M}_+\,\vec{\beta}_+^{(1)} + \mathbf{M}_-\,\vec{\beta}_-^{(1)} + \mathbf{M}_+\,\vec{\beta}_-^{(1)}\, e^{2\,i\Omega\,t} + \mathbf{M}_-\,\vec{\beta}_+^{(1)}\, e^{-2\,i\Omega\,t}\right)\,. \tag{3.C.24}$$

As usual in the AdS/CFT program, given a regular solution, the vectors $\vec{\beta}_\pm^{(1)}$ and $\vec{\beta}_\pm^{(0)}$ will no more be independent. From the linearity of the equations of motion it follows that this relation is also linear

$$\vec{\beta}_\pm^{(1)} = \mathbf{X}_\pm\,\vec{\beta}_\pm^{(0)} = -\frac{i}{\omega}\,\mathbf{X}_\pm\,\mathbf{M}_\pm\,\vec{\epsilon}, \tag{3.C.25}$$

where $\mathbf{X}_\pm$ are 2×2 matrices to be computed and (3.C.23) has been used. Plugging this into (3.C.24) allows to find a relation between the current $\delta\mathcal{J}$ and the applied electric field $\vec{\epsilon}$

USC DE SANTIAGO

which defines $\boldsymbol{\sigma}$, $\boldsymbol{\sigma}_+$ and $\boldsymbol{\sigma}_-$ as the 2×2 conductivity matrices of the three current modes, one with frequency ω and two with $\omega \pm 2\Omega$ (the heterodyning mixing modes [150])

$$\delta\vec{\mathcal{J}} = \left[\boldsymbol{\sigma}(\omega)\, e^{-i\omega\, t} \,+\, \boldsymbol{\sigma}^{+}(\omega)\, e^{-i(\omega+2\Omega)\, t} \,+\, \boldsymbol{\sigma}^{-}(\omega)\, e^{-i(\omega-2\Omega)\, t}\right]\vec{\epsilon}\,, \tag{3.C.26}$$

where

$$\begin{aligned} \boldsymbol{\sigma}(\omega) &= -\frac{i}{\omega}\left(\mathbf{M}_+\mathbf{X}_+\mathbf{M}_+ + \mathbf{M}_-\mathbf{X}_-\mathbf{M}_-\right) \\ \boldsymbol{\sigma}^{+}(\omega) &= -\frac{i}{\omega}\,\mathbf{M}_-\mathbf{X}_-\mathbf{M}_+ \\ \boldsymbol{\sigma}^{-}(\omega) &= -\frac{i}{\omega}\,\mathbf{M}_+\mathbf{X}_+\mathbf{M}_-\ . \end{aligned} \tag{3.C.27}$$

The procedure to compute $\mathbf{X}_\pm$ starts by solving the differential equation system (3.C.20) from the pseudohorizon $r_* \to -\infty$ to the AdS boundary at $r_* = 0$. At the horizon we impose the ingoing boundary condition $\vec{\xi}_\pm(r_*) \simeq \vec{c}\, e^{-i\omega_\pm r_*}$, where $\vec{c}$ are constant vectors $(1,0,0),(0,1,0)$ and $(0,0,1)$. Due to linearity of the equations we obtain in this way two complex 3×3 matrices $P_\pm$ and $Q_\pm$ such that $\vec{\xi}^{(0)}_\pm = P_\pm\vec{c}_\pm$, and $\vec{\xi}^{(1)}_\pm = Q_\pm\vec{c}_\pm$. In this way we can solve for $\vec{\xi}^{(1)}_\pm = Q_\pm P_\pm^{-1}\vec{\xi}^{(0)}_\pm$. Since we will be setting the source for the embedding fluctuations to zero, i.e. $\xi^{(0)}_{\pm,3} \equiv \gamma^{(0)}_\pm = 0$ and we only care about $\xi^{(1)}_{\pm,1,2}$, the searched for matrices $\mathbf{X}_\pm$ in (3.C.25) will be given by the 2×2 submatrix of the product $Q_\pm P_\pm^{-1}$

$$\mathbf{X}_{\pm\, ij} = [Q_\pm P_\pm^{-1}]_{ij=1,2}\,.$$

From them, the conductivities are extracted using (3.C.27).

3.C.1 More on optical conductivities

In Fig. 3.19 we show some plots for the heterodyning optical conductivities $\boldsymbol{\sigma}^{\pm}(\omega)$. As proven in [30], a set of non-trivial relations among the components of $\boldsymbol{\sigma}$ and $\boldsymbol{\sigma}^{\pm}$ allows to take as independent components σ_{xx}, σ_{xy} and $\sigma^{\pm}_{xx}$. The relation $\boldsymbol{\sigma}(-\omega) = \boldsymbol{\sigma}(\omega)^*$ implies that the DC conductivity will be real. For the heterodyning conductivities, in contrast, $\boldsymbol{\sigma}^{\pm}(-\omega) = \boldsymbol{\sigma}^{\mp}(\omega)^*$ and, hence, the associated DC limits will be complex.

They exhibit a similar pattern of oscillations whose amplitude increases as we approach the critical point. Eventually they sharpen into peaks as well. Comparing for example the peaks in $\sigma^{\pm}_{xx}$ with those in σ_{xx} in Fig. 3.9 it seems apparent that they share half of them each. This is apparent in the heterodyning version of Figs.3.10 shown below in Fig.3.20. Namely, while σ^{-}_{xx} has only the central stable peaks, σ^{+}_{xx} has the external peaks whose average value is Ω.

USC
UNIVERSIDADE
DE SANTIAGO
DE COMPOSTELA

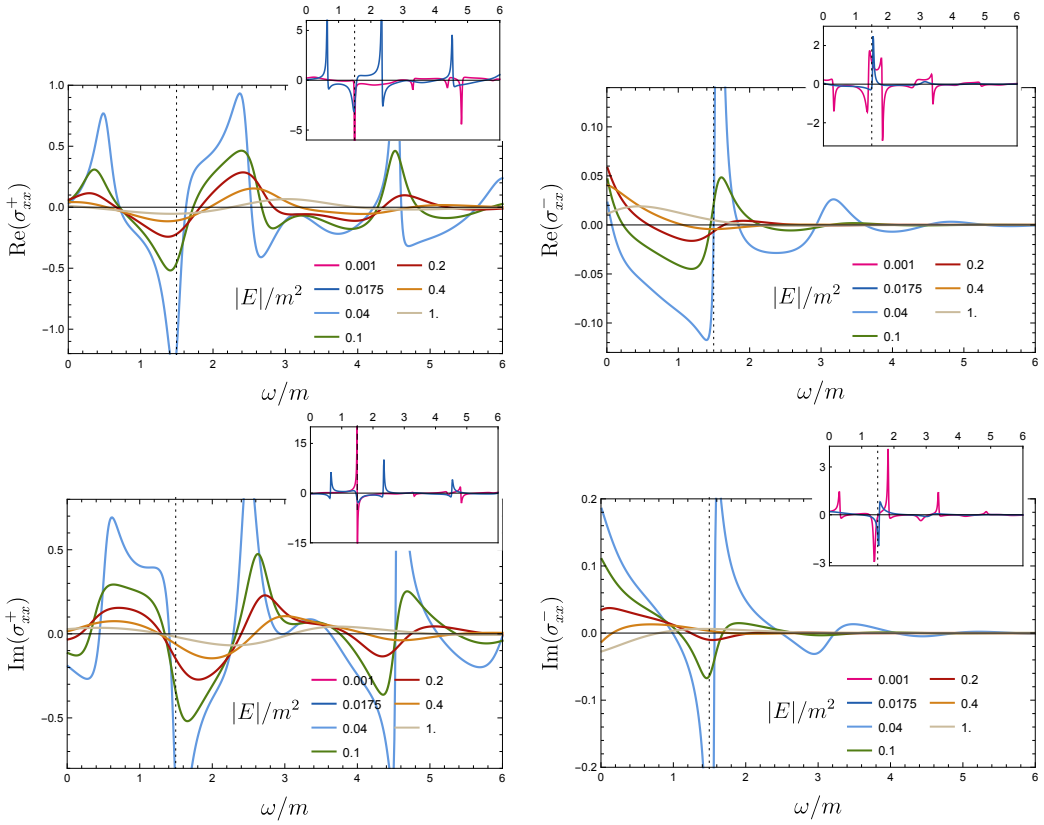


Figure 3.19: AC Conductivities for fixed value of $\Omega/m = 1.496$ and different values of $|E|/m^2$. They correspond to the vertically aligned dots in Fig. 3.11 with the same color code. In the insets, the curves for low values of $|E|/m^2 \to 0$ deep into the critical wedge, where they develop peak resonances. The value $\omega/m \to \Omega/m = 1.496$ is signalled with a dashed vertical line.

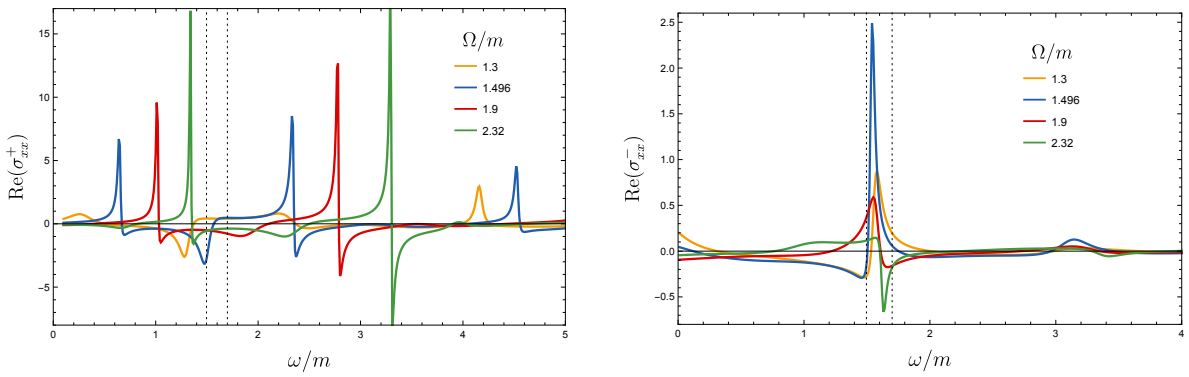


Figure 3.20: Peaks in the AC conductivities along the critical line to the right of the first Floquet condensate (see Fig.3.11). The vertical dashed lines signal the critical Floquet and the meson mass frequencies respectively. The central peaks bunch in this region whereas the two lateral peaks move with ω while keeping their inter-spacing almost constant.

USC UNIVERSIDADE DE SANTIAGO DE COMPOSTELA

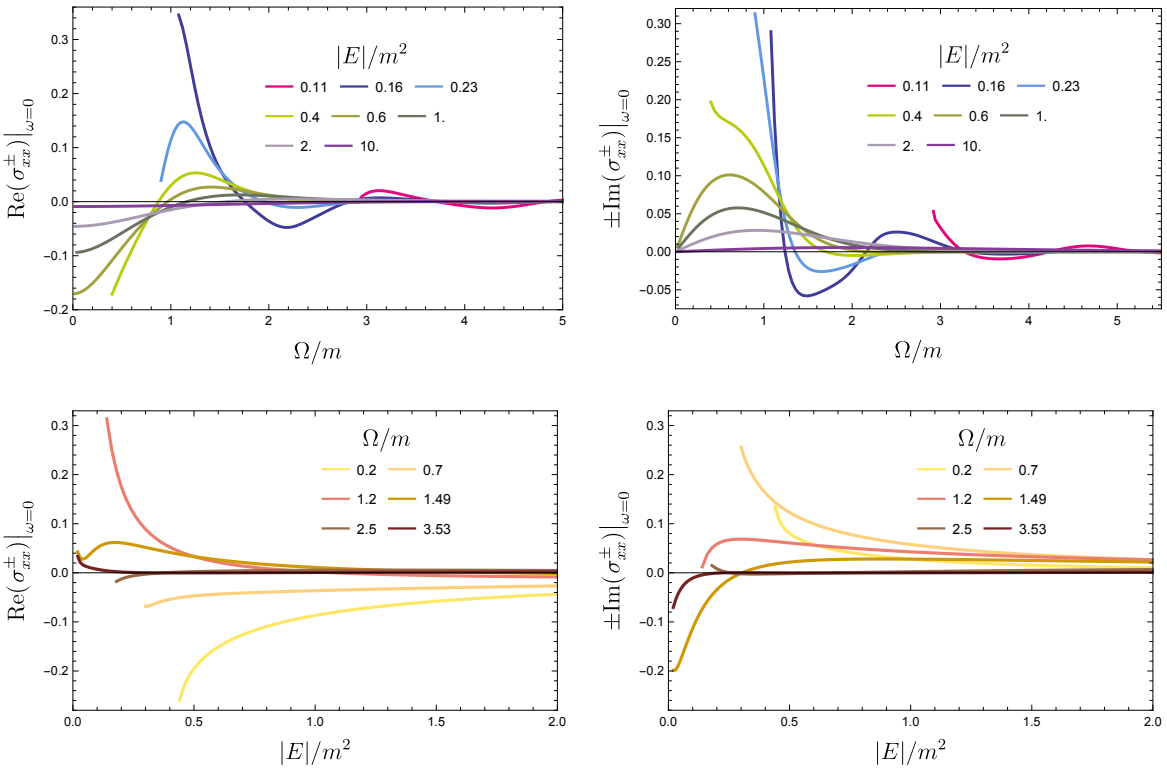


Figure 3.21: DC conductivities $\sigma^{\pm}_{xx}$ as function of either Ω/m or $|E|/m^2$.

USC
UNIVERSIDADE
DE SANTIAGO
DE COMPOSTELA

USC
UNIVERSIDADE
DE SANTIAGO
DE COMPOSTELA

4 Analytic results

There are two limits where the equations are amenable to analytic solution. These are the low mass limit $m \to 0$, both for finite and vanishing temperature, and the high frequency limit $\Omega \to \infty$ in the zero-temperature case. In the former case all embeddings are of black hole type, while in the latter all three configurations can be found.

In this chapter we present these analytic computations. The first section will be devoted to the massless limit, in which we derive a constant b field solution to the equations of motion as well as the conductivity for finite temperature (the zero temperature result amounts to setting $r_{\rm h} = 0$ in this one). On the other hand, the second section analyzes the high frequency limit for vanishing temperature, which is only accessible numerically in the general $T \neq 0$ case (see appendix 3.A in the previous chapter). All detailed computations can be found in the appendices.

4.1 Massless limit

4.1.1 Black hole embeddings in the massless limit

When the mass parameter m is zero or small it is possible to find analytic solutions of the equations of motion. These solutions are much easier to find in the angular coordinates (r, θ) with $\theta = \theta(r)$ as defined in (2.A.12). It is straightforward to prove that the Lagrangian density with this parameterization is

$$\mathcal{L} = \frac{\cos^2\theta}{\sqrt{r^4 - r_{\rm h}^4}} \sqrt{\left(r^4 - r_{\rm h}^4 - \Omega^2 b^2\right)\left(\left(r^4 - r_{\rm h}^4\right)\left(b'^2 + r^2\theta'^2\right) + r^4\right) + b^2\left(r^4 - r_{\rm h}^4\right)^2 \chi'^2} \ . \tag{4.1.1}$$

Moreover, the cyclic coordinate χ is now related to $\theta(r)$ and $b(r)$ as

$$\chi'(r) = \frac{q\sqrt{r^4 - r_{\rm h}^4 - \Omega^2 b^2}\sqrt{\left(r^4 - r_{\rm h}^4\right)\left(b'^2 + r^2\theta'^2\right) + r^4}}{b\,\left(r^4 - r_{\rm h}^4\right)\sqrt{b^2\,\Omega^2\,\left(r^4 - r_{\rm h}^4\right)\cos^4\theta - q^2}} \ . \tag{4.1.2}$$

USC UNIVERSIDADE DE SANTIAGO DE COMPOSTELA

The Routhian that is obtained after eliminating χ' from $\mathcal{L}$ is

$$\mathcal{R} \,=\, \frac{\sqrt{(r^4-r_{\rm h}^4)\,(b'^2+r^2\theta'^2)+r^4}}{\Omega\, b\,\,(r^4-r_{\rm h}^4)}\sqrt{r^4-r_{\rm h}^4-\Omega^2 b^2}\sqrt{\Omega^2 b^2\,(r^4-r_{\rm h}^4)\cos^4\theta-q^2}\ . \tag{4.1.3}$$

The tortoise coordinates in this (τ, r_*) parameterization are defined as

$$d\tau \,=\, dt \,-\, A_\theta(r)\,dr\ , \qquad\qquad dr_* \,=\, B_\theta(r)\,dr\ , \tag{4.1.4}$$

where $A_\theta(r)$ and $B_\theta(r)$ are the following functions

$$A_\theta(r) \,=\, \frac{\Omega\, b^2\chi'}{r^4-r_{\rm h}^4-b^2\Omega^2}\,, \qquad B_\theta(r) \,=\, \frac{\mathcal{L}}{\cos^2\theta\,(r^4-r_{\rm h}^4-b^2\Omega^2)}\ , \tag{4.1.5}$$

with $\mathcal{L}$ being the Lagrangian density (4.1.1). In terms of (τ, r_*) the (t, r) part of the effective metric takes the form

$$\frac{r^4-r_{\rm h}^4-b^2\Omega^2}{r^2}\,(-d\tau^2+dr_*^2)\ , \tag{4.1.6}$$

which means that, indeed, these new coordinates are tortoise coordinates for the effective open string metric.

Let us now consider a massless embedding with $\theta = 0$. The Routhian (4.1.3) for this case takes the form

$$\mathcal{R}_0 = \frac{\sqrt{(r^4-r_{\rm h}^4)\,b'^2+r^4}\sqrt{[\Omega^2 b^2-r^4+r_{\rm h}^4]\,[\Omega^2 b^2\,(r^4-r_{\rm h}^4)-q^2]}}{\Omega b\,(r^4-r_{\rm h}^4)}\ . \tag{4.1.7}$$

Both factors in the second square root in (4.1.7) must vanish simultaneously at the pseudo-horizon $r_{\rm c}$ in order to keep the Routhian real. From this condition, we get

$$b_0^2 = \frac{q}{\Omega^2} = \frac{r_{\rm c}^4-r_{\rm h}^4}{\Omega^2}\ , \tag{4.1.8}$$

where, in the second step, we have used that $q = r_{\rm c}^4 - r_{\rm h}^4$ for the massless embeddings. Actually, one can verify from the equation of motion of $\mathcal{R}_0$ that $b = b_0$ is a solution of this equation in which b is constant. Moreover, plugging $b = b_0$ into the right-hand side of (4.1.2), we get that the phase $\chi(r)$ in this massless case satisfies

$$\chi'_{m=0} = \Omega\frac{r^2}{r^4-r_{\rm h}^4} \,=\, \frac{\Omega}{r^2\,f(r)}\ . \tag{4.1.9}$$

In order to write explicitly the function $\chi_{m=0}(r)$, let as define a new function $\Lambda(x)$ as

$$\Lambda(x) \,\equiv\, \log\frac{x-1}{x+1} \,-\, 2\,\mathrm{arccot}\,x\ , \qquad\qquad \frac{d\Lambda}{dx} \,=\, \frac{4x^2}{x^4-1}\ . \tag{4.1.10}$$

One has

$$\chi_{m=0}(r) \,=\, \frac{\Omega}{4r_{\rm h}}\,\Lambda(r/r_{\rm h})\ , \tag{4.1.11}$$

USC UNIVERSIDADE DE SANTIAGO DE COMPOSTELA

where we have fixed the integration constant in such a way that $\Lambda(x) \to 0$ for $x \to \infty$ ($\Lambda(x) \approx -4/x$ for large x). Therefore, the complexified gauge potential $c(r) = b_0\, e^{i\chi_{m=0}(r)}$ in the rotating wave frame is

$$c(r) = \frac{\sqrt{r_{\rm c}^4 - r_{\rm h}^4}}{\Omega}\, e^{\frac{i\Omega}{4r_{\rm h}}\Lambda(r/r_{\rm h})} \ . \tag{4.1.12}$$

By expanding the right-hand side of (4.1.12) for large r and comparing the result with (2.1.15), we get the electric field E and the current j, namely

$$E \,=\, j \,=\, -i\sqrt{r_{\rm c}^4 - r_{\rm h}^4} \,=\, -i\,\sqrt{q}\ . \tag{4.1.13}$$

Thus, E and j are parallel and equal, which corresponds to $\gamma_{xx} = 1$ and $\gamma_{xy} = 0$ in the conductivity tensor. Using (2.1.16) it is easy to derive the correctly normalised physical conductivity, relating the the physical electric field and the physical current, as

$$\sigma(\Omega) \,=\, \frac{\sqrt{2}N_{\rm f}N_{\rm c}}{\pi\sqrt{\lambda}}\,. \tag{4.1.14}$$

Up to a convention factor of $\sqrt{2}$ this result matches the one obtained in [52], (see eq. (5.8)), where the authors made the observation that this conductivity is nothing else than $1/g^2$ in terms of the effective defect field theory gauge coupling on the D5-brane. This normalisation should affect all the conductivities obtained in chapter 3. Importantly, our result also agrees with the findings in [33] in that the response of the system is not only linear, but instantaneous.

The effective temperature in angular coordinates is given by

$$T_{\rm eff} \,=\, \frac{1}{2\pi}\,\frac{2\,r_{\rm c}^3 \,-\, b_0\,b_1\,\Omega^2}{\Omega\,b_0^2\,\chi_1}\ , \tag{4.1.15}$$

where $b_1 = b'(r = r_{\rm c})$ and $\chi_1 = \chi'(r = r_{\rm c})$. In the massless solution found above $b_1 = 0$ and the value of χ_1 can be read from (4.1.9) by taking $r = r_{\rm c}$. We get

$$T_{\rm eff} \,=\, \frac{r_{\rm c}}{\pi} \,=\, \frac{\left(q + r_{\rm h}^4\right)^{\frac{1}{4}}}{\pi}\ . \tag{4.1.16}$$

4.1.2 Optical conductivities in the masless limit

When the unperturbed embedding of the probe brane is massless, *i.e.*, when $\theta = 0$, the equations for $\delta\theta$ and $\delta\vec{c}$ decouple and we can take safely $\delta\theta = 0$. The unperturbed configuration in this case is the analytic solution discussed previously in this section. The equations of motion for δc_x and δc_y greatly simplify for this solution. Amazingly, the general solution of these coupled equations can be obtained analytically, as shown in detail in appendix 4.B. Using these results one can extract the exact value of the conductivity matrices, which turn out to be

$$\boldsymbol{\sigma}(\omega) \,= c\,\mathbb{I}\ , \qquad\qquad \boldsymbol{\sigma}^{+}(\omega) \,=\, \boldsymbol{\sigma}^{-}(\omega) \,=\, 0\ . \tag{4.1.17}$$

USC UNIVERSIDADE DE SANTIAGO DE COMPOSTELA

with $c = 1$. As mentioned before, this analytic result controls the limits in the previous sections where $|E|/m^2$ and Ω/m both become very large.

Of course, the coefficient c in Eq. (4.1.17) is not equal to 1. Using (2.1.16) it is easy to derive the correctly normalised physical conductivity, relating the physical electric field and the physical current, which coincides with (4.1.14).

4.2 High frequency limit for vanishing temperature

In the present section, it will be useful to use the parametrization described in appendix 2.B.

If the frequency Ω is large, the boundary condition at the UV (2.B.11) fixes that $|c(\rho \to \infty)| = E/\Omega \ll 1$ and this enforces $c(\rho)$ to be small for all values of ρ. The gauge field can then be treated as a perturbation around the state with $c = 0$ and, as we shall see, admits an analytic solution. To start with, using the scaling symmetry (2.1.19) we can choose to linearise the equations of motion derived from (2.B.9) near the solution with $c = 0$ and $w = 1$. Writing $w = 1 + \delta w$ we get

$$c'' + \frac{2}{\rho} c' + \frac{\Omega^2}{(1+\rho^2)^2} c = 0 , \tag{4.2.1}$$

$$\delta w'' + \frac{2}{\rho} \delta w' = \frac{2\Omega^2}{(1+\rho^2)^3} |c|^2 , \tag{4.2.2}$$

where c and δw are small. Notice that, although at linear order the equations decouple, as in [31] we have included the lowest order contribution to the coupling of modes, $\mathcal{O}(|\delta c|^2)$, in the equation of δw. The general solution of the equation of δc is

$$c(\rho) = c_1\, g_1(\rho) + c_2\, g_2(\rho) , \tag{4.2.3}$$

where c_1 and c_2 are constants and $g_1(\rho)$ and $g_2(\rho)$ are the functions

$$\begin{aligned} g_1(\rho) &= \frac{\sqrt{1+\rho^2}}{\rho} \sin\left(\sqrt{1+\Omega^2}\, \arctan(\rho)\right) , \\ g_2(\rho) &= \frac{\sqrt{1+\rho^2}}{\rho} \cos\left(\sqrt{1+\Omega^2}\, \arctan(\rho)\right) , \end{aligned} \tag{4.2.4}$$

with asymptotic behaviour as $\rho \to \infty$ given by

$$\begin{aligned} g_1(\rho) &= \sin\left(\frac{\pi}{2}\sqrt{1+\Omega^2}\right) - \sqrt{1+\Omega^2} \cos\left(\frac{\pi}{2}\sqrt{1+\Omega^2}\right) \frac{1}{\rho} + \cdots , \\ g_2(\rho) &= \cos\left(\frac{\pi}{2}\sqrt{1+\Omega^2}\right) + \sqrt{1+\Omega^2} \sin\left(\frac{\pi}{2}\sqrt{1+\Omega^2}\right) \frac{1}{\rho} + \cdots \end{aligned} \tag{4.2.5}$$

USC UNIVERSIDADE DE SANTIAGO DE COMPOSTELA

Similarly near $\rho = 0$, g_1 and g_2 behave as

$$g_1(\rho) \;=\; \sqrt{1+\Omega^2} \;-\; \frac{\Omega^2\sqrt{1+\Omega^2}}{6}\,\rho^2 \;+\; \cdots$$

$$g_2(\rho) \;=\; \frac{1}{\rho} \;-\; \frac{\Omega^2}{2}\,\rho \;+\; \cdots \tag{4.2.6}$$

At the linearised level the Joule heating q of Eq. (2.B.12) is proportional to the Wronskian of c and c^*

$$q \;=\; i\,\frac{\Omega\,\rho^2}{2}\left(c\,c'^{\,*} \;-\; c^*\,c'\right) . \tag{4.2.7}$$

Since q is independent of ρ, we could compute it by using the expansions (4.2.5) around $\rho = \infty$ or (4.2.6) around $\rho = 0$. The result one obtains is the same and given by

$$q \;=\; \Omega\,\sqrt{1+\Omega^2}\;\mathrm{Im}\,(c_1\,c_2^*) \;. \tag{4.2.8}$$

The solution for $\delta w(\rho)$ can be written as

$$\delta w(\rho) \;=\; -\frac{2\Omega^2}{\rho}\int_0^\rho \frac{s^2}{(s^2+1)^3}\,|c(s)|^2 \;-\; 2\Omega^2\int_\rho^\infty \frac{s}{(s^2+1)^3}\,|c(s)|^2 \;+\; c_3 \;, \tag{4.2.9}$$

with c_3 being a new integration constant.

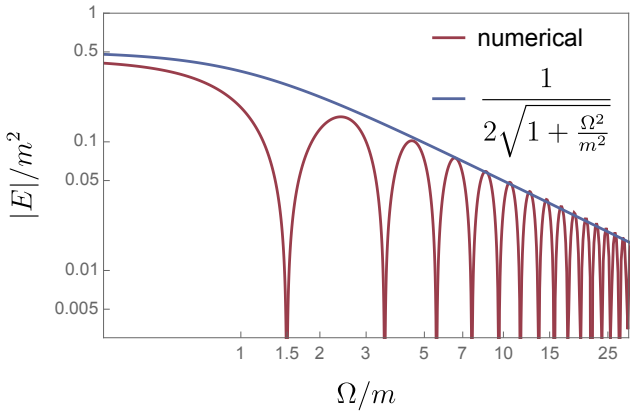


Figure 4.1: Logarithmic version of the plot in Fig. 3.17 for $r_\mathrm{h} = 0$. The high Ω/m fitting is derived in Sec. 4.C.3 (see eq. (4.C.44)).

Since we obtained the general solution of our equations, we can now analyze the different types of embeddings. The details of this study are deferred to appendix 4.C. Let us summarise here the results that we obtain there.

1. Regularity of the Minkowski embeddings at $\rho = 0$ enforces that the constant c_2 in (4.2.3) has to vanish.

2. By imposing the additional condition $E = 0$ or $j = 0$ to these Minkowski solutions, we obtain the resonant frequencies (3.1.4), corresponding to the meson masses of the D3-D5 model and to the endpoint of the line of Floquet suppression points (see figure 3.6), respectively.

3. To construct black hole embeddings we have to build up a pseudohorizon in our linearised theory and impose the corresponding infalling boundary conditions.

4. Although the linear approximation breaks down for the critical embeddings, it turns out that one can use the linear Minkowski solution to represent the critical configuration in the UV region of large ρ and one can use this result to represent features of the phase diagram, such as the envelope curve of figure 4.1.

USC
UNIVERSIDADE
DE SANTIAGO
DE COMPOSTELA

Appendices for chapter 4

4.A Black hole embeddings in the small mass limit

Let us now consider small mass solutions in which $b(r)$ and $\theta(r)$ are given by

$$b(r) \,=\, b_0 \,+\, \beta(r)\ , \qquad\qquad \theta(r) \,=\, \lambda(r)\ , \tag{4.A.1}$$

where the functions $\beta(r)$ and $\lambda(r)$ are small. At first order in these functions, they satisfy the following linear equations of motion

$$\begin{aligned} &\frac{d}{dr}\Big[(r^4\,f-q)\,\lambda'\Big] \,+\, 2r^2\lambda \,=\, 0\ , \\ &\frac{d}{dr}\Big[\frac{r^4\,f-q}{r^2}\,\beta'\Big] \,+\, \frac{4r^2\Omega^2}{r^4\,f-q}\,\beta \,=\, 0\ , \end{aligned} \tag{4.A.2}$$

which can be written as

$$\begin{aligned} &(r^4-r_{\rm c}^4)\lambda'' \,+4r^3\,\lambda' \,+\, 2r^2\,\lambda \,=\, 0\ , \\ &r^2(r^4-r_{\rm c}^4)\,\beta'' \,+\, 2r(r^4+r_{\rm c}^4)\beta' \,+\, 4\Omega^2\,\frac{r^6}{r^4-r_{\rm c}^4}\,\beta \,=\, 0\ . \end{aligned} \tag{4.A.3}$$

Let us start by writing the general solution for the differential equation satisfied by $\lambda(r)$

$$\lambda(r) \,=\, c_1\ F\Big(\frac{1}{4}\,,\,\frac{1}{2}\,;\,\frac{3}{4}\,;\,\frac{r^4}{r_{\rm c}^4}\Big) \,+\, c_2\,r\,F\Big(\frac{1}{2}\,,\,\frac{3}{4}\,;\,\frac{5}{4}\,;\,\frac{r^4}{r_{\rm c}^4}\Big)\ , \tag{4.A.4}$$

where c_1 and c_2 are constants. The hypergeometric functions written in (4.A.4) have a logarithmic singularity as we approach the pseudohorizon at $r = r_{\rm c}$. Indeed, from the general equation

$$F\Big(\alpha,\beta;\alpha+\beta;z\Big) \approx -\frac{\Gamma(\alpha+\beta)}{\Gamma(\alpha)\Gamma(\beta)}\ \log(1-z)\ , \qquad\qquad \text{as } z\to 1^-\ , \tag{4.A.5}$$

we get

$$\lambda(r) \approx -\frac{r_{\rm c}}{\sqrt{\pi}}\left[c_1\,\frac{\Gamma\left(\frac{3}{4}\right)}{\Gamma\left(\frac{1}{4}\right)} \,+\, c_2\,r_{\rm c}\,\frac{\Gamma\left(\frac{5}{4}\right)}{\Gamma\left(\frac{3}{4}\right)}\right]\,\log\left(1-\frac{r^4}{r_{\rm c}^4}\right)\ , \qquad\qquad \text{as } r\to r_{\rm c}\ . \tag{4.A.6}$$

USC UNIVERSIDADE DE SANTIAGO DE COMPOSTELA

The absence of this logarithmic singularity imposes the following ratio between the constants c_1 and c_2

$$\frac{c_1}{c_2} \,=\, -\frac{r_{\rm c}}{4}\,\left[\frac{\Gamma\left(\frac{1}{4}\right)}{\Gamma\left(\frac{3}{4}\right)}\right]^2 \,. \tag{4.A.7}$$

Let us now look at the UV behavior $r \to \infty$. In general, for large z, one has

$$F(\alpha,\beta;\alpha+\beta;z) \,\approx\, \Gamma(\alpha+\beta)\left[e^{-i\pi\alpha}\,\frac{\Gamma(\beta-\alpha)}{\Gamma^2(\beta)}\,z^{-\alpha} \,+\, e^{-i\pi\beta}\,\frac{\Gamma(\alpha-\beta)}{\Gamma^2(\alpha)}\,z^{-\beta}\right] . \tag{4.A.8}$$

Applying this last equation to our case, we get the UV behavior of the two functions in (4.A.4)

$$\begin{aligned} F\Big(\frac{1}{4}\,,\,\frac{1}{2}\,;\,\frac{3}{4}\,;\,\frac{r^4}{r_{\rm c}^4}\Big) \,&\approx\, r_{\rm c}\,\Gamma\Big(\frac{3}{4}\Big)\left[\frac{e^{-\frac{i\pi}{4}}}{\pi}\,\Gamma\Big(\frac{1}{4}\Big)\,\frac{1}{r} \,+\, r_{\rm c}\,\frac{e^{-\frac{i\pi}{2}}\,\Gamma\Big(-\frac{1}{4}\Big)}{\Gamma^2\Big(\frac{1}{4}\Big)}\,\frac{1}{r^2}\right] , \\ r\,F\Big(\frac{1}{2}\,,\,\frac{3}{4}\,;\,\frac{5}{4}\,;\,\frac{r^4}{r_{\rm c}^4}\Big) \,&\approx\, r_{\rm c}\,\Gamma\Big(\frac{5}{4}\Big)\left[r_{\rm c}\,e^{-\frac{i\pi}{2}}\,\frac{\Gamma\Big(\frac{1}{4}\Big)}{\Gamma^2\Big(\frac{3}{4}\Big)}\,\frac{1}{r} + \,r_{\rm c}^2\,\frac{e^{-\frac{3i\pi}{2}}}{\pi}\Gamma\Big(-\frac{1}{4}\Big)\,\frac{1}{r^2}\right] . \end{aligned} \tag{4.A.9}$$

Therefore, the coefficient of the leading term in $\lambda(r)$ as $r \to \infty$ is

$$q^{\frac{1}{4}}\,c_1\,e^{-\frac{i\pi}{4}}\,\frac{\Gamma\Big(\frac{3}{4}\Big)\Gamma\Big(\frac{1}{4}\Big)}{\pi} \,+\, q^{\frac{1}{2}}\,c_2\,e^{-\frac{i\pi}{2}}\,\Gamma\Big(\frac{5}{4}\Big)\,\frac{\Gamma\Big(\frac{1}{4}\Big)}{\Gamma^2\Big(\frac{3}{4}\Big)} \,. \tag{4.A.10}$$

The imaginary part of this leading term in the UV is zero if the ratio of c_1 and c_2 is

$$\frac{c_1}{c_2} \,=\, -\frac{r_{\rm c}}{4}\,\frac{\sqrt{2}\,\Gamma\Big(\frac{5}{4}\Big)}{\Gamma^3\Big(\frac{3}{4}\Big)} \,, \tag{4.A.11}$$

which can be seen to be equivalent to (4.A.7).

Let us write the UV behavior of $\theta(r)$ as

$$\theta(r) \approx \frac{m}{r} \,+\, \frac{\mathcal{C}}{r^2} \,+\, \cdots \,, \qquad\qquad (r \to \infty) \,, \tag{4.A.12}$$

where m and $\mathcal{C}$ are the mass and condensate parameters respectively. They are related to c_1 and c_2 as

$$\begin{aligned} m \,&=\, r_{\rm c}\,c_1\,\frac{\Gamma\Big(\frac{3}{4}\Big)\,\Gamma\Big(\frac{1}{4}\Big)}{\sqrt{2}\,\pi} \,=\, r_{\rm c}\,c_1 \\ \mathcal{C} \,&=\, -r_{\rm c}^3\,c_2\,\frac{\Gamma\Big(\frac{5}{4}\Big)\,\Gamma\Big(-\frac{1}{4}\Big)}{\sqrt{2}\,\pi} \,=\, r_{\rm c}^3\,c_2 \,. \end{aligned} \tag{4.A.13}$$

USC UNIVERSIDADE DE SANTIAGO DE COMPOSTELA

It follows that $\mathcal{C}$ and m are linearly related in this small mass solutions

$$\mathcal{C} \,=\, -r_{\rm c}\left[\frac{2\,\Gamma\left(\frac{3}{4}\right)}{\Gamma\left(\frac{1}{4}\right)}\right]^2\, m\ . \tag{4.A.14}$$

Moreover, the function $\theta(r)$ can be written as

$$\theta(r) \,=\, \frac{m}{r_{\rm c}}\,F\Big(\frac{1}{4}\,,\,\frac{1}{2}\,;\,\frac{3}{4}\,;\,\frac{r^4}{r_{\rm c}^4}\Big) \,+\, \frac{\mathcal{C}}{r_{\rm c}^3}\,r\,F\Big(\frac{1}{2}\,,\,\frac{3}{4}\,;\,\frac{5}{4}\,;\,\frac{r^4}{r_{\rm c}^4}\Big)\ . \tag{4.A.15}$$

Let us next look at the equation satisfied by the gauge field perturbation $\beta(r)$ in the system (4.A.3). Its general solution is

$$\beta(r) \,=\, d\,\exp\Big[-\frac{i\,\Omega}{2r_{\rm c}}\,\Lambda(r/r_{\rm c})\Big] \,+\, \bar{d}\,\exp\Big[\frac{i\,\Omega}{2r_{\rm c}}\,\Lambda(r/r_{\rm c})\Big]\ , \tag{4.A.16}$$

where d is a complex constant. It is interesting to find the solution for the complex potential $c = be^{i\chi}$. For the massless solution $c(r)$ takes the value

$$c_0(r) \,=\, b_0\,e^{i\chi_{m=0}(r)} \,=\, b_0\,e^{\frac{i\Omega}{4r_{\rm h}}\Lambda(r/r_{\rm h})}\ . \tag{4.A.17}$$

Let us denote

$$\delta c(r) \equiv c(r) - c_0(r)\ . \tag{4.A.18}$$

This function satisfies the following differential equation at linear order

$$r(r^4-r_{\rm c}^4)(r^4-r_{\rm h}^4)^2\delta c'' \,+\, 2(r^4-r_{\rm h}^4)\Big[r^8+(r_{\rm c}^4-r_{\rm h}^4)r^3(r+i\Omega) \,-\, r_{\rm c}^4r_{\rm h}^4\Big]\delta c' \,+$$

$$+r^5\Omega\,\Big[\Omega r^4+(r_{\rm c}^4-2r_{\rm h}^4)\Omega-4i(r_{\rm c}^4-r_{\rm h}^4)r\Big]\delta c \,=\, 0 \tag{4.A.19}$$

Instead of trying to solve directly this equation we notice that δc, at first order, can be written as

$$\delta c \,=\, e^{i\,\chi_{m=0}(r)}\,\Big(\beta \,+\, i\,b_0\,\delta\chi\Big)\ , \tag{4.A.20}$$

where $\delta\chi(r) = \chi(r) - \chi_{m=0}(r)$. The equation satisfied by $\delta\chi(r)$ is rather simple, namely

$$\delta\,\chi' \,=\, -\frac{2\,r^2\,\Omega}{b_0\,(r^4\,-\,r_{\rm c}^4)}\,\beta\ , \tag{4.A.21}$$

and can be readily integrated

$$\delta\chi(r) \,=\, -\frac{id}{b_0}\,\exp\Big[-\frac{i\,\Omega}{2r_{\rm c}}\,\Lambda(r/r_{\rm c})\Big] \,+\, \frac{i\bar{d}}{b_0}\exp\Big[\frac{i\,\Omega}{2r_{\rm c}}\,\Lambda(r/r_{\rm c})\Big] \,+\, \varphi\ , \tag{4.A.22}$$

where φ is a constant. Plugging (4.A.16) and (4.A.22) into (4.A.20), we obtain

$$\delta c(r) = A\,\exp\left[i\frac{\Omega}{4}\Big(\frac{1}{r_{\rm h}}\,\Lambda(r/r_{\rm h}) \,-\, \frac{2}{r_{\rm c}}\,\Lambda(r/r_{\rm c})\Big)\right] \,+\, B\exp\Big[\frac{i\,\Omega}{4r_{\rm h}}\,\Lambda(r/r_{\rm h})\Big]\ , \tag{4.A.23}$$

USC UNIVERSIDADE DE SANTIAGO DE COMPOSTELA

where $A = 2d$ and $B = i\frac{\varphi}{\Omega}\sqrt{r_{\rm c}^4 - r_{\rm h}^4}$. To proceed further we have to impose a regularity condition to the general solution (4.A.23). With this purpose let us write $\delta c(r)$ in terms of the tortoise coordinates (4.1.4) for the open string metric. In this massless case it is easy to demonstrate that (4.1.4) can be integrated to give the following relation between the tortoise coordinates (τ, r_*) and our original coordinates (t, r)

$$\tau \,=\, t \,+\, \frac{1}{4r_{\rm h}}\Lambda\left(\frac{r}{r_{\rm h}}\right) - r_* \;, \qquad\qquad r_* \,=\, \frac{1}{4r_{\rm c}}\Lambda\left(\frac{r}{r_{\rm c}}\right) \;. \tag{4.A.24}$$

The new radial coordinate r_* varies from $r_* = -\infty$ at the pseudohorizon to $r_* = 0$ at the UV boundary. Actually, one can prove that in these regions it can be related to r as

$$r_* \,=\, -\frac{1}{r} + \mathcal{O}(r^{-5}) \;, \qquad (r \to \infty) \;, \qquad\qquad r_* \,\sim\, \frac{1}{4r_{\rm c}}\,\log(r - r_{\rm c}) \;, \qquad (r \to r_{\rm c}) \;. \tag{4.A.25}$$

Let us next consider the time-dependent gauge potential $\delta a(r, t)$, given by

$$\delta a(r, t) \,=\, \delta c(r)\, e^{i\Omega\, t} \;. \tag{4.A.26}$$

By combining (4.A.23) and (4.A.24) it straightforward to prove that δa can be written in terms of (τ, r_*) simply as

$$\delta a(\tau, r_*) \,=\, A\, e^{i\Omega(\tau - r_*)} \,+\, B\, e^{i\Omega(\tau + r_*)} \;. \tag{4.A.27}$$

We next impose an infalling boundary condition, which amounts to select the solutions with $A = 0$ in (4.A.27). Therefore, the regular solutions we are looking for are

$$\delta a(\tau, r_*) \,=\, B\, e^{i\Omega(\tau + r_*)} \;. \tag{4.A.28}$$

Equivalently, $\delta c(r)$ is given by

$$\delta c(r) \,=\, B \exp\left[\frac{i\,\Omega}{4r_{\rm h}}\,\Lambda(r/r_{\rm h})\right] \;. \tag{4.A.29}$$

We can now read off the electric field and current from the asymptotic behaviour of δc, namely

$$\delta c(r) \,\approx\, B \,-\, \frac{i\Omega B}{r} \,+\, \cdots \;, \qquad\qquad (r \to \infty) \;. \tag{4.A.30}$$

Thus, we have

$$\delta E \,=\, \delta j \,=\, -i\Omega B \;, \tag{4.A.31}$$

which means that the equality of E and j of the massless solution is mantained at first order in these small mass solutions.

USC DE SANTIAGO

4.B Derivation of the optical conductivities in the massless limit

In the massless case the fluctuations of the embedding function decouple from those of the gauge field $\delta\vec{c}$. Therefore, since we are interested in computing conductivities, we can concentrate in studying the equations for δc_x and δc_y. In order to write these equations in a more convenient form, let us define the following differential operators

$$\begin{aligned}\mathcal{O}_1 \equiv \partial_t^2 \,+\, \frac{(r^4-r_{\rm h}^4)^2(r_{\rm c}^4-r^4)}{r^4(r_{\rm c}^4+r^4-2r_{\rm h}^4)}\partial_r^2 - \frac{2(r^4-r_{\rm h}^4)(r_{\rm c}^4-r_{\rm h}^4)}{r^2(r_{\rm c}^4+r^4-2r_{\rm h}^4)}\partial_t\partial_r + \\ \frac{4r(r_{\rm c}^4-r_{\rm h}^4)}{(r_{\rm c}^4+r^4-2r_{\rm h}^4)}\partial_t - \frac{2(r^4-r_{\rm h}^4)^2(r_{\rm c}^4+r^4)}{r^5(r_{\rm c}^4+r^4-2r_{\rm h}^4)}\partial_r \,, \\ \mathcal{O}_2 \equiv -2\partial_t \,+\, \frac{2(r^4-r_{\rm h}^4)(r_{\rm c}^4-r_{\rm h}^4)}{r^2(r_{\rm c}^4+r^4-2r_{\rm h}^4)}\partial_r \,+\, \frac{4r(r^4-r_{\rm h}^4)}{r_{\rm c}^4+r^4-2r_{\rm h}^4} \,. \end{aligned} \tag{4.B.1}$$

Then, one can show that δc_x and δc_y satisfy the following system of coupled second-order differential equations

$$\Big(\mathcal{O}_1-\Omega^2\Big)\,\delta c_x \,+\, \Omega\,\mathcal{O}_2\,\delta c_y \,=\, 0 \,, \qquad\qquad \Big(\mathcal{O}_1-\Omega^2\Big)\,\delta c_y \,-\, \Omega\,\mathcal{O}_2\,\delta c_x \,=\, 0 \,. \tag{4.B.2}$$

To decouple these equations, let us consider the following complex combinations of δc_x and δc_y

$$\eta(t,r) \,\equiv\, \delta c_x(t,r) \,+\, i\delta c_y(t,r) \,, \qquad\qquad \tilde{\eta}(t,r) \,\equiv\, \delta c_x(t,r) \,-\, i\delta c_y(t,r) \,. \tag{4.B.3}$$

Notice that $\tilde{\eta}$ is not the complex conjugate of η since δc_x and δc_y are not necessarily real. It is straightforward to verify that the equations for η and $\tilde{\eta}$ are indeed decoupled and given by

$$\Big(\mathcal{O}_1-\Omega^2\Big)\,\eta \,-\, i\Omega\,\mathcal{O}_2\,\eta \,=\, 0 \,, \qquad\qquad \Big(\mathcal{O}_1-\Omega^2\Big)\,\tilde{\eta} \,+\, i\Omega\,\mathcal{O}_2\,\tilde{\eta} \,=\, 0 \,. \tag{4.B.4}$$

Let us now separate variables as

$$\eta(t,r) \,=\, \beta(r)\,e^{-i\omega\,t} \,, \qquad\qquad \tilde{\eta}(t,r) \,=\, \tilde{\beta}(r)\,e^{-i\omega\,t} \,, \tag{4.B.5}$$

for some frequency ω. Then, we obtain the following differential equations for β

$$\begin{aligned} r(r^4-r_{\rm c}^4)(r^4-r_{\rm h}^4)^2\beta'' = -2(r^4-r_{\rm h}^4)\Big[r^8-r_{\rm c}^4r_{\rm h}^4+r^4(r_{\rm c}^4-r_{\rm h}^4)-ir^3(r_{\rm c}^4-r_{\rm h}^4)(\omega-\Omega)\Big]\beta' - \\ -r^5(\omega-\Omega)\Big[4ir(r_{\rm c}^4-r_{\rm h}^4)+r^4(\omega-\Omega)+(r_{\rm c}^4-2r_{\rm h}^4)(\omega-\Omega)\Big]\beta \,. \end{aligned} \tag{4.B.6}$$

The equation for $\tilde{\beta}$ is the same, but with $(\omega+\Omega)$ instead of $(\omega-\Omega)$. Then, remarkably, one can find the following general solutions

$$\begin{aligned} \beta(r) \,&=\, e^{\,i\,\frac{\Omega-\omega}{4r_{\rm h}}\Lambda\left(\frac{r}{r_{\rm h}}\right)}\left[A+B\,e^{-i\,\frac{\Omega-\omega}{2r_{\rm c}}\Lambda\left(\frac{r}{r_{\rm c}}\right)}\right] \,, \\ \tilde{\beta}(r) \,&=\, e^{-i\,\frac{\Omega+\omega}{4r_{\rm h}}\Lambda\left(\frac{r}{r_{\rm h}}\right)}\left[\tilde{A}+\tilde{B}\,e^{\,i\,\frac{\Omega+\omega}{2r_{\rm c}}\Lambda\left(\frac{r}{r_{\rm c}}\right)}\right] \,, \end{aligned} \tag{4.B.7}$$

USC UNIVERSIDADE DE SANTIAGO DE COMPOSTELA

where Λ is the function defined in (4.1.10) and A, B, $\tilde{A}$ and $\tilde{B}$ are complex constants which are determined by imposing boundary conditions both at the IR and UV. First of all, we write the solutions we found in terms of the tortoise coordinates (τ, r_*) of (4.A.24). Actually, by inspecting the expression of η obtained from (4.B.7) one easily demonstrates that, in terms of the tortoise variables, it can be simply written as

$$\eta(\tau, r_*) \,=\, e^{\frac{\Omega}{4r_{\rm h}}\Lambda\left(\frac{r}{r_{\rm h}}\right)}\left[A\, e^{-i\omega(\tau+r_*)} \,+\, B\, e^{-2i\Omega\, r_*}\, e^{-i\omega(\tau-r_*)}\right] \tag{4.B.8}$$

It is now clear that $\eta(\tau, r_*)$ is the superposition of ingoing and outgoing waves at the pseudohorizon. The infalling regularity condition requires that B vanishes. Then, writing η in our original (t, r) coordinates, we have

$$\eta(t, r) \,=\, A\, e^{-i\,\frac{\omega-\Omega}{4r_{\rm h}}\Lambda\left(\frac{r}{r_{\rm h}}\right)}\, e^{-i\omega\, t}\ . \tag{4.B.9}$$

We can proceed similarly with $\tilde{\eta}$ and conclude that we should require that $\tilde{B} = 0$. Therefore

$$\tilde{\eta}(t, r) \,=\, \tilde{A}\, e^{-i\,\frac{\omega+\Omega}{4r_{\rm h}}\Lambda\left(\frac{r}{r_{\rm h}}\right)}\, e^{-i\omega\, t}\ . \tag{4.B.10}$$

Therefore, we obtain that the fluctuations δc_x and δc_y regular at the pseudohorizon are

$$\begin{aligned}
\delta c_x(t, r) \,&=\, \frac{1}{2}\Big[\, A\, e^{-i\,\frac{\omega-\Omega}{4r_{\rm h}}\Lambda\left(\frac{r}{r_{\rm h}}\right)} \,+\, \tilde{A}\, e^{-i\,\frac{\omega+\Omega}{4r_{\rm h}}\Lambda\left(\frac{r}{r_{\rm h}}\right)}\Big]\, e^{-i\omega\, t}\ , \\
\delta c_y(t, r) \,&=\, \frac{1}{2i}\Big[\, A\, e^{-i\,\frac{\omega-\Omega}{4r_{\rm h}}\Lambda\left(\frac{r}{r_{\rm h}}\right)} \,-\, \tilde{A}\, e^{-i\,\frac{\omega+\Omega}{4r_{\rm h}}\Lambda\left(\frac{r}{r_{\rm h}}\right)}\Big]\, e^{-i\omega\, t}\ .
\end{aligned} \tag{4.B.11}$$

Let us now impose the boundary conditions at the UV. To fulfil the UV boundary condition (3.C.17) we sum two solutions of the form (4.B.11) with frequencies $\omega_+ = \omega + \Omega$ and $\omega_- = \omega - \Omega$. Let $A_\pm$ and $\tilde{A}_\pm$ denote the constants in (4.B.11) with frequency $\omega_\pm$. From the leading UV terms we get that, in order to satisfy the boundary condition (3.C.23), the constants $A_\pm$ and $\tilde{A}_\pm$ must be related to ϵ_x and ϵ_y as

$$A_+ \,=\, -\frac{i}{\omega}\left(\epsilon_x + i\epsilon_y\right)\,, \qquad \tilde{A}_- \,=\, -\frac{i}{\omega}\left(\epsilon_x - i\epsilon_y\right)\,, \qquad \tilde{A}_+ \,=\, A_- \,=\, 0\ . \tag{4.B.12}$$

Moreover, from the analysis of the subleading UV terms we conclude that

$$\vec{\beta}^{(1)}_\pm \,=\, \mathbf{M}_\pm\, \vec{\epsilon}\ . \tag{4.B.13}$$

By comparing (4.B.13) and (3.C.25), we get that the matrices $\mathbf{X}_\pm$ are given by

$$\mathbf{X}_\pm \,=\, i\omega\, \mathbf{I}\ . \tag{4.B.14}$$

Plugging these $\mathbf{X}_\pm$ matrices in (3.C.27), we obtain the conductivity matrices in these massless case, namely

$$\boldsymbol{\sigma}(\omega) \,=\, \mathbf{I}\,, \qquad\qquad \boldsymbol{\sigma}^+(\omega) \,=\, \boldsymbol{\sigma}^-(\omega) \,=\, 0\,, \tag{4.B.15}$$

Note this result is valid at both finite and vanishing temperature. As in the case of the non-linear current, here also the result confirms the expectations put forward in [33].

USC DE SANTIAGO

4.C Embeddings in the linearised approximation at $T = 0$

In this appendix we study in detail the three types of embeddings in the linearised approximation of section 4.2 (valid for large driving frequency Ω or small electric field E).

4.C.1 Minkowski embeddings

To obtain the Minkowski embeddings that reach $\rho = 0$ we impose regularity of the function $c(\rho)$ at $\rho = 0$. This implies that the constant c_2 must vanish and, therefore the gauge field $c(\rho)$ is given by

$$c(\rho) \,=\, c_1\, g_1(\rho) \,=\, c_1\, \frac{\sqrt{1\,+\,\rho^2}}{\rho}\, \sin\left(\sqrt{1+\Omega^2}\, \arctan(\rho)\right) . \tag{4.C.1}$$

From the boundary expansion (2.B.11) we find the electric field and current hence

$$E \;=\; -i\, c_1\, \Omega\, \sin\left(\frac{\pi}{2}\, \sqrt{1+\Omega^2}\right) , \tag{4.C.2}$$

$$j \;=\; -c_1\, \sqrt{1+\Omega^2}\, \cos\left(\frac{\pi}{2}\, \sqrt{1+\Omega^2}\right) . \tag{4.C.3}$$

Eliminating the constant c_1 we obtain the current in terms of the electric field E

$$j \,=\, -\frac{i\, E}{\Omega}\, \sqrt{1+\Omega^2}\, \cot\left(\frac{\pi}{2}\, \sqrt{1+\Omega^2}\right) . \tag{4.C.4}$$

We can also eliminate c_1 in (4.C.1) using (4.C.2)

$$c(\rho) \,=\, \frac{i\, E}{\Omega\, \sin\left[\frac{\pi}{2}\, \sqrt{1+\Omega^2}\right]}\, \frac{\sqrt{1+\rho^2}}{\rho}\, \sin\left[\sqrt{1+\Omega^2}\, \arctan\rho\right] . \tag{4.C.5}$$

Let us now look at the embedding function δw given in (4.2.9). Imposing $\delta w(\rho = 0) = 0$ fixes the value of the integration constant c_3

$$c_3 \,=\, 2\, \Omega^2\, |c_1|^2 \int_0^\infty ds\, \frac{s}{(s^2+1)^3}\, g_1^2(s) . \tag{4.C.6}$$

Then, the resulting $\delta w(\rho)$ can be written as

$$\begin{aligned} \delta w(\rho) \,=\, 2\, \Omega^2\, |c_1|^2 \int_0^\rho ds\, \frac{\sin^2\left[\sqrt{1+\Omega^2}\, \arctan(s)\right]}{s(s^2+1)^2} \,-\\ -\, \frac{2\, \Omega^2\, |c_1|^2}{\rho} \int_0^\rho ds\, \frac{\sin^2\left[\sqrt{1+\Omega^2}\, \arctan(s)\right]}{(s^2+1)^2} . \end{aligned} \tag{4.C.7}$$

USC UNIVERSIDADE DE SANTIAGO DE COMPOSTELA

From the UV expansion (2.B.11) we find the mass and the condensate

$$m \,=\, 1 \,+\, 2\,\Omega^2\,|c_1|^2\,\int_0^\infty\,ds\,\frac{\sin^2\left[\sqrt{1+\Omega^2}\,\arctan(s)\right]}{s(s^2+1)^2}\,,$$

$$\mathcal{C} \,=\, -2\,\Omega^2\,|c_1|^2\,\int_0^\infty\,ds\,\frac{\sin^2\left[\sqrt{1+\Omega^2}\,\arctan(s)\right]}{(s^2+1)^2}\,. \tag{4.C.8}$$

In terms of the electric field at the boundary, using (4.C.2) we obtain

$$m \,=\, 1 \,+\, \frac{2\,|E|^2}{\sin^2\left(\frac{\pi}{2}\,\sqrt{1+\Omega^2}\right)}\,\int_0^\infty\,ds\,\frac{\sin^2\left[\sqrt{1+\Omega^2}\,\arctan(s)\right]}{s(s^2+1)^2}\,,$$

$$\mathcal{C} \,=\, -\frac{|E|^2}{4\,\sin^2\left(\frac{\pi}{2}\,\sqrt{1+\Omega^2}\right)}\,\left(\pi+\frac{\sin\left(\pi\sqrt{1+\Omega^2}\right)}{\Omega^2\sqrt{1+\Omega^2}}\right)\,. \tag{4.C.9}$$

To find the resonant frecuencies of the Floquet condensates we impose that $E = 0$ in (4.C.2), which means that the Ω's must satisfy

$$\sqrt{1+\Omega_n^2} \,=\, 2(n+1)\,, \tag{4.C.10}$$

for $n \,=\, 0, 1, 2, \cdots$. This gives the following discrete set

$$\Omega_n \,=\, 2\sqrt{\left(n+\frac{1}{2}\right)\left(n+\frac{3}{2}\right)}\,, \tag{4.C.11}$$

which are the same as the masses of the vector mesons in the D3-D5 model [139]. Conversely, if instead of $E = 0$ we require $j = 0$, we arrive at the following set of frequencies

$$\Omega_k = 2\sqrt{k\,\,(k+1)} = 2.828, 4.899, ...\,, \tag{4.C.12}$$

which are related to the Floquet suppression points, as studied in chapter 3 (see section 3.1.1).

4.C.2 Black hole embeddings

We now determine $c(\rho)$ for a black hole embedding by imposing the appropriate in-falling boundary condition at the pseudohorizon. Now the phase $\chi(\rho)$ is not constant and, in fact, χ' is related to the Joule heating q. To obtain this relation in the linearised approximation, let us take into account that $c\,c'^{*} \,-\, c^{*}\,c' = -2i\,\chi'\,b^2$. Since the Lagrangian density $\mathcal{L} = \rho^2$ in the linear approximation, we get from (2.B.6) that

$$\chi'(\rho) \,=\, \frac{q}{\Omega}\,\frac{1}{\rho^2\,b^2(\rho)}\,. \tag{4.C.13}$$

USC UNIVERSIDADE DE SANTIAGO DE COMPOSTELA

Let us now take $\rho = \rho_c$ in this last expression and use (2.B.15) and (2.B.21) to relate $b_0 = b(\rho_c)$ and q to $w_0 = w(\rho_c)$ and ρ_c. We immediately get

$$\chi'(\rho_c) \,=\, \frac{\Omega}{w_0^2 + \rho_c^2} \,, \tag{4.C.14}$$

which is an initial condition for $\chi(\rho)$. We begin by introducing a new variable y, related to ρ as[1]

$$y \,=\, \arctan(\rho) \,, \tag{4.C.15}$$

and let y_c be the y coordinate of the pseudohorizon $y_c = \arctan(\rho_c)$. In terms of the variable y, the initial condition (4.C.14), for $w_0 = 1$, takes the form

$$\left.\frac{d\chi}{dy}\right|_{y=y_c} \,=\, \Omega \,. \tag{4.C.16}$$

We will impose the following infalling condition at the pseudohorizon

$$\left.\frac{dc}{dy}\right|_{y=y_c} \,=\, i\,\Omega\, c(y_c) \,. \tag{4.C.17}$$

Taking into account that, in general

$$\frac{dc}{dy} \,=\, \left[\, i\frac{d\chi}{dy} \,+\, \frac{1}{b}\,\frac{db}{dy}\right] c \,, \tag{4.C.18}$$

this is equivalent to requiring that

$$\left.\frac{db}{dy}\right|_{y=y_c} \,=\, 0 \tag{4.C.19}$$

or, equivalently, that the infalling frequency is real. To simplify the calculation, let us now introduce a new complex field

$$\psi(y) \,=\, \frac{\rho}{\sqrt{1+\rho^2}}\, c(\rho) \,. \tag{4.C.20}$$

As $c = \psi(y)/\sin y$, the infalling boundary condition (4.C.17) takes the following form in terms of ψ

$$\left.\frac{d\psi}{dy}\right|_{y=y_c} \,=\, \Big(i\,\Omega \,+ \cot y_c\Big)\,\psi(y_c) \,. \tag{4.C.21}$$

Taking into account that $\cot y_c = 1/\rho_c$, we finally get

$$\left.\frac{d\psi}{dy}\right|_{y=y_c} \,=\, \left(i\,\Omega \,+\, \frac{1}{\rho_c}\right)\psi(y_c) \,. \tag{4.C.22}$$

The general solution (4.2.3) can be written as

$$\psi(y) \,=\, d_1\, e^{i\overline{\Omega}\, y} \,+\, d_2\, e^{-i\overline{\Omega}\, y} \,, \tag{4.C.23}$$

[1] The coordinate y is nothing but the tortoise coordinate ρ_* in this linear approximation. Indeed, in this case the function $B(\rho)$ defined in (2.B.27) is $B(\rho) \approx 1/(1+\rho^2)$ and (2.B.26) is easily integrated to give $\rho_* = \arctan y$, as claimed.

where d_1 and d_2 are complex constants and $\overline{\Omega}$ is defined as

$$\overline{\Omega} \equiv \sqrt{1+\Omega^2} \ . \tag{4.C.24}$$

We now impose the pseudohorizon boundary condition (4.C.17). It is easy to demonstrate that (4.C.17) is satisfied if the ratio of the constants d_1 and d_2 is given by

$$\frac{d_1}{d_2} \ = \ \frac{(\overline{\Omega}+\Omega)\rho_{\rm c} \ - \ i}{(\overline{\Omega}-\Omega)\rho_{\rm c} \ + \ i} \, e^{-2i\,\overline{\Omega}\,y_{\rm c}} \ . \tag{4.C.25}$$

To rewrite this condition in a more convenient form, define the phases $\Lambda_{\rm c}$ and $\overline{\Lambda}_{\rm c}$

$$\Lambda_{\rm c} \equiv \arctan\left[\frac{\overline{\Omega}-\Omega}{\rho_{\rm c}}\right] , \qquad\qquad \overline{\Lambda}_{\rm c} \equiv \arctan\left[\frac{\overline{\Omega}+\Omega}{\rho_{\rm c}}\right] , \tag{4.C.26}$$

in terms of which we can write

$$\begin{aligned} (\overline{\Omega}+\Omega)\rho_{\rm c}+i \ &= \ \sqrt{(\overline{\Omega}+\Omega)^2\rho_{\rm c}^2+1}\ e^{i\Lambda_{\rm c}} \ , \\ (\overline{\Omega}-\Omega)\rho_{\rm c}+i \ &= \ \sqrt{(\overline{\Omega}-\Omega)^2\rho_{\rm c}^2+1}\ e^{i\overline{\Lambda}_{\rm c}} \ , \end{aligned} \tag{4.C.27}$$

and d_1/d_2 takes the form

$$\frac{d_1}{d_2} \ = \ \frac{\sqrt{(\overline{\Omega}+\Omega)^2\rho_{\rm c}^2+1}}{\sqrt{(\overline{\Omega}-\Omega)^2\rho_{\rm c}^2+1}} \ \ e^{-2i\,\overline{\Omega}\,y_{\rm c}-i\Lambda_{\rm c}-i\overline{\Lambda}_{\rm c}} \ . \tag{4.C.28}$$

It is now straightforward to relate the value of ψ at $y=y_{\rm c}$ with the constant d_1 and to obtain the value of c at the pseudohorizon. We get

$$c(y_{\rm c}) \ = \ \frac{2\overline{\Omega}\,\sqrt{1+\rho_{\rm c}^2}}{\sqrt{(\overline{\Omega}+\Omega)^2\rho_{\rm c}^2+1}} \ \ d_1 \ e^{i\overline{\Omega}\,y_{\rm c}\,+\,i\Lambda_{\rm c}} \tag{4.C.29}$$

We choose the phase of $c(y_{\rm c})$ to vanish at $\rho=\rho_{\rm c}$. This requirement determines the phase of d_1, which must be of the form

$$d_1 \ = \ |d_1|\, e^{-i\overline{\Omega}\,y_{\rm c}\,-\,i\Lambda_{\rm c}} \ . \tag{4.C.30}$$

Moreover, since

$$|c(y_{\rm c})| \ = \ \frac{2\overline{\Omega}\,\sqrt{1+\rho_{\rm c}^2}}{\sqrt{(\overline{\Omega}+\Omega)^2\rho_{\rm c}^2+1}} \ |d_1| \ , \tag{4.C.31}$$

we can fulfill (2.B.15) with $w_0=1$ by choosing $|d_1|$ to be

$$|d_1| \ = \ \frac{\sqrt{1+\rho_{\rm c}^2}}{2\,\overline{\Omega}\,\Omega}\,\sqrt{(\overline{\Omega}+\Omega)^2\rho_{\rm c}^2+1} \ . \tag{4.C.32}$$

USC UNIVERSIDADE DE SANTIAGO DE COMPOSTELA

The value of $|d_2|$ can be obtained from (4.C.28)

$$|d_2| \,=\, \frac{\sqrt{1+\rho_{\rm c}^2}}{2\,\overline{\Omega}\,\Omega}\,\sqrt{(\overline{\Omega}-\Omega)^2\rho_{\rm c}^2+1}\;. \tag{4.C.33}$$

From these values of $|d_1|$ and $|d_2|$ one can readily check that the Joule heating q is given by

$$q \,=\, \Omega\,\bar{\Omega}\Big(\,|d_1|^2\,-\,|d_2|^2\,\Big) \,=\, (1+\rho_{\rm c}^2)\,\rho_{\rm c}^2\;, \tag{4.C.34}$$

in agreement with (2.B.21), as it should. Taking into account these results, we can write d_1 and d_2 as

$$\begin{aligned}
d_1 \,&=\, \frac{\sqrt{1+\rho_{\rm c}^2}}{2\,\overline{\Omega}\,\Omega}\,\sqrt{(\overline{\Omega}+\Omega)^2\rho_{\rm c}^2+1}\;\,e^{-i\overline{\Omega}\,y_{\rm c}\,-\,i\Lambda_{\rm c}} \,=\, \frac{\sqrt{1+\rho_{\rm c}^2}}{2\,\overline{\Omega}\,\Omega}\,\Big[(\overline{\Omega}+\Omega)\rho_{\rm c}-i\Big]\,e^{-i\overline{\Omega}\,y_{\rm c}}\;,\\
d_2 \,&=\, \frac{\sqrt{1+\rho_{\rm c}^2}}{2\,\overline{\Omega}\,\Omega}\,\sqrt{(\overline{\Omega}-\Omega)^2\rho_{\rm c}^2+1}\;\,e^{i\overline{\Omega}\,y_{\rm c}\,+\,i\overline{\Lambda}_{\rm c}} \,=\, \frac{\sqrt{1+\rho_{\rm c}^2}}{2\,\overline{\Omega}\,\Omega}\,\Big[(\overline{\Omega}-\Omega)\rho_{\rm c}+i\Big]\,e^{i\overline{\Omega}\,y_{\rm c}}\;,
\end{aligned} \tag{4.C.35}$$

and the complexified gauge potential $c(y)$ is given by

$$\begin{aligned}
c(y) \,=\, \frac{\sqrt{1+\rho_{\rm c}^2}}{2\,\overline{\Omega}\,\Omega\,\sin y}\Bigg[&\sqrt{(\overline{\Omega}+\Omega)^2\rho_{\rm c}^2+1}\;e^{i\overline{\Omega}\,(y-y_{\rm c})\,-\,i\Lambda_{\rm c}}\;+\\
&+\sqrt{(\overline{\Omega}-\Omega)^2\rho_{\rm c}^2+1}\;e^{-i\overline{\Omega}\,(y-y_{\rm c})\,+\,i\overline{\Lambda}_{\rm c}}\Bigg]\;.
\end{aligned} \tag{4.C.36}$$

This expression can also be rewritten as

$$c(y) \,=\, \frac{\sqrt{1+\rho_{\rm c}^2}}{2\,\overline{\Omega}\,\Omega\,\sin y}\Bigg[\Big[(\overline{\Omega}+\Omega)\rho_{\rm c}-i\Big]e^{i\overline{\Omega}\,(y-y_{\rm c})}\,+\,\Big[(\overline{\Omega}-\Omega)\rho_{\rm c}+i\Big]e^{-i\overline{\Omega}\,(y-y_{\rm c})}\Bigg]\;. \tag{4.C.37}$$

From (4.C.37) we can obtain the phase χ

$$\tan\chi(y) \,=\, \frac{\rho_{\rm c}\,\Omega\,\sin\Big[\overline{\Omega}(y-y_{\rm c})\Big]}{\rho_{\rm c}\,\overline{\Omega}\cos\Big[\overline{\Omega}(y-y_{\rm c})\Big]\,+\,\sin\Big[\overline{\Omega}(y-y_{\rm c})\Big]}\;. \tag{4.C.38}$$

Finally, we can expand this result near $\rho=\infty$ to obtain the electric field E

$$\begin{aligned}
E \,=\, -i\,\frac{\sqrt{1+\rho_{\rm c}^2}}{2\,\overline{\Omega}}\Bigg[&\sqrt{(\overline{\Omega}+\Omega)^2\rho_{\rm c}^2+1}\;e^{-i\overline{\Omega}\,(y_{\rm c}-\frac{\pi}{2})\,-\,i\Lambda_{\rm c}}\;+\\
&+\sqrt{(\overline{\Omega}-\Omega)^2\rho_{\rm c}^2+1}\;e^{i\overline{\Omega}\,(y_{\rm c}-\frac{\pi}{2})\,+\,i\overline{\Lambda}_{\rm c}}\Bigg]\;,
\end{aligned} \tag{4.C.39}$$

USC UNIVERSIDADE DE SANTIAGO DE COMPOSTELA

and the current j

$$j \;=\; -i\,\frac{\sqrt{1+\rho_{\rm c}^2}}{2\,\Omega}\left[\sqrt{(\overline{\Omega}+\Omega)^2\rho_{\rm c}^2+1}\;e^{-i\overline{\Omega}\,(y_{\rm c}-\frac{\pi}{2})\,-\,i\Lambda_{\rm c}}\;-\right.$$
$$\left.-\sqrt{(\overline{\Omega}-\Omega)^2\rho_{\rm c}^2+1}\;e^{i\overline{\Omega}\,(y_{\rm c}-\frac{\pi}{2})+i\bar{\Lambda}_{\rm c}}\right]\,. \qquad (4.C.40)$$

As a check one can verify that these results reduce to the ones obtained for Minkowski embeddings when we take $\rho_{\rm c}=y_{\rm c}=0$.

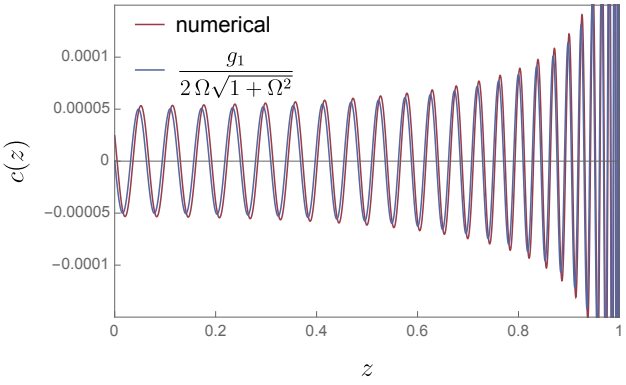


Figure 4.2: Comparison of the critical solution for c obtained by numerically solving the non-linear full equation of motion and (4.C.43) for $\Omega = 100$, $m = 1$ and $\epsilon = \frac{1}{2}$, using $z^2 = \frac{1}{1+\rho^2}$.

4.C.3 Critical embeddings

According to (2.B.15), and taking into account that critical solutions have $\rho_{\rm c}=0$, they must satisfy $\Omega\, b(\rho=0) \;=\; w_0^2$. Therefore, if we define the parameter ϵ as

$$\epsilon \;\equiv\; \Omega\, b(\rho=0)\;, \qquad (4.C.41)$$

these embeddings must satisfy $\epsilon = w_0^2$. In our linearised analysis we have $w_0=1$. Thus, we are tempted to describe the critical embeddings by means of the solution $g_1(\rho)$ of (4.C.1) with $\epsilon=1$. Indeed, contrary to the other solution $g_2(\rho)$, the function $g_1(\rho)$ is regular at $\rho=0$ and one can easily find ϵ as a function of Ω and the constant c_1

$$\epsilon \;=\; \Omega\, c_1\,\sqrt{1+\Omega^2}\;. \qquad (4.C.42)$$

Plugging this relation in (4.C.1), we get $c(\rho)$ as

$$c(\rho) \;=\; \frac{\epsilon}{\Omega\sqrt{1+\Omega^2}}\,g_1(\rho)\;. \qquad (4.C.43)$$

USC UNIVERSIDADE DE SANTIAGO DE COMPOSTELA

It turns out, however, that this linearised solution cannot describe accurately the critical embedding near $\rho = 0$. Indeed, we found in section 2.B.2 that the b field behaves linearly in ρ around its value at $\rho = 0$, whereas the function $g_1(\rho)$ behaves quadratically (see (4.2.6)). As argued in [31] for the analogous D3-D7 case, the critical solutions behave highly non-linearly around $\rho = 0$. Nevertheless the linear solution can describe rather accurately the true non-linear solution for $\rho \gg 1$ if we change the value of ϵ from its naive value $\epsilon = 1$. To illustrate this we compare the linear analytic solution for $\epsilon = 1/2$ with the numerical results. In figure 4.2 we plot the values of $c(\rho)$ calculated by these two procedures.

For a general value of ϵ, the electric field E, the current j and the condensate $\mathcal{C}$ in the linear approximation are

$$
\begin{aligned}
E &= -i\frac{\epsilon}{\sqrt{1+\Omega^2}}\sin\left(\frac{\pi}{2}\sqrt{1+\Omega^2}\right) , \\
j &= -\frac{\epsilon}{\Omega}\cos\left(\frac{\pi}{2}\sqrt{1+\Omega^2}\right) \\
\mathcal{C} &= -\frac{1}{4}\frac{\epsilon^2}{1+\Omega^2}\left(\pi + \frac{\sin\left(\pi\sqrt{1+\Omega^2}\right)}{\Omega^2\sqrt{1+\Omega^2}}\right) .
\end{aligned}
\tag{4.C.44}
$$

In figure 4.3 we compare the approximate linear expressions (4.C.44) for E and $\mathcal{C}$ (again for $\epsilon = 1/2$) to the numerical result of the full non-linear calculation. A reasonable agreement for large Ω is found. The discrepancies can be attributed to the intrinsic non-linearity of the critical solutions. In particular, eq. (4.C.44) implies that the critical electric field decreases as $(\Omega/m)^{-1}$ for large Ω/m.

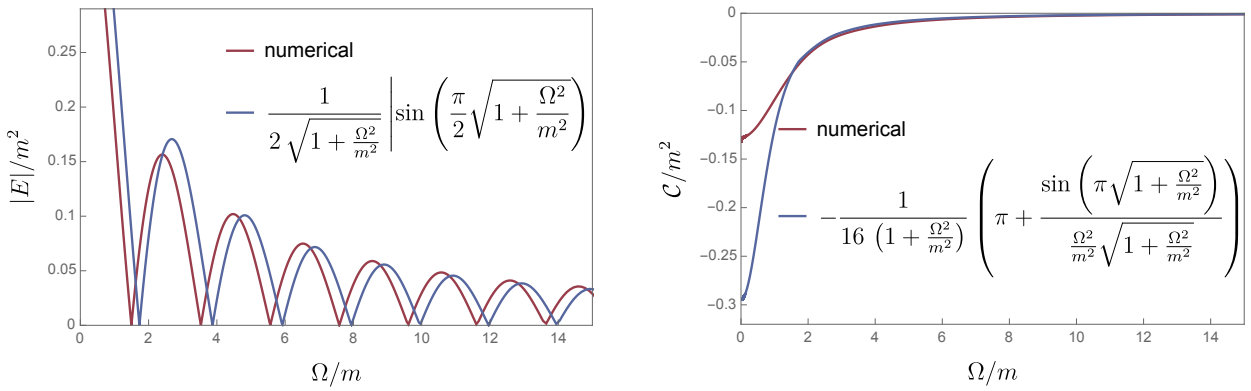


Figure 4.3: E and $\mathcal{C}$ for critical solutions obtained numerically and using (4.C.44) with $\epsilon = 1/2$.

USC
UNIVERSIDADE DE SANTIAGO DE COMPOSTELA

USC
UNIVERSIDADE
DE SANTIAGO
DE COMPOSTELA

5 Some final remarks

We have pursued, along the line of previous works [30, 31], the study of holographic Floquet flavor systems driven by an external rotating electric field. We focus on the D3/D5 system but we find that most of the results are qualitatively robust and shared by the D3/D7 setup. Besides, we analyzed the finite temperature effects.

The system can be in two phases (insulator and conductor) depending on the type of embedding of the probe brane. In agreement with the (3+1)-dimensional results of [30, 31] we have found that for certain frequencies the driving field resonates with the vector meson excitations of the gauge theory and gives rise to zero field Floquet resonances. The lobbed structure shown in Fig. 3.1 may be a universal feature.

Many distinguishing features are present for configurations approaching the critical line separating the conducting from the isolating phase. The strong enhancement of the oscillations deforming into sharp peaks is one such. These peaks seem to point to bound states that are shifted from the meson masses. At this point, a very relevant question is that of stability of the embeddings. The exact point where, say, Black Hole embeddings decay into Minkowski embeddings and viceversa is a problem that can be addressed in equilbrium thermodynamics, and has a practical answer in terms of the equal area law. Here however, the similar tools are not available from a would be periodic thermodynamics [151], and this certainly an important aspect that will need further study in the future.

We studied the effects of having the system heated at some non-zero temperature. In this case, the dual geometry has two types of horizons: the usual event horizon of the closed string geometry in the bulk, and the effective horizon of the open string metric on the brane. Respectively, we can associate two temperatures to them: the Hawking temperature T of the background (see (2.1.4)) and the effective one T_{eff} written in (2.1.13) experienced by the worldsheet degrees of freedom. We have scanned throughout all our phase space and checked that $T_{\text{eff}} > T$.

The main effect of the background temperature is the addition of deconfined charged carriers to the system. Such carriers add to the ones produced by the electric field through the Schwinger mechanism of dielectric breakdown. We show that one of the main results in previous works, namely, the presence of vector meson Floquet condensates, persists at finite temperature, signaling the robustness of this non-perturbative effect. The lobbed structure

USC DE SANTIAGO

of the line of critical embeddings is also found here, but gets depleted in height and is completely washed away for high enough values of the temperature, namely, for a radius horizon $r_{\rm h}/m \geq 0.8897$ in units of the quark mass (see Fig. 3.1).

At high temperatures, some interesting effects occur when the background and effective horizons come close together. These include a multi-valuedness that resemble a secondary phase transition within the conductive black hole phase (Fig. 3.2). Also new solutions with vanishing $|E| = |j| = 0$ appear within this phase (Fig. 3.3).

On the other hand, we have remarked the relevance of the so called *Floquet suppression points*. These states were missed in previous analysis but are common to both D3/D5 and D3/D7 systems both at zero and finite temperature. We have shown that the phase portrait very close to these points is strikingly similar to the one in the vicinity of the vector meson Floquet condensates, up to an exchange of j with E. This calls for a deeper study in search for a sounder duality. From the physical point of view, these new points exhibit a dynamical suppression of the vacuum polarizability. It could be attributed to a dynamical screening of the effective dipole charge of the meson fluctuations at strong coupling and for precise frequencies. It bears resemblance to similar effects in the realm of Floquet condensed matter systems where, for example, hopping terms can be seen to vanish at fined tuned frequencies of the driving (see section 1.5.2). This is the type of effects that make Floquet driving an appealing paradigm in the search for mechanisms that could help in suppressing quantum decoherence.

Moreover, we have analised the non-linear rotating conductivity in section 3.2.1. The relative phase (angle) between j and E has an interesting information that we interpret in terms of a possible variable admixture of two types of currents: rotating polarization and charge flow. The polarization current is the only one present in the Minkowski phase while both are present in the BH states. The global picture that emerges from the analysis, shows that the Floquet suppressed states are points where the polarizability of the vacuum switches smoothly from positive to negative. This is remarkable as it states that, for ample intervals in the range of driving frequencies, Ω, the meson condensate is polarised *antiparallel* to the applied electric field! Again here, this result is amongst the class of remarkable effects that one can find in the context of Floquet engineering [16] of condensed matter systems. For example, it is worth citing ref. [152], where paramagnetism can be turned into diamagnetism under a strong driving in the Rabi model coupled to a heat bath.

In the limit of large electric field, and/or large temperature, we agree with the results in [33]. In this limit the polarization rotating current gets suppressed, $j_{\rm pol}(t) \to 0$, whereas the conduction currect satisfies an Ohmic instantaneous response for an arbitrary frequency of the rotating driving $j(t) \sim j_{\rm con}(t) = \sigma E(t)$ with σ a real constant. Linearity suggests the possibility of this being also true for any electric field time dependence in 2+1 dimensions.

Last but not least, we have investigated the AC and DC conductivities. Transport properties are an important benchmark, and they exhibit substantial differences in the two dimensionalities. In (2+1) dimensions, the massless case turns out to be trivial. In the massive situation, however, the conductivity tensor exhibits a rich structure. We have payed special attention to the first resonant frequency $\Omega = \Omega_{\rm c} = 1.4965$ which is close to the meson mass frequency. In this situation the system creates efficiently charged carriers and holes. In ex-

perimental setups, the asymmetry in the electron-hole pairs for different chiralities gives rise to the so called “optically induced valley polarization". This might be the closest physical realization to our setup at the resonant point. Whether or not the double peak structure observed in Fig: 3.10 may have some meaning in this direction is something that deserves further scrutiny. Otherwise, it would probably mean this model is too crude to capture the chiral asymmetry in the splitting of the Dirac point.

This interesting pattern with peaks deep inside the wedges between the lobes in phase space still exists for low to moderate temperatures, but gets dissolved as soon as the height of the lobes is depleted at high temperature. The highest peaks shift with growing $|E|$ and stay close to the position of the (also drifting) Floquet suppression points. However we haven't found exact numerical agreement, so this stays a qualitative observation. We also find agreement with the predictions in [33] in the limit of small mass.

Our work could be continued along several directions. The comparison of our results with the D3-D7 model points towards some universality in the phase space. To strengthen this point, a natural strategy is to extend the study to other brane setups. Most prominently, the (2+1) dimensional ABJM model is an example of superconformal QFT with a well stablished gravity dual [153]. The flavor branes in this case are D6-branes [154, 155] (see [156] for an analysis of the thermodynamics of the flavor branes in ABJM). The ABJM supergravity background has a non-trivial topological structure which allows to switch on fluxes of the gauge fields and realise the quantum Hall effect [157]. This suggests that it could be the right place to find non-trivial topological effects induced by an external driving in an holographic setup like the ones we are missing here.

Another direction worth pushing is to consider other types of drivings. The brane picture of gauge theories allow for several possibilities. For example, instead of an electric field we could consider a magnetic field, or let the brane oscillate periodically. This type of configurations were considered in [62, 158], and are the natural setup to find resonances that could be interpreted as Floquet condensates of other type of mesons, like scalar mesons.

One could also study the effects of backreaction for a large number of flavor branes. Interestingly, backreacted D3-D5 backgrounds have been constructed in [76–78] using the smearing approximation. Furthermore, in part II of this thesis we will construct another one.

Finally, another aspect that deserves further attention is the actual nature of the phase transition. It can be triggered by an admixture of both temperature and/or electric field. While the multi-valuedness of the state curves in Fig. 3.2 suggest an area law for the transition point, the actual location it is not consistent for the $(|j|/m^2, |E|/m^2)$ and the $(\mathcal{C}, |E|/m^2)$ curves. This points to the difficulties, out of equilibrium, in defining a *bona fide* free energy from which the 1-point functions are derived [140]. Techniques developed specifically for open non equilibrium steady states should be used instead. In particular, it would be very interesting to apply the Schwinger-Keldysh approach of [159,160] to these systems in order to calculate properties of the corresponding steady states like equilibrium of phases and phase transitions.

USC
UNIVERSIDADE
DE SANTIAGO
DE COMPOSTELA

USC
UNIVERSIDADE
DE SANTIAGO
DE COMPOSTELA

Part II

Black holes in the backreacted flavored D3/D5 system

USC
UNIVERSIDADE
DE SANTIAGO
DE COMPOSTELA

USC
UNIVERSIDADE
DE SANTIAGO
DE COMPOSTELA

6 Overview and holographic setup

We present in this chapter a top-down holographic dual that realises a system with finite quark density and spatial anisotropy, and could then be applied to model systems with those characteristics.

The proposed supergravity background is based on a low energy limit of D-brane intersections. As introduced in 1.3, we will be dealing with two classes of branes: color and flavor branes. The anisotropy will then be naturally induced in the system as a result of the different orientation of the intersecting stacks.

On the one hand, we will consider N_c color D3-branes placed at the tip of a cone over a five-dimensional Sasaki-Einstein space and containing the color degrees of freedom that are dual to the supergravity fluxes. The second class of branes will be N_f flavor D5 branes, dual to degrees of freedom transforming in the fundamental representation of the gauge group. Besides, we will assume $N_f \sim N_c$, so that the probe approximation breaks down and it is necessary to take into account the backreaction of the flavor branes on the geometry.

In particular, we will study an intersection in which the flavor branes share two spatial directions with the color branes, giving rise to an anisotropy between the two common spatial directions and the third one, as promised. The field theory dual to this configuration is well-known and consists of a theory with hypermultiplets living in a $(2+1)$-dimensional defect, coupled to the ambient four-dimensional super Yang-Mills theory [110, 134, 161].

We construct the (backreacted) geometry for this D3-D5-brane intersection by using the smearing technique outlined in 1.3.2, which is accurate in the Veneziano limit. Specifically, the D5-branes are smeared both in the cartesian direction orthogonal to the defect and on the internal directions and, therefore, this configuration is dual to a system of multiple $(2+1)$-dimensional layers in a $(3+1)$-dimensional ambient gauge theory. For vanishing quark density, the supersymmetric ten-dimensional supergravity equations corresponding to this multilayer setup were first introduced in [76] and further studied in [77–81]. However, in this case we present a different branch of solutions, that can be continuously connected with flavorless backgrounds.[1]

We find a background that solves the equations of motion of ten-dimensional type IIB

[1] In [77–81] the limit $N_f \to 0$ is singular, a blight which however does not blemish the applicability of finite flavor solutions.

USC SANTIAGO DE COMPOSTELA

supergravity with (smeared) D5-brane sources. The corresponding metric has a horizon, which means that our solution is a black hole that is dual to a field theory at non-zero temperature. Moreover, since our sources are dynamical objects, rather than fluxes, they have a worldvolume action which can contain a gauge field. This feature can be used to construct gravity duals of gauge theories at non-zero baryon density.[2]

Indeed, as was shown in [162, 163] for the D3-D7 system in the probe approximation, in order to introduce a non-vanishing baryon density, one should switch on a radially dependent time component of a gauge potential on the worldvolume of the flavor brane. To obtain the backreacted geometry we have to determine how the ten-dimensional metric and fluxes of type IIB supergravity are modified by the presence of this gauge field in the DBI plus WZ action.

This part is organised as follows. In what remains of this chapter we present our ansatz for the different fields of type IIB supergravity. The equations of motion are derived in detail in appendix 6.A. These equations are complicated and we have not been able to integrate them analytically. Instead, we followed the same procedure as in refs. [87, 88] and found a perturbative solution at first order in certain expansion parameters, reviewed in chapter 7. In section 7.1 we present our solution in the case in which the chemical potential vanishes. Details of the calculations leading to this results are given in appendix 7.A. The solution found is first-order in an expansion in a temperature dependent parameter, proportional to $\lambda^{\frac{1}{2}}\, n_{\rm f}/(N_{\rm c}\, T)$, where λ is the 't Hooft coupling, $n_{\rm f}$ is the density of flavors per unit length in the direction orthogonal to the defects, and T is the temperature.

In section 7.2 we continue to the case of nontrivial gauge potential and thereby present the solution with nonzero chemical potential at finite temperature. The calculations are detailed in appendix 7.B. In this case the solution is (doubly) perturbative. The expansion parameters are the one we introduced above for zero chemical potential plus another one proportional to $\lambda^{\frac{1}{2}}\, n_{\rm b}^2/(N_{\rm c}\, n_{\rm f}\, T^5)$, where $n_{\rm b}$ is the baryon density per unit volume.

In section 7.3 we analyze the thermodynamic properties of the background. We first compute the temperature and entropy and then we obtain the internal energy density by calculating the ADM energy of the background. In order to completely characterise the anisotropic thermodynamics of our model we employ the formalism of [164], which requires introducing a brane potential that measures the energy cost of adding flavor branes in the system. This analysis allows us to compute the pressures and the speeds of sound along the different field theory directions. Moreover, we check these results by computing directly the vacuum expectation value of the stress-energy tensor and the Euclidean on-shell action.

Chapter 8 is devoted to the calculation of several observables. First of all we calculate the hydrodynamic coefficients in the shear channel at zero quark density. The calculation requires dealing with the dimensionally reduced theory. The dimensionally reduced action was derived in [77] and is reviewed in appendix 8.A, where the detailed calculation of the hydrodynamic transport coefficients is performed. In section 8.2 we compute the quark-antiquark potentials in directions parallel and orthogonal to the D5-brane layers. Similarly,

[2] We identify the baryon symmetry with the $U(1)$ that acts equally at each defect D5-brane on the fields localised there. Due to the smearing, this effectively becomes a global $U(1)$ symmetry in 3+1 dimensions.

in section 8.3 we calculate the entanglement entropy of parallel and orthogonal slabs.

Finally, in chapter 9 we summarise our results and discuss possible extensions and further applications of our work.

6.1 D3/D5 system in the unquenched approximation

In this section we will briefly describe our general ten-dimensional background geometry. The specific characteristics of our ansatz are presented in the subsequent sections, while the details of the calculations are relegated to the appendices.

Our top-down model is based on the following array representing the intersection of $N_{\rm c}$ D3-branes and $N_{\rm f}$ D5-branes:

$$\begin{array}{rccccccccc} & 1 & 2 & 3 & 4 & 5 & 6 & 7 & 8 & 9 \\ (N_{\rm c})\ \text{D3}: & \times & \times & \times & \cdot & \cdot & \cdot & \cdot & \cdot & \cdot \\ (N_{\rm f})\ \text{D5}: & \times & \times & \cdot & \times & \times & \times & \cdot & \cdot & \cdot \end{array} \tag{6.1.1}$$

The branes are extended in directions marked by $\times$ and localised otherwise. In (6.1.1) the D3-branes are color branes which, in the absence of the D5-branes, generate the $AdS_5 \times \mathcal{M}_5$ geometry dual to a supersymmetric Yang-Mills theory in four dimensions. In the following we will assume that $\mathcal{M}_5$ is a compact Sasaki-Einstein manifold and, therefore, the D3-branes are placed at the tip of a six-dimensional cone over $\mathcal{M}_5$.

The D5-branes are flavor branes dual to matter hypermultiplets living in (2+1)-dimensional defects of the ambient (3+1)-dimensional theory. We want to obtain a black hole geometry incorporating the backreaction of the flavor branes. We will assume that $N_{\rm f}$ is large and, following the approach reviewed in [86], we will consider a continuous distribution of flavor branes. The total action of the system is the sum of the one corresponding to ten-dimensional type IIB supergravity action $S_{\rm IIB}$ and the action of the branes

$$S \,=\, S_{\rm IIB} + S_{\rm branes}\ . \tag{6.1.2}$$

The ten-dimensinal metric g, the dilaton ϕ, the Ramond-Ramond (RR) forms F_1, F_3, and F_5 and the Neveu-Schwarz (NS) three-form H_3 enter in the supergravity action

$$\begin{aligned} S_{\rm IIB} \,=\, \frac{1}{2\kappa_{10}^2}\int {\rm d}^{10}x\sqrt{-g}\Big(R - \frac{1}{2}(\partial\phi)^2 - \frac{e^{-\phi}}{2\cdot 3!}H_3^2 - \frac{e^{2\phi}}{2}F_1^2 - \frac{e^{\phi}}{2\cdot 3!}F_3^2 - \frac{1}{4\cdot 5!}F_5^2\Big) \\ -\frac{1}{2\kappa_{10}^2}\int \frac{1}{2}C_4\wedge H_3\wedge F_3\ , \end{aligned} \tag{6.1.3}$$

and $S_{\rm branes}$ is the sum of the Dirac-Born-Infeld (DBI) and Wess-Zumino (WZ) action of the flavor D5-branes

$$S_{\rm branes} \,=\, -T_5\sum_{N_{\rm f}}\int_{\mathcal{M}_6}{\rm d}^6\xi e^{\frac{\phi}{2}}\sqrt{-\det\big(\hat{g} - e^{-\frac{\phi}{2}}\mathcal{F}\big)} \,+\, S_{\rm WZ}\ . \tag{6.1.4}$$

USC UNIVERSIDADE DE SANTIAGO DE COMPOSTELA

In (6.1.4) $\hat{g}$ is the pullback of the ten-dimensional metric to the D5-brane worldvolume, $\mathcal{F} = \hat{B}_2 + F$, where $\hat{B}_2$ is the pullback of the two-form potential for H_3 ($H_3 = \mathrm{d}F_2$) and the two-form $F = \mathrm{d}A$ is the worldvolume gauge field strength. Moreover, the WZ term S_{WZ} can be written as

$$S_{\mathrm{WZ}} \,=\, T_5 \int \Xi \wedge \left(C_6 - C_4 \wedge \mathcal{F} + \frac{1}{2!}\, C_2 \wedge \mathcal{F} \wedge \mathcal{F} - \frac{1}{3!}\, C_0\, \mathcal{F} \wedge \mathcal{F} \wedge \mathcal{F} \right) , \tag{6.1.5}$$

where C_i ($i = 0, 2, 4, 6$) are RR potentials and the four-form Ξ is the so-called smearing form, which encodes the distribution of the D5-brane charge of the stack of flavor branes. The ten-dimensional gravitational constant in (6.1.3) and the D5-brane tension in (6.1.4) and (6.1.5) are given by

$$2\,\kappa_{10}^2 \,=\, (2\pi)^7\, g_{\mathrm{s}}^2\, \alpha'^4 \qquad , \qquad T_5 \,=\, \frac{1}{(2\pi)^5\, g_{\mathrm{s}}\, \alpha'^3} \ , \tag{6.1.6}$$

with g_{s} and α' being the string constant and the Regge slope, respectively.

Let us now specify our ansatz to solve the equations of motion stemming from the action (6.1.2). The ten-dimensional metric in Einstein frame is written as

$$\begin{aligned} \mathrm{d}s_{10}^2 \,=\, h^{-\frac{1}{2}} \Big[- b\, \mathrm{d}t^2 \,+\, \mathrm{d}x_1^2 \,+\, \mathrm{d}x_2^2 \,+\, \alpha^2\, \mathrm{d}x_3^2 \Big] \\ + h^{\frac{1}{2}} \left[\frac{G^2}{b}\, \mathrm{d}\rho^2 \,+\, S^2\, \mathrm{d}s_{\mathrm{KE}}^2 \,+\, F^2\, (\mathrm{d}\tau + \mathcal{A})^2 \right] , \end{aligned} \tag{6.1.7}$$

where all the functions h, b, α, G, S, and F depend on the non-compact holographic radial coordinate ρ; the boundary, corresponding to the UV, is at $\rho \to \infty$. Notice that the third cartesian coordinate x_3 is distinguished from x_1 and x_2. This anisotropy along the gauge theory directions is to be expected from the brane setup (6.1.1).

The function $G(\rho)$ in the metric (6.1.7) can be chosen at will by selecting the radial coordinate ρ. It is quite convenient to choose the gauge in which $G(\rho)$ is related to the other functions of the metric as

$$G \,=\, \frac{b\, \alpha\, S^4\, F}{\rho\, (\rho^4 - \rho_{\mathrm{h}}^4)} \ , \tag{6.1.8}$$

where ρ_{h} is a constant corresponding to the radius the event horizon of the black hole. Indeed, the blackening function $b(\rho)$ vanishes at $\rho = \rho_{\mathrm{h}}$ and the Hawking temperature of the black hole can be obtained from the surface gravity, and it is given by

$$T \,=\, \frac{1}{2\pi} \frac{1}{\sqrt{g_{\rho\rho}}} \frac{\mathrm{d}}{\mathrm{d}\rho} \left(\sqrt{-g_{tt}} \right) \Big|_{\rho \to \rho_{\mathrm{h}}} = \frac{1}{4\pi\, G(\rho_{\mathrm{h}})}\, \partial_\rho \Big(b h^{-\frac{1}{2}} \Big) \Big|_{\rho = \rho_{\mathrm{h}}} . \tag{6.1.9}$$

Let us now describe the internal part of the metric (6.1.7). Before adding the deformation induced by the flavor branes, the internal space is a five-dimensional Sasaki-Einstein (SE) manifold $\mathcal{M}_5$, whose line element can be written as a $U(1)$-bundle over a Kähler-Einstein (KE) space $\mathcal{M}_4$: $\mathrm{d}s_{\mathrm{SE}}^2 \,=\, \mathrm{d}s_{\mathrm{KE}}^2 + (\mathrm{d}\tau + \mathcal{A})^2$. Let $\{e^i\}$, $i = 1, \ldots, 4$, be a canonical basis of

vielbein one-forms for the KE space ($\mathrm{d}s^2_{\mathrm{KE}} = \sum_i (e^i)^2$). In this basis the Kähler two-form J_{KE} of $\mathcal{M}_4$ is

$$J_{\mathrm{KE}} = e^1 \wedge e^2 + e^3 \wedge e^4 \ , \tag{6.1.10}$$

and is related to the one-form $\mathcal{A}$ of the metric (6.1.7) as $J_{\mathrm{KE}} = \mathrm{d}\mathcal{A}/2$. Let us next define the two-form $\hat{\Omega}_2$ as

$$\hat{\Omega}_2 = e^{3i\tau}\Big(e^1 + ie^2) \wedge (e^3 + ie^4) \ . \tag{6.1.11}$$

We will use the real and imaginary parts of $\hat{\Omega}_2$ in our ansatz for the RR forms F_5 and F_3. They satisfy

$$\mathrm{d}\,\mathrm{Re}\,(\hat{\Omega}_2) = -3\,\mathrm{Im}(\hat{\Omega}_2) \wedge (\mathrm{d}\tau + \mathcal{A}) \ , \qquad \mathrm{d}\,\mathrm{Im}\,(\hat{\Omega}_2) = 3\,\mathrm{Re}(\hat{\Omega}_2) \wedge (\mathrm{d}\tau + \mathcal{A}) \ . \tag{6.1.12}$$

We are now ready to write our ansatz for the different forms of the type IIB background. First of all, we will take $F_1 = H_3 = 0$. Moreover, the RR five-form F_5 can be decomposed as

$$F_5 = F_5^{(0)} + F_5^{\mathrm{cp}} + \star F_5^{\mathrm{cp}} \ , \tag{6.1.13}$$

where $\star$ is the ten-dimensional Hodge star operator and $F_5^{(0)}$ is the standard five-form sourced by the D3-branes

$$F_5^{(0)} = K(\rho)(1+\star)\,\mathrm{d}^4x \wedge \mathrm{d}\rho \ . \tag{6.1.14}$$

We will require that $F_5^{(0)}$ is a closed form, which in turn implies that the function $K(\rho)$ must be related to the other functions of the metric as

$$K = Q_{\mathrm{c}}\,\frac{b\,\alpha^2}{h^2\,\rho(\rho^4 - \rho_{\mathrm{h}}^4)} \ , \tag{6.1.15}$$

with Q_{c} being a constant. Using standard arguments to quantise the flux of F_5, we can relate the constant Q_{c} to the number of color D3-branes N_{c} as

$$Q_{\mathrm{c}} = \frac{(2\pi)^4\,g_{\mathrm{s}}\,\alpha'^2\,N_{\mathrm{c}}}{\mathrm{Vol}\Big(\mathcal{M}_5\Big)} \ . \tag{6.1.16}$$

In order to construct a gravity dual of a flavored theory with non-zero chemical potential we need to have a non-vanishing worldvolume gauge field A of the form

$$A = A_t(\rho)\,\mathrm{d}t \ . \tag{6.1.17}$$

This worldvolume gauge field acts as a source of the RR forms due to the coupling of A to the RR potentials in the WZ action (6.1.5). In particular, the presence of the worldvolume gauge field (6.1.17) induces extra components of F_5 that should be added to $F_5^{(0)}$ as in (6.1.13). As our ansatz, we will take (below cp stands for chemical potential)

$$F_5^{\mathrm{cp}} = \mathrm{d}C_4^{\mathrm{cp}} \ , \tag{6.1.18}$$

USC UNIVERSIDADE DE SANTIAGO DE COMPOSTELA

where the four-form $C_4^{\rm cp}$ depends on a new function $J(\rho)$ and is given by

$$C_4^{\rm cp} = J(\rho)\mathrm{d}x^1 \wedge \mathrm{d}x^2 \wedge \mathrm{Re}(\hat{\Omega}_2) \ . \tag{6.1.19}$$

We will also adopt the following ansatz for the RR three-form F_3

$$F_3 = Q_{\rm f}\, \mathrm{d}x^3 \wedge \mathrm{Im}(\hat{\Omega}_2) \ + \ F_{123}\, \mathrm{d}x^1 \wedge \mathrm{d}x^2 \wedge \mathrm{d}x^3 \ , \tag{6.1.20}$$

where F_{123} is constant. The first term in (6.1.20) enforces the violation of the Bianchi identity which, according to the WZ action (6.1.5), takes the form

$$\mathrm{d}F_3 \ = \ 2\kappa_{10}^2\, T_5\, \Xi \ . \tag{6.1.21}$$

By using (6.1.12) we can find the explicit expression of the smearing form Ξ, namely

$$2\kappa_{10}^2 T_5\, \Xi = -3 Q_{\rm f}\, \mathrm{d}x^3 \wedge \mathrm{Re}(\hat{\Omega}_2) \wedge (\mathrm{d}\tau + \mathcal{A}) \ . \tag{6.1.22}$$

Notice that Ξ has the same form as the one introduced in [76] to smear massless flavors. The component of F_3 proportional to F_{123} in (6.1.20) is needed in order to satisfy the equations of motion when the worldvolume gauge field (6.1.17) is present. A similar term was introduced in [88] in the D3-D7 system.

Notice that Ξ determines the D5-brane charge distribution of the smeared stack of flavor branes. As the four-form Ξ does not depend on the coordinate x^3, although it contains $\mathrm{d}x^3$ in its expression, our stack of flavor branes is a homogeneous continuous distribution of D5-branes along the x^3-direction, which is dual to a system of multiple (2+1)-dimensional layers. As shown in [78], the parameter $Q_{\rm f}$ is proportional to the density of smeared branes along the x^3-direction. The precise relation between $Q_{\rm f}$ and this density depends on the internal Sasaki-Einstein manifold $\mathcal{M}_5$. If we distribute $N_{\rm f}$ D5-branes along a distance L_3 in the third cartesian direction, we can define the density of flavor branes $n_{\rm f}$ as

$$n_{\rm f} \ = \ \frac{N_{\rm f}}{L_3} \ . \tag{6.1.23}$$

The D5-branes wrap a two-dimensional submanifold $\mathcal{M}_2$ within the five-dimensional compact manifold $\mathcal{M}_5$. Let us define the transverse volume $v_\perp$ of $\mathcal{M}_2$ as the ratio

$$v_\perp \ = \ \frac{\mathrm{Vol}(\mathcal{M}_5)}{\mathrm{Vol}(\mathcal{M}_2)} \ . \tag{6.1.24}$$

Then, $Q_{\rm f}$ is just given by

$$Q_{\rm f} \ = \ \frac{2\pi^2\, g_{\rm s}\, \alpha'}{3}\, \frac{n_{\rm f}}{v_\perp} \ . \tag{6.1.25}$$

Interestingly, $Q_{\rm f}$ can be rewritten as

$$Q_{\rm f} \ = \ \frac{2\kappa_{10}^2\, T_5}{3!}\, \frac{n_{\rm f}}{v_\perp} \ , \tag{6.1.26}$$

USC UNIVERSIDADE DE SANTIAGO DE COMPOSTELA

and it is just proportional to the ratio between the tension of the D5-brane and the gravitational constant $(2\kappa_{10}^2)^{-1}$. When $\mathcal{M}_5 = \mathbb{S}^5$, the embedding of the D5-branes has been analyzed in detail in [78], where it was shown that

$$Q_{\rm f}(\mathbb{S}^5) \,=\, \frac{4\pi\, g_{\rm s}\, \alpha'\, n_{\rm f}}{9\sqrt{3}}\ . \tag{6.1.27}$$

Similarly, one can study the embeddings in the case in which $\mathcal{M}_5 = T^{1,1}$, leading to the result

$$Q_{\rm f}(T^{1,1}) \,=\, \frac{3\pi\, g_{\rm s}\, \alpha'\, n_{\rm f}}{8}\ . \tag{6.1.28}$$

The equations of motion for our ansatz are worked out in appendix 6.A. In chapter 7 we present our solutions of these equations.

USC
UNIVERSIDADE
DE SANTIAGO
DE COMPOSTELA

USC
UNIVERSIDADE
DE SANTIAGO
DE COMPOSTELA

Appendices for chapter 6

6.A Equations of motion

In this appendix we write down in detail the equations of motion for the total action (6.1.2), as well as the resulting equations for the different functions of our ansatz. Let us begin by writing the equations satisfied by the forms, which are [165]

$$\begin{aligned}
\mathrm{d}\Big(e^{2\phi}\star F_1\Big) + e^{\phi} H_3\wedge\star F_3 - \frac{1}{3}\kappa_{10}^2 T_5\,\Xi\wedge\mathcal{F}\wedge\mathcal{F}\wedge\mathcal{F} &= 0\\
\mathrm{d}\Big(e^{\phi}\star F_3\Big) - F_5\wedge H_3 + \kappa_{10}^2\,T_5\,\Xi\wedge\mathcal{F}\wedge\mathcal{F} &= 0\\
\mathrm{d}\star F_5 - H_3\wedge F_3 - 2\kappa_{10}^2 T_5\,\Xi\wedge\mathcal{F} &= 0\\
\mathrm{d}\Big(e^{-\phi}\star H_3\Big) + F_5\wedge F_3 + e^{\phi}\star F_3\wedge F_1 - 2\kappa_{10}^2\,\delta_{\mathcal{F}} S_{\text{branes}} &= 0\ . \qquad (6.A.1)
\end{aligned}$$

Notice that the last term in the equations (6.A.1) is due to the brane sources. The equations of motion for the RR forms contain the smearing form Ξ since they are coupled to the D5-brane through the WZ term (6.1.5). The last term in the equation for H_3 in (6.A.1) is an eight-form which arises from the smeared DBI term of the brane action. Its expression is given below in (6.A.15). The RR forms have to satisfy the Bianchi identities, namely

$$\begin{aligned}
\mathrm{d}F_1 &= 0\\
\mathrm{d}F_3 - H_3\wedge F_1 - 2\kappa_{10}^2 T_5\,\Xi &= 0\\
\mathrm{d}F_5 - H_3\wedge F_3 - 2\kappa_{10}^2 T_5\,\Xi\wedge\mathcal{F} &= 0\ , \qquad (6.A.2)
\end{aligned}$$

where the NSNS three-form is such that $\mathrm{d}H_3 = 0$. The equation for the dilaton is given by

$$\Box\phi = e^{2\phi}F_1^2 + \frac{1}{2\cdot 3!}e^{\phi}F_3^2 - \frac{1}{2\cdot 3!}e^{-\phi}H_3^2 - \frac{2\kappa_{10}^2}{\sqrt{-g}}\frac{\delta S_{\text{branes}}}{\delta\phi}\ . \qquad (6.A.3)$$

In addition, we have to impose Einstein equations, which are also written below in (6.A.17), but we first need to introduce our ansatz for the metric.

USC DE SANTIAGO

We will consider solutions for which

$$F_1 \,=\, 0\,, \qquad\qquad H_3 \,=\, 0\ . \tag{6.A.4}$$

It is convenient to write the equations of motion in terms of a new radial coordinate σ, related to the ρ coordinate used in the main text as

$$e^{4\rho_{\rm h}^4\sigma} = 1 - \frac{\rho_{\rm h}^4}{\rho^4}\ . \tag{6.A.5}$$

In terms of σ, our metric ansatz (6.1.7) takes the form

$$\begin{aligned} {\rm d}s_{10}^2 \;&=\; h^{-\frac{1}{2}}\left[-b\,({\rm d}t)^2+({\rm d}x^1)^2+({\rm d}x^2)^2+\alpha^2({\rm d}x^3)^2\right] \\ &\quad +h^{\frac{1}{2}}\left[b\,\alpha^2 S^8F^2{\rm d}\sigma^2+S^2{\rm d}s_{\rm KE}^2+F^2({\rm d}\tau+\mathcal{A})^2\right]\,, \end{aligned} \tag{6.A.6}$$

where the radial functions h, b, α, F, and S should be understood as functions of σ through the change of variables (6.A.5). The ansatz for the RR three-form F_3 has been written in (6.1.20), whereas F_5 can be readily obtained from (6.1.13)-(6.1.19), and is given by

$$\begin{aligned} F_5 \;&=\; Q_{\rm c}\frac{b\,\alpha^2}{h^2}\,(1+\star){\rm d}^4x\wedge{\rm d}\sigma+(1+\star)\partial_\sigma J(\sigma){\rm d}\sigma\wedge{\rm d}x^1\wedge{\rm d}x^2\wedge{\rm Re}(\hat{\Omega}_2) \\ &\quad -3J(\sigma)(1+\star){\rm d}x^1\wedge{\rm d}x^2\wedge{\rm Im}(\hat{\Omega}_2)\wedge({\rm d}\tau+\mathcal{A})\ . \end{aligned} \tag{6.A.7}$$

The Bianchi identity for F_5 gives the following differential equation for J

$$\partial_\sigma^2 J - 4\frac{\partial_\sigma S}{S}\,\partial_\sigma J - 9\,\alpha^2 b\,S^8 J + 3\,Q_{\rm f}\,S^4\,\partial_\sigma A_t = 0\ , \tag{6.A.8}$$

where we have used the expression (6.1.22) of the smearing form Ξ and an ansatz for the worldvolume gauge field strength $\mathcal{F}$, which in the σ coordinate takes the form

$$\mathcal{F} = {\rm d}A = \partial_\sigma A_t(\sigma){\rm d}\sigma\wedge{\rm d}t\ . \tag{6.A.9}$$

Let us now write down in detail the equation (6.A.3) for the dilaton. To compute the last term in this equation we need to know the expression for the smeared DBI action. With this purpose, we define the modulus $|\Xi|$ of the smearing form as

$$|\Xi| = \sqrt{\frac{1}{4!}\Xi_{\alpha_1\alpha_2\alpha_3\alpha_4}\Xi_{\beta_1\beta_2\beta_3\beta_4}g^{\alpha_1\beta_1}g^{\alpha_2\beta_2}g^{\alpha_3\beta_3}g^{\alpha_4\beta_4}}\ . \tag{6.A.10}$$

Using (6.1.22), we get

$$|\Xi| \;=\; \frac{3\,Q_{\rm f}}{\sqrt{2}\,\kappa_{10}^2\,T_5}\,\frac{1}{\sqrt{h}\,\alpha\,F\,S^2}\ . \tag{6.A.11}$$

USC UNIVERSIDADE DE SANTIAGO DE COMPOSTELA

Let us also introduce a shorthand

$$\Lambda = \sqrt{1 + e^{-\phi}\mathcal{F}_{\mu\nu}\mathcal{F}^{\mu\nu}} \,=\, \sqrt{1 - \frac{e^{-\phi}(\partial_\sigma A_t)^2}{\alpha^2 b^2 F^2 S^8}} \ . \tag{6.A.12}$$

Then, the smeared DBI action takes the form

$$S_{\rm DBI}^{smeared} \,=\, -T_5 \int \mathrm{d}^{10}x \sqrt{-g}\, e^{\frac{\phi}{2}}\, \sqrt{2}|\Xi|\, \Lambda \ , \tag{6.A.13}$$

which can be expressed explicitly by plugging in the expressions in (6.A.11) and (6.A.12). The resulting equation for ϕ is

$$\partial_\sigma^2\phi - \alpha\, b\, F\, S^4 \left(3\frac{Q_{\rm f}\, \alpha\, b\, F\, e^{\frac{\phi}{2}}\, S^6}{\sqrt{\alpha^2 b^2 F^2 S^8 - e^{-\phi}\,(\partial_\sigma A_t)^2}} + \frac{F\, e^{\phi}}{2\,\alpha}\, \left(F_{123}^2 h^2 S^4 + 2\, Q_{\rm f}^2 \right) \right) = 0 \ . \tag{6.A.14}$$

Notice that, even though $H_3 = 0$, its equation of motion is non-trivial. In order to write this equation in detail we need to determine the eight-form $\delta_{\mathcal{F}} S_{\rm branes}$, which arises when the DBI term of the brane action is varied with respect to the NSNS two-form potential. This one reads

$$\delta_{\mathcal{F}} S_{\rm branes} \,=\, \frac{1}{\kappa_{10}^2} \frac{3\, Q_{\rm f}\, e^{-\frac{\phi}{2}}\, S^2\, \partial_\sigma A_t}{\sqrt{\alpha^2 b^2 F^2 S^8 - e^{-\phi}\,(\partial_\sigma A_t)^2}}\, \mathrm{d}x^1 \wedge \mathrm{d}x^2 \wedge \mathrm{d}x^3 \wedge e^1 \wedge e^2 \wedge e^3 \wedge e^4 \wedge e^5 \ . \tag{6.A.15}$$

Using this last expression, the equation for H_3 becomes

$$6\, Q_{\rm f}\, e^{-\phi/2}\, S^2 \partial_\sigma A_t + \, (Q_{\rm c} F_{123} + 6 Q_{\rm f} J) \sqrt{\alpha^2 b^2 F^2 S^8 - e^{-\phi}(\partial_\sigma A_t)^2} = 0 \ . \tag{6.A.16}$$

Let us now write down the Einstein equations that follow from the action (6.1.2). When $F_1 = H_3 = 0$, these equations read

$$\begin{aligned} R_{\mu\nu} - \frac{1}{2} g_{\mu\nu} R - \frac{1}{2}(\partial_\mu\phi\partial_\nu\phi - \frac{1}{2} g_{\mu\nu}(\partial\phi)^2) \ - \frac{1}{2\cdot 3!} e^{\phi}(3 F_{3\,\mu\rho\sigma} F_3{}_{\nu}{}^{\rho\sigma} - \frac{1}{2} g_{\mu\nu} F_3^2) \\ - \frac{1}{4\cdot 5!}(5 F_{5\mu\rho\sigma\tau\gamma} F_{5\nu}{}^{\rho\sigma\tau\gamma} - \frac{1}{2} g_{\mu\nu} F_5^2) \,=\, 2\kappa_{10}^2 T_{\mu\nu} \ , \end{aligned} \tag{6.A.17}$$

where $T_{\mu\nu}$ is the energy-momentum tensor for the distribution of D5-branes. Using the methods of [86], $T_{\mu\nu}$ can be easily obtained. It is useful to write it in flat components with respect to the following basis of vielbein one-forms

$$\begin{aligned} &E^{x^0} = h^{-\frac{1}{4}} b^{\frac{1}{2}} \mathrm{d}t \ , \qquad E^{x^{1,2}} = h^{-\frac{1}{4}} \mathrm{d}x^{1,2} \, , \qquad E^{x^3} = h^{-\frac{1}{4}} \alpha \mathrm{d}x^3 \ , \\ &E^{\sigma} = h^{\frac{1}{4}} \alpha S^4 F b^{\frac{1}{2}} \mathrm{d}\sigma \, , \qquad E^{i} = h^{\frac{1}{4}} S e^i, \quad i = \{1,2,3,4\} \, , \\ &E^{5} = h^{\frac{1}{4}} F e^5 \ . \end{aligned} \tag{6.A.18}$$

USC UNIVERSIDADE DE SANTIAGO DE COMPOSTELA

Written in flat components $T_{\mu\nu}$, it is given by

$$T_{\hat{\mu}\hat{\nu}} = T_5 e^{\frac{\phi}{2}}\sqrt{2}\Big[-\frac{1}{2}|\Xi|\Lambda g_{\hat{\mu}\hat{\nu}} + \frac{|\Xi|}{2\Lambda}e^{-\phi}(\partial_\sigma A_t)^2\left(E^t{}_{\hat{\mu}}E^t{}_{\hat{\nu}}g^{\sigma\sigma} + E^\sigma{}_{\hat{\mu}}E^\sigma{}_{\hat{\nu}}g^{tt}\right) + \frac{\Lambda}{12|\Xi|}\Xi_{\hat{\mu}\hat{\alpha}_1\hat{\alpha}_2\hat{\alpha}_3}\Xi_{\hat{\nu}}{}^{\hat{\alpha}_1\hat{\alpha}_2\hat{\alpha}_3}\Big] . \tag{6.A.19}$$

One can readily verify that the only non-vanishing components of $T_{\hat{\mu}\hat{\nu}}$ are

$$\begin{aligned} T_{\hat{x}^0\hat{x}^0} &= -T_{\hat{\sigma}\hat{\sigma}} = \frac{3Q_{\rm f}}{2\kappa_{10}^2 T_5}\,\frac{e^{\frac{\phi}{2}}}{\Lambda\,\alpha\,F\sqrt{h}\,S^2} \\ T_{\hat{x}^1\hat{x}^1} &= T_{\hat{x}^2\hat{x}^2} = -\frac{3Q_{\rm f}}{2\kappa_{10}^2 T_5}\,\frac{\Lambda e^{\frac{\phi}{2}}}{\alpha\,F\,\sqrt{h}\,S^2} \\ T_{\hat{5}\hat{5}} = T_{\hat{6}\hat{6}} &= T_{\hat{7}\hat{7}} = T_{\hat{8}\hat{8}} = -\frac{3Q_{\rm f}}{4\kappa_{10}^2 T_5}\,\frac{\Lambda e^{\frac{\phi}{2}}}{\alpha\,F\,\sqrt{h}\,S^2}\ . \end{aligned} \tag{6.A.20}$$

In order to massage the equations derived from (6.A.17) in more compact form, let us first define the quantities X, Y, and Z as follows

$$X = e^{-\phi}S^2(\partial_\sigma A_t)^2\,, \qquad Y = \sqrt{\alpha^2 b^2 F^2 e^{\phi}S^8 - (\partial_\sigma A_t)^2}\,, \qquad Z = F_{123}^2 b F^2 h^2 e^{\phi}S^8\ . \tag{6.A.21}$$

Then, the Einstein equations (6.A.17) are equivalent to the following system of second order differential equations

$$\begin{aligned} \partial_\sigma^2 \log F &= \frac{1}{2}Q_{\rm f}^2 b F^2 e^{\phi}S^4 - \frac{3Q_{\rm f}\alpha^2 b^2 F^2 e^{\phi}S^{10}}{2Y} + 4\alpha^2 b F^4 S^4 - 9\alpha^2 b J^2 S^4 - \frac{Z}{4} \\ \partial_\sigma^2 \log S &= 6\alpha^2 b F^2 S^6 - 2\alpha^2 b F^4 S^4 - \frac{9}{2}\alpha^2 b J^2 S^4 - \frac{(\partial_\sigma J)^2}{2S^4} - \frac{3Q_{\rm f}X e^{\phi}}{2Y} - \frac{Z}{4} \\ \partial_\sigma^2 \log h &= -bS^4\left(-\frac{2(\partial_\sigma J)^2}{bS^8} + Q_{\rm f}^2 F^2 e^{\phi} - 18\alpha^2 J^2\right) - \frac{3Q_{\rm f}e^{\phi}S^2\left(\alpha^2 b^2 F^2 S^8 - \frac{2X}{S^2}\right)}{Y} - \frac{Q_{\rm c}^2\alpha^2\, b}{h^2} + \frac{3Z}{2} \\ \partial_\sigma^2 \log b &= 18\alpha^2 b J^2 S^4 + \frac{2(\partial_\sigma J)^2}{S^4} + \frac{6Q_{\rm f}X e^{\phi}}{Y} + Z \\ \partial_\sigma^2 \log \alpha &= -Q_{\rm f}^2 b F^2 e^{\phi}S^4 + \frac{(\partial_\sigma J)^2}{S^4} - 3Q_{\rm f}Y S^2 + 9\alpha^2 b J^2 S^4\ , \end{aligned} \tag{6.A.22}$$

USC UNIVERSIDADE DE SANTIAGO DE COMPOSTELA

together with the first-order constraint

$$
\begin{aligned}
&-\partial_\sigma \log\alpha\,\partial_\sigma \log b - \partial_\sigma \log F\,\partial_\sigma \log b - \frac{1}{2}\partial_\sigma \log h\,\partial_\sigma \log b - 4\partial_\sigma \log S\,\partial_\sigma \log b - \partial_\sigma \log\alpha\,\partial_\sigma \log h \\
&-2\partial_\sigma \log F\,\partial_\sigma \log\alpha - 8\partial_\sigma \log F\,\partial_\sigma \log S - 8\partial_\sigma \log\alpha\,\partial_\sigma \log S - 12\,(\partial_\sigma \log S)^2 + \frac{1}{2}\,(\partial_\sigma \log h)^2 \\
&-Q_f^2 b F^2 e^{\phi} S^4 - \frac{2\;3Q_f \alpha^2 b^2 F^2 e^{\phi} S^{10}}{Y} + 24\alpha^2 b F^2 S^6 - 4\alpha^2 b F^4 S^4 - \frac{Q_c^2 \alpha^2 b}{2h^2} \\
&-9\alpha^2 b J^2 S^4 + \frac{(\partial_\sigma J)^2}{S^4} + \frac{1}{2}(\partial_\sigma \phi)^2 - \frac{Z}{2} = 0\ .
\end{aligned}
\tag{6.A.23}
$$

The equations of motion written above contain $\partial_\sigma A_t$. As standard, though, it can be eliminated algebraically by using (6.A.16) which casts $\partial_\sigma A_t$ in terms of other functions. This exercise yields

$$
\partial_\sigma A_t \;=\; -\frac{(Q_{\rm c}\,F_{123} \;+\; 6\,Q_{\rm f}\,J)\,\alpha\,b\,F\,S^4\,e^{\frac{\phi}{2}}}{\left[36\,Q_{\rm f}^2\,S^4 \;+\; (Q_{\rm c}\,F_{123} \;+\; 6Q_{\rm f}\,J)^2\right]^{\frac{1}{2}}}\ . \tag{6.A.24}
$$

Since all the functions depend only on the coordinate σ we can describe the system in terms of a one-dimensional effective action of the form

$$
S^{\rm eff} = \int {\rm d}\sigma\, L_{1D} \;=\; \int {\rm d}\sigma\;\; (L_g + L_{F_3} + L_{F_5} + L_{\rm DBI} + L_{\rm WZ})\ , \tag{6.A.25}
$$

where

$$
\begin{aligned}
L_g \;&=\; 24\alpha^2 b F^2 S^6 - 4\alpha^2 b F^4 S^4 - \frac{1}{2}(\partial_\sigma \phi)^2 - \frac{1}{2}\,(\partial_\sigma \log h)^2 + 12\,(\partial_\sigma \log S)^2 \\
&\quad +\partial_\sigma \log b\left(\partial_\sigma \log\alpha + \partial_\sigma \log F + \frac{1}{2}\partial_\sigma \log h + 4\partial_\sigma \log S\right) \\
&\quad +\partial_\sigma \log\alpha\,(2\partial_\sigma \log F + \partial_\sigma \log h + 8\partial_\sigma \log S) + 8\partial_\sigma \log F\,\partial_\sigma \log S \\
L_{F_3} \;&=\; -\frac{1}{2} b\,F^2 e^{\phi} S^4\left(F_{123}^2 h^2 S^4 + 2Q_{\rm f}^2\right) \\
L_{F_5} \;&=\; -\frac{1}{4}\left(\frac{\alpha^2 b\;(Q_{\rm c}^2 - 18h^2 J^2 S^4)}{h^2} + \frac{2(\partial_\sigma J)^2}{S^4}\right) \\
L_{\rm DBI} \;&=\; -6Q_{\rm f}\alpha\,b\,F\,e^{\frac{\phi}{2}} S^6 \sqrt{1 - \frac{e^{-\phi}(\partial_\sigma A_t)^2}{\alpha^2 b^2 F^2 S^8}} \\
L_{\rm WZ} \;&=\; 6\,Q_{\rm f}\,J\,\partial_\sigma A_t\ .
\end{aligned}
\tag{6.A.26}
$$

The one-dimensional effective action (6.A.25) can be used to obtain the equation of motion of the worldvolume gauge field A_t. Since A_t only enters $S^{\rm eff}$ through its derivative $\partial_\sigma A_t$, it

is a cyclic variable and hence its equation of motion can be written as a conservation law, namely

$$\frac{\delta}{\delta(\partial_\sigma A_t)}\Big(L_{\rm DBI}+L_{\rm WZ}\Big) \,=\, C\ , \tag{6.A.27}$$

where C is a constant. Remarkably, this equation of motion is consistent with the bulk equations for the backreacted ansatz. Indeed, one can directly show that (6.A.27) is equivalent to (6.A.16) if we identify F_{123} and the constant C as

$$C \,=\, -Q_{\rm c}\,F_{123}\ . \tag{6.A.28}$$

We regard this equivalence as a non-trivial consistency condition of our backreacted ansatz.

The constant F_{123} is related to the quark charge density $n_{\rm q}$ as we will demonstrate next. According to the holographic dictionary, the latter is given by the boundary value of the displacement field $D(\sigma)$, *i.e.*,

$$n_{\rm q}=D(\sigma=0)\equiv\frac{{\rm Vol}(\mathcal{M}_5)}{2\kappa_{10}^2}\,2\pi\,\alpha'\,\frac{\partial L_{\rm DBI}}{\partial(\partial_\sigma A_t)}\bigg|_{\sigma\to 0}\ . \tag{6.A.29}$$

Using the worldvolume equation (6.A.27) we can relate $D(\sigma)$ to the constant C and the function $J(\sigma)$, since

$$\frac{\partial L_{\rm DBI}}{\partial(\partial_\sigma A_t)} \,=\, C\,-\,6\,Q_{\rm f}\,J(\sigma) \,=\, -Q_{\rm c}\,F_{123}\,-\,6\,Q_{\rm f}\,J(\sigma)\ . \tag{6.A.30}$$

Therefore, taking into account that $Q_{\rm c}\,{\rm Vol}(\mathcal{M}_5) \,=\, (2\pi)^4\,g_{\rm s}\,\alpha'^2\,N_{\rm c}$ and that $2\kappa_{10}^2 \,=\, (2\pi)^7\,g_{\rm s}^2\,\alpha'^4$, we can write the displacement field as

$$D(\sigma) \,=\, -\frac{N_{\rm c}}{4\pi^2\,g_{\rm s}\,\alpha'}\,F_{123}\,+\,\frac{6\pi\alpha'}{\kappa_{10}^2}\,Q_{\rm f}\,{\rm Vol}(\mathcal{M}_5)\,J(\sigma)\ . \tag{6.A.31}$$

In our solutions the regularity condition of A_t at the UV boundary requires the vanishing of the function $J(\sigma)$ as $\sigma\to 0$. Therefore, the second term in (6.A.31) does not contribute to the quark density $n_{\rm q}$, which thereby eventually leads to the relation

$$n_{\rm q} \,=\, -\frac{N_{\rm c}}{4\pi^2\,g_{\rm s}\,\alpha'}\,F_{123}\ . \tag{6.A.32}$$

USC
UNIVERSIDADE
DE SANTIAGO
DE COMPOSTELA

7 Flavored anisotropic black holes

In what follows, we will solve the equations of motion derived in chapter 6. First we will consider the system without charges (see section 7.1), and we will include them later in section 7.2. Finally, section 7.3 analyses the thermodynamic properties of the system.

7.1 Black holes without charges

In this section we consider the background in which the worldvolume gauge field vanishes, the gravity dual of the flavored theory at zero chemical potential but at non-zero temperature. The details of the integration of the equations of motion leading to this solution are relegated to appendix 7.A. Our solution is a black hole which has a horizon at $\rho = \rho_{\rm h}$. The blackening factor in the metric (6.1.7) is given by

$$b \,=\, 1 \,-\, \frac{\rho_{\rm h}^4}{\rho^4} \ . \tag{7.1.1}$$

In these zero chemical potential solutions the function $\alpha(\rho)$ encoding the anisotropy is related to the dilaton $\phi(\rho)$ as

$$\alpha \,=\, e^{-\phi} \ . \tag{7.1.2}$$

Moreover, the warp factor h can be written in terms of the dilaton ϕ as

$$h \,=\, \frac{Q_{\rm c}}{4\rho^4}\, e^{-\phi} \ . \tag{7.1.3}$$

The equations for the remaining functions of the ansatz are quite involved and are in general only amenable for numerical study. To prosecute toward analytic solutions, we introduce a small expansion parameter ϵ,

$$\epsilon \,=\, \frac{Q_{\rm f}}{5\,\rho_{\rm h}} \ , \tag{7.1.4}$$

where the factor 5 has been included for convenience. This allows us to find explicit solutions, perturbatively in ϵ. To this end, let $\tilde{\rho}$ be the following rescaled radial coordinate

$$\tilde{\rho} \,=\, \frac{\rho}{\rho_{\rm h}} \ , \tag{7.1.5}$$

USC UNIVERSIDADE DE SANTIAGO DE COMPOSTELA

and $\Omega(\tilde{\rho})$ the following function

$$\Omega(\tilde{\rho}) \equiv \frac{5}{4}\left[2\arctan\tilde{\rho} + \log\left(\frac{\tilde{\rho}^4}{(\tilde{\rho}+1)^2(\tilde{\rho}^2+1)}\right) - \pi\right] . \tag{7.1.6}$$

Then, at first order in ϵ, we have

$$\begin{aligned} b(\tilde{\rho}) &= 1 - \frac{1}{\tilde{\rho}^4} , & \phi(\tilde{\rho}) &= \epsilon\,\Omega\left(\tilde{\rho}\right) , \\ \alpha(\tilde{\rho}) &= 1 - \epsilon\,\Omega\left(\tilde{\rho}\right) , & h(\tilde{\rho}) &= \frac{Q_{\rm c}}{4\rho_{\rm h}^4\tilde{\rho}^4}\left(1 - \epsilon\,\Omega\left(\tilde{\rho}\right)\right) , \\ G(\tilde{\rho}) &= 1 + \epsilon\Big(\frac{1}{2}\,\tilde{\rho}^4\Omega(\tilde{\rho}) + \frac{5}{8}\Big(4\tilde{\rho}^3 - 1\Big)\Big) , \end{aligned} \tag{7.1.7}$$

while the functions $F(\tilde{\rho})$ and $S(\tilde{\rho})$, that characterise the deformation of the internal manifold, can be written as

$$\frac{F(\tilde{\rho})}{\rho_{\rm h}} = \tilde{\rho}\left(1 + \epsilon\,F_1(\tilde{\rho})\right) , \qquad \frac{S(\tilde{\rho})}{\rho_{\rm h}} = \tilde{\rho}\left(1 + \epsilon\,S_1(\tilde{\rho})\right) . \tag{7.1.8}$$

Due to their lengthy nature, the explicit expressions of $F_1(\tilde{\rho})$ and $S_1(\tilde{\rho})$ are collected inside (7.A.18) of appendix 7.A, however.

7.2 Charged black holes

When the worldvolume gauge field $A_t(\rho)$ is non-trivial our background is dual to a gauge theory at non-zero chemical potential. The presence of this non-trivial worldvolume gauge field induces in extra components of the RR fields F_3 and F_5 written in eqs. (6.1.18)-(6.1.20), which involve the constant F_{123} and the function $J(\tilde{\rho})$. As shown in appendix 6.A, the constant F_{123} is proportional to the quark density $n_{\rm q}$ (see eq. (6.A.32)). We proceed to seek for a perturbative solution of the equations of motion in which these new components are small. With this purpose, let us redefine F_{123} and $J(\tilde{\rho})$ as

$$F_{123} = \epsilon\,\delta \quad , \quad J(\tilde{\rho}) = \epsilon\,\delta\,j(\tilde{\rho}) , \tag{7.2.1}$$

where δ is a new expansion parameter. By using (6.A.32) we can relate $n_{\rm q}$ to ϵ and δ as

$$n_{\rm q} = -\frac{N_{\rm c}}{4\pi^2\,g_{\rm s}\,\alpha'}\,\epsilon\,\delta . \tag{7.2.2}$$

Actually, in our expansion of the solution for non-vanishing chemical potential, the different functions of the background get an additional term proportional to $\epsilon\,\tilde{\delta}^2$, where $\tilde{\delta}$ is related to δ as

$$\tilde{\delta} = \frac{Q_{\rm c}}{10\sqrt{6}}\,\frac{\delta}{\rho_{\rm h}^3} . \tag{7.2.3}$$

USC UNIVERSIDADE DE SANTIAGO DE COMPOSTELA

To make the physics in the expansion parameters more transparent, let us relate $\tilde{\delta}$ to the parameters of the dual theory. A simple calculation using eq. (6.A.32) shows that $\tilde{\delta}$ is related to the temperature T and quark density $n_{\rm q}$ as

$$\tilde{\delta} \,=\, -\frac{4\sqrt{2}\,\alpha'\,g_{\rm s}}{\sqrt{3}}\,\frac{n_{\rm q}}{N_{\rm c}}\,\frac{1}{n_{\rm f}\,T^2}\Big(1+\mathcal{O}\Big(\frac{n_{\rm f}}{T}\Big)\Big) \,=\, -\frac{4\sqrt{2}\,\alpha'\,g_{\rm s}}{\sqrt{3}}\,\frac{n_{\rm b}}{n_{\rm f}}\,\frac{1}{T^2}\Big(1+\mathcal{O}\Big(\frac{n_{\rm f}}{T}\Big)\Big)\,, \tag{7.2.4}$$

where, in the last step, we have introduced the baryon density $n_{\rm b} = n_{\rm q}/N_{\rm c}$.

To method of obtaining the perturbative solution to the equations of motion is explained in detail in appendix 7.B. As compared with the one found in section 7.1, the functions of the ansatz get an extra correction of order $\epsilon\,\tilde{\delta}^2$. For example, the blackening factor is now

$$b(\tilde{\rho}) = \left(1-\frac{1}{\tilde{\rho}^4}\right)\left(1-4\,\epsilon\,\tilde{\delta}^2\left(\Omega\,(\tilde{\rho})+\frac{5}{\tilde{\rho}}\right)\right)\,, \tag{7.2.5}$$

where $\Omega\,(\tilde{\rho})$ is the function defined in (7.1.6). Notice that, at the order we are working, the apparent horizon read of from the metric (*i.e.*, the zero of $b(\tilde{\rho})$) still occurs at $\tilde{\rho}=1$. The expressions for the functions $\phi(\tilde{\rho})$, $\alpha(\tilde{\rho})$, $h(\tilde{\rho})$, and $G(\tilde{\rho})$ are given by

$$\begin{aligned}
\phi(\tilde{\rho}) &= \epsilon\,\Omega\,(\tilde{\rho}) - \epsilon\,\tilde{\delta}^2\left(\Omega\,(\tilde{\rho})+\frac{5}{\tilde{\rho}}\right)\\
\alpha(\tilde{\rho}) &= 1-\epsilon\,\Omega\,(\tilde{\rho}) - \epsilon\,\tilde{\delta}^2\left(\Omega\,(\tilde{\rho})+\frac{5}{\tilde{\rho}}\right)\\
h(\tilde{\rho}) &= \frac{Q_{\rm c}}{4\rho_{\rm h}^4\tilde{\rho}^4}\left(1-\epsilon\,\Omega\,(\tilde{\rho}) - 3\,\epsilon\,\tilde{\delta}^2\left(\Omega\,(\tilde{\rho})+\frac{5}{\tilde{\rho}}\right)\right)\\
G(\tilde{\rho}) &= 1-\frac{1}{2}\epsilon\left(\frac{5}{4}\left(1-4\tilde{\rho}^3\right)-\tilde{\rho}^4\,\Omega(\tilde{\rho})\right)\\
&\qquad -\epsilon\,\tilde{\delta}^2\left(\frac{5}{8}\left(20\tilde{\rho}^3-5+\frac{4}{\tilde{\rho}}\right)+\frac{5}{2}\,\tilde{\rho}^4\,\Omega(\tilde{\rho})\right)\,.
\end{aligned} \tag{7.2.6}$$

Moreover, the functions $F(\tilde{\rho})$ and $S(\tilde{\rho})$ can now be written as

$$\begin{aligned}
\frac{F(\tilde{\rho})}{\rho_{\rm h}} &\,=\, \tilde{\rho}\left(1+\epsilon\,F_1(\tilde{\rho})\,+\,\epsilon\,\tilde{\delta}^2\,F_2(\tilde{\rho})\right)\\
\frac{S(\tilde{\rho})}{\rho_{\rm h}} &\,=\, \tilde{\rho}\left(1+\epsilon\,S_1(\tilde{\rho})\,+\,\epsilon\,\tilde{\delta}^2\,S_2(\tilde{\rho})\right)\,,
\end{aligned} \tag{7.2.7}$$

where $F_1(\tilde{\rho})$ and $S_1(\tilde{\rho})$ are the same as in (7.1.8) and the new functions $F_2(\tilde{\rho})$ and $S_2(\tilde{\rho})$ are written in (7.B.16).

To complete the solution we must give the flux function $j(\tilde{\rho})$ and the worldvolume gauge field $A_t'(\tilde{\rho})$. They are displayed in eqs. (7.B.20) and (7.B.21) respectively.

It is interesting to write down the asymptotic forms of the different functions of the background in the UV region $\tilde{\rho} \to \infty$. In this region, the metric becomes $AdS_5 \times \mathcal{M}_5$, with subleading flavor corrections. These corrections can be straightforwardly obtained from our equations. The expansions of the functions ϕ, α, h, and G can be easily obtained by expanding the function $\Omega(\tilde{\rho})$ for large $\tilde{\rho}$, finally leading to the expansions

$$\begin{aligned}
\phi(\tilde{\rho}) &= -\frac{5\,\epsilon}{\tilde{\rho}} + \frac{5}{4}\frac{\epsilon - \epsilon\,\tilde{\delta}^2}{\tilde{\rho}^4} + \dots\,, \qquad\qquad \alpha(\tilde{\rho}) = 1 + \frac{5\,\epsilon}{\tilde{\rho}} - \frac{5}{4}\frac{\epsilon + \epsilon\,\tilde{\delta}^2}{\tilde{\rho}^4} + \dots \\
h(\tilde{\rho}) &= \frac{Q_{\rm c}}{4\rho_{\rm h}^4\,\tilde{\rho}^4}\left(1 + \frac{5\,\epsilon}{\tilde{\rho}} - \frac{5}{4}\frac{\epsilon + 3\epsilon\,\tilde{\delta}^2}{\tilde{\rho}^4} + \dots\right) \\
G(\tilde{\rho}) &= 1 - \frac{\epsilon}{2\tilde{\rho}} + \frac{5}{16}\frac{\epsilon - 5\,\epsilon\,\tilde{\delta}^2}{\tilde{\rho}^4} + \dots\,.
\end{aligned} \tag{7.2.8}$$

Moreover, the UV expansion of the functions F and S can be found from (7.A.18) and (7.B.16) and is given by

$$\begin{aligned}
\frac{F(\tilde{\rho})}{\rho_{\rm h}} &= \tilde{\rho}\Big(1 - \frac{7}{10}\frac{\epsilon}{\tilde{\rho}} + \frac{5}{16}\frac{\epsilon + 3\epsilon\,\tilde{\delta}^2}{\tilde{\rho}^4} + \dots\Big) \\
\frac{S(\tilde{\rho})}{\rho_{\rm h}} &= \tilde{\rho}\Big(1 - \frac{6}{5}\frac{\epsilon}{\tilde{\rho}} + \frac{5}{48}\frac{8\epsilon + 9\epsilon\,\tilde{\delta}^2}{\tilde{\rho}^4} + \dots\Big)\,.
\end{aligned} \tag{7.2.9}$$

7.3 Thermodynamics

Now that we have found the solution for our geometry in the presence of flavor and a non-trivial gauge potential, let us work out the corresponding thermodynamics of the field theory. First of all, we obtain the temperature of the system by equating it with the Hawking temperature, using (6.1.9). We get

$$T = \frac{2\,\rho_{\rm h}}{\pi\,Q_{\rm c}^{1/2}}\left(1 - \frac{15}{8}\,\epsilon - \frac{5}{8}\,\epsilon\,\tilde{\delta}^2\right)\,. \tag{7.3.1}$$

The entropy density s is identified with the entropy of the black hole, given by the Bekenstein-Hawking formula

$$s = \frac{2\pi}{\kappa_{10}^2}\frac{A_8}{V_3}\,, \tag{7.3.2}$$

where A_8 is the volume at the horizon of the eight-dimensional space orthogonal to the $(t,\tilde{\rho})$-plane and V_3 is the infinite constant volume of the three-dimensional Minkowski directions (x^1,x^2,x^3). For our geometry, we obtain

$$s = \frac{{\rm Vol}\big(\mathcal{M}_5\big)}{(2\pi)^6\,\alpha'^4\,g_{\rm s}^2}\,Q_{\rm c}^{1/2}\,\rho_{\rm h}^3\left(1 + \frac{15}{8}\,\epsilon + \frac{5}{8}\epsilon\,\tilde{\delta}^2\right)\,. \tag{7.3.3}$$

USC UNIVERSIDADE DE SANTIAGO DE COMPOSTELA

In order to obtain the internal energy density $\mathcal{E}$ of our system, we calculate the ADM energy of the background, which is given by the standard formula [87]

$$E_{ADM} = -\frac{1}{\kappa_{10}^2}\sqrt{-g_{tt}}\int_{\mathcal{M}_{t,\rho_\infty}} \mathrm{d}^8x\sqrt{g_8}\,(K_{T,\mu} - K_0)\ . \tag{7.3.4}$$

In (7.3.4) $K_{T,\mu}$ is the extrinsic curvature of the eight-dimensional subspace within the nine-dimensional (constant time) space. For our metric ansatz (6.1.7), $K_{T,\mu}$ is given by

$$K_{T,\mu} = \frac{1}{\sqrt{\det g_9}}\partial_\mu\left(\sqrt{\det g_9}\,\frac{1}{\sqrt{g_{\rho\rho}}}\delta^\mu_\rho\right) \,=\, \frac{\sqrt{b}}{h^{\frac{3}{4}}\,G\,\alpha\,F\,S^4}\,\partial_\rho\Big(h^{\frac{1}{2}}\,\alpha\,F\,S^4\Big)\ . \tag{7.3.5}$$

Moreover, K_0 is the extrinsic curvature at zero temperature and zero quark density. At first order in $Q_{\rm f}$, K_0 is given by

$$K_0 \,=\, \frac{3\,\sqrt{2}}{Q_{\rm c}^{\frac{1}{4}}}\left(1\,-\,\frac{17}{60}\,\frac{Q_{\rm f}}{\rho}\right)\ . \tag{7.3.6}$$

The integral in (7.3.4) is taken at constant time and at a fixed radial position (which is then sent to infinity). We get

$$\mathcal{E} = \frac{E_{ADM}}{V_3} \,=\, \frac{3\,\mathrm{Vol}\Big(\mathcal{M}_5\Big)}{(2\pi)^7\,\alpha'^4\,g_{\rm s}^2}\,\rho_{\rm h}^4\left(1\,-\,\frac{5}{6}\,\epsilon\,+\,\frac{25}{6}\epsilon\,\tilde{\delta}^2\right)\ . \tag{7.3.7}$$

We can now compute the free energy density as

$$f = \mathcal{E} - T\,s \,=\, -\frac{\mathrm{Vol}\Big(\mathcal{M}_5\Big)}{(2\pi)^7\,\alpha'^4\,g_{\rm s}^2}\,\rho_{\rm h}^4\left(1\,+\,\frac{5}{2}\,\epsilon\,-\,\frac{25}{2}\epsilon\,\tilde{\delta}^2\right)\ . \tag{7.3.8}$$

Note that one can as well read the free energy from the euclidean action, as shown in appendix 7.C. All these expressions contain the combination $\epsilon\,\tilde{\delta}^2$, which can be written in terms of the quark density $n_{\rm q}$ as

$$\epsilon\,\tilde{\delta}^2 \,=\, \gamma\,\frac{n_{\rm q}^2}{Q_{\rm f}\,\rho_{\rm h}^5}\ , \tag{7.3.9}$$

where the coefficient γ depends on the internal manifold $\mathcal{M}_5$ and is given by

$$\gamma \,=\, \frac{2^9\,\pi^{12}\,g_{\rm s}^4\,\alpha'^6}{15\left(\mathrm{Vol}\Big(\mathcal{M}_5\Big)\right)^2}\ . \tag{7.3.10}$$

Let us next obtain s, $\mathcal{E}$, and f in terms of physical quantities. With this purpose, let us define λ as

$$\lambda \,=\, 4\pi\,g_{\rm s}\,N_{\rm c}\ , \tag{7.3.11}$$

which, in the case in which the internal manifold $\mathcal{M}_5$ is the five-sphere $\mathbb{S}^5$ and the unflavored geometry it is the dual of $\mathcal{N}=4$ super Yang-Mills theory, is just the 't Hooft coupling written in terms of string variables. Furthermore, the 'a' coefficient of the conformal anomaly is

USC DE SANTIAGO

inversely proportional to the internal volume [166], so we can define the ratio between the a coefficients of the field theory dual to the D3-branes on the cone and $\mathcal{N}=4$ super Yang-Mills as the ratio between the volume of $\mathcal{M}_5$ with the five-sphere

$$\bar{a} = \frac{a_{\mathcal{M}_5}}{a_{\mathcal{N}=4}} = \frac{\pi^3}{\mathrm{Vol}\,(\mathcal{M}_5)}\ . \tag{7.3.12}$$

It will be convenient recall the definition of the baryon density

$$n_{\mathrm{b}} = \frac{n_{\mathrm{q}}}{N_{\mathrm{c}}} \tag{7.3.13}$$

so that we can then invert (7.3.1) and write ρ_{h} in terms of N_{c}, λ, n_{f}, and T as

$$\rho_{\mathrm{h}} = \pi\,\lambda^{\frac{1}{2}}\bar{a}^{\frac{1}{2}}\,\alpha' T\left[1+\frac{\lambda^{\frac{1}{2}}}{N_{\mathrm{c}}\bar{a}^{\frac{1}{2}}}\left(\frac{1}{16\,v_\perp}\frac{n_{\mathrm{f}}}{T}+\frac{v_\perp}{2\,\pi^4}\frac{n_{\mathrm{b}}^2}{n_{\mathrm{f}}T^5}\right)\right]\ . \tag{7.3.14}$$

Thereby the expansion parameters ϵ and $\epsilon\tilde{\delta}^2$ in terms of physical quantities read

$$\epsilon = \frac{\lambda^{\frac{1}{2}}}{30\,v_\perp\,N_{\mathrm{c}}\,\bar{a}^{\frac{1}{2}}}\frac{n_{\mathrm{f}}}{T}+\dots\quad,\quad \epsilon\,\tilde{\delta}^2 = \frac{4\,v_\perp}{5\,\pi^4}\frac{\lambda^{\frac{1}{2}}}{N_{\mathrm{c}}\,\bar{a}^{\frac{1}{2}}}\frac{n_{\mathrm{b}}^2}{n_{\mathrm{f}}T^5}+\dots\ . \tag{7.3.15}$$

Using (7.3.14), (7.3.15), and (7.3.9) we finally arrive at the following expressions for the entropy and energy densities

$$\begin{aligned} s &= \frac{\pi^2 N_{\mathrm{c}}^2}{2}\,\bar{a}\,T^3\left[1+\frac{\lambda^{\frac{1}{2}}}{N_{\mathrm{c}}\bar{a}^{\frac{1}{2}}}\left(\frac{1}{4\,v_\perp}\frac{n_{\mathrm{f}}}{T}+\frac{2v_\perp}{\pi^4}\frac{n_{\mathrm{b}}^2}{n_{\mathrm{f}}T^5}\right)\right] \\ \mathcal{E} &= \frac{3\pi^2 N_{\mathrm{c}}^2}{8}\,\bar{a}\,T^4\left[1+\frac{\lambda^{\frac{1}{2}}}{N_{\mathrm{c}}\bar{a}^{\frac{1}{2}}}\left(\frac{2}{9\,v_\perp}\frac{n_{\mathrm{f}}}{T}+\frac{16v_\perp}{3\,\pi^4}\frac{n_{\mathrm{b}}^2}{n_{\mathrm{f}}T^5}\right)\right]\ , \end{aligned} \tag{7.3.16}$$

while the free energy density is given by

$$f = -\frac{\pi^2\,N_{\mathrm{c}}^2}{8}\,\bar{a}\,T^4\left[1+\frac{\lambda^{\frac{1}{2}}}{N_{\mathrm{c}}\bar{a}^{\frac{1}{2}}}\left(\frac{1}{3\,v_\perp}\frac{n_{\mathrm{f}}}{T}-\frac{8v_\perp}{\pi^4}\frac{n_{\mathrm{b}}^2}{n_{\mathrm{f}}T^5}\right)\right]\ . \tag{7.3.17}$$

In the case in which $\mathcal{M}_5 = \mathbb{S}^5$, we have $\bar{a}=1$ and the leading terms in (7.3.16) and (7.3.17) reproduce the standard values of s, $\mathcal{E}$, and f for $\mathcal{N}=4$ super Yang-Mills theory. Notice that the flavor corrections in these equations depend on the ratios n_{f}/T and $n_{\mathrm{b}}^2/(n_{\mathrm{f}}T^5)$, which are dimensionless, since $[T]=[n_{\mathrm{f}}]=[\text{length}]^{-1}$ and $n_{\mathrm{b}} = [\text{length}]^{-3}$. The flavor contribution increases the value of the entropy and the energy densities, indicating an increase in the number of degrees of freedom. This is expected since each D5-brane introduces additional fields localised at the intersection with the color D3-branes.

Following the approach of [38, 164], to unravel a better understanding of the thermodynamics of the anisotropic system it is convenient to consider the situation in which the

number of flavor D5-branes change. Therefore, we allow $n_{\rm f}$ to vary and write the first law of thermodynamics as

$$\mathrm{d}\mathcal{E} \;=\; T\,\mathrm{d}s + \Phi\,\mathrm{d}n_{\rm f} + \mu\,\mathrm{d}n_{\rm q}\;, \tag{7.3.18}$$

where μ is the ordinary (baryon) chemical potential and Φ is a brane potential which measures the energy cost of introducing additional flavor branes in the system. Taking into account that $f = \mathcal{E} - T\,s$, we can write the variation of the free energy as

$$\mathrm{d}f = -s\,\mathrm{d}T + \Phi\,\mathrm{d}n_{\rm f} + \mu\,\mathrm{d}n_{\rm q}\;. \tag{7.3.19}$$

It follows from (7.3.19) that

$$s = -\left(\frac{\partial f}{\partial T}\right)_{n_{\rm f},n_{\rm q}}\;, \tag{7.3.20}$$

which can be easily checked directly using (7.3.16) and (7.3.17) and can be regarded as a consistency check of our expression (7.3.17) for f. Similarly, the brane potential Φ can be obtained from f as

$$\Phi = \left(\frac{\partial f}{\partial n_{\rm f}}\right)_{T,n_{\rm q}}\;. \tag{7.3.21}$$

Computing the derivative in (7.3.21) using (7.3.17), we arrive at the following expression for the brane potential Φ

$$\Phi = -\frac{\pi^2\,\lambda^{\frac{1}{2}}\,N_{\rm c}\,\bar{a}^{\frac{1}{2}}}{24\,v_\perp}T^3\left(1+\frac{24\,v_\perp^2}{\pi^4}\,\frac{n_{\rm b}^2}{n_{\rm f}^2\,T^4}\right)\;. \tag{7.3.22}$$

Moreover, the baryonic chemical potential μ can be obtained as

$$\mu = \left(\frac{\partial f}{\partial n_{\rm q}}\right)_{T,n_{\rm f}}\;, \tag{7.3.23}$$

and is given by

$$\mu = \frac{2\,\lambda^{\frac{1}{2}}\,\bar{a}^{\frac{1}{2}}\,v_\perp}{\pi^2}\,\frac{n_{\rm b}}{n_{\rm f}\,T}\;\;. \tag{7.3.24}$$

For the Gibbs free energy $g = f - \Phi n_{\rm f} - \mu n_{\rm q}$ we get

$$g \;\;=\;\; -\frac{\pi^2\,N_{\rm c}^2}{8}\bar{a}\,T^4\,. \tag{7.3.25}$$

From f and g we get the pressures along the xy- and z-directions as

$$p_{xy} \;=\; -f \;+\; \mu\,n_{\rm q} \;=\; -g \;-\; \Phi\,n_{\rm f}\;, \qquad\qquad p_z \;=\; -g\;. \tag{7.3.26}$$

More explicitly, these two pressures can be written as

$$\begin{aligned} p_{xy} \;&=\; \frac{\pi^2\,N_{\rm c}^2}{8}\,\bar{a}\,T^4\left[1+\frac{\lambda^{\frac{1}{2}}}{N_{\rm c}\bar{a}^{\frac{1}{2}}}\left(\frac{1}{3\,v_\perp}\frac{n_{\rm f}}{T}+\frac{8v_\perp}{\pi^4}\frac{n_{\rm b}^2}{n_{\rm f}\,T^5}\right)\right] \\ p_z \;&=\; \frac{\pi^2\,N_{\rm c}^2}{8}\,\bar{a}\,T^4\;. \end{aligned} \tag{7.3.27}$$

USC UNIVERSIDADE DE SANTIAGO DE COMPOSTELA

Notice that p_{xy} becomes larger, while p_z in (7.3.27) is not affected by the addition of D5-branes, which is consistent with having flavors living in layers extended along the xy-directions. Actually, we can easily check that

$$\frac{\partial p_{xy}}{\partial \mu} \,=\, n_{\rm q}\ , \qquad\qquad \frac{\partial p_z}{\partial \mu} \,=\, 0\ . \tag{7.3.28}$$

We have checked these thermodynamic results in several ways. First of all, we verified that the regulated euclidean on-shell action divided by the inverse temperature equals the grand canonical potential $\Omega = f - \mu\, n_{\rm q}$. To perform this calculation we have to regulate the on-shell action by subtracting its zero temperature value, both for the bulk and Gibbons-Hawking terms (for details, see appendix 7.C).

We have also checked the expressions of the energy density and pressures that we have just found using the following thermodynamic arguments. Indeed, one can compute the vacuum expectation value (VEV) of the stress-energy tensor from the Brown-York tensor at the boundary, by using the proposal of [167]. The Brown-York tensor of the ten-dimensional gravity theory is

$$\tau_{ij} \,=\, \frac{1}{\kappa_{10}^2}\Big(K_{ij} \,-\, K\,\gamma_{ij}\Big)\ , \tag{7.3.29}$$

where γ_{ij} is the induced metric at a $r=$ constant surface, K_{ij} is the extrinsic curvature of the surface, and $K = \gamma^{ij}\,K_{ij}$. The VEV of the stress-energy tensor of the dual theory is related to the Minkowski components of the Brown-York tensor evaluated at the boundary [167]

$$\langle T^{\mu}{}_{\nu}\rangle \,=\, V_{\rm SE}\,\sqrt{-\gamma_{\rm min}}\ \tau^{\mu}{}_{\nu}\Big|_{\rm reg\,,\,\rho\to\infty}\ , \tag{7.3.30}$$

where $V_{\rm SE} = h^{\frac{5}{4}}\,F\,S^4\,{\rm Vol}(\mathcal{M}_5)$ is the volume for the compact 5d part of the metric. The right-hand side of (7.3.30) is singular at the UV boundary. To regulate it we subtract its zero temperature value (given by supersymmetry), similarly as was done in [88]. Therefore, we obtain the VEV of the stress-energy tensor as

$$\langle T^{\mu}{}_{\nu}\rangle = V_{\rm SE}\lim_{\rho_\Lambda\to\infty}\left[\sqrt{-\gamma_{\rm min}}\tau^{\mu}{}_{\nu} - \left[b^{1/2}\lim_{\rho_{\rm h}\to 0}\Big(\sqrt{-\gamma_{\rm min}}\tau^{\mu}{}_{\nu}\Big)\right]_{\tilde\delta\to 0}\right]_{\rho=\rho_\Lambda}\ , \tag{7.3.31}$$

where $\gamma_{\rm min}$ is the determinant of the Minkowski part of the induced metric and the $b^{\frac{1}{2}}$ factor, needed to match the geometries at the cutoff, is evaluated at zero chemical potential. After some calculation, we get

$$\begin{aligned}
\langle T^{t}{}_{t}\rangle \;&=\; -\frac{3\,{\rm Vol}\big(\mathcal{M}_5\big)}{(2\pi)^7\,\alpha'^4\,g_{\rm s}^2}\,\rho_{\rm h}^4\left(1\,-\,\frac{5}{6}\,\epsilon\,+\,\frac{25}{6}\epsilon\,\tilde\delta^2\right)\\
\langle T^{x^1}{}_{x^1}\rangle \;&=\; \langle T^{x^2}{}_{x^2}\rangle \;=\; \frac{{\rm Vol}\big(\mathcal{M}_5\big)}{(2\pi)^7\,\alpha'^4\,g_{\rm s}^2}\,\rho_{\rm h}^4\left(1\,+\,\frac{5}{2}\,\epsilon\,+\,\frac{15}{2}\epsilon\,\tilde\delta^2\right)\\
\langle T^{x^3}{}_{x^3}\rangle \;&=\; \frac{{\rm Vol}\big(\mathcal{M}_5\big)}{(2\pi)^7\,\alpha'^4\,g_{\rm s}^2}\,\rho_{\rm h}^4\left(1\,-\,\frac{15}{2}\,\epsilon\,-\,\frac{15}{6}\epsilon\,\tilde\delta^2\right)\ .
\end{aligned} \tag{7.3.32}$$

USC UNIVERSIDADE DE SANTIAGO DE COMPOSTELA

We can check that $\mathcal{E} = -\langle T^t{}_t \rangle$ and that the pressures along the parallel and transverse directions are indeed given by the expectation values of the corresponding components of the stress-energy tensor, namely

$$p_{xy} = \langle T^{x^1}{}_{x^1} \rangle = \langle T^{x^2}{}_{x^2} \rangle \,, \qquad\qquad p_{zz} = \langle T^{x^3}{}_{x^3} \rangle \,. \tag{7.3.33}$$

In addition, in appendix 8.A we present a further check of the VEV of $T^\mu{}_\nu$ in the case of zero chemical potential. In this case we can make use of the reduction to five dimensions found in [77]. The reduced theory contains gravity and three scalars, whose contribution to the VEV of the stress-energy tensor must be regulated by using their superpotential. The final results coincide with those in (7.3.32) for $\tilde{\delta} = 0$.

As in [77] the anisotropy of the system is manifested through a pressure difference, measured by the potential Φ. Indeed, one can readily check that

$$p_z - p_{xy} = \Phi \, n_{\rm f} \,. \tag{7.3.34}$$

Actually, using (7.3.32) we can write, at $\mathcal{O}(\epsilon^2)$, the two pressures in terms of the energy density as

$$p_{xy} = \left(\frac{1}{3} + \frac{10}{9} \left(1 + \tilde{\delta}^2 \right) \epsilon \right) \mathcal{E} \,, \qquad p_z = \left(\frac{1}{3} - \frac{20}{9} \left(1 + \tilde{\delta}^2 \right) \epsilon \right) \mathcal{E} \,. \tag{7.3.35}$$

The speeds of sound along the two different directions are now easily computed, with the result

$$v_{xy}^2 = \left(\frac{\partial p_{xy}}{\partial \mathcal{E}} \right) = \frac{1}{3} + \frac{10}{9} \left(1 + \tilde{\delta}^2 \right) \epsilon \,, \qquad v_z^2 = \left(\frac{\partial p_z}{\partial \mathcal{E}} \right) = \frac{1}{3} - \frac{20}{9} \left(1 + \tilde{\delta}^2 \right) \epsilon \,, \tag{7.3.36}$$

where we have calculated the derivatives by keeping the expansion parameters $\epsilon, \tilde{\delta}$ fixed. Recall that this means to keep the density of flavor branes and/or the baryon density, appropriately scaled with the powers of the temperature, fixed, see (7.3.15). Rewriting these speeds in this vein leads to

$$\begin{aligned} v_{xy}^2 &= \frac{1}{3} \left[1 + \frac{\lambda^{\frac{1}{2}}}{N_{\rm c} \bar{a}^{\frac{1}{2}}} \left(\frac{1}{9\, v_\perp} \frac{n_{\rm f}}{T} + \frac{8 v_\perp}{3\pi^4} \frac{n_{\rm b}^2}{n_{\rm f} T^5} \right) \right] \\ v_z^2 &= \frac{1}{3} \left[1 - 2 \frac{\lambda^{\frac{1}{2}}}{N_{\rm c} \bar{a}^{\frac{1}{2}}} \left(\frac{1}{9\, v_\perp} \frac{n_{\rm f}}{T} + \frac{8 v_\perp}{3\pi^4} \frac{n_{\rm b}^2}{n_{\rm f} T^5} \right) \right] \,. \end{aligned} \tag{7.3.37}$$

To gain some intuition on the above expressions, let us first recall how the speed of sound works out for massless probe D5-branes immersed in the geometry induced by D3-branes. There the speed of sound for collective modes localised on a (single) defect D5-brane coincides with that of a conformal $(2+1)$-dimensional theory $v_{\rm s}^2 = 1/2$ [69]. One should bear in mind though that there are actually two types of sound waves: these faster ones propagating along

USC DE SANTIAGO

the directions of the defects, but also those slower that are blind to defects, propagating in the whole 3+1 dimensions with innate conformal speed $v_s^2 = 1/3$.

In the current setup, where the backreaction is taken into account and the defects are smeared in the transverse directions, there is an interesting interplay of collective phenomena leading to speeding and braking from the conformal value 1/3. The speed along the defect directions is larger than in the orthogonal directions: The interaction between the adjoint and fundamental degrees of freedom leads to slowing down the defect degrees of freedom, while at the same time speeding up the fields mixing mode that moves at an intermediate speed. This suggests that the interaction inborn from defect degrees of freedom with the degrees of freedom outside the defects is such that it "pushes" the motion of the collective modes to higher speeds along the defect directions. On the contrary, the motion in the direction transverse to the defects slows down, which can be seen in part as a consequence of the equation of state below (7.3.38). In a sense, the total kinetic energy of the fluid is conserved but more of it is put in the direction of the defects, so that there is less available for the transverse motion.

The deviation from the value 1/3 in (7.3.37) naively reflects the breaking of conformality along the (x^1, x^2)-plane and the x^3-direction. Values for the speed of sound above the conformal value in holography [168, 169] are now abound in various settings [170]. However, here the full equation of state

$$2p_{xy} + p_z = \mathcal{E} \tag{7.3.38}$$

should be regarded as the "conformal" analog in homogeneous, but anisotropic system. Indeed, we have not introduced any further energy scale in the system as the D3- and D5-branes are not separated and the corresponding fundamental quark masses vanish. One can also easily check the following relations

$$\begin{aligned} &p_{xy} = \frac{1}{3}\left(\mathcal{E} - \Phi\, n_{\rm f}\right) \ , \qquad\qquad p_z = \frac{1}{3}\left(\mathcal{E} + 2\Phi\, n_{\rm f}\right) \ , \\ &\mathcal{E} = \frac{1}{4}\left(3\,T\,s + 3\mu\, n_{\rm q} + \Phi\, n_{\rm f}\right) \ , \\ &p_{xy} = T\,s + \mu\, n_{\rm q} - \mathcal{E} \ , \qquad\qquad p_z = T\,s + \mu\, n_{\rm q} + \Phi\, n_{\rm f} - \mathcal{E} \ . \end{aligned} \tag{7.3.39}$$

We now compare the chemical potential μ with the UV value of the worldvolume gauge field A_t. For this purpose, it is quite convenient to rewrite μ as

$$\mu \;=\; -\frac{\rho_{\rm h}}{\sqrt{6}\,\pi\,\alpha'}\,\tilde{\delta}\left(1 + \frac{15}{8}\,\epsilon\right) . \tag{7.3.40}$$

On the other hand, in appendix 7.B we found, by imposing the condition that A_t vanishes at the horizon, that

$$\frac{A_{t,\rm UV}}{2\pi\alpha'} \;=\; -\frac{\rho_{\rm h}}{\sqrt{6}\,\pi\,\alpha'}\,\tilde{\delta}\left(1 - \Delta_1\,\epsilon\right) , \tag{7.3.41}$$

USC UNIVERSIDADE DE SANTIAGO DE COMPOSTELA

where $\Delta_1 \approx 1.06$. These two results coincide at leading order in $\tilde{\delta}$, but they differ at $\mathcal{O}(\epsilon\tilde{\delta})$. Indeed, one can easily demonstrate that

$$\frac{A_{t,\mathrm{UV}}}{2\pi\alpha'} = \mu\left(1 - \left(\frac{15}{8} + \Delta_1\right)\epsilon\right) . \tag{7.3.42}$$

This result is similar to the one found in [88] for the D3-D7 system at finite baryon density and may be regarded as an effect due to the backreaction of the flavors.

USC
UNIVERSIDADE
DE SANTIAGO
DE COMPOSTELA

USC
UNIVERSIDADE
DE SANTIAGO
DE COMPOSTELA

Appendices for chapter 7

7.A Solution at vanishing chemical potential

In this appendix we integrate the equations of motion found in appendix 6.A in the case in which the chemical potential vanishes. This particular case corresponds to taking $A_t = F_{123} = J = 0$ in eqs. (6.A.8), (6.A.14), (6.A.16), (6.A.22), and (6.A.23). The equation for the blackening factor b in (6.A.22) becomes simply $\partial_\sigma^2 \log b = 0$, which can be integrated as

$$b = e^{4\rho_{\rm h}^4 \sigma} , \tag{7.A.1}$$

where we have conveniently fixed the integration constants. In terms of the radial coordinate ρ, this blackening factor b becomes the one written in (7.1.1).

By comparing the equations satisfied by the warp factor h and the dilaton ϕ, one readily concludes that they can be related as

$$h = \frac{Q_{\rm c}}{4\rho_{\rm h}^4} \left(1 - e^{4\rho_{\rm h}^4 \sigma}\right) e^{-\phi} , \tag{7.A.2}$$

which, in terms of the coordinate ρ, is equivalent to (7.1.3). Therefore, the dilaton determines the warp factor. Let us now write the reduced system of equations for F, S, and ϕ. It is convenient to define the new functions $\tilde{F}$ and $\tilde{S}$ as

$$\tilde{F} = e^{-\frac{3}{2}\phi} F , \qquad \tilde{S} = e^{-\frac{3}{2}\phi} S , \tag{7.A.3}$$

which, together with the dilaton ϕ, satisfy the following system of three coupled ordinary differential equations

$$\begin{aligned}
\partial_\sigma^2 \log \tilde{F} &= \tilde{F}\tilde{S}^4 e^{4\rho_{\rm h}^4 \sigma + 10\phi} \left(4\tilde{F}^3 - 6Q_{\rm f}\tilde{S}^2 - Q_{\rm f}^2 \tilde{F}\right) \\
\partial_\sigma^2 \log \tilde{S} &= \tilde{F}\tilde{S}^4 e^{4\rho_{\rm h}^4 \sigma + 10\phi} \left(6\tilde{F}\tilde{S}^2 - 2\tilde{F}^3 - \frac{9}{2}Q_{\rm f}\tilde{S}^2 - \frac{3}{2}Q_{\rm f}^2 \tilde{F}\right) \\
\partial_\sigma^2 \phi &= Q_{\rm f}\tilde{F}\tilde{S}^4 e^{4\rho_{\rm h}^4 \sigma + 10\phi} \left(Q_{\rm f}\tilde{F} + 3\tilde{S}^2\right) .
\end{aligned} \tag{7.A.4}$$

We will solve the system (7.A.4) at first-order in the parameter ϵ defined in (7.1.4). Let us

USC UNIVERSIDADE DE SANTIAGO

represent ϕ, $\tilde{F}$, and $\tilde{S}$ in terms of the reduced radial coordinate $\tilde{\rho}$ introduced in (7.1.5)

$$\begin{aligned}\phi &= \epsilon\,\phi_1(\tilde{\rho}) \\ \tilde{F} &= \rho_{\rm h}\,\tilde{\rho}\left(1+\epsilon\,\tilde{F}_1(\tilde{\rho})\right) \\ \tilde{S} &= \rho_{\rm h}\,\tilde{\rho}\left(1+\epsilon\,\tilde{S}_1(\tilde{\rho})\right)\ .\end{aligned} \tag{7.A.5}$$

In (7.A.5) the zeroth order term corresponds to the $AdS_5\times\mathcal{M}_5$ geometry with a constant dilaton (set to zero). The first-order contribution $\phi_1(\tilde{\rho})$ to the dilaton satisfies a second-order differential equation which can be obtained by plugging the expansions (7.A.5) into the system (7.A.4) and then keeping first-order terms. We find

$$\phi_1'' + \frac{(5\tilde{\rho}^4-1)\,\phi_1'}{\tilde{\rho}\,(\tilde{\rho}^4-1)} - \frac{15\tilde{\rho}}{\tilde{\rho}^4-1} = 0\ , \tag{7.A.6}$$

where the primes denote derivatives with respect to $\tilde{\rho}$. The general solution of (7.A.6) is

$$\phi_1 = c_2 + \frac{1}{4}\left(c_1\log\left(\frac{\tilde{\rho}^4}{\tilde{\rho}^4-1}\right) + 5\log\left(\frac{\tilde{\rho}-1}{\tilde{\rho}+1}\right) + 10\arctan(\tilde{\rho})\right)\ , \tag{7.A.7}$$

where c_1 and c_2 are integration constants. The equations for $\tilde{F}_1$ and $\tilde{F}_2$ derived from the system (7.A.4) are coupled. They can be decoupled by introducing new functions f_1 and f_2 as follows

$$\tilde{F}_1(\tilde{\rho}) = \frac{1}{\sqrt{2}}f_1(\tilde{\rho}) - \frac{4}{\sqrt{17}}f_2(\tilde{\rho})\ , \qquad \tilde{S}_1(\tilde{\rho}) = \frac{1}{\sqrt{2}}f_1(\tilde{\rho}) + \frac{1}{\sqrt{17}}f_2(\tilde{\rho})\ . \tag{7.A.8}$$

The decoupled equations for f_1 and f_2 are thus

$$\begin{aligned} f_1'' + \frac{(5\tilde{\rho}^4-1)\,f_1'}{\tilde{\rho}\,(\tilde{\rho}^4-1)} - \frac{32\tilde{\rho}^2\,f_1}{\tilde{\rho}^4-1} + \frac{24\sqrt{2}\tilde{\rho}}{\tilde{\rho}^4-1} - \frac{40\sqrt{2}\tilde{\rho}^2\phi_1}{\tilde{\rho}^4-1} &= 0 \\ f_2'' + \frac{(5\tilde{\rho}^4-1)\,f_2'}{\tilde{\rho}\,(\tilde{\rho}^4-1)} - \frac{12\tilde{\rho}^2 f_2}{\tilde{\rho}^4-1} - \frac{3\sqrt{17}\tilde{\rho}}{2\,(\tilde{\rho}^4-1)} &= 0\ . \end{aligned} \tag{7.A.9}$$

The equation for f_1 contains ϕ_1 as a source and can be integrated as

$$\begin{aligned} f_1 &= \frac{1}{\sqrt{2}}\left(\tilde{\rho}^3 + \frac{1}{4}\left(\tilde{\rho}^4-13\right)\left(\log\left(\frac{\tilde{\rho}-1}{\tilde{\rho}+1}\right)+2\arctan(\tilde{\rho})\right)\right) \\ &\quad -\frac{c_3}{2} - 2c_4 + \tilde{\rho}^4\left(\frac{5c_1}{2\sqrt{2}} - \frac{5c_2}{\sqrt{2}} + c_3\right) + \log\left(\frac{\tilde{\rho}^4-1}{\tilde{\rho}^4}\right)\left(\frac{5c_1\tilde{\rho}^4}{4\sqrt{2}} - 2c_4\tilde{\rho}^4 + c_4\right)\ , \end{aligned} \tag{7.A.10}$$

USC UNIVERSIDADE DE SANTIAGO DE COMPOSTELA

where c_3 and c_4 are new constants of integration. In order to integrate the equation satisfied by f_2, let us define functions $P(z)$ and $Q(z)$ as follows

$$\begin{aligned} P(z) &= F\Big(-\frac{1}{2}\,,\,\frac{3}{2}\,;1\,;\,1-z^4\Big) \\ Q(z) &= (2z^4-1)^{-\frac{3}{2}}\,F\left(\frac{5}{4}\,,\,\frac{3}{4}\,;2\,;\,\frac{1}{(2z^4-1)^2}\right)\,. \end{aligned} \tag{7.A.11}$$

The functions $F(\ldots) = {}_2F_1(a,b;c;z)$ here are standard hypergeometric functions, but we have dropped the subscripts to avoid extra clutter. The functions $P(\tilde\rho)$ and $Q(\tilde\rho)$ are two independent solutions of the homogeneous equation for $f_2(\tilde\rho)$ in (7.A.9). To find a solution of the inhomogeneous equation we apply the Wronskian method. The general solution for $f_2(\tilde\rho)$ is

$$f_2(\tilde\rho) \,=\, c_5\,P(\tilde\rho) \,+\, c_6\,Q(\tilde\rho) \,+\, I_1(\tilde\rho)\,P(\tilde\rho) \,+\, I_2(\tilde\rho)\,Q(\tilde\rho)\,. \tag{7.A.12}$$

In (7.A.12) c_5 and c_6 are constants of integration and $I_1(\tilde\rho)$ and $I_2(\tilde\rho)$ are the following integrals

$$I_1(\tilde\rho) \,=\, \int_{\tilde\rho}^{\infty}\,\frac{Q(z)\,g(z)}{W(P,Q)}\,dz\,, \qquad\qquad I_2(\tilde\rho) \,=\, \int_{1}^{\tilde\rho}\,\frac{P(z)\,g(z)}{W(P,Q)}\,\mathrm{d}z\,, \tag{7.A.13}$$

where $g(z)$ is the inhomogeneous term in (7.A.9)

$$g(z) \,=\, \frac{3\sqrt{17}\,z}{2(z^4-1)}\,, \tag{7.A.14}$$

and $W(P,Q)$ is the Wronskian of the functions $P(z)$ and $Q(z)$, given by

$$W(P,Q) \,=\, P(z)\,Q'(z) \,-\, Q(z)\,P'(z) \,=\, \frac{8\,\sqrt{2}}{\pi\,z\,(1-z^4)}\,. \tag{7.A.15}$$

We have found a solution for ϕ_1, F_1, and S_1 which depends on six integration constants $c_1\,,\,\cdots\,,c_6$. These constants can be determined by requiring the fulfilment of the constraint (6.A.23), as well as regularity both at the horizon $\tilde\rho = 1$ and at the boundary $\tilde\rho \to \infty$. Doing this we get

$$c_1 = 5, \qquad c_2 = -\frac{5\pi}{4}, \qquad c_3 = -\frac{25+13\pi}{2\sqrt{2}}, \qquad c_4 = \frac{13}{4\sqrt{2}}, \qquad c_5 = c_6 = 0\,. \tag{7.A.16}$$

Let us now write the final form of our $\mathcal{O}(\epsilon)$ solution. The dilaton $\phi(\tilde\rho)$, the warp factor $h(\tilde\rho)$, and the functions $\alpha(\tilde\rho)$ and $G(\tilde\rho)$ are written in (7.1.7) in terms of the function $\Omega(\tilde\rho)$ defined in (7.1.6). The internal deformation functions $F(\tilde\rho)$ and $S(\tilde\rho)$ are written in (7.1.8) in terms of the first-order functions $F_1(\tilde\rho)$ and $S_1(\tilde\rho)$. In order to present compact expressions for these functions, let us define the integrals $\mathcal{I}_P(x)$ and $\mathcal{I}_{Q(x)}$ as

$$\mathcal{I}_P^{(1)}(x) \,=\, \int_1^x\,z^2P(z)\,\mathrm{d}z\,, \qquad\qquad \mathcal{I}_Q^{(1)}(x) \,=\, \int_x^\infty\,z^2Q(z)\,\mathrm{d}z\,. \tag{7.A.17}$$

USC UNIVERSIDADE DE SANTIAGO DE COMPOSTELA

This procedure finally yields

$$\begin{aligned} F_1(\tilde{\rho}) &= \frac{3\sqrt{2}\,\pi}{8}\left(P(\tilde{\rho})\,\mathcal{I}_Q^{(1)}(\tilde{\rho}) + Q(\tilde{\rho})\,\mathcal{I}_P^{(1)}(\tilde{\rho})\right) + \frac{1}{2}\,\tilde{\rho}^3 - \frac{1}{8} + \frac{1}{10}\,(\tilde{\rho}^4+2)\,\Omega(\tilde{\rho}) \\ S_1(\tilde{\rho}) &= -\frac{3\sqrt{2}\,\pi}{32}\left(P(\tilde{\rho})\,\mathcal{I}_Q^{(1)}(\tilde{\rho}) + Q(\tilde{\rho})\,\mathcal{I}_P^{(1)}(\tilde{\rho})\right) + \frac{1}{2}\,\tilde{\rho}^3 - \frac{1}{8} + \frac{1}{10}\,(\tilde{\rho}^4+2)\,\Omega(\tilde{\rho})\ . \end{aligned} \tag{7.A.18}$$

7.B Solution with non-zero chemical potential

Let us now add non-zero chemical potential to the black hole solution of appendix 7.A. We will first expand the dilaton in powers of ϵ and δ as

$$\phi = \epsilon\,\phi_1(\tilde{\rho}) \,+\, \epsilon\,\delta^2\,\phi_2(\tilde{\rho})\ , \tag{7.B.1}$$

where $\phi_1(\tilde{\rho})$ is the solution found in appendix 7.A in (7.A.7). It turns out that the equation for ϕ_2 is completely decoupled and given by

$$\phi_2'' + \frac{(5\tilde{\rho}^4-1)}{\tilde{\rho}\,(\tilde{\rho}^4-1)}\phi_2' - \frac{Q_{\rm c}^2}{120\,\rho_{\rm h}^6\,\tilde{\rho}^3\,(\tilde{\rho}^4-1)} = 0\ . \tag{7.B.2}$$

The solution for this equation is

$$\phi_2 = d_2 + d_1\log\left(1-\frac{1}{\tilde{\rho}^4}\right) - \frac{Q_{\rm c}^2}{480\rho_{\rm h}^6\tilde{\rho}}\left(\tilde{\rho}\left(\log\left(\frac{\tilde{\rho}-1}{\tilde{\rho}+1}\right)+2\arctan(\tilde{\rho})\right)+4\right)\ , \tag{7.B.3}$$

where d_1 and d_2 are integration constants. Similarly, we expand $\alpha(\tilde{\rho})$ and $b(\tilde{\rho})$ as

$$\alpha(\tilde{\rho}) \,=\, \alpha_0 \,+\, \epsilon\,\alpha_1(\tilde{\rho}) \,+\, \epsilon\,\delta^2\,\alpha_2(\tilde{\rho})\ , \qquad\qquad b(\tilde{\rho}) \,=\, b_0(\tilde{\rho}) \,+\, \epsilon\,\delta^2\,b_2(\tilde{\rho})\ , \tag{7.B.4}$$

where α_0, $\alpha_1(\tilde{\rho})$, and $b_0(\tilde{\rho})$ are the zeroth and first order terms in (7.1.7) per subscript labeling. Notice that $b(\tilde{\rho})$ does not contain $\mathcal{O}(\epsilon)$) terms, in agreement with our result (7.1.7) for the black hole with vanishing chemical potential. The equations for $\alpha_2(\tilde{\rho})$ and $b_2(\tilde{\rho})$ are

$$\begin{aligned} \alpha_2'' + \frac{5\tilde{\rho}^4-1}{\tilde{\rho}\,(\tilde{\rho}^4-1)}\alpha_2' - \frac{Q_{\rm c}^2}{120\rho_{\rm h}^6\,\tilde{\rho}^3\,(\tilde{\rho}^4-1)} &= 0 \\ b_2'' - \frac{5\tilde{\rho}^4-9}{\tilde{\rho}\,(\tilde{\rho}^4-1)}b_2' + \frac{16}{\tilde{\rho}^2\,(\tilde{\rho}^4-1)^2}b_2 - \frac{Q_{\rm c}^2}{30\,\rho_{\rm h}^6\,\tilde{\rho}^7} &= 0\ , \end{aligned} \tag{7.B.5}$$

and, remarkably, can be solved in terms of $\phi_2(\tilde{\rho})$ as

$$\alpha_2(\tilde{\rho}) \,=\, \phi_2(\tilde{\rho})\ , \qquad\qquad b_2(\tilde{\rho}) \,=\, 4\left(1-\frac{1}{\tilde{\rho}^4}\right)\phi_2(\tilde{\rho})\ . \tag{7.B.6}$$

USC UNIVERSIDADE DE SANTIAGO DE COMPOSTELA

Similarly, we can expand the warp factor $h(\tilde{\rho})$ as

$$h(\tilde{\rho}) \,=\, h_0(\tilde{\rho}) \,+\, \epsilon\, h_1(\tilde{\rho}) \,+\, \epsilon\,\delta^2\, h_2(\tilde{\rho}) \ , \tag{7.B.7}$$

where $h_0(\tilde{\rho})$ and $h_1(\tilde{\rho})$ can be extracted from (7.1.7). The second order contribution $h_2(\tilde{\rho})$ satisfies the equation

$$\begin{aligned} &h_2'' + \frac{13\tilde{\rho}^4-9}{\tilde{\rho}\,(\tilde{\rho}^4-1)}h_2' - \frac{16}{\tilde{\rho}^2\,(\tilde{\rho}^4-1)}h_2 \\ &\qquad + \frac{4Q_{\rm c}\,\tilde{\rho}^2}{\rho_{\rm h}^4\,(\tilde{\rho}^4-1)^2}b_2 + \frac{8Q_{\rm c}}{\rho_{\rm h}^4\,\tilde{\rho}^2\,(\tilde{\rho}^4-1)}\alpha_2 - \frac{Q_{\rm c}^3}{160\rho_{\rm h}^{10}\,\tilde{\rho}^7\,(\tilde{\rho}^4-1)} = 0 \ , \end{aligned} \tag{7.B.8}$$

which can also be solved in terms of the dilaton function $\phi_2(\tilde{\rho})$ as

$$h_2(\tilde{\rho}) = \frac{3Q_{\rm c}}{4\rho_{\rm h}^4\tilde{\rho}^4}\,\phi_2(\tilde{\rho}) \ . \tag{7.B.9}$$

Let us next represent $F(\tilde{\rho})$ and $S(\tilde{\rho})$ as in (7.2.7). The differential equations for $F_2(\tilde{\rho})$ and $S_2(\tilde{\rho})$ are coupled and contain $\alpha_2(\tilde{\rho})$ and $b_2(\tilde{\rho})$ as sources. These equations can be decoupled by performing the same linear combinations as in (7.A.8), *i.e.*, by introducing new functions $g_1(\tilde{\rho})$ and $g_2(\tilde{\rho})$ as

$$F_2(\tilde{\rho}) = \frac{1}{\sqrt{2}}g_1(\tilde{\rho}) - \frac{4}{\sqrt{17}}g_2(\tilde{\rho}) \qquad\qquad S_2(\tilde{\rho}) = \frac{1}{\sqrt{2}}g_1(\tilde{\rho}) + \frac{1}{\sqrt{17}}g_2(\tilde{\rho}) \ . \tag{7.B.10}$$

The equations satisfied by g_1 and g_2 are

$$\begin{aligned} &g_1'' + \frac{1-5\tilde{\rho}^4}{\tilde{\rho}-\tilde{\rho}^5}\,g_1' - \frac{32\tilde{\rho}^2}{\tilde{\rho}^4-1}\,g_1 - \frac{24\sqrt{2}\,\tilde{\rho}^2}{\tilde{\rho}^4-1}\Big(d_1\log\left(1-\frac{1}{\tilde{\rho}^4}\right)+d_2\Big) \\ &\qquad + \frac{Q_{\rm c}^2\,\tilde{\rho}^3}{10\sqrt{2}\,\rho_{\rm h}^6\,(\tilde{\rho}^4-1)}\Big(\log\left(\frac{\tilde{\rho}-1}{\tilde{\rho}+1}\right)+2\arctan(\tilde{\rho})\Big) + \frac{Q_{\rm c}^2\,(80\tilde{\rho}^4+3)}{200\sqrt{2}\,\rho_{\rm h}^6\,\tilde{\rho}^3(\tilde{\rho}^4-1)} = 0 \\ &g_2'' + \frac{1-5\tilde{\rho}^4}{\tilde{\rho}-\tilde{\rho}^5}\,g_2' - \frac{12\tilde{\rho}^2}{\tilde{\rho}^4-1}\,g_2 + \frac{\sqrt{17}\,Q_{\rm c}^2}{1200\,\rho_{\rm h}^6\,\tilde{\rho}^3\,(\tilde{\rho}^4-1)} = 0 \ . \end{aligned} \tag{7.B.11}$$

The equation for g_1 can be explicitly integrated as

$$\begin{aligned} g_1(\tilde{\rho}) \;=\; &-\frac{1}{2400\sqrt{2}\rho_{\rm h}^6\tilde{\rho}}\Bigg(7200\rho_{\rm h}^6\tilde{\rho}^5\left(d_1\log\left(1-\frac{1}{\tilde{\rho}^4}\right)+2d_1+d_2\right)+4Q_{\rm c}^2\left(5\tilde{\rho}^4-9\right) \\ &+5Q_{\rm c}^2\tilde{\rho}\left(\tilde{\rho}^4-2\right)\left(\log\left(\frac{\tilde{\rho}-1}{\tilde{\rho}+1}\right)+2\arctan(\tilde{\rho})\right)\Bigg)+d_3\left(1-2\tilde{\rho}^4\right) \\ &+\frac{1}{2}d_4\left(2-\left(1-2\tilde{\rho}^4\right)\log\left(1-\frac{1}{\tilde{\rho}^4}\right)\right) \ , \end{aligned} \tag{7.B.12}$$

USC UNIVERSIDADE DE SANTIAGO DE COMPOSTELA

where d_3 and d_4 are new integration constants. To integrate the equation for g_2 in (7.B.11) we again make use of the Wronskian method. The homogeneous part of the equation is the same as the one in the equation for f_2 in (7.A.9) and, therefore, is solved by the functions P and Q defined in (7.A.11). To write a special solution of the second-order inhomogeneous equation in (7.B.11), we define new functions $\mathcal{I}_P^{(2)}(x)$ and $\mathcal{I}_Q^{(2)}(x)$ as

$$\mathcal{I}_P^{(2)}(x) \,=\, \int_1^x \frac{P(z)}{z^2}\,\mathrm{d}z \;, \qquad\qquad \mathcal{I}_Q^{(2)}(x) \,=\, \int_x^\infty \frac{Q(z)}{z^2}\,\mathrm{d}z \;. \tag{7.B.13}$$

Then, the general solution for $g_2(\tilde\rho)$ can be written as

$$g_2(\tilde\rho) = d_5\,P(\tilde\rho) + d_6\,Q(\tilde\rho) + \frac{\sqrt{17}\,\pi\,Q_{\rm c}^2}{9600\,\sqrt{2}\,\rho_{\rm h}^6}\Big(P(\tilde\rho)\,\mathcal{I}_Q^{(2)}(\tilde\rho) \,+\, Q(\tilde\rho)\,\mathcal{I}_P^{(2)}(\tilde\rho)\Big)\;, \tag{7.B.14}$$

where d_5 and d_6 are two new integration constants. By imposing regularity of ϕ_2, g_1, and g_2, both at the horizon $\tilde\rho = 1$ and at the UV $\tilde\rho \to \infty$, we can determine the constants of integration, which can be shown to be given by

$$\begin{aligned} d_1 \,&=\, \frac{d_2}{\pi} \,=\, \frac{Q_{\rm c}^2}{480\,\rho_{\rm h}^6}\;, \qquad\qquad d_3 \,=\, -\frac{3+2\pi}{480\,\sqrt{2}}\,\frac{Q_{\rm c}^2}{\rho_{\rm h}^5} \\ d_4 \,&=\, \frac{Q_{\rm c}^2}{120\,\sqrt{2}\,\rho_{\rm h}^5}\;, \qquad\qquad d_5 \,=\, d_6 \,=\, 0\;. \end{aligned} \tag{7.B.15}$$

Using these values for the d_i's we get the expressions of $\phi(\tilde\rho)$, $\alpha(\tilde\rho)$, $b(\tilde\rho)$, and $h(\tilde\rho)$ displayed in eqs. (7.2.5) and (7.2.6) of the main text. The expression for $G(\tilde\rho)$ in 7.2.6) can be obtained from the other functions by using (6.1.8). The functions $F(\tilde\rho)$ and $G(\tilde\rho)$ can be written as in (7.2.7), with $F_2(\tilde\rho)$ and $S_2(\tilde\rho)$ given by

$$\begin{aligned} F_2(\tilde\rho) \;&=\; -\frac{\pi}{4\sqrt{2}}\Big(P(\tilde\rho)\,\mathcal{I}_Q^{(2)}(\tilde\rho) + Q(\tilde\rho)\,\mathcal{I}_P^{(2)}(\tilde\rho)\Big) \,-\, \frac{5}{2}\,\tilde\rho^3 + \frac{5}{8} \,+\, \frac{9}{2\,\tilde\rho} + \frac{1}{2}(2-\tilde\rho^4)\,\Omega(\tilde\rho) \\ S_2(\tilde\rho) \;&=\; \frac{\pi}{16\sqrt{2}}\Big(P(\tilde\rho)\,\mathcal{I}_Q^{(2)}(\tilde\rho) + Q(\tilde\rho)\,\mathcal{I}_P^{(2)}(\tilde\rho)\Big) \,-\, \frac{5}{2}\,\tilde\rho^3 + \frac{5}{8} \,+\, \frac{9}{2\,\tilde\rho} + \frac{1}{2}(2-\tilde\rho^4)\,\Omega(\tilde\rho)\;. \end{aligned} \tag{7.B.16}$$

To complete the solution it remains to find $j(\tilde\rho)$. Its equation at leading order can be easily found from (6.A.8) and is given by

$$j'' + \frac{\tilde\rho^4+3}{\tilde\rho\,(\tilde\rho^4-1)}\,j' - \frac{9\,\tilde\rho^2}{\tilde\rho^4-1}\,j - \frac{Q_{\rm c}\,\tilde\rho}{2\rho_{\rm h}\,(\tilde\rho^4-1)} = 0\;. \tag{7.B.17}$$

The homogeneous version of this equation has the following two independent solutions

$$J_1(\tilde\rho) = F\Big(-\frac{3}{4},\frac{3}{4};1;1-\tilde\rho^4\Big)\;, \qquad J_2(\tilde\rho) = \big(\tilde\rho^4-1\big)^{-3/4}\;F\left(\frac{3}{4},\frac{3}{4};\frac{5}{2};\frac{1}{1-\tilde\rho^4}\right)\;. \tag{7.B.18}$$

USC UNIVERSIDADE DE SANTIAGO DE COMPOSTELA

The general solution for $j(\tilde{\rho})$ can be found by adding a linear combination of $J_1(\tilde{\rho})$ and $J_2(\tilde{\rho})$ and a special solution of the complete equation obtained again by the Wronskian method. Notice that $J_1(\tilde{\rho})$ is regular at $\tilde{\rho}=1$ and blows up at $\tilde{\rho}\to\infty$, whereas $J_2(\tilde{\rho})$ has the opposite behavior and diverges at the horizon and is regular at the UV. By taking these facts into account, it is not difficult to find the regular solution for $j(\tilde{\rho})$. If we define $\mathcal{I}_1(\tilde{\rho})$ and $\mathcal{I}_2(\tilde{\rho})$ as

$$\mathcal{I}_1(\tilde{\rho}) \,=\, \int_1^{\tilde{\rho}} \frac{J_1(z)}{z^2}\mathrm{d}z \;, \qquad\qquad \mathcal{I}_2(\tilde{\rho}) \,=\, \int_{\tilde{\rho}}^{\infty} \frac{J_2(z)}{z^2}\mathrm{d}z \tag{7.B.19}$$

then we have

$$j(\tilde{\rho}) \,=\, -\frac{Q_{\mathrm{c}}\Big[\Gamma\left(\frac{3}{4}\right)\Big]^2}{8\sqrt{\pi}\,\rho_{\mathrm{h}}}\left(J_1(\tilde{\rho})\,\mathcal{I}_2(\tilde{\rho})+J_2(\tilde{\rho})\,\mathcal{I}_1(\tilde{\rho})\right) \;. \tag{7.B.20}$$

On the other hand, we can use these results to find the worldvolume gauge field A_t'. Let us write

$$\frac{1}{2\pi\alpha'}A_t'(\tilde{\rho}) = \frac{1}{2\pi\alpha'}\Big(A_t'^{(0)}(\tilde{\rho})+\epsilon\, A_t'^{(1)}(\tilde{\rho})\Big) = \tilde{\delta}\;\left(a_0(\tilde{\rho})+\epsilon\, a_1(\tilde{\rho})\right) \;, \tag{7.B.21}$$

where

$$\begin{aligned} a_0(\tilde{\rho}) \;&=\; -\frac{\rho_{\mathrm{h}}}{\sqrt{6}\pi\alpha'}\frac{1}{\tilde{\rho}^2} \\ a_1(\tilde{\rho}) \;&=\; -\frac{\sqrt{3}\,\rho_{\mathrm{h}}}{16\,\alpha'\tilde{\rho}^2}\Big(P(\tilde{\rho})\,I_Q(\tilde{\rho})+Q(\tilde{\rho})\,I_P(\tilde{\rho})-\frac{\sqrt{2}\left(3\,(1-4\tilde{\rho}^3)-(3\tilde{\rho}^4+1)\,\frac{4}{5}\Omega(\tilde{\rho})\right)}{3\pi} \\ &\quad +\frac{80\sqrt{2}\,\rho_{\mathrm{h}}}{\pi\,Q_{\mathrm{c}}}j(\tilde{\rho})\Big) \;. \end{aligned} \tag{7.B.22}$$

The UV value of $A_t/(2\pi\alpha')$ is related to the chemical potential μ. This value can be obtained by integrating (7.B.21) with respect to $\tilde{\rho}$. Doing this integration with the condition that $A_t(\tilde{\rho}=1)=0$, we get

$$\frac{A_{t,UV}}{2\pi\alpha'} \,=\, \frac{A_t(\tilde{\rho}\to\infty)}{2\pi\alpha'} \,=\, \frac{1}{2\pi\alpha'}\int_1^{\infty} A_t'(\tilde{\rho})\,\mathrm{d}\tilde{\rho} \,=\, \tilde{\delta}\;\left(a_{0,UV}\,+\,\epsilon\, a_{1,UV}\right) \;, \tag{7.B.23}$$

where $a_{0,\mathrm{UV}}$ and $a_{1,\mathrm{UV}}$ are given by

$$\begin{aligned} a_{0,\mathrm{UV}} \;&=\; \int_1^{\infty} a_0(\tilde{\rho})\,\mathrm{d}\tilde{\rho} \,=\, -\frac{\rho_{\mathrm{h}}}{\sqrt{6}\,\pi\alpha'} \\ a_{1,\mathrm{UV}} \;&=\; \int_1^{\infty} a_1(\tilde{\rho})\,\mathrm{d}\tilde{\rho} \,\approx\, -1.06\,a_{0,\mathrm{UV}} \;, \end{aligned} \tag{7.B.24}$$

The integration of $a_{0,\mathrm{UV}}$ in (7.B.24) can be done analytically, whereas the one needed to get $a_{1,\mathrm{UV}}$ has to be done numerically. By comparing these results with the chemical potential calculated in (7.3.40), we notice that the $\mathcal{O}(\epsilon\tilde{\delta})$ terms are different (see (7.3.42)). This difference can be attributed to the backreaction of the flavors.

USC
UNIVERSIDAD DE SANTIAGO

7.C Grand canonical potential from the euclidean action

As a crosscheck, one can as well compute the grand canonical potential from the on-shell euclidean action $\mathcal{I}$ as

$$\Omega = \frac{1}{\beta}\left(\mathcal{I}_{bulk} - \mathcal{I}_{bulk,T,\mu=0} + \mathcal{I}_{surface} - \mathcal{I}_{surface,T,\mu=0}\right) \ , \tag{7.C.1}$$

where we are subtracting the zero temperature and chemical potential values, and β is the period of the Euclidean time in the non-zero temperature solution. Moreover, we will be rescaling the zero temperature and chemical actions with a factor $\sqrt{1-\frac{\rho_{\rm h}^4}{\rho^4}}$, which is simply the squared root of $b(\rho)$ in the absence of chemical potential, given by equation (7.1.1). The bulk action is (6.1.2) and the surface action is given by the Gibbons-Hawking term

$$\mathcal{I}_{surface} = -\frac{1}{\kappa_{10}^2}\int_{\mathcal{M}_{\rho\infty}} d^9x\,\sqrt{g_9}\,K \ , \tag{7.C.2}$$

with K being the extrinsic curvature of the nine dimensional hypersurface with constant ρ within the full space

$$\sqrt{g_9}\,K = \frac{\sqrt{g_9}}{\sqrt{g_{10}}}\partial_\mu\left(\sqrt{g_{10}}\frac{1}{\sqrt{g_{\rho\rho}}}\delta^\mu_\rho\right) = \frac{\rho\,(\rho^4-\rho_{\rm h}^4)}{h^{1/4}b^{1/2}\alpha\,S^4\,F}\partial_\rho\left(h^{1/4}\alpha\,b^{1/2}\,S^4\,F\right) \ . \tag{7.C.3}$$

We start by computing the contribution of the bulk action

$$\begin{aligned}
&-\frac{(2\pi)^7\,\alpha'^4\,g_{\rm s}^2}{V_3\,{\rm Vol}\left(\mathcal{M}_5\right)}\frac{1}{\beta}\left(\mathcal{I}_{bulk}-\mathcal{I}_{bulk,T,\mu=0}\right) = \\
&= \lim_{\rho_\Lambda\to\infty}\left[\int_{\rho_{\rm h}}^{\rho_\Lambda}\left(-8\,\rho^3 - Q_{\rm f}\,\frac{3}{2}\,\rho^2 + \frac{n_q^2}{Q_{\rm f}}\,\frac{15}{2}\,\gamma\,\frac{1}{\rho^2}\right) - \sqrt{1-\frac{\rho_{\rm h}^4}{\rho^4}}\int_0^{\rho_\Lambda}\left(-8\,\rho^3 - Q_{\rm f}\,\frac{3}{2}\,\rho^2\right)\right] = \\
&= \rho_{\rm h}^4\left(1 + \frac{Q_{\rm f}}{\rho_{\rm h}}\,\frac{1}{2} + \frac{n_q^2}{Q_{\rm f}}\,\frac{15}{2}\,\gamma\,\frac{1}{\rho_{\rm h}^5}\right) = \rho_{\rm h}^4\left(1+\epsilon\,\frac{5}{2}+\epsilon\,\tilde{\delta}^2\,\frac{15}{2}\right) \ ,
\end{aligned} \tag{7.C.4}$$

where we have made use of (7.1.4) and (7.3.9). On the other hand, for the surface action we find

$$\begin{aligned}
&-\frac{(2\pi)^7\,\alpha'^4\,g_{\rm s}^2}{V_3\,{\rm Vol}\left(\mathcal{M}_5\right)}\frac{1}{\beta}\left(\mathcal{I}_{surface}-\mathcal{I}_{surface,T,\mu=0}\right) = \\
&= \lim_{\rho_\Lambda\to\infty}\left[4\,\rho_\Lambda^4 - Q_{\rm f}\,\frac{3}{20}\,\rho_\Lambda^3 - 2\,\rho_{\rm h}^4 - \sqrt{1-\frac{\rho_{\rm h}^4}{\rho_\Lambda^4}}\left(4\,\rho_\Lambda^4 - Q_{\rm f}\,\frac{3}{20}\,\rho_\Lambda^3\right)\right] = 0 \ ,
\end{aligned} \tag{7.C.5}$$

which vanishes. Thus, we arrive at

$$\Omega = \frac{V_3\,{\rm Vol}\left(\mathcal{M}_5\right)}{(2\pi)^7\,\alpha'^4\,g_{\rm s}^2}\rho_{\rm h}^4\left(1+\epsilon\,\frac{5}{2}+\epsilon\,\tilde{\delta}^2\,\frac{15}{2}\right) = f - \mu\,n_q \ , \tag{7.C.6}$$

where f is given by (7.3.8). This result coincides with the $\langle T^{x^1}{}_{x^1}\rangle$ and $\langle T^{x^2}{}_{x^2}\rangle$ components of the energy momentum tensor in (7.3.32).

USC DE SANTIAGO

8 Applications

In this chapter we make use of the background geometry to compute several observable quantities in the dual field theory. We are specifically interested in determining the dependence on the flavor deformation parameters of these observables. We start by analyzing the transport properties at zero chemical potential.

8.1 Hydrodynamics at zero chemical potential

Let us start by studying the hydrodynamic properties of our system. We will compute the transport coefficients of perturbations propagating along the (x^1, x^2)-plane. In order to do that we consider the dimensionally reduced theory to four dimensions and perform a suitably chosen perturbation of the 4d metric. This calculation is done in detail in appendix 8.A.1, following the lines of ref. [77], whereas in this section we will summarise the results. We will restrict our analysis to the so-called shear channel. Our main purpose is to obtain the dispersion relation $\omega = \omega(q)$ of these shear modes at low momentum q. Let us assume that, as in the $AdS_5 \times \mathbb{S}^5$ geometry, this dispersion relation has the form

$$\omega \;=\; -i\, D_\eta\, q^2 \left(1 + \tau_s\, D_\eta\, q^2\right) + \dots \;, \tag{8.1.1}$$

where we are keeping terms up to quartic power of q. The dispersion relation (8.1.1) depends on two transport coefficients D_η and τ_s, which we calculate next. We will work in dimensionless variables $\hat{q}$ and $\hat{\omega}$, defined as

$$\hat{q} = \frac{q}{2\pi\, T} \;, \qquad\qquad \hat{\omega} = \frac{\omega}{2\pi\, T} \;. \tag{8.1.2}$$

Moreover, we define rescaled coefficients $\hat{D}_\eta$ and $\hat{\tau}_s$ as

$$\hat{D}_\eta \;=\; 2\pi\, T\, D_\eta \;, \qquad\qquad \hat{\tau}_s \;=\; 2\pi\, T\, \tau_s \;. \tag{8.1.3}$$

USC
UNIVERSIDADE
DE SANTIAGO
DE COMPOSTELA

In terms of the rescaled quantities, the dispersion relation (8.1.1) takes the form

$$\hat{\omega} \;=\; -i\, \hat{D}_\eta\, \hat{q}^2 \left(1 + \hat{\tau}_s\, \hat{D}_\eta\, \hat{q}^2\right) + \dots \;. \tag{8.1.4}$$

The coefficient $\hat{D}_\eta$ determines the ratio of the shear viscosity η to the entropy density s, namely

$$\frac{\eta}{s} = \frac{\hat{D}_\eta}{2\pi} \ . \tag{8.1.5}$$

From the results of appendix 8.A we get

$$\hat{D}_\eta = \frac{1}{2} \ , \qquad \hat{\tau}_s = 1 - \log 2 + \frac{5}{2}(\pi - 3)\,\epsilon \ . \tag{8.1.6}$$

Notice that the coefficient $\hat{D}_\eta$ is not corrected by the flavor. Its value corresponds to having $\eta/s = 1/(4\pi)$. On the contrary, the coefficient $\hat{\tau}_s$ is modified by the flavor. The $\epsilon = 0$ value $\hat{\tau}_s = 1 - \log 2 \simeq 0.307$ is the result found for the $AdS_5 \times \mathbb{S}^5$ geometry. The $\mathcal{O}(\epsilon)$ correction written in (8.1.6) encodes the effect of flavors, and of the corresponding anisotropy, on this transport coefficient. At the intersection between the D3 and D5 branes there is $(2+1)$-dimensional CFT, which it would be expected to have a holographic dual AdS_4 geometry. In this case the coefficient $\hat{D}_\eta$ would take the same value as in AdS_5, but $\hat{\tau}_s$ takes a larger value [171]

$$\hat{\tau}_s^{CFT_{2+1}} = \frac{3}{4}\,(1 - \log 3) + \frac{\pi}{4\sqrt{3}} \simeq 0.379. \tag{8.1.7}$$

The flavor correction in (8.1.6) increases the value of τ_s relative to the AdS_5 result thus maybe indicating that it is tending towards the AdS_4 value.

It would be interesting to calculate the transport coefficients for perturbations propagating along the x^3-direction. This calculation must be done in the five-dimensional supergravity theory constructed in [77]. Besides 5d gravity and scalars, this theory contains a codimension one defect whose fluctuations are very difficult to analyze. For this reason we will not attempt to carry out this calculation here.

8.2 Quark-antiquark potentials

In this section we will be using the (dimensionful) radial coordinate ρ. We will follow the standard holographic prescription [172,173] to find the potential between a quark and an antiquark and will solve the equations of motion of a fundamental string with its two endpoints lying at the UV boundary. These equations are obtained by extremizing the Nambu-Goto action

$$S = \frac{1}{2\pi\alpha'} \int_\Sigma \mathrm{d}\tau\, \mathrm{d}\sigma\, e^{\phi/2} \sqrt{-\det(g_2)} \ , \tag{8.2.1}$$

where τ and σ are coordinates of the string worldsheet Σ and g_2 is the induced metric on Σ in the Einstein frame. Since our geometry is anisotropic, we have to consider two different cases, depending on whether the string is extended along the directions x^1 and x^2 of the layers of D5-branes or along the orthogonal direction x^3. These two cases are treated in different subsections in what follows.

USC DE SANTIAGO

8.2.1 Intra-layer potential

We first consider a fundamental string hanging from the UV boundary and extended along x^1 with no dependence on the other two cartesian coordinates x^2, x^3; otherwise one ends up with partial differential equations in general. Let us take $\tau = x^0$, $\sigma = x^1$, and $\rho = \rho(x^1)$. Then, (8.2.1) becomes

$$S_\parallel = \frac{1}{2\pi\alpha'} \int \mathrm{d}x^0\, \mathrm{d}x^1\, e^{\phi/2} \sqrt{\frac{b^2 F^2 S^8 \alpha^2}{\rho^2 \left(\rho^4 - \rho_\mathrm{h}^4\right)^2}\, \rho'^2 + \frac{b}{h}}\ , \tag{8.2.2}$$

where ρ' denotes the derivative of $\rho(x^1)$ with respect to x^1. From the action (8.2.2) we obtain the following equation of motion for ρ'

$$\rho' = \pm \sqrt{\frac{b}{b_0}} \frac{\sqrt{h_0\, b\, e^{\phi - \phi(\rho_0)} - b_0\, h}}{\sqrt{B_1}\, h}\ , \tag{8.2.3}$$

with ρ_0 being the turning point of ρ (*i.e.*, the minimal value of the coordinate ρ) and h_0 and b_0 are the metric functions b and h evaluated at $\rho = \rho_0$. Moreover, $B_1 = B_1(\rho)$ is defined as

$$B_1 = \frac{b^2 F^2 S^8 \alpha^2}{\rho^2 \left(\rho^4 - \rho_\mathrm{h}^4\right)^2}\ . \tag{8.2.4}$$

We can invert (8.2.3) to obtain x^1 as a function of ρ, namely

$$x_1(\rho) = \pm \int_{\rho_0}^{\rho} \mathrm{d}\rho \sqrt{\frac{b_0}{b}} \frac{\sqrt{B_1}\, h}{\sqrt{h_0\, b\, e^{\phi - \phi(\rho_0)} - b_0\, h}}\ . \tag{8.2.5}$$

It follows that the quark-antiquark distance $d_\parallel$ at the boundary is

$$d_\parallel = 2 \int_{\rho_0}^{\infty} \mathrm{d}\rho \sqrt{\frac{b_0}{b}} \frac{\sqrt{B_1}\, h}{\sqrt{h_0\, b\, e^{\phi - \phi(\rho_0)} - b_0\, h}}\ . \tag{8.2.6}$$

Numerical integration of $d_\parallel$ is shown in Fig. 8.1, where we plot the dimensionless quark-antiquark distance $\tilde{d}_\parallel = \pi\, T\, d_\parallel$ versus the turning point coordinate $\tilde{\rho}_0 = \frac{\rho_0}{\rho_\mathrm{h}}$. We fast forward with representing the numerical results and leave the physical interpretation later in Sec. 8.2.3.

In order to find the quark-antiquark potential we have to evaluate the on-shell action. Plugging (8.2.3) into (8.2.2), we obtain

$$2\pi\, \alpha' S_\parallel^{\mathrm{on-shell}} = 2 \int_{\rho_0}^{\rho_\mathrm{max}} \mathrm{d}\rho\, \frac{\sqrt{h_0}\, b^{3/2}\, F\, S^4\, \alpha\, e^{\phi - \frac{\phi(\rho_0)}{2}}}{\rho\, \left(\rho^4 - \rho_\mathrm{h}^4\right)\, \sqrt{h_0\, b\, e^{\phi - \phi(\rho_0)} - b_0\, h}} \equiv \int_{\rho_0}^{\rho_\mathrm{max}} \mathrm{d}\rho\, \mathcal{L}_\parallel^{\mathrm{on-shell}}\ . \tag{8.2.7}$$

It is straightforward to see that the on-shell Lagrangian $\mathcal{L}_\parallel^{\mathrm{on-shell}}$ diverges at the UV boundary $\rho \to \infty$. We regularise this divergence by subtracting the action of two fundamental strings

USC Santiago

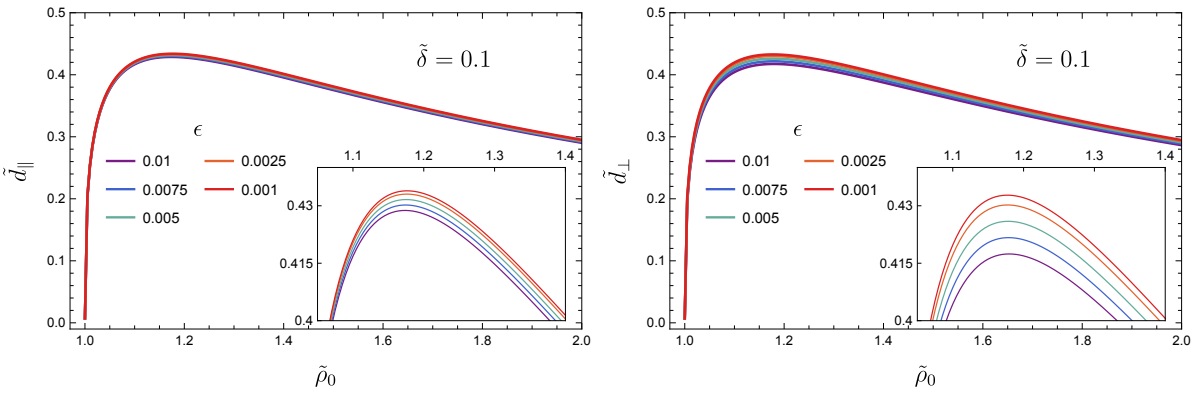


Figure 8.1: Quark-antiquark distances $\tilde{d}_{\parallel} = \pi\, T\, d_{\parallel}$ and $\tilde{d}_{\perp} = \pi\, T\, d_{\perp}$ versus the turning point $\tilde{\rho}_0 = \frac{\rho_0}{\rho_{\rm h}}$ for different ϵ at fixed $\tilde{\delta}$.

going straight from $\rho = \rho_{\rm h}$ to the boundary at $\rho \to \infty$. The regularised on-shell action is identified with the quark-antiquark potential. We get

$$\begin{aligned} 2\pi\,\alpha'\,V^{\parallel}_{q\bar{q}} &= 2\pi\left(S^{\rm on-shell}_{\parallel} - \int_{\rho_{\rm h}}^{\infty} {\rm d}\rho\,\mathcal{L}^{\rm straight}_{\parallel}\right) \\ &= 2\int_{\rho_0}^{\infty} {\rm d}\rho\,\frac{\sqrt{h_0}\,b^{3/2}\,F\,S^4\,\alpha\,e^{\phi-\frac{\phi(\rho_0)}{2}}}{\rho\,(\rho^4-\rho_{\rm h}^4)\,\sqrt{h_0\,b\,e^{\phi-\phi(\rho_0)}-b_0\,h}} - 2\int_{\rho_{\rm h}}^{\infty} {\rm d}\rho\; e^{\frac{\phi}{2}}\,\frac{\alpha\,F\,S^4}{\rho^5} \\ &= 2\int_{\rho_0}^{\infty} {\rm d}\rho\left(\frac{\sqrt{h_0}\,b^{3/2}\,F\,S^4\,\alpha\,e^{\phi-\frac{\phi(\rho_0)}{2}}}{\rho\,(\rho^4-\rho_{\rm h}^4)\,\sqrt{h_0\,b\,e^{\phi-\phi(\rho_0)}-b_0\,h}} - e^{\frac{\phi}{2}}\,\frac{\alpha\,F\,S^4}{\rho^5}\right) - 2\int_{\rho_{\rm h}}^{\rho_0} {\rm d}\rho\; e^{\frac{\phi}{2}}\,\frac{\alpha\,F\,S^4}{\rho^5}\,. \end{aligned} \tag{8.2.8}$$

As for the quark-antiquark distance, these integrals cannot be performed analytically. The numerical results are shown in Fig. 8.2.

Examining the anisotropic and finite density contribution separately, the order ϵ correction increases the maximum parallel distance $\tilde{d}^{\rm max}_{\parallel}$, while the order $\epsilon\tilde{\delta}^2$ correction does not change significantly the numerical results. We represent these contributions as

$$d_{\parallel} = d^{(0)}_{\parallel} + \epsilon\, d^{(\epsilon)}_{\parallel} + \epsilon\,\tilde{\delta}^2\, d^{(\epsilon\,\tilde{\delta}^2)}_{\parallel}\,, \qquad V^{\parallel}_{q\bar{q}} = V^{(0)}_{\parallel} + \epsilon\, V^{(\epsilon)}_{\parallel} + \epsilon\,\tilde{\delta}^2\, V^{(\epsilon\,\tilde{\delta}^2)}_{\parallel}\,. \tag{8.2.9}$$

USC UNIVERSIDADE DE SANTIAGO

In Fig. 8.3 we plot separately these contributions to the distance and to the potential.

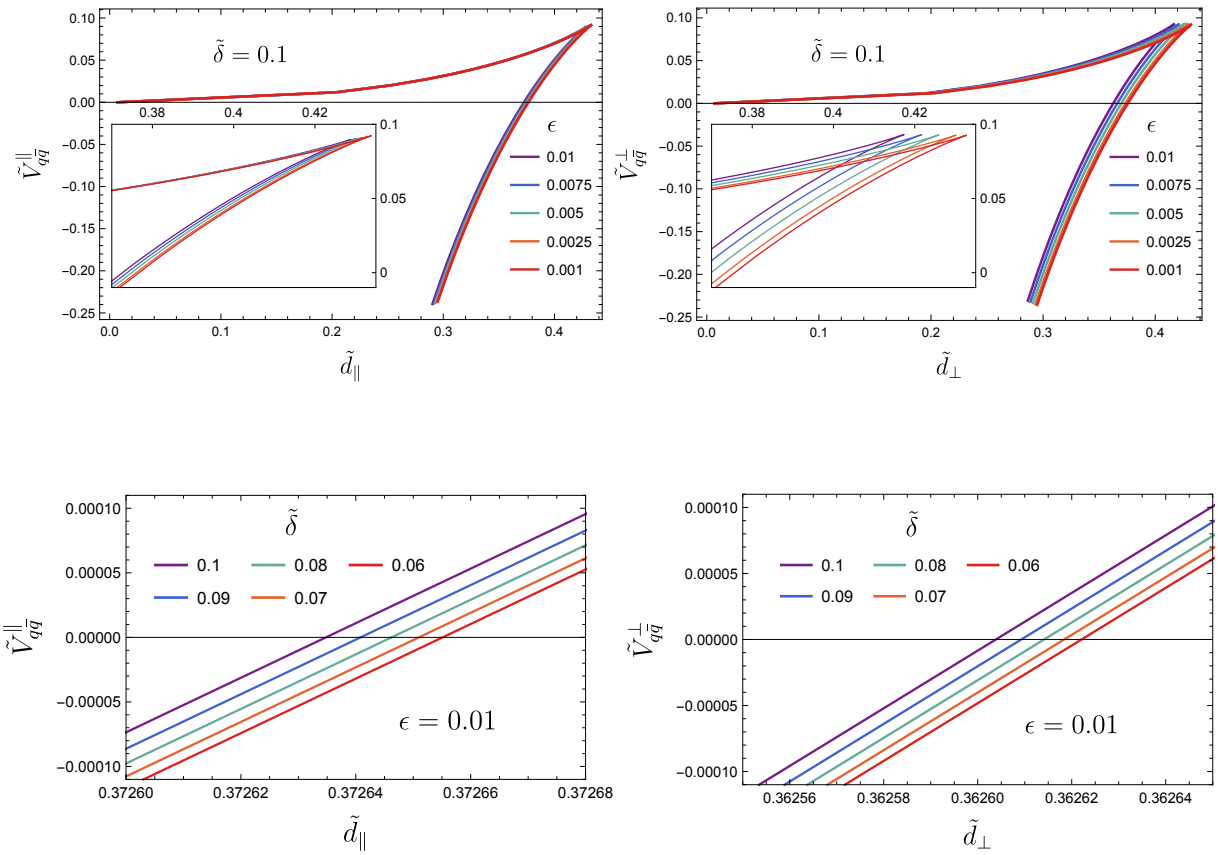


Figure 8.2: Quark-antiquark potential $\tilde{V}^a_{q\bar{q}} = \frac{\mathrm{Vol}(\mathcal{M}_5)^{\frac{1}{2}}}{\pi^{\frac{3}{2}}\,\lambda^{\frac{1}{2}}\,T}\,V^a_{q\bar{q}}$ versus $\tilde{d}_a = \pi\,T\,d_a$ $(a = \parallel, \perp)$. The upper plots are for different ϵ and fixed $\tilde{\delta}$, while the lower ones correspond to different values of $\tilde{\delta}$ and fixed ϵ. The left plot shows the intra-layer potential, while the right one is the inter-layer one.

8.2.2 Inter-layer potential

We now consider a fundamental string hanging from the UV boundary and extended along x^3 with the other two cartesian coordinates being constant. We now take $\rho = \rho(x^3)$. Eq. (8.2.1) becomes

$$S_\perp = \frac{1}{2\pi\alpha'}\int \mathrm{d}\tau\,\mathrm{d}x^3\,e^{\phi/2}\sqrt{\frac{b^2F^2S^8\alpha^2}{\rho^2\left(\rho^4-\rho_{\mathrm{h}}^4\right)^2}\,\rho'^2+\frac{b\,\alpha^2}{h}}\ , \tag{8.2.10}$$

from which we obtain the following equation for ρ'

$$\rho' = \pm\sqrt{\frac{b}{b_0}}\,\frac{\alpha\sqrt{h_0\,b\,\alpha^2\,e^{\phi-\phi(\rho_0)}-b_0\,\alpha_0^2\,h}}{\sqrt{B_2}\,h\,\alpha_0}\ , \tag{8.2.11}$$

USC UNIVERSIDADE DE SANTIAGO DE COMPOSTELA

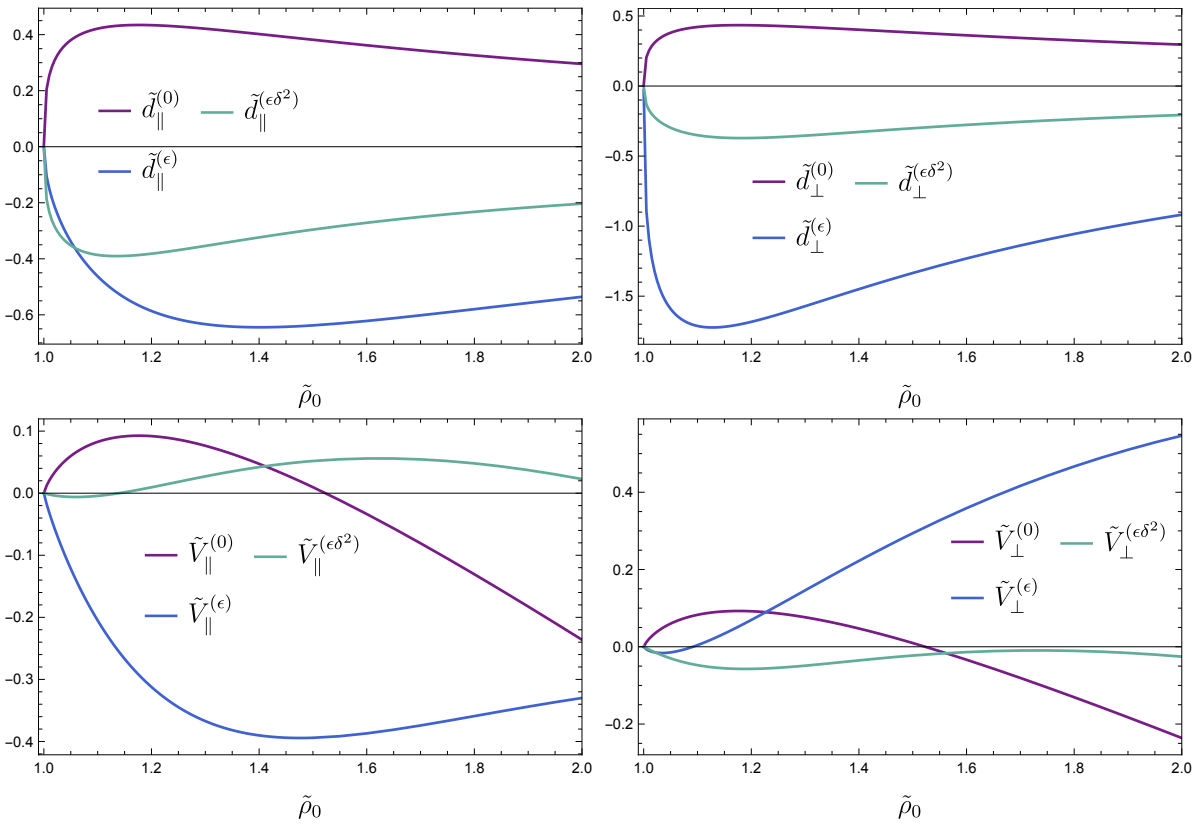


Figure 8.3: Comparison between the corrections at different orders. In these plots $\tilde{V}_a = \frac{\mathrm{Vol}(\mathcal{M}_5)^{\frac{1}{2}}}{\pi^{\frac{3}{2}}\,\lambda^{\frac{1}{2}}\,T} V_a$ and $\tilde{d}_a = \pi\, T\, d_a$ for $a = \parallel, \perp$ and $\tilde{\rho}_0 = \rho_0/\rho_{\mathrm{h}}$.

where B_2 is the following function

$$B_2 = \frac{b^2 F^2 S^8 \alpha^{\,2}}{\rho^2 \left(\rho^4 - \rho_{\mathrm{h}}^4\right)^2} \,. \tag{8.2.12}$$

As before, we can invert it to obtain x^3 as a function of ρ

$$x_3(\rho) = \pm \int_{\rho_0}^{\rho} \mathrm{d}\rho \sqrt{\frac{b_0}{b}} \frac{\sqrt{B_2}\, h\, \alpha_0}{\alpha \sqrt{h_0\, b\, \alpha^2\, e^{\phi-\phi(\rho_0)} - b_0\, \alpha_0^2\, h}} \,. \tag{8.2.13}$$

It follows that the quark-antiquark distance $d_\perp$ at the boundary is given by the following integral

$$d_\perp = 2 \int_{\rho_0}^{\infty} \mathrm{d}\rho \sqrt{\frac{b_0}{b}} \frac{\sqrt{B_2}\, h\, \alpha_0}{\alpha \sqrt{h_0\, b\, \alpha^2\, e^{\phi-\phi(\rho_0)} - b_0\, \alpha_0^2\, h}} \,, \tag{8.2.14}$$

USC UNIVERSIDADE DE SANTIAGO DE COMPOSTELA

which, as in the intra-layer case must be performed numerically. The result is shown in Fig. 8.1. We next calculate the on-shell action for these configuration, which reads

$$2\pi\,\alpha'\,S_{\perp}^{\rm on-shell}=2\int_{\rho_0}^{\rho_{\rm max}}{\rm d}\rho\frac{\sqrt{h_0}\,b^{3/2}FS^4\alpha^2e^{\phi-\frac{\phi(\rho_0)}{2}}}{\rho\,(\rho^4-\rho_{\rm h}^4)\,\sqrt{h_0\,\alpha^2\,be^{\phi-\phi(\rho_0)}-b_0\,\alpha_0^2\,h}}=\int_{\rho_0}^{\rho_{\rm max}}{\rm d}\rho\,\mathcal{L}_{\perp}^{\rm on-shell}\ , \tag{8.2.15}$$

which is again divergent at the UV. As above, we regularise this divergence by subtracting the action of two fundamental strings going straight from $\rho=\rho_{\rm h}$ to the boundary at $\rho\to\infty$. The regularised on-shell action is identified with the quark-antiquark potential along the x^3-direction, and is given by

$$\begin{aligned}2\pi\,\alpha'\,V_{q\bar{q}}^{\perp}&=2\pi\,\left(S_{\perp}^{\rm on-shell}-\int_{\rho_{\rm h}}^{\infty}{\rm d}\rho\,\mathcal{L}_{\perp}^{\rm straight}\right)\\&=2\int_{\rho_0}^{\infty}{\rm d}\rho\,\frac{\sqrt{h_0}\,b^{3/2}FS^4\alpha^2e^{\phi-\frac{\phi(\rho_0)}{2}}}{\rho\,(\rho^4-\rho_{\rm h}^4)\,\sqrt{h_0\,\alpha\,be^{\phi-\phi(\rho_0)}-b_0\,\alpha_0\,h}}-2\int_{\rho_{\rm h}}^{\infty}{\rm d}\rho\,e^{\frac{\phi}{2}}\,\frac{\alpha\,F\,S^4}{\rho^5}\\&=2\int_{\rho_0}^{\infty}{\rm d}\rho\left(\frac{\sqrt{h_0}\,b^{3/2}FS^4\alpha^2e^{\phi-\frac{\phi(\rho_0)}{2}}}{\rho\,(\rho^4-\rho_{\rm h}^4)\,\sqrt{h_0\,\alpha\,be^{\phi-\phi(\rho_0)}-b_0\,\alpha_0\,h}}-e^{\frac{\phi}{2}}\,\frac{\alpha\,F\,S^4}{\rho^5}\right)\\&\qquad-2\int_{\rho_{\rm h}}^{\rho_0}{\rm d}\rho\,e^{\frac{\phi}{2}}\,\frac{\alpha\,F\,S^4}{\rho^5}\ .\end{aligned} \tag{8.2.16}$$

These integrals can be performed numerically. The results are shown in Fig. 8.2. In addition, we consider the anisotropic and finite density corrections similarly, introducing an expansion in ϵ and $\tilde{\delta}$ similar to (8.2.9), but for the inter-layer separation and potential. The results are represented in Fig. 8.3.

8.2.3 Physical interpretation

Let us now comment on the results shown in Fig. 8.2. At small separations between the quark and the antiquark, the potential follows the colored curves, until it reaches the horizontal line. At this point the disconnected configuration becomes dominant and the potential is flat, thus the color charges are screened by the plasma. We observe that as the density of defects, parameterised by ϵ, increases, the separation where the charges are screened becomes smaller, and that the effect is more pronounced in the direction transverse to the defects. The enhanced screening could be taken as a natural consequence of having more color nonsinglet degrees of freedom in the plasma, from the fields at the defects. Note also that strings can end on D5-branes so a connected configuration can break in two separate strings with the new endpoints localised at the D5-branes. In principle the breaking might be expected to be more favorable if the string is extended in the direction transverse to the D5-brane, since the string should be orthogonal to the D5-brane worldvolume at the endpoint. This would serve

USC DE SANTIAGO

as a possible explanation for the difference in screening between the transverse and parallel directions.

Dialing the baryon charge density, through changes in $\tilde{\delta}$, also affects the screening. Although the effect is relatively mild (recall that the baryon density is small compared to the defect density), increasing the baryon density seems to also increase the screening. Note that the purple and blue curves in the lower plots of Fig. 8.2 are slightly displaced to the right compared to the upper plots, and that $\tilde{\delta}$ should be smaller for those. This is natural in view that increasing the baryon density would increase the number of degrees of freedom that can contribute to the screening. Notice also that in this case the effect seems to be stronger in the directions parallel to the defect, as might have been expected since in principle the charges would be localised along these directions.

8.3 Entanglement entropy

The holographic entanglement entropy [174, 175] between a spatial region A in the gauge theory and its complement is obtained by finding the eight-dimensional spatial surface Σ whose boundary coincides with the boundary of A and minimises the functional

$$S_A = \frac{1}{4G_{10}} \int_\Sigma \mathrm{d}^8\xi \, \sqrt{\det g_8} \ , \tag{8.3.1}$$

where $G_{10} = 8\,\pi^6\, g_s^2\, \alpha'^4$ is the ten-dimensional Newton constant satisfying $16\pi\, G_{10} = 2\kappa_{10}^2$ and g_8 is the induced metric on Σ. We will minimise S_A for the case in which the region A is a slab of infinite extent in two of the spatial gauge theory directions and has a finite width in the third one. There are clearly two different cases to be studied, depending on whether the direction with finite width is parallel or transverse to the defect. We study these two possibilities in the two subsections that follow.

8.3.1 Parallel slab

Let A be the region

$$A = \left\{ -\frac{l_\parallel}{2} < x^1 < \frac{l_\parallel}{2}, -\frac{L_2}{2} \leq x^2 < \frac{L_2}{2}, -\frac{L_3}{2} \leq x^3 < \frac{L_3}{2} \right\} \ . \tag{8.3.2}$$

We consider both x^2- and x^3-directions to be periodic with periods L_2 and L_3, otherwise one ends up with partial differential equations. Eventually, we are interested in the $L_2, L_3 \to \infty$ limit. We will consider a surface Σ ending on the boundary of A at the UV $\rho \to \infty$, which penetrates into the bulk and reaches a minimal value ρ_0 of the holographic coordinate ρ. Actually, in this section we will use the dimensionless variable y defined as

$$y = \frac{\rho}{\rho_0} \ . \tag{8.3.3}$$

USC UNIVERSIDADE DE SANTIAGO DE COMPOSTELA

We will parameterise Σ by a function $y = y(x^1)$ and, to compute the entanglement functional S_A, we will integrate over all variables except x^1. We get

$$S_{\parallel} = \frac{L_2\, L_3\, \mathrm{Vol}\big(\mathcal{M}_5\big)}{4G_{10}} \int \mathrm{d}x^1 \sqrt{\frac{b\, F^4\, h^2\, S^{16} \alpha^4}{y^2\, (\rho_0^4 y^4 - \rho_{\mathrm{h}}^4)^2}\, y'^2 + F^2\, h\, S^8\, \alpha^2}\ , \tag{8.3.4}$$

The functional $S_{\parallel}$ has a first integral that allows to obtain y' as

$$\frac{\mathrm{d}y}{\mathrm{d}x^1} = \pm\, F\, h^{1/2}\, S^4\, \alpha \frac{\sqrt{F^2\, h\, S^8\, \alpha^2 - \alpha_0^2\, F_0^2\, h_0\, S_0^8}}{B_3^{1/2} \alpha_0\ F_0\, h_0^{1/2}\, S_0^4}\ , \tag{8.3.5}$$

where the subscript 0 implies the functions are evaluated at $y = y_0 = 1$ and B_3 is given by

$$B_3 = \frac{b\, F^4\, h^2\, S^{16}\, \alpha^4}{y^2\, (\rho_0^4 y^4 - \rho_{\mathrm{h}}^4)^2}\ . \tag{8.3.6}$$

Thus, we have

$$x^1 = \pm \int_1^y \mathrm{d}y\, \frac{B_3^{1/2} \alpha_0\ F_0\, h_0^{1/2}\, S_0^4}{F\, h^{1/2}\, S^4\, \alpha \sqrt{F^2\, h\, S^8\, \alpha^2 - \alpha_0^2\, F_0^2\, h_0\, S_0^8}}\ , \tag{8.3.7}$$

and therefore, the length $l_{\parallel}$ in this direction is

$$l_{\parallel} = 2 \int_1^{\infty} \mathrm{d}y\, \frac{B_3^{1/2} \alpha_0\ F_0\, h_0^{1/2}\, S_0^4}{F\, h^{1/2}\, S^4\, \alpha \sqrt{F^2\, h\, S^8\, \alpha^2 - \alpha_0^2\, F_0^2\, h_0\, S_0^8}}\ . \tag{8.3.8}$$

Plugging this result in (8.3.4), we obtain that $S_{\parallel}$ has the following on-shell value

$$\frac{4G_{10}}{L_2\, L_3\, \mathrm{Vol}\big(\mathcal{M}_5\big)} S_{\parallel} = 2 \int_1^{\infty} \mathrm{d}y\, \frac{b^{1/2} F^3 h^{3/2} S^{12} \alpha^3}{y\ (\rho_0^4 y^4 - \rho_{\mathrm{h}}^4) \sqrt{F^2\, h\, S^8 \alpha^2 - \alpha_0^2 F_0^2 h_0\, S_0^8}} \equiv 2 \int_1^{\infty} \mathrm{d}y\, \mathcal{L}_{\parallel}\ , \tag{8.3.9}$$

where, in the last step, we have defined the function $\mathcal{L}_{\parallel}$. If we now want to evaluate the entropy for this configuration, we need to subtract the divergent contributions that come from the upper limit of the integral, $y \to \infty$. When $y \to \infty$, $\mathcal{L}_{\parallel}$ behaves as

$$\mathcal{L}_{\parallel} = \rho_0\, Q_{\mathrm{c}}\, \left(\frac{\rho_0}{4} y + \epsilon\, \rho_{\mathrm{h}}\right) + \mathcal{O}(y^{-3}) \tag{8.3.10}$$

leading to asymptotic behavior for $S_{\parallel}$ as

$$\frac{4G_{10}}{L_2\, L_3\, \mathrm{Vol}\big(\mathcal{M}_5\big)} S_{\parallel} = \ 2\, \rho_0\, Q_{\mathrm{c}}\, \left(\frac{\rho_0}{8} y_{\mathrm{max}}^2 + \epsilon\, \rho_{\mathrm{h}}\, y_{\mathrm{max}}\right) + \mathcal{O}(y^{-2})\ , \tag{8.3.11}$$

where the last term vanishes when $y_{\mathrm{max}} \to \infty$. Defining the cutoff (in units of length) as $\varepsilon_{\mathrm{UV}} = Q_{\mathrm{c}}^{1/2}/(2\rho_{\mathrm{max}}) \to 0$, the divergent part is

$$S_{\parallel}^{\mathrm{div}} = \frac{N_{\mathrm{c}}^2}{2\pi} \bar{a}\, \frac{L_2 L_3}{\varepsilon_{\mathrm{UV}}^2} + N_{\mathrm{f}}\, N_{\mathrm{c}}\, \bar{a}^{\frac{1}{2}}\, \frac{2}{15} \frac{\lambda^{\frac{1}{2}}}{v_{\perp}} \frac{L_2}{\varepsilon_{\mathrm{UV}}}\, . \tag{8.3.12}$$

USC UNIVERSIDADE DE SANTIAGO DE COMPOSTELA

The first term reproduces the area law for the theory in the absence of flavors. The second term is a subleading correction proportional to the number of flavors that has the form of an area law for a $(2+1)$-dimensional theory, so it naturally captures the contribution to the entanglement entropy from the fields localised at the defects.

Subtracting the divergent part, we can write

$$\begin{aligned}\frac{4G_{10}}{L_2\,L_3\,\mathrm{Vol}\big(\mathcal{M}_5\big)}S_{\parallel}^{\mathrm{reg}} &= \frac{4G_{10}}{L_2\,L_3\,\mathrm{Vol}\big(\mathcal{M}_5\big)}\left(S_{\parallel}-S_{\parallel}^{\mathrm{div}}\right)\\ &= 2\int_1^{\infty}\mathrm{d}y\,\left(\mathcal{L}_{\parallel}-\mathcal{L}_{\parallel}^{\mathrm{div}}\right)-2\,\rho_0\,Q_{\mathrm{c}}\,\left(\frac{\rho_0}{8}+\epsilon\,\rho_{\mathrm{h}}\right)\,. \end{aligned}\tag{8.3.13}$$

The parallel distance $l_{\parallel}$ and the regulated entanglement entropy $S_{\parallel}^{\mathrm{reg}}$ are plotted in Fig. 8.4. The ϵ correction increases the value of the width, while it decreases slightly the value of the entanglement entropy for small $\tilde{l}_{\parallel}$, and increases it for big $\tilde{l}_{\parallel}$. The contributions of the different orders are represented in Fig. 8.5, using a notation similar to the one employed in (8.2.9). See also Fig. 8.6, where we compare the entanglement entropies of the flavored and unflavored theories in the two directions at the same slab widths.

The entanglement entropy found above matches the results of section 7.3 for the thermal entropy density of the black hole in the limit in which $T\,l_{\parallel}$ is large [176–178]. Indeed, let us use the prescription given in [179] to compute the derivative of the entanglement entropy with respect to $l_{\parallel}$ from the derivatives of both $l_{\parallel}$ and $S_{\parallel}$ with respect to the turning point y_0 when $y_0=1$. From (8.3.8) we get

$$\left.\frac{\mathrm{d}l_{\parallel}}{\mathrm{d}y_0}\right|_{y_0=1}=\frac{2\,b_0^{1/2}\,F_0^2\,h_0\,S_0^8\,\alpha_0^2}{\rho_0^4-\rho_{\mathrm{h}}^4}\lim_{y\to 1}\left(\frac{1}{\sqrt{F^2\,h\,S^8\,\alpha^2-\alpha_0^2\,F_0^2\,h_0\,S_0^8}}\right)\,.\tag{8.3.14}$$

Moreover, from (8.3.9) we arrive at

$$\frac{4\,G_{10}}{L_2\,L_3\;\mathrm{Vol}\big(\mathcal{M}_5\big)}\left.\frac{\mathrm{d}S_{\parallel}^{\mathrm{reg}}}{\mathrm{d}y_0}\right|_{y_0=1}=\frac{2\,b_0^{1/2}F_0^3h_0^{3/2}S_0^{12}\alpha_0^3}{\rho_0^4-\rho_{\mathrm{h}}^4}\lim_{y\to 1}\left(\frac{1}{\sqrt{F^2\,h\,S^8\,\alpha^2-\alpha_0^2\,F_0^2\,h_0\,S_0^8}}\right)\tag{8.3.15}$$

Thus, we can write

$$\begin{aligned}\frac{4G_{10}}{\mathrm{Vol}\big(\mathcal{M}_5\big)\,L_2\,L_3}\frac{\mathrm{d}S_{\parallel}^{\mathrm{reg}}}{\mathrm{d}l_{\parallel}} &= \frac{4G_{10}}{\mathrm{Vol}\big(\mathcal{M}_5\big)\,L_2\,L_3}\frac{\mathrm{d}S_{\parallel}^{\mathrm{reg}}}{\mathrm{d}y_0}\frac{\mathrm{d}y_0}{\mathrm{d}l_{\parallel}}\\ &= F_0\,h_0^{1/2}S_0^4\alpha_0\\ &= \frac{\rho_0^3}{2}\,Q_{\mathrm{c}}^{1/2}\Bigg(1+\frac{5\epsilon}{2\rho_{\mathrm{h}}^4}\Bigg(\frac{1}{5}\left(\rho_0^4-\rho_{\mathrm{h}}^4\right)\Omega\left(\frac{\rho_0}{\rho_{\mathrm{h}}}\right)+\rho_0^3\rho_{\mathrm{h}}-\frac{\rho_{\mathrm{h}}^4}{4}\\ &\quad+\tilde{\delta}^2\left(-\left(\rho_0^4-\rho_{\mathrm{h}}^4\right)\Omega\left(\frac{\rho_0}{\rho_{\mathrm{h}}}\right)-5\rho_0^3\rho_{\mathrm{h}}+\frac{4\rho_{\mathrm{h}}^5}{\rho_0}+\frac{5\rho_{\mathrm{h}}^4}{4}\right)\Bigg)\Bigg)\end{aligned}\tag{8.3.16}$$

USC UNIVERSIDADE DE SANTIAGO DE COMPOSTELA

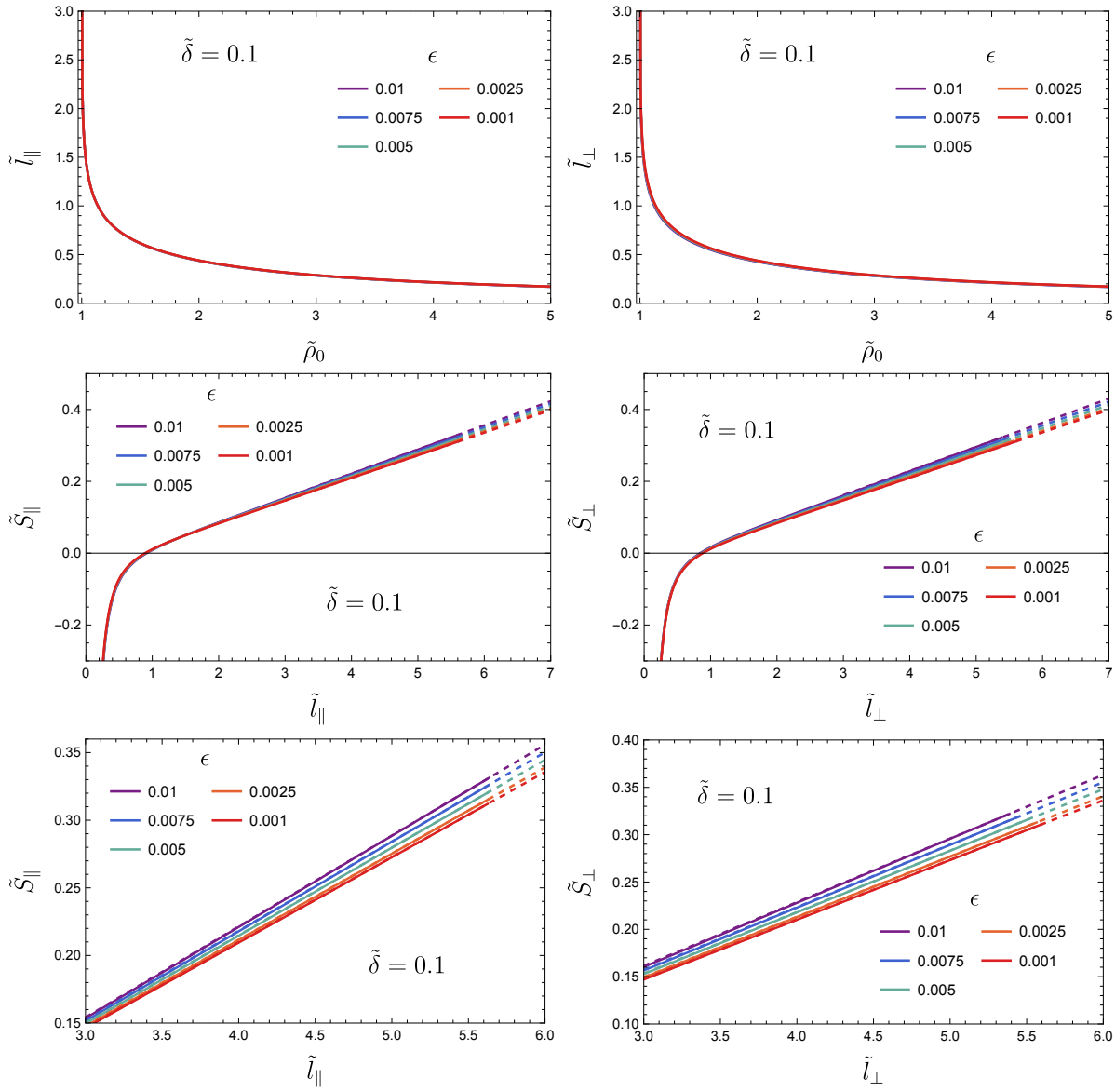


Figure 8.4: *First row*: rescaled parallel (left) and transverse (right) width $\tilde{l} = \pi\, T\, l$ versus the rescaled turning point $\tilde{\rho}_0 = \frac{\rho_0}{\rho_{\rm h}}$. *Second and third rows*: rescaled parallel (left) and transverse (right) entanglement entropy $\tilde{S} = \frac{\mathrm{Vol}(\mathcal{M}_5)}{8\,\pi^4\,L_2\,L_3\,N_{\rm c}^2\,T^2}\,S^{\rm reg}$ versus the rescaled width. The slope of the dashed lines are fixed by the thermal entropy density according to (8.3.19) and (8.3.34).

When $\rho_0 \to \rho_{\rm h}$ this last expression becomes

$$\frac{4G_{10}}{\mathrm{Vol}\big(\mathcal{M}_5\big)\,L_2\,L_3}\,\frac{\mathrm{d}S_\parallel^{\rm reg}}{\mathrm{d}l_\parallel} = \frac{\rho_{\rm h}^3}{2}\,Q_{\rm c}^{1/2}\left(1+\epsilon\,\frac{15}{8}+\epsilon\,\tilde{\delta}^2\,\frac{5}{8}\right)\,, \tag{8.3.17}$$

which agrees with the thermal entropy density of the black hole obtained in section 7.3.

USC UNIVERSIDADE DE SANTIAGO

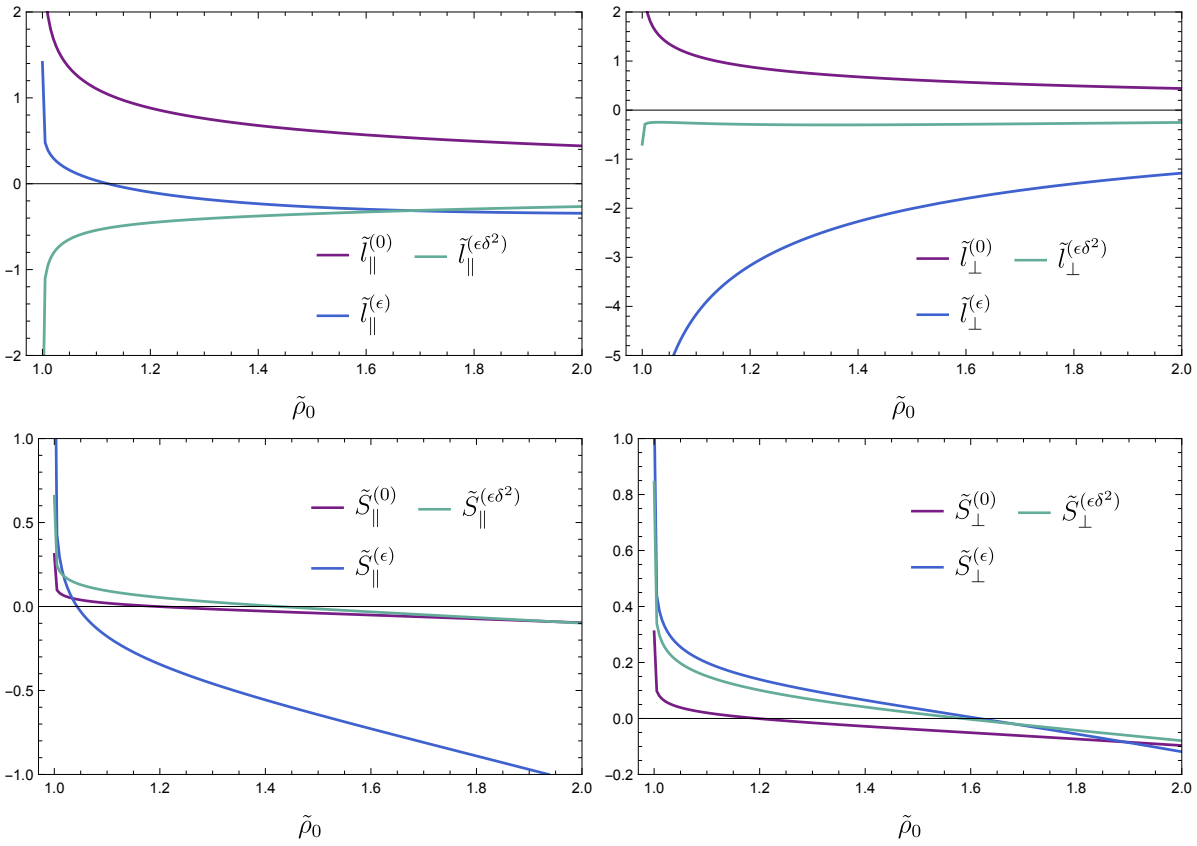


Figure 8.5: Comparison between the corrections at different orders of the widths and entanglement entropies, defined in way similar to (8.2.9).

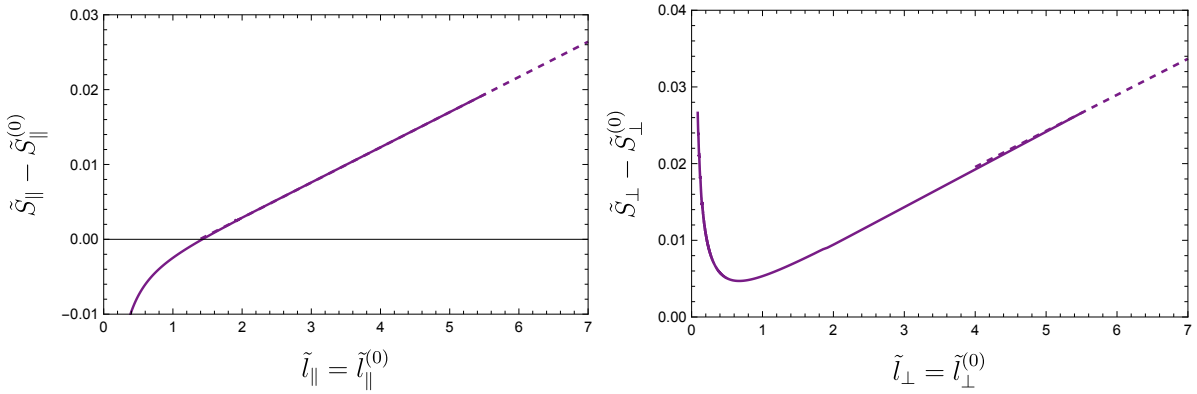


Figure 8.6: Differences in the finite contributions to the entanglement entropy between the flavored and unflavored theories. We have set $\epsilon = 0.01$ and $\tilde{\delta} = 0.1$. The slope of the dashed lines are fixed by the flavor contribution to the thermal entropy density.

Actually, taking into account the value of G_{10}, one can rewrite (7.3.3) as

$$\frac{4G_{10}}{\mathrm{Vol}\big(\mathcal{M}_5\big)} s \;=\; \frac{\rho_{\mathrm{h}}^3}{2}\, Q_{\mathrm{c}}^{1/2} \left(1 + \epsilon\, \frac{15}{8} + \epsilon\, \tilde{\delta}^2\, \frac{5}{8}\right) \;. \tag{8.3.18}$$

USC UNIVERSIDADE DE SANTIAGO DE COMPOSTELA

By comparing (8.3.17) and (8.3.18), it follows that, when $\rho_0 \to \rho_{\rm h}$ and $T\,l_\parallel$ is large, we have the following approximate equality between the entanglement entropy density and the thermal entropy density s

$$\frac{1}{L_2\,L_3}\frac{{\rm d}S_\parallel}{{\rm d}l_\parallel}\Big|_{\rho_0\to\rho_{\rm h}} = s \tag{8.3.19}$$

in agreement with the analysis of [176–178]. By looking at the slope of the entanglement entropy versus the parallel width, we have also verified that, for different values of the expansion parameters ϵ and $\epsilon\,\tilde{\delta}^2$, our numerical results fulfill (8.3.19) in the limit in which $Tl_\parallel$ is large (see Fig. 8.4). Both (8.3.19) and the numerical results capture the increase in the number of degrees of freedom that enter through the fields localised at the defects, consistently with the thermodynamic quantities we computed previously.

8.3.2 Transverse slab

Let us now consider the region

$$A = \left\{-\frac{l_\perp}{2} < x^3 < \frac{l_\perp}{2}, -\frac{L_1}{2} \le x^1 < \frac{L_1}{2}, -\frac{L_2}{2} \le x^2 < \frac{L_2}{2}\right\}\,, \tag{8.3.20}$$

which is a slab with finite width in the transverse direction. As before, we take x^1 and x^2 to be periodic with periods L_1 and L_2 respectively, and we are ultimately interested in the $L_1, L_2 \to \infty$ limit. Let us use again the variable y defined in (8.3.3) and take $y = y(x^3)$. By integrating over all variables except x^3, we get

$$S_\perp = \frac{L_1\,L_2\,{\rm Vol}\big(\mathcal{M}_5\big)}{4G_{10}}\int {\rm d}x_3\,F\,h^{1/2}\,S^4\,\alpha\,\sqrt{1+\frac{b\,F^2\,h\,S^8}{y^2\,\left(\rho_0^4\,y^4-\rho_{\rm h}^4\right)^2}y'^2}\,, \tag{8.3.21}$$

where now y' denotes the derivative with respect to x^3. From the first integral of $S_\perp$ we can get the value of y', namely

$$\frac{{\rm d}y}{{\rm d}x_3} = \pm\frac{F\,h^{1/2}\,S^4\,\alpha\,\sqrt{F^2\,h\,S^8\,\alpha^2-\alpha_0^2\,F_0^2\,h_0\,S_0^8}}{\alpha_0\,B_4^{1/2}\,F_0\,h_0^{1/2}S_0^4}\,, \tag{8.3.22}$$

where the subscript 0 implies the functions are evaluated at $y = y_0 = 1$ and B_4 is the function

$$B_4 = \frac{b\,F^4\,h^2\,S^{16}\,\alpha^2}{y^2\,\left(\rho_0^4\,y^4-\rho_{\rm h}^4\right)^2}\,. \tag{8.3.23}$$

Thus, we have

$${\rm d}x^3 = {\rm d}y\,\frac{\alpha_0\,F_0\,h_0^{1/2}\,S_0^4\,b^{1/2}\,F\,h^{1/2}\,S^4}{y\,\left(\rho_0^4\,y^4-\rho_{\rm h}^4\right)\sqrt{F^2\,h\,S^8\,\alpha^2-\alpha_0^2\,F_0^2\,h_0\,S_0^8}}\,, \tag{8.3.24}$$

USC UNIVERSIDADE DE SANTIAGO DE COMPOSTELA

and the length $l_\perp$ in the transverse direction is

$$l_\perp = 2\int_1^\infty \mathrm{d}y\, \frac{\alpha_0\, F_0\, h_0^{1/2}\, S_0^4\, b^{1/2}\, F\, h^{1/2}\, S^4}{y\, (\rho_0^4\, y^4 - \rho_{\rm h}^4)\, \sqrt{F^2\, h\, S^8\, \alpha^2 - \alpha_0^2\, F_0^2\, h_0\, S_0^8}}\ . \tag{8.3.25}$$

Moreover, by using (8.3.22) in (8.3.21), the on-shell entanglement entropy functional $S_\perp$ becomes

$$\begin{aligned}\frac{4G_{10}}{L_1\, L_2\, \mathrm{Vol}\big(\mathcal{M}_5\big)} S_\perp &= 2\int_1^\infty \mathrm{d}y\, \frac{b^{1/2}\, F^3\, h^{3/2}\, S^{12}\, \alpha^2}{y\, (\rho_0^4\, y^4 - \rho_{\rm h}^4)\, \sqrt{F^2\, h\, S^8\, \alpha^2 - \alpha_0^2\, F_0^2\, h_0\, S_0^8}} \\ &\equiv 2\int_1^\infty \mathrm{d}y\, \mathcal{L}_\perp\ ,\end{aligned} \tag{8.3.26}$$

where, in the last step, we have defined $\mathcal{L}_\perp$. If we now want to evaluate the finite entropy for this configuration, we need to subtract the divergent contributions that come from the upper limit of the integral, $y \to \infty$. As $y \to \infty$, $\mathcal{L}_\perp$ goes like

$$\mathcal{L}_\perp = \frac{1}{4}\, Q_{\rm c}\, \rho_0\, \rho_{\rm h}\, (y\, \rho_0 - \epsilon \rho_{\rm h}) + \mathcal{O}(y^{-2})\ . \tag{8.3.27}$$

Thus, the leading behavior of $S_\perp$ reads as

$$\frac{4G_{10}}{L_1\, L_2\, \mathrm{Vol}\big(\mathcal{M}_5\big)} S_\perp = \frac{1}{2}\, Q_{\rm c}\, \rho_0\, \rho_{\rm h}\, \left(\frac{y_{\rm max}^2}{2}\, \rho_0 - \epsilon\, \rho_{\rm h}\, y_{\rm max}\right) + \mathcal{O}(y^{-1})\ , \tag{8.3.28}$$

where the last term vanishes when $y_{\rm max} \to \infty$. In terms of field theory quantities, the divergent part is therefore

$$S_\perp^{\rm div} = \frac{N_{\rm c}^2}{2\pi} \bar{a} \frac{L_1 L_2}{\varepsilon_{\rm UV}^2} - N_{\rm c}\, \bar{a}^{\frac{1}{2}}\, \frac{1}{30}\, \frac{\lambda^{\frac{1}{2}}}{v_\perp}\, \frac{n_{\rm f}\, L_1\, L_2}{\varepsilon_{\rm UV}}\ . \tag{8.3.29}$$

As in the case of a parallel slab, the first term reproduces the area law in the absence of flavors. The cutoff dependence of the second term is similar to the one expected for the area law in a $(2+1)$-dimensional theory, but it gives a negative contribution and depends on the flavor density, rather than on the number of flavors. Comparing with (8.3.12), the negative contribution suggests that the number of degrees of freedom that propagate in the directions transverse to the defects is effectively reduced, at least concerning their contribution to the entanglement entropy.

Removing the divergent pieces, we define the regulated entanglement entropy $S_\perp^{\rm reg}$ as

$$\begin{aligned}\frac{4G_{10}}{L_1\, L_2\, \mathrm{Vol}\big(\mathcal{M}_5\big)} S_\perp^{\rm reg} &= \frac{4G_{10}}{L_1\, L_2 \mathrm{Vol}\big(\mathcal{M}_5\big)} \left(S_\perp - S_\perp^{\rm div}\right) \\ &= 2\int_1^\infty \mathrm{d}y\, \left(\mathcal{L}_\perp - \mathcal{L}_\perp^{\rm div}\right) - \frac{1}{2}\, Q_{\rm c}\, \rho_0\, \rho_{\rm h}\, \left(\frac{1}{2}\, \rho_0 - \epsilon\right)\ .\end{aligned} \tag{8.3.30}$$

USC UNIVERSIDADE DE SANTIAGO DE COMPOSTELA

Both $l_\perp$ and $S_\perp^{\rm reg}$ are plotted in Fig. 8.4. In this transverse case, the width decreases with the epsilon corrections, and the entanglement entropy increases for big $l_\perp$ and decreases for small $l_\perp$.

As we did for the parallel slab, one can compute the entanglement entropy density for large $Tl_\perp$ and compare the result with the thermal entropy density of the flavored black hole. By following the same steps as before, we calculate the derivative of the entanglement entropy with respect to $l_\perp$ from the derivatives of both $l_\perp$ and $S_\perp$ with respect to the turning point. From (8.3.25), we have

$$\left.\frac{{\rm d}l_\perp}{{\rm d}y_0}\right|_{y_0=1} = \frac{2\,b_0^{1/2}\,F_0^2\,h_0\,S_0^8\,\alpha_0}{(\rho_0^4-\rho_{\rm h}^4)}\lim_{y\to 1}\left(\frac{1}{\sqrt{F^2\,h\,S^8\,\alpha^2-\alpha_0^2\,F_0^2\,h_0\,S_0^8}}\right)\,, \tag{8.3.31}$$

and from (8.3.26) we get

$$\frac{4G_{10}}{L_1\,L_2{\rm Vol}\big(\mathcal{M}_5\big)}\left.\frac{{\rm d}S_\perp^{\rm reg}}{{\rm d}y_0}\right|_{y_0=1} = \frac{2\,b_0^{1/2}F_0^3h_0^{3/2}S_0^{12}\alpha_0^2}{\rho_0^4-\rho_{\rm h}^4}\lim_{y\to 1}\left(\frac{1}{\sqrt{F^2\,h\,S^8\,\alpha^2-\alpha_0^2\,F_0^2\,h_0\,S_0^8}}\right) \tag{8.3.32}$$

Thus, for large $Tl_\perp$ we can write

$$\frac{4G_{10}}{L_1\,L_2{\rm Vol}\big(\mathcal{M}_5\big)}\frac{{\rm d}S_\perp^{\rm reg}}{{\rm d}l_\perp} = \frac{4G_{10}}{L_1\,L_2{\rm Vol}\big(\mathcal{M}_5\big)}\left.\frac{{\rm d}S_\perp^{\rm reg}}{{\rm d}y_0}\right|_{y_0=1}\frac{{\rm d}y_0}{{\rm d}l_\perp} = F_0\,h_0^{1/2}S_0^4\alpha_0\,, \tag{8.3.33}$$

which is the same result as the one found for the parallel slab (see 8.3.16). Thus, when $\rho_0\to\rho_{\rm h}$ we find a result which coincides with the thermal entropy of the black hole that we obtained in Sec. 7.3,

$$\frac{1}{L_1\,L_2}\left.\frac{{\rm d}S_\perp}{{\rm d}l_\perp}\right|_{\rho_0\to\rho_{\rm h}} = s\,. \tag{8.3.34}$$

The agreement between the entanglement entropy and thermal entropy densities for large $T\,l_\perp$ can also be verified from the results plotted in Fig. 8.4.

Similarly to the parallel case in (8.3.19), (8.3.34) and the numerical results for the entanglement entropy in the transverse slab also capture the increase in the number of degrees of freedom. Although asymptotically the transverse and parallel entanglement entropies have the same slopes, in the plots of Fig. 8.4 the transverse entanglement entropy increases faster for smaller widths.

8.3.3 Mutual information and correlations among flavors

To gain complementary information on the entanglement, it is useful to consider the mutual information of a bipartite system. This quantity is better suited to capture quantum entanglement than the entanglement entropy which is prone to temperature effects. In addition, there are no subtleties in regard to regularization.

USC DE SANTIAGO

Given two regions A and B, their mutual information $I(A,B)$ is defined through the entanglement entropies as

$$I(A,B) = S(A) + S(B) - S(A \cup B) \ . \tag{8.3.35}$$

The value of the mutual information is finite, positive semidefinite, and it provides an upper bound on the correlations between the two regions [180]. If we consider the regions A and B to be two slabs of some fixed sise, the value of the mutual information is usually determined by two competing configurations [176, 181]. If the separation between the two slabs is relatively small, then the minimal surface area that determines $S(A \cup B)$ consists of the union of a surface joining the closer edges of the two region with another surface connecting the edges that are further away. When the separation becomes larger, then the minimal area is the union of the minimal surface associated to region A with the minimal surface associated to region B, in which case $S(A \cup B) = S(A) + S(B)$ and the mutual information vanishes. So regions that are far enough separated contain degrees of freedom that are uncorrelated.

Let us consider now two slabs of equal width and a separation between them which is of the same length or larger. If the entanglement entropy is monotonically increasing, then the mutual information vanishes for this configuration. This is the case for the total entanglement entropy and the contribution of flavor in the parallel directions shown in Figs. 8.4 and 8.6 (left). This indicates that the theory remains "local", with degrees of freedom in spatially separated regions begin independent of each other, and it is the typical situation in holographic duals.

On the other hand, we observe a strikingly different behavior in the flavor contribution to the transverse entanglement entropy, in Fig. 8.6 (right). In this case the entanglement entropy is increasing for widths larger than the scale set by the temperature, but it shows a minimum and it is decreasing for smaller widths. This implies that even if the separation between the two slabs is larger than their width, the mutual information can be nonzero, with larger values reached when the width of the two slabs is very small and the separation is close to the minimum of the entanglement entropy. This indicates that the flavor degrees of freedom are correlated in the transverse direction through distances below or of the order of the temperature scale. This implies that flavor degrees of freedom separated in the transverse direction are not completely independent. It is then tempting to interpret the scale set by the minimum of the entanglement entropy as an "effective width" for the D5-branes that carry those degrees of freedom.

USC
UNIVERSIDADE
DE SANTIAGO
DE COMPOSTELA

Appendices for chapter 8

8.A Dimensional reduction

The ten-dimensional supergravity action can be dimensionally reduced both to four and five dimensions. The details of these constructions were given in [77] and will be briefly reviewed in this appendix. Since this reduced theory corresponds to vanishing chemical potential, in this appendix we restrict ourselves to this $\mu = 0$ case. In the reduction to five dimensions we adopt the following ansatz for the metric

$$\mathrm{d}s_{10}^2 = e^{\frac{10}{3}\gamma} g_{pq} \mathrm{d}z^p \mathrm{d}z^q + e^{-2(\gamma+\lambda)} \mathrm{d}s_{\mathrm{KE}}^2 + e^{2(4\lambda-\gamma)} \left(\mathrm{d}\tau + \mathcal{A}\right)^2 \ , \tag{8.A.1}$$

where g_{pq} is a metric for the coordinates $z^p = (t, x^1, x^2, x^3, \rho)$ and (γ, λ) are scalar fields depending on the 5d coordinates z^p. In our ansatz γ and λ depend only on the radial coordinate ρ and are related to the functions of the ten-dimensional metric as

$$\lambda = \frac{1}{5}\left(\log F - \log S\right) \ , \qquad \gamma = \frac{1}{10}\left(-2\log F - 8\log S - \frac{5}{2}\log h\right) \ . \tag{8.A.2}$$

Moreover, the reduced 5d metric takes the form

$$\mathrm{d}s_5^2 = -c_1^2\,\mathrm{d}t^2 + c_2^2\left((\mathrm{d}x^1)^2 + (\mathrm{d}x^2)^2\right) + c_3^2\,(\mathrm{d}x^3)^2 + c_\rho^2\,\mathrm{d}\rho^2 \ , \tag{8.A.3}$$

where the different coefficients are

$$\begin{aligned} c_1 &= F^{1/3} S^{4/3} b^{1/2} h^{1/6} \ , & c_2 &= F^{1/3} S^{4/3} h^{1/6} \\ c_3 &= \alpha\, F^{1/3} S^{4/3} h^{1/6} \ , & c_\rho &= \frac{\alpha\, F^{4/3} h^{2/3} S^{16/3}}{\rho^5 b^{1/2}} \ . \end{aligned} \tag{8.A.4}$$

We will use the reduced theory to compute the VEV of the stress-energy tensor. This calculation makes use of the holographic renormalization formalism to regulate the on-shell action. The VEV of the stress-energy tensor of the dual theory is obtained by taking the functional derivative of the renormalised theory with respect to the boundary metric. The result is [77]

$$\langle T^\mu{}_\nu \rangle = \frac{V_5}{2\kappa_{10}^2}\sqrt{\gamma}\left(-2K^\mu{}_\nu + \delta^\mu{}_\nu\left(2K + W_{5d}\right)\right)\Big|_{\rho\to\infty} + Q_{\mathrm{f}}\frac{V_5}{\kappa_{10}^2}\sqrt{\hat{\gamma}} e^{2\gamma+2\lambda+\frac{\phi}{2}}\delta^\mu{}_\nu\Big|_{\rho\to\infty} \ , \tag{8.A.5}$$

USC UNIVERSIDADE DE SANTIAGO DE COMPOSTELA

where γ is the determinant of the metric induced on constant ρ slices, $K^{\mu}{}_{\nu}$ is the extrinsic curvature of these constant ρ surfaces ($K = K^{\mu}{}_{\mu}$), and W_{5d} is the superpotential, given by

$$W_{5d} = -6e^{\frac{8}{3}\gamma - 4\lambda} - 4e^{\frac{8}{3}\gamma + 6\lambda} + Q_{\rm c} e^{\frac{20}{3}\gamma} \ . \tag{8.A.6}$$

In the last term in (8.A.5), $\hat{\gamma}$ is the determinant of the metric induced on constant ρ and x^3 slices. It is not difficult to show that, at first order in ϵ, that

$$\langle T^{\mu}{}_{\nu} \rangle = \text{diag}(-\mathcal{E}, p_{xy}, p_{xy}, p_z) = \mathcal{E}\, \text{diag}\left(-1\,,\, \frac{1}{3} + \frac{10}{9}\epsilon\,,\, \frac{1}{3} + \frac{10}{9}\epsilon\,,\, \frac{1}{3} - \frac{20}{9}\epsilon \right) , \tag{8.A.7}$$

where $\mathcal{E}$ is the energy density

$$\mathcal{E} = \frac{3\,\text{Vol}\big(\mathcal{M}_5\big)}{(2\pi)^7\,\alpha'^4\,g_{\rm s}^2}\,\rho_{\rm h}^4 \left(1 - \frac{5}{6}\epsilon\right) \ . \tag{8.A.8}$$

This result matches with the one found by thermodynamic methods in section 7.3.

8.A.1 Hydrodynamics in the shear channel

The five-dimensional supergravity theory can be further reduced along the x^3-direction. The $5d \to 4d$ ansatz for the reduction takes the form [77]

$$\text{d}s_5^2 \,=\, e^{-\beta}\,\text{d}s_4^2 \,+\, e^{2\beta}\,(\text{d}x^3)^2 \ , \tag{8.A.9}$$

where β is a new scalar field of the $4d$ supergravity. For our ansatz $e^{\beta} = c_3$, where c_3 is the function displayed in (8.A.4). This $4d$ theory can be used to compute the VEV of the stress-energy tensor of the dual theory along the (t, x^1, x^2)-directions. The result of this calculation coincides with the one displayed in (8.A.7) and will not be repeated here. Moreover, we can use the $4d$ theory to obtain the transport coefficients for perturbations propagating along the (x^1, x^2)-plane. In this appendix we will analyze the so-called shear channel. With this purpose we fluctuate the $4d$ metric about the background solution via the substitution

$$g_{mn} \,\to\, g_{mn} \,+\, h_{mn} \ , \tag{8.A.10}$$

where g_{mn} is the reduced metric of the first-order solution at zero chemical potential. We will work in the radial gauge for the metric, in which

$$h_{m\rho} = 0 \ , \qquad\qquad (m = t, x^1, x^2, \rho) \ . \tag{8.A.11}$$

Without loss of generality we consider a perturbation propagating along the x^2-direction. In the shear channel only the metric fluctuations h_{tx^1} and $h_{x^1\,x^2}$ are excited. Let us assume that these fluctuations (in the Fourier space) have frequency ω and momentum q and, accordingly, let us parametrise them as

$$h_{tx^1} = e^{-i\left(\omega t - q x^2\right)} c_2^2(\rho)\, H_{tx^1}(\rho) \ , \qquad\qquad h_{x^1\,x^2} = e^{-i\left(\omega t - q x^2\right)} c_2^2(\rho)\, H_{x^1\,x^2}(\rho) \ . \tag{8.A.12}$$

USC UNIVERSIDADE DE SANTIAGO DE COMPOSTELA

It turns out that the equations for the fluctuations can be reduced to a single second-order differential equation for a gauge invariant combination $X = X_0 + \epsilon\, X_1$, defined as

$$X(\rho) = q\, H_{tx^1}(\rho) + \omega H_{x^1\, x^2}(\rho)\ . \tag{8.A.13}$$

In order to write the fluctuation equation in a simple form, let us perform the following change of the radial variable

$$x\ =\ \sqrt{b(\rho)}\ =\ \sqrt{1-\frac{\rho_{\rm h}^4}{\rho^4}}\ . \tag{8.A.14}$$

In this new variable, the horizon is at $x = 0$, while the boundary resides at $x = 1$. Moreover, let us work with the dimensionless frequency and momentum $\hat{q}$ and $\hat{\omega}$ defined in (8.1.2). Then, if now the prime denotes derivative with respect to x, the fluctuation equation becomes

$$X''\ -\ \frac{\hat{q}^2x^2+\hat{\omega}^2}{x\,(\hat{q}^2x^2-\hat{\omega}^2)}\,X'\ +\ \Gamma\,\frac{\hat{q}^2x^2-\hat{\omega}^2}{x^2\sqrt{1-x^2}\,k(x)}\,X=0\ , \tag{8.A.15}$$

where Γ is the constant

$$\Gamma=\frac{\pi^2T^2Q_{\rm c}}{\rho_{\rm h}^2}=4\ -\ 15\,\epsilon\ , \tag{8.A.16}$$

and $k(x)$ is the following function

$$k(x)=4\left(x^2-1\right)+5\epsilon\left(x^2-1+4\left(1-x^2\right)^{1/4}+\frac{4}{5}\,x^2\,\Omega\left(\frac{1}{(1-x^2)^{1/4}}\right)\right)\ . \tag{8.A.17}$$

Notice that Γ and $k(x)$ contain terms which are zeroth-order in the flavor parameter, together with the ones that are first-order in ϵ. We want to find solutions of (8.A.15) which satisfy infalling boundary conditions at the horizon $x = 0$, as well as Dirichlet boundary conditions at the UV boundary $x = 1$. These solutions only exist if certain dispersion relation $\hat{\omega} = \hat{\omega}(\hat{q})$ is satisfied. Our objective in this section is to find such dispersion relation in a power series of $\hat{q}$. Actually, we will only keep quadratic and quartic terms of $\hat{q}$, as in (8.1.4), which contains two transport coefficients $\hat{D}_\eta$ and $\hat{\tau}_s$.

In order to impose infalling boundary conditions at the horizon $x = 0$, we adopt an ansatz for $X(x)$

$$X(x)\ =\ x^{-i\hat{\omega}}\,S(x)\ , \tag{8.A.18}$$

where $S(x)$ must be regular at $x = 0$. Let us expand $S(x)$ in powers of $\hat{q}$ as

$$S(x)\ =\ S_0(x)\ +\ \hat{q}^2\,S_2(x)\ +\ \dots\ . \tag{8.A.19}$$

Plugging (8.A.18) and the expansion (8.A.19) into (8.A.15) we get the following two differential equations for $S_0(x)$ and $S_2(x)$

$$\begin{aligned} S_0''-\frac{1}{x}\,S_0' &= 0\\ S_2''-\frac{1}{x}S_2' &= -\left[\frac{2\hat{D}_\eta}{x^2}+\frac{\Gamma}{\sqrt{1-x^2}\,k(x)}\right]S_0-\frac{2\hat{D}_\eta\,\left(\hat{D}_\eta-x^2\right)}{x^3}\,S_0'\ . \end{aligned} \tag{8.A.20}$$

USC UNIVERSIDADE DE SANTIAGO DE COMPOSTELA

We can immediately integrate the equation for S_0 in (8.A.20), yielding

$$S_0(x) \,=\, c_1 \frac{x^2}{2} \,+\, c_2 \;, \tag{8.A.21}$$

where c_1 and c_2 are integration constants. The differential equation for S_2 in (8.A.20) contains terms which depend on the flavor expansion parameter ϵ. Since we are working at first order in ϵ, it is convenient to expand the transport coefficients in powers of ϵ as

$$\hat{D}_\eta \,=\, \hat{D}_0 \,+\, \epsilon\, \hat{D}_1 \;, \qquad\qquad \hat{\tau}_s \,=\, \hat{\tau}_0 \,+\, \epsilon\, \hat{\tau}_1 \;, \tag{8.A.22}$$

as well as for the function S_2

$$S_2(x) \,=\, s(x) + \epsilon\, \tilde{s}(x) \;. \tag{8.A.23}$$

Proceeding in this way we generate two second-order differential equations for $s(x)$ and $\tilde{s}(x)$, which can be analytically integrated (these functions have rather long expressions and will not be written here). This integration generates two new integration constants c_3 and c_4 for $s(x)$ and another two c_5 and c_6 for $\tilde{s}(x)$. Expanding our analytic result for $s(x)$ near $x = 0$, up to second order in x, we get

$$\begin{aligned} s(x) \;\;=\;\; & \frac{1}{2}\Big(2\hat{D}_0(c_1\hat{D}_0 + c_2)\log x - c_1 - c_2 + 2c_4\Big) \\ & + \frac{1}{4}x^2\left(c_1\hat{D}_0(2\log x - 1) + c_1 + 2c_2\log\left(\frac{x}{2}\right) + c_2 + 2c_3\right) + \dots \;. \end{aligned} \tag{8.A.24}$$

Similarly, $\tilde{s}(x)$ near $x = 0$ takes the form

$$\begin{aligned} \tilde{s}(x) \;\;=\;\; & -\Big[(6\hat{D}_1 + 5i\pi - 5 - 10\log 2)c_1 + \Big((15+25i)\pi - 70 + 40\log 2\Big)c_2 - 12c_5\Big]\frac{x^2}{24} \\ & + \left[\frac{c_1}{2}x^2 + 2c_1\hat{D}_0 + c_2\right]\hat{D}_1\,\log x \,+\, \frac{1}{12}\Big(10i\pi + 35 - 20\log 2)c_1 \\ & + \frac{1}{12}\Big(5i\pi - 5 - 10\log 2\Big)c_2 \,+\, c_6 + \dots \;. \end{aligned} \tag{8.A.25}$$

Combining all these equations, we get $S(x) = S_0(x) + \hat{q}^2(s(x) + \epsilon\tilde{s}(x))$ for small $\hat{q}$ and small x. Let us now obtain an expression by expanding $S(x)$ in opposite order and demand that it should be consistent with the above. We first expand near $x = 0$ and write

$$S(x) = 1 + \sigma_2\, x^2 + \sigma_4\, x^4 + \dots \;. \tag{8.A.26}$$

Plugging the expansion (8.A.26) into (8.A.15) we get σ_2 and s_4 in terms of $\hat{\omega}$ and $\hat{q}$. Expanding this result for small $\hat{q}$ and ϵ, σ_2, we obtain

$$\begin{aligned} \sigma_2 \;\;=\;\; & -\frac{1}{2\hat{D}_0} + \frac{1}{4}\hat{q}^2(2\hat{\tau}_0 - 1) + \epsilon\left(\frac{\hat{D}_1}{2\hat{D}_0^2} + \frac{\hat{q}^2\hat{\tau}_1}{2}\right) + \dots \\ \sigma_4 \;\;=\;\; & -\frac{(4 - 12\hat{D}_0)\hat{q}^2}{64\hat{D}_0} - \epsilon\frac{\hat{q}^2\left(5\pi\hat{D}_0^2 - 30\hat{D}_0^2 + 30\hat{D}_0^2\log 2 - 4\hat{D}_1\right)}{64\hat{D}_0^2} + \dots \;. \end{aligned} \tag{8.A.27}$$

USC UNIVERSIDADE DE SANTIAGO DE COMPOSTELA

Thus, an expansion for small x and small $\hat{q}$ (8.A.26) leads to the following expressions for $S_0(x)$ and $S_2(x)$

$$\begin{aligned} S_0(x) &= 1 - \frac{x^2}{2\hat{D}_0} + \epsilon \frac{\hat{D}_1 x^2}{2\hat{D}_0^2} \\ S_2(x) &= \frac{12x^4\hat{D}_0^2 \,+\, 16(2\hat{\tau}_0 - 1)\hat{D}_0^2\, x^2 \,-\, 4\hat{D}_0\, x^4}{64\hat{D}_0^2} \\ &\quad + \frac{\epsilon}{64\,\hat{D}_0^2}\left[(30 - 5\pi - 30\log 2)\hat{D}_0^2\, x^4 \,+\, 4\hat{D}_1\, x^4 \,+\, 32\hat{\tau}_1\,\hat{D}_0^2\, x^2\right] . \end{aligned} \tag{8.A.28}$$

Let us now compare (8.A.28) and (8.A.21). Since the right-hand side of (8.A.21) does not depend on ϵ, we conclude that

$$\hat{D}_1 = 0 \ . \tag{8.A.29}$$

Moreover, by comparing the expression for S_2 in (8.A.28) and the one that follows from (8.A.24) and (8.A.25), we can relate the different integration constants and the transport coefficients as

$$\begin{aligned} &c_1 = -\frac{1}{\hat{D}_0}\ , \qquad c_2 = 1 \qquad c_3 = \frac{\hat{D}_0(2\hat{\tau}_0 - 3 + \log 4) + 1}{2\hat{D}_0}\ , \qquad c_4 = \frac{1}{2} - \frac{1}{2\hat{D}_0} \\ &c_5 = \frac{\hat{D}_0(12\hat{\tau}_1 + \pi(15 + 25i) - 70 + 20\log 4) + 5(1 - i\pi + \log 4)}{12\hat{D}_0} \\ &c_6 = \frac{5(\hat{D}_0(2 - 2i\pi + \log(16)) + 14 + 4i\pi - \log(256))}{24\hat{D}_0}\ . \end{aligned} \tag{8.A.30}$$

With these constants, the function S_0 becomes

$$S_0(x) = 1 - \frac{1}{2\,\hat{D}_0} x^2 \ . \tag{8.A.31}$$

Imposing the Dirichlet boundary condition $S_0(x = 1) = 0$ at $x = 1$ leads to the result for $\hat{D}_0$,

$$\hat{D}_0 = \frac{1}{2}\ . \tag{8.A.32}$$

Using this new condition and (8.A.30) we arrive at the following expressions for $s(x)$

$$\begin{aligned} s(x) &= \frac{1}{2}\Bigg(x^2\left(\tau_0 - \log\left(x/2\right)\right) - 1 + \sqrt{1 - x^2} + \frac{1}{2}\log\left(\frac{1 - \sqrt{1 - x^2}}{\sqrt{1 - x^2} + 1}\right) \\ &\quad + \left(1 - x^2\right)\operatorname{arctanh}\left(\sqrt{1 - x^2}\right)\Bigg)\ , \end{aligned} \tag{8.A.33}$$

USC UNIVERSIDADE DE SANTIAGO DE COMPOSTELA

and $\tilde{s}(x)$

$$\begin{aligned}\tilde{s}(x) &= -\frac{5\left(1-x^2\right)^{3/4}}{x^2}\left(\frac{1}{3}F\left(1,1;\frac{7}{4};1-\frac{1}{x^2}\right)-\frac{1}{21}2\left(1-x^2\right)F\left(1,2;\frac{11}{4};1-\frac{1}{x^2}\right)+\frac{2x^2}{3}\right)\\ &+\frac{1}{4}x^2(2\tau_1+5(\log(4)-2))-\sqrt{1-x^2}\left(\Omega\left(\frac{1}{(1-x^2)^{\frac{1}{4}}}\right)+\frac{15}{4}\right)\\ &+\frac{5}{4}\left(x^2+2\right)\operatorname{arctanh}\left(\sqrt{1-x^2}\right)-\frac{5}{4}(\pi-5+\log(4))\ . \end{aligned} \tag{8.A.34}$$

Requiring that $s(x=1)=0$ determines the value of $\hat{\tau}_0$, which turns out to be

$$\hat{\tau}_0 = 1-\log 2\ . \tag{8.A.35}$$

Moreover, the Dirichlet boundary condition $\tilde{s}(x=1)=0$ is satisfied if $\hat{\tau}_1$ is given by

$$\hat{\tau}_1 = \frac{5}{2}(\pi-3)\ . \tag{8.A.36}$$

USC
UNIVERSIDADE DE SANTIAGO DE COMPOSTELA

9 Some final remarks

In this work we studied the holographic dual to an intersection of multiple color D3-branes and flavor D5-branes beyond the probe or equivalently the quenched approximation. We found geometries that solve the supergravity equations of motion with D3-brane fluxes and smeared D5-brane sources. In our setup the D5-branes share two spatial directions with the D3-branes and are continuously distributed along the third direction forming a multilayer structure. The solutions we found are charged black holes corresponding to a field theory configuration with non-zero temperature and chemical potential. In the dual ambient four-dimensional supersymmetric gauge field theory, the D5-branes give rise to massless flavors on a codimension one defect.

We solved the complete set of equations of motion in a first-order perturbative expansion in two parameters. This solution is valid when these two parameters are small, let us now comment on this further. Taking into account the parametric dependence of the densities on the number of colors $N_{\rm c}$, flavors $N_{\rm f}$, and the 't Hooft coupling λ, we can introduce the quantities

$$n_{\rm f} = N_{\rm f}\ \bar{n}_{\rm f}\ \ ,\ \ n_{\rm b} = N_{\rm f}\ \bar{n}_{\rm b}\ , \tag{9.1}$$

where $n_{\rm f}$ is the density of the smeared flavors in the direction transverse to the defect and $n_{\rm b}$ is the baryon density. In terms of these quantities the solutions are valid when the following conditions are satisfied

$$\frac{N_{\rm c}}{\lambda^{1/2} N_{\rm f}} \gg \frac{\bar{n}_{\rm f}}{T} \gg \frac{\bar{n}_{\rm b}^2}{\bar{n}_{\rm f} T^5}\ . \tag{9.2}$$

Alternatively, the second condition can be expressed as

$$\frac{n_{\rm f}}{T} \gg \frac{n_{\rm b}}{T^3}\ . \tag{9.3}$$

Therefore, both the defect and baryon densities (in units of the temperature) should be small, with the latter being much smaller than the former.

In this regime of validity we have been able to obtain a consistent anisotropic thermodynamics and to compute several observables such as transport coefficients, quark-antiquark potentials, and entanglement entropies. Our results for the entropy and energy density (7.3.16), as well as for the pressures (7.3.27) reflect that there are additional degrees of freedom along

the $(2+1)$-dimensional intersections between the color and flavor branes, contributing to the entropy, energy density and pressure along the intersection but not to the transverse pressure. The enhancement in the number of degrees of freedom also shows in the entanglement entropy of a slab, see Fig. 8.4, which becomes larger when the density of defects (implicit in the parameter ϵ) increases. A more precise statement reflecting the same facts is captured by the formulas (8.3.19) and (8.3.34) that determine the increase of the entanglement entropy with the sise of the entangling region as proportional to the thermal entropy. Curiously, in this limit the entanglement entropy shows a similar behavior independently of whether the slab is oriented parallel or transverse to the intersection.

The results for the quark-antiquark potential, depicted in Fig. 8.2, indicate that the degrees of freedom at the intersections contribute significantly to the screening of color charges, in any direction, although the effect is more pronounced in the transverse direction. On the other hand, the effect of the charge density is more noticeable along the directions parallel to the defect. We did not study the effect of the charge density in hydrodynamics, but we observed that the second order transport coefficient in the shear channel along the intersection increases slightly with the number of D5-branes (8.1.6). This might be an indication of $(2+1)$-dimensional dynamics, where the value of the coefficient is larger, modifying the transport properties. Another possible indication is that the value of the speed of sound along the intersection is increased (7.3.37), going above the conformal value in $3+1$ dimensions but still below the conformal value in a $(2+1)$-dimensional theory (that one finds in isolated D5-branes [69]), at least in the approximation of small flavor density that we use. Since the equation of state remains conformal (7.3.38), the transverse speed of sound goes below the conformal value in (7.3.37). In addition to these thermodynamic insights, we also infer from the behavior of mutual information that flavor degrees of freedom are correlated in the transverse direction, thus not being completely independent at separations close or below the temperature scale. One could take this as a signal of increasing inter-layer mobility and decreasing intra-layer mobility, which is interesting from the point of view of condensed matter physics, where multilayered materials with strongly correlated electrons constrained to move in $2+1$ dimensions show strange metallic behavior and high-T_c superconductivity.

Let us now comment on some possible extensions of our work. It would be certainly desirable to obtain a solution valid beyond the perturbative expansions performed here. Most likely this would require a numerical analysis of the equations of motion, such us the ones written in the system (7.A.4) for the case of vanishing chemical potential. The black hole solution studied of this system found here is not unique. Indeed, in [76] an exact solution for zero chemical potential was found. This black hole geometry has a Lifshifz-like scaling symmetry, is non-analytic in n_f and, as a consequence, one cannot take the flavorless limit $n_f \to 0$. It would be interesting to construct new backgrounds interpolating between that geometry and the asymptotically AdS metric found here. More generally, in order to classify all possible solutions one should study different boundary conditions to be imposed both at the UV and at the IR.

The solutions at nonzero baryon density display the phenomenon of having two types of charged degrees of freedom, those that are fractionalised, corresponding to those sitting behind the horizon, and coherent ones which correspond to those that are hovering above the

horizon. This situation has been encountered elsewhere, in electron cloud solutions [182, 183] to various probe brane configurations [157, 184, 185] with entrancing connections to quantum Hall physics. Constructing observables such as the butterfly velocity or the generalised charged entanglement entropy discussed in [186] would yield probes for distinguishing how the degrees of freedom flow under external fields, complementarily to the obvious magneto-transport coefficients readily available. A really captivating scenario would be to establish the entanglement first law using the latter probe, addressing the long-standing open problem in the field.

The setup considered here can be generalised in several other directions. One possibility could be adding four-dimensional flavors by introducing D7-branes, which as a start could be treated as probes as in [79]. This analysis would shed more light to the anisotropic physics of the holographic multilayer theories. Another possible generalization could be extending the analysis to different dimensions both for the ambient theory or for the defect. For example, viable chassis for this exercise include the D2-D6 backreacted geometry of [187] or the D3-D3' backreacted geometry constructed in [188].

USC
UNIVERSIDADE
DE SANTIAGO
DE COMPOSTELA

USC
UNIVERSIDADE
DE SANTIAGO
DE COMPOSTELA

Conclusions

After a brief review on the holographic correspondence and its applications, we have studied D3 and D5 branes intersections in two special limits. The first part of this thesis was devoted to the analysis of the D3/D5 intersection in the so-called quenched approximation, while the second part aimed to study the same system when the backreaction of the flavor branes is taken into account. Even though the most important features and conclusions have been detailed in previous chapters of this thesis (see chapters 5 and 9), let us summarise here the main results.

In part I we employed holographic techniques to analyze the response of a (2+1)-dimensional gauge theory to an external rotating electric field. By doing so, we found many resemblances to the (3+1)-dimensional system, previously studied in [30] and [31]. In particular, different kinds of embeddings lead to two distinguished phases of the system, which can either behave as an insulator or a conductor. Roughly, the lobbed lines in Fig. 3.1 show the separation of the phase space into the conductor phase (black hole embeddings, above the line) and the insulator one (Minkowski embeddings, below the line). The line itself correspond to the so-called critical embeddings. Note that for some range of frequencies along the critical line we find states with zero electric field, but non-zero induced current, and viceversa, that are termed vector meson Floquet condensates and Floquet suppression points, respectively.

Moreover, we extended the analysis to the finite temperature case, so that we have two horizons. The inner one is the usual event horizon, while the outer one is an effective horizon that appears as a consequence of the background electric field. We have checked that the Hawking temperature T always turns out to be smaller than the effective one T_{eff}, $T < T_{\text{eff}}$. The three mentioned kinds of embeddings are defined considering whether the brane crosses or not the effective horizon.

Mainly, the effect of the background temperature is equivalent to that of increasing the module of the electric field. The lobbed structure is depleted as we increase the background temperature, until we completely lose the Minkowski embeddings at a horizon radius $r_{\text{h}}/m \geq 0.8897$, in units of the quark mass. Actually, one has to reach values of $r_{\text{h}}/m \geq 0.8$ in order to see significant effects of the non-vanishing temperature. At these high temperatures, where both horizons come closer, we start seeing multi-valuedness within the conductive phase (Fig. 3.2), as well as solutions with vanishing $|E| = |j| = 0$, that are only found in the insulator phase for smaller temperatures.

On the other hand, we studied both the non-linear rotating conductivity and the AC and DC conductivities. The former one, and in particular the analysis of the angle between j

USC DE SANTIAGO

and E led us to consider a possible mixture of two types of currents: rotating polarization and charge flow. The charge flow is not present in the insulating phase. Also, in the Floquet suppression points, the polarizability of the vacuum goes smoothly from positive to negative, which means that in some given ranges of the driving frequency the meson condensate is polarised antiparallel to the applied electric field. We can cite [152] as an example of this kind of effect in the Floquet engineering realm, where paramagnetism turns into diamagnetism under a strong driving. It is worth mentioning that in the large electric field or large temperature limits the results in [33] are recovered: the current is purely a conductive current and $j_{\text{con}}(t) = \sigma E(t)$ with σ a real constant.

As for the AC and DC conductivities, they can be computed analytically in the massless limit, where the conductivity tensor turns out to be trivial and again agrees with [33]. In the massive case, it displays a rich structure. In particular, we studied the system close to (or at) the first critical frequency, where the system creates efficiently charged carriers and holes. This interesting pattern is still present for finite temperature, but dissolves very fast as we increase it.

Future extensions of this work could go in the direction of adding new components to the gauge field, in order to study the effects of, for example, chemical potential and magnetic fields. Moreover, the use of other brane setups, as the ABJM model, could lead to interesting non-trivial topological effects. Another direction would be to consider the backreaction of the D5 branes into the D3 background. Finally, it is worth mentioning that the nature of the phase transition needs to be further studied.

Part II of this thesis is devoted to the study of a D3/D5 system in the unquenched approximation. We applied the smearing technique and found geometries solving the equations of motion. In particular, we found solutions that are black holes, with and without charges, corresponding to a field theory with finite temperature and with or without chemical potential.

In order to solve the equations of motion we used a perturbative expansion in two parameters, related to the density of the smeared flavors in the direction transverse to the defect, n_{f}, and the baryon density, n_{b} (see (7.3.15)).

These solutions were later used to compute different (anisotropic) thermodynamic quantities, as well as observables such as transport coefficients, quark-antiquark potentials, and entanglement entropies. From these results, we can infer that there are additional degrees of freedom along the intersection of the D3 and D5 branes that contribute to the pressure along the intersection (as well as to other quantities such as the entropy or the energy density), but not to the transverse pressure. The effects related to the enhancement in the number of degrees of freedom can also be found when looking at the entanglement entropy or the quark-antiquark potentials. It is worth mentioning that, in the latter ones, the degrees of freedom at the intersections have a significant impact on the screening of color charges, both in the transverse and the parallel directions.

Although the effect of charge density was not considered in hydrodynamics, we noticed that the second order transport coefficient in the shear channel along the intersection increases with the number of D5-branes (see (8.1.6)).

One possible extension of this work would be looking for solutions valid beyond the limits

of our perturbative expansions, which would more probably require a numerical analysis of the system. Furthermore, another solution to this background (in the absence of chemical potential) had already been found in [76]. This black hole geometry is not analytic in the flavorless limit; thus, it would be interesting to obtain some interpolation between both limits.

Besides, our setup can be generalised in different ways. On the one hand, one can introduced D7-branes in order to add four-dimensional flavors (these new branes could be treated as probes, as in [79]). Moreover, the analysis could be extended to the D2-D6 backreacted geometry of [187] or the D3-D3' backreacted geometry constructed in [188].

USC
UNIVERSIDADE
DE SANTIAGO
DE COMPOSTELA

USC
UNIVERSIDADE
DE SANTIAGO
DE COMPOSTELA

Bibliography

[1] J. Maldacena, *The Large-N Limit of Superconformal Field Theories and Supergravity*, *International Journal of Theoretical Physics* **38** (1999) 1113 [hep-th/9711200].

[2] J. Casalderrey-Solana, H. Liu, D. Mateos, K. Rajagopal and U.A. Wiedemann, *Gauge/String Duality, Hot QCD and Heavy Ion Collisions*, *arXiv e-prints* (2011) arXiv:1101.0618 [1101.0618].

[3] J. McGreevy, *Holographic duality with a view toward many-body physics*, *arXiv e-prints* (2009) arXiv:0909.0518 [0909.0518].

[4] A.V. Ramallo, *Introduction to the AdS/CFT correspondence*, *arXiv e-prints* (2013) arXiv:1310.4319 [1310.4319].

[5] J.D. Edelstein, J.P. Shock and D. Zoakos, *The AdS/CFT Correspondence and Non-perturbative QCD*, in *Particles and Fields*, A. Ayala, C. Calcaneo-Roldan, B. Morales-Ruiz, A. Perez-Lorenzana, A. Sanchez, M.E. Tejada-Yeomans et al., eds., vol. 1116 of *American Institute of Physics Conference Series*, pp. 265–284, Apr., 2009, DOI [0901.2534].

[6] M. Ammon and J. Erdmenger, *Gauge/Gravity Duality: Foundations and Applications*, Cambridge University Press (2015), 10.1017/CBO9780511846373.

[7] J. Zaanen, Y. Liu, Y.-W. Sun and K. Schalm, *Holographic Duality in Condensed Matter Physics*, Cambridge University Press (2015), 10.1017/CBO9781139942492.

[8] L. Susskind, *The world as a hologram*, *Journal of Mathematical Physics* **36** (1995) 6377 [hep-th/9409089].

[9] A. Karch and E. Katz, *Adding flavor to AdS/CFT*, *Journal of High Energy Physics* **2002** (2002) 043 [hep-th/0205236].

[10] J. Erdmenger, N. Evans, I. Kirsch and E.J. Threlfall, *Mesons in gauge/gravity duals*, *European Physical Journal A* **35** (2008) 81 [0711.4467].

[11] G. Floquet, *Sur les équations différentielles linéaires à coefficients périodiques*, *Annales scientifiques de l'École Normale Supérieure* **2e série, 12** (1883) 47.

USC DE SANTIAGO

[12] M. Bukov, L. D'Alessio and A. Polkovnikov, *Universal high-frequency behavior of periodically driven systems: from dynamical stabilization to Floquet engineering*, *Advances in Physics* **64** (2015) 139 [1407.4803].

[13] P. Weinberg, M. Bukov, L. D'Alessio, A. Polkovnikov, S. Vajna and M. Kolodrubetz, *Adiabatic perturbation theory and geometry of periodically-driven systems*, *Phys. Rept.* **688** (2017) 1 [1606.02229].

[14] M. Holthaus, *Floquet engineering with quasienergy bands of periodically driven optical lattices*, *Journal of Physics B Atomic Molecular Physics* **49** (2016) 013001 [1510.09042].

[15] T. Oka and S. Kitamura, *Floquet Engineering of Quantum Materials*, *Annual Review of Condensed Matter Physics* **10** (2019) 387 [1804.03212].

[16] U.D. Giovannini and H. Hübener, *Floquet analysis of excitations in materials*, *Journal of Physics: Materials* **3** (2019) 012001.

[17] M.S. Rudner and N.H. Lindner, *The Floquet Engineer's Handbook*, *arXiv e-prints* (2020) arXiv:2003.08252 [2003.08252].

[18] D. Fausti, R. Tobey, N. Dean, S. Kaiser, A. Dienst, M. Hoffmann et al., *Light-induced superconductivity in a stripe-ordered cuprate*, *Science (New York, N.Y.)* **331** (2011) 189.

[19] M. Mitrano, A. Cantaluppi, D. Nicoletti, S. Kaiser, A. Perucchi, S. Lupi et al., *Possible light-induced superconductivity in k3c60 at high temperature*, *Nature* **530** (2016) .

[20] T. Oka and H. Aoki, *Photovoltaic Hall effect in graphene*, *Physical Review B* **79** (2009) 081406 [0807.4767].

[21] T. Kitagawa, T. Oka, A. Brataas, L. Fu and E. Demler, *Transport properties of nonequilibrium systems under the application of light: Photoinduced quantum hall insulators without landau levels*, *Phys. Rev. B* **84** (2011) 235108.

[22] J. Cayssol, B. Dóra, F. Simon and R. Moessner, *Floquet topological insulators*, *Physica Status Solidi Rapid Research Letters* **7** (2013) 101 [1211.5623].

[23] N.H. Lindner, G. Refael and V. Galitski, *Floquet topological insulator in semiconductor quantum wells*, *Nature Physics* **7** (2011) 490 [1008.1792].

[24] M.C. Rechtsman, J.M. Zeuner, Y. Plotnik, Y. Lumer, D. Podolsky, F. Dreisow et al., *Photonic Floquet topological insulators*, *Nature* **496** (2013) 196 [1212.3146].

[25] G. Jotzu, M. Messer, R. Desbuquois, M. Lebrat, T. Uehlinger, D. Greif et al., *Experimental realization of the topological Haldane model with ultracold fermions*, *Nature* **515** (2014) 237 [1406.7874].

[26] Y.H. Wang, H. Steinberg, P. Jarillo-Herrero and N. Gedik, *Observation of Floquet-Bloch States on the Surface of a Topological Insulator*, *Science* **342** (2013) 453 [1310.7563].

[27] X.-X. Zhang, T.T. Ong and N. Nagaosa, *Theory of photoinduced Floquet Weyl semimetal phases*, *Phys. Rev. B* **94** (2016) 235137 [1607.05941].

[28] H. Hübener, M.A. Sentef, U. de Giovannini, A.F. Kemper and A. Rubio, *Creating stable Floquet-Weyl semimetals by laser-driving of 3D Dirac materials*, *Nature Communications* **8** (2017) 13940 [1604.03399].

[29] L. Bucciantini, S. Roy, S. Kitamura and T. Oka, *Emergent weyl nodes and fermi arcs in a floquet weyl semimetal*, *Phys. Rev. B* **96** (2017) 041126.

[30] K. Hashimoto, S. Kinoshita, K. Murata and T. Oka, *Holographic Floquet states I: a strongly coupled Weyl semimetal*, *Journal of High Energy Physics* **2017** (2017) 127 [1611.03702].

[31] S. Kinoshita, K. Murata and T. Oka, *Holographic floquet states ii: Floquet condensation of vector mesons in nonequilibrium phase diagram*, *Journal of High Energy Physics* **2018** (2017) .

[32] D. Mateos, R.C. Myers and R.M. Thomson, *Thermodynamics of the brane*, *Journal of High Energy Physics* **2007** (2007) 067 [hep-th/0701132].

[33] A. Karch and S.L. Sondhi, *Non-linear, finite frequency quantum critical transport from AdS/CFT*, *Journal of High Energy Physics* **2011** (2011) 149 [1008.4134].

[34] R.A. Janik and P. Witaszczyk, *Towards the description of anisotropic plasma at strong coupling*, *JHEP* **09** (2008) 026 [0806.2141].

[35] P.M. Chesler and L.G. Yaffe, *Horizon formation and far-from-equilibrium isotropization in supersymmetric Yang-Mills plasma*, *Phys. Rev. Lett.* **102** (2009) 211601 [0812.2053].

[36] T. Azeyanagi, W. Li and T. Takayanagi, *On String Theory Duals of Lifshitz-like Fixed Points*, *JHEP* **06** (2009) 084 [0905.0688].

[37] D. Mateos and D. Trancanelli, *The anisotropic N=4 super Yang-Mills plasma and its instabilities*, *Phys. Rev. Lett.* **107** (2011) 101601 [1105.3472].

[38] D. Mateos and D. Trancanelli, *Thermodynamics and Instabilities of a Strongly Coupled Anisotropic Plasma*, *JHEP* **07** (2011) 054 [1106.1637].

[39] J.-i. Koga, K. Maeda and K. Tomoda, *Holographic superconductor model in a spatially anisotropic background*, *Phys. Rev.* **D89** (2014) 104024 [1401.6501].

USC DE SANTIAGO

[40] S. Jain, N. Kundu, K. Sen, A. Sinha and S.P. Trivedi, *A Strongly Coupled Anisotropic Fluid From Dilaton Driven Holography*, *JHEP* **01** (2015) 005 [1406.4874].

[41] L. Cheng, X.-H. Ge and S.-J. Sin, *Anisotropic plasma at finite $U(1)$ chemical potential*, *JHEP* **07** (2014) 083 [1404.5027].

[42] E. Banks and J.P. Gauntlett, *A new phase for the anisotropic N=4 super Yang-Mills plasma*, *JHEP* **09** (2015) 126 [1506.07176].

[43] D. Roychowdhury, *On anisotropic black branes with Lifshitz scaling*, *Phys. Lett.* **B759** (2016) 410 [1509.05229].

[44] D. Roychowdhury, *Holography for anisotropic branes with hyperscaling violation*, *JHEP* **01** (2016) 105 [1511.06842].

[45] V. Jahnke and A.S. Misobuchi, *Probing strongly coupled anisotropic plasmas from higher curvature gravity*, *Eur. Phys. J. C* **76** (2016) 309 [1510.03774].

[46] E. Banks, *Phase transitions of an anisotropic N=4 super Yang-Mills plasma via holography*, *JHEP* **07** (2016) 085 [1604.03552].

[47] D. Ávila, D. Fernández, L. Patiño and D. Trancanelli, *Thermodynamics of anisotropic branes*, *JHEP* **11** (2016) 132 [1609.02167].

[48] A. Donos, J.P. Gauntlett and O. Sosa-Rodriguez, *Anisotropic plasmas from axion and dilaton deformations*, *JHEP* **11** (2016) 002 [1608.02970].

[49] D. Giataganas, U. Gürsoy and J.F. Pedraza, *Strongly-coupled anisotropic gauge theories and holography*, *Phys. Rev. Lett.* **121** (2018) 121601 [1708.05691].

[50] G. Itsios, N. Jokela, J. Järvelä and A.V. Ramallo, *Low-energy modes in anisotropic holographic fluids*, *Nucl. Phys.* **B940** (2019) 264 [1808.07035].

[51] I. Aref'eva and K. Rannu, *Holographic Anisotropic Background with Confinement-Deconfinement Phase Transition*, *JHEP* **05** (2018) 206 [1802.05652].

[52] A. Karch and A. O'Bannon, *Metallic AdS/CFT*, *Journal of High Energy Physics* **2007** (2007) 024 [0705.3870].

[53] T. Albash, V.G. Filev, C.V. Johnson and A. Kundu, *Quarks in an external electric field in finite temperature large N gauge theory*, *JHEP* **08** (2008) 092 [0709.1554].

[54] T. Albash, V.G. Filev, C.V. Johnson and A. Kundu, *Finite temperature large N gauge theory with quarks in an external magnetic field*, *JHEP* **07** (2008) 080 [0709.1547].

[55] J. Erdmenger, R. Meyer and J.P. Shock, *AdS/CFT with flavour in electric and magnetic Kalb-Ramond fields*, *JHEP* **12** (2007) 091 [0709.1551].

[56] E. D'Hoker and P. Kraus, *Magnetic Brane Solutions in AdS*, *JHEP* **10** (2009) 088 [0908.3875].

[57] E. D'Hoker and P. Kraus, *Charged Magnetic Brane Solutions in AdS (5) and the fate of the third law of thermodynamics*, *JHEP* **03** (2010) 095 [0911.4518].

[58] K. Jensen, A. Karch and E.G. Thompson, *A Holographic Quantum Critical Point at Finite Magnetic Field and Finite Density*, *JHEP* **05** (2010) 015 [1002.2447].

[59] N. Evans, A. Gebauer, K.-Y. Kim and M. Magou, *Phase diagram of the D3/D5 system in a magnetic field and a BKT transition*, *Phys. Lett.* **B698** (2011) 91 [1003.2694].

[60] E. D'Hoker and P. Kraus, *Holographic Metamagnetism, Quantum Criticality, and Crossover Behavior*, *JHEP* **05** (2010) 083 [1003.1302].

[61] K.-Y. Kim, B. Sahoo and H.-U. Yee, *Holographic chiral magnetic spiral*, *JHEP* **10** (2010) 005 [1007.1985].

[62] C. Hoyos, T. Nishioka and A. O'Bannon, *A chiral magnetic effect from AdS/CFT with flavor*, *Journal of High Energy Physics* **2011** (2011) 84 [1106.4030].

[63] M. Ammon, V.G. Filev, J. Tarrío and D. Zoakos, *D3/D7 Quark-Gluon Plasma with Magnetically Induced Anisotropy*, *JHEP* **09** (2012) 039 [1207.1047].

[64] U. Gürsoy, M. Järvinen, G. Nijs and J.F. Pedraza, *Inverse Anisotropic Catalysis in Holographic QCD*, *JHEP* **04** (2019) 071 [1811.11724].

[65] N. Evans, K.-Y. Kim, J.P. Shock and J.P. Shock, *Chiral phase transitions and quantum critical points of the D3/D7(D5) system with mutually perpendicular E and B fields at finite temperature and density*, *JHEP* **09** (2011) 021 [1107.5053].

[66] D.E. Kharzeev and H.-U. Yee, *Chiral helix in AdS/CFT with flavor*, *Phys. Rev.* **D84** (2011) 125011 [1109.0533].

[67] A. Donos, J.P. Gauntlett and C. Pantelidou, *Magnetic and Electric AdS Solutions in String- and M-Theory*, *Class. Quant. Grav.* **29** (2012) 194006 [1112.4195].

[68] N. Jokela and A.V. Ramallo, *Universal properties of cold holographic matter*, *Phys. Rev.* **D92** (2015) 026004 [1503.04327].

[69] G. Itsios, N. Jokela and A.V. Ramallo, *Collective excitations of massive flavor branes*, *Nucl. Phys.* **B909** (2016) 677 [1602.06106].

[70] S.S. Gubser and S.S. Pufu, *The Gravity dual of a p-wave superconductor*, *JHEP* **11** (2008) 033 [0805.2960].

USC DE SANTIAGO

[71] M. Ammon, J. Erdmenger, M. Kaminski and P. Kerner, *Superconductivity from gauge/gravity duality with flavor*, *Phys. Lett.* **B680** (2009) 516 [0810.2316].

[72] P. Basu, J. He, A. Mukherjee and H.-H. Shieh, *Superconductivity from D3/D7: Holographic Pion Superfluid*, *JHEP* **11** (2009) 070 [0810.3970].

[73] N. Iizuka, S. Kachru, N. Kundu, P. Narayan, N. Sircar and S.P. Trivedi, *Bianchi Attractors: A Classification of Extremal Black Brane Geometries*, *JHEP* **07** (2012) 193 [1201.4861].

[74] A. Donos and J.P. Gauntlett, *Helical superconducting black holes*, *Phys. Rev. Lett.* **108** (2012) 211601 [1203.0533].

[75] N. Iizuka and K. Maeda, *Study of Anisotropic Black Branes in Asymptotically anti-de Sitter*, *JHEP* **07** (2012) 129 [1204.3008].

[76] E. Conde, H. Lin, J.M. Penín, A.V. Ramallo and D. Zoakos, *D3-D5 theories with unquenched flavors*, *Nuclear Physics B* **914** (2017) 599 [1607.04998].

[77] J.M. Penín, A.V. Ramallo and D. Zoakos, *Anisotropic D3-D5 black holes with unquenched flavors*, *Journal of High Energy Physics* **2018** (2018) 139 [1710.00548].

[78] N. Jokela, J.M. Penín, A.V. Ramallo and D. Zoakos, *Gravity dual of a multilayer system*, *JHEP* **03** (2019) 064 [1901.02020].

[79] U. Gran, N. Jokela, D. Musso, A.V. Ramallo and M. Tornsö, *Holographic fundamental matter in multilayered media*, *JHEP* **12** (2019) 38 [1909.01864].

[80] C. Hoyos, N. Jokela, J.M. Penín and A.V. Ramallo, *Holographic spontaneous anisotropy*, *JHEP* **04** (2020) 062 [2001.08218].

[81] C. Hoyos, N. Jokela, J.M. Penín, A.V. Ramallo and J. Tarrío, *Risking your NEC*, *JHEP* **10** (2021) 112 [2104.11749].

[82] E. Fradkin, S.A. Kivelson, M.J. Lawler, J.P. Eisenstein and A.P. MacKenzie, *Nematic Fermi Fluids in Condensed Matter Physics*, *Annual Review of Condensed Matter Physics* **1** (2010) 153 [0910.4166].

[83] K. Yagi and N. Yunes, *Relating follicly-challenged compact stars to bald black holes: A link between two no-hair properties*, *Phys. Rev.* **D91** (2015) 103003 [1502.04131].

[84] K. Yagi and N. Yunes, *I-Love-Q Relations: From Compact Stars to Black Holes*, *Class. Quant. Grav.* **33** (2016) 095005 [1601.02171].

[85] F. Bigazzi, R. Casero, A.L. Cotrone, E. Kiritsis and A. Paredes, *Non-critical holography and four-dimensional CFT's with fundamentals*, *Journal of High Energy Physics* **2005** (2005) 012 [hep-th/0505140].

[86] C. Núñez, A. Paredes and A.V. Ramallo, *Unquenched Flavor in the Gauge/Gravity Correspondence*, *Adv. High Energy Phys.* **2010** (2010) 196714 [1002.1088].

[87] F. Bigazzi, A.L. Cotrone, J. Mas, A. Paredes, A.V. Ramallo and J. Tarrío, *D3-D7 Quark-Gluon Plasmas*, *JHEP* **11** (2009) 117 [0909.2865].

[88] F. Bigazzi, A.L. Cotrone, J. Mas, D. Mayerson and J. Tarrío, *D3-D7 Quark-Gluon Plasmas at Finite Baryon Density*, *JHEP* **04** (2011) 060 [1101.3560].

[89] A. Garbayo, J. Mas and A.V. Ramallo, *Holographic Floquet states in low dimensions*, *Journal of High Energy Physics* **2020** (2020) 13 [2007.12115].

[90] M. Berenguer, A. Garbayo, J. Mas and A.V. Ramallo, *Holographic Floquet states in low dimensions (II)*, *arXiv e-prints* (2022) arXiv:2209.03884 [2209.03884].

[91] A. Garbayo, C. Hoyos, N. Jokela, J.M. Penín and A.V. Ramallo, *Flavored anisotropic black holes*, *Journal of High Energy Physics* **2022** (2022) 61 [2208.04958].

[92] K. Becker, M. Becker and J.H. Schwarz, *String Theory and M-Theory: A Modern Introduction*, Cambridge University Press (2006), 10.1017/CBO9780511816086.

[93] E. Kiritsis, *String theory in a nutshell*, Princeton University Press, USA (2019).

[94] J. Polchinski, *String theory. Vol. 1: An introduction to the bosonic string*, Cambridge Monographs on Mathematical Physics, Cambridge University Press (12, 2007), 10.1017/CBO9780511816079.

[95] J. Polchinski, *String theory. Vol. 2: Superstring theory and beyond*, Cambridge Monographs on Mathematical Physics, Cambridge University Press (12, 2007), 10.1017/CBO9780511618123.

[96] M.B. Green, J.H. Schwarz and E. Witten, *SUPERSTRING THEORY. VOL. 1: INTRODUCTION*, Cambridge Monographs on Mathematical Physics, Cambridge University Press (7, 1988).

[97] M.B. Green, J.H. Schwarz and E. Witten, *SUPERSTRING THEORY. VOL. 2: LOOP AMPLITUDES, ANOMALIES AND PHENOMENOLOGY*, Cambridge Monographs on Mathematical Physics, Cambridge University Press (7, 1988).

[98] S.P. Martin, *A Supersymmetry Primer*, in *Perspectives on Supersymmetry. Edited by KANE GORDON L. Published by World Scientific Publishing Co. Pte. Ltd*, pp. 1–98 (1998), DOI.

[99] S. Coleman and J. Mandula, *All possible symmetries of the s matrix*, *Phys. Rev.* **159** (1967) 1251.

[100] F. Gliozzi, J. Scherk and D. Olive, *Supersymmetry, supergravity theories and the dual spinor model*, *Nuclear Physics B* **122** (1977) 253.

[101] G. Hooft, *A planar diagram theory for strong interactions*, *Nuclear Physics B* **72** (1974) 461.

[102] G. Veneziano, *Some aspects of a unified approach to gauge, dual and gribov theories*, *Nuclear Physics B* **117** (1976) 519.

[103] F. Benini, F. Canoura, S. Cremonesi, C. Núñez and A.V. Ramallo, *Unquenched flavors in the Klebanov-Witten model*, *JHEP* **02** (2007) 090 [hep-th/0612118].

[104] R. Casero, C. Núñez and A. Paredes, *Towards the string dual of N=1 supersymmetric QCD-like theories*, *Phys. Rev. Lett.* **73** (2006) 086005 [hep-th/0602027].

[105] R. Casero, C. Núñez and A. Paredes, *Elaborations on the string dual to N=1 SQCD*, *Phys. Rev. Lett.* **77** (2008) 046003 [0709.3421].

[106] F. Benini, S. Cremonesi, F. Canoura, A.V. Ramallo and C. Núñez, *Backreacting flavors in the Klebanov-Strassler background*, *Journal of High Energy Physics* **2007** (2007) 109 [0706.1238].

[107] E. Conde and A.V. Ramallo, *On the gravity dual of Chern-Simons-matter theories with unquenched flavor*, *Journal of High Energy Physics* **2011** (2011) 99 [1105.6045].

[108] E. Conde, J. Gaillard and A.V. Ramallo, *On the holographic dual of mathcal{N} = 1 SQCD with massive flavors*, *Journal of High Energy Physics* **2011** (2011) 23 [1107.3803].

[109] A. Karch and L. Randall, *Localized Gravity in String Theory*, *Phys. Rev. Lett.* **87** (2001) 061601 [hep-th/0105108].

[110] O. Dewolfe, D.Z. Freedman and H. Ooguri, *Holography and defect conformal field theories*, *Phys. Rev. D* **66** (2002) 025009 [hep-th/0111135].

[111] A.F. Faedo, A. Kundu, D. Mateos, C. Pantelidou and J. Tarrío, *Three-dimensional super Yang-Mills with compressible quark matter*, *Journal of High Energy Physics* **2016** (2016) 154 [1511.05484].

[112] L. Girardello, M. Petrini, M. Porrati and A. Zaffaroni, *Novel local CFT and exact results on perturbations of N = 4 super Yang Mills from AdS dynamics*, *Journal of High Energy Physics* **1998** (1998) 022 [hep-th/9810126].

[113] L. Girardello, M. Petrini, M. Porrati and A. Zaffaroni, *The supergravity dual of N = 1 super yang-mills theory*, *Nuclear Physics B* **569** (2000) 451 [hep-th/9909047].

[114] V.G. Filev, C.V. Johnson, R.C. Rashkov and K. Sankaran Viswanathan, *Flavoured large N gauge theory in an external magnetic field*, *Journal of High Energy Physics* **2007** (2007) 019 [hep-th/0701001].

[115] D.T. Son and A.O. Starinets, *Viscosity, Black Holes, and Quantum Field Theory*, *Annual Review of Nuclear and Particle Science* **57** (2007) 95 [0704.0240].

[116] A. Buchel and J.T. Liu, *Universality of the Shear Viscosity from Supergravity Duals*, *Phys. Rev. Lett.* **93** (2004) 090602 [hep-th/0311175].

[117] S. Rahav, I. Gilary and S. Fishman, *Effective hamiltonians for periodically driven systems*, *Phys. Rev. A* **68** (2003) 013820.

[118] N. Goldman and J. Dalibard, *Periodically Driven Quantum Systems: Effective Hamiltonians and Engineered Gauge Fields*, *Physical Review X* **4** (2014) 031027 [1404.4373].

[119] M.M. Maricq, *Application of average hamiltonian theory to the nmr of solids*, *Phys. Rev. B* **25** (1982) 6622.

[120] M.M. Maricq, *Relaxation and equilibrium of a spin system coupled to a radiation field*, *Phys. Rev. B* **37** (1988) 7215.

[121] A. Verdeny, A. Mielke and F. Mintert, *Accurate effective hamiltonians via unitary flow in floquet space*, *Phys. Rev. Lett.* **111** (2013) 175301.

[122] N. Goldman, J. Dalibard, M. Aidelsburger and N.R. Cooper, *Periodically driven quantum matter: The case of resonant modulations*, *Phys. Rev. A* **91** (2015) 033632.

[123] A. Eckardt and E. Anisimovas, *High-frequency approximation for periodically driven quantum systems from a floquet-space perspective*, *New Journal of Physics* **17** (2015) 093039.

[124] W. Magnus, *On the exponential solution of differential equations for a linear operator*, *Communications on Pure and Applied Mathematics* **7** (1954) 649 [https://onlinelibrary.wiley.com/doi/pdf/10.1002/cpa.3160070404].

[125] S. Ebihara, K. Fukushima and T. Oka, *Chiral pumping effect induced by rotating electric fields*, *Phys. Rev. B* **93** (2016) 155107 [1509.03673].

[126] A. Eckardt, *Colloquium: Atomic quantum gases in periodically driven optical lattices*, *Reviews of Modern Physics* **89** (2017) 011004 [1606.08041].

[127] J. Dalibard, "*Des cages de lumières pour les atomes: La physique des pièges et des réseaux optiques*." Cours au Collège de France, 2013.

[128] R. Peierls, *Zur Theorie des Diamagnetismus von Leitungselektronen*, *Zeitschrift fur Physik* **80** (1933) 763.

[129] H. Lignier, C. Sias, D. Ciampini, Y. Singh, A. Zenesini, O. Morsch et al., *Dynamical control of matter-wave tunneling in periodic potentials*, *Phys. Rev. Lett.* **99** (2007) 220403.

USC DE SANTIAGO COMPOSTELA

[130] S. Takayoshi, J. Wu and T. Oka, *Nonadiabatic Nonlinear Optics and Quantum Geometry – Application to the Twisted Schwinger Effect*, *arXiv e-prints* (2020) arXiv:2005.01755 [2005.01755].

[131] J. Berges, S. Borsányi and C. Wetterich, *Prethermalization*, *Physical Review Letters* **93** (2004) 142002 [hep-ph/0403234].

[132] J. Sonner and A.G. Green, *Hawking Radiation and Nonequilibrium Quantum Critical Current Noise*, *Physical Review Letters* **109** (2012) 091601 [1203.4908].

[133] S. Nakamura and H. Ooguri, *Out of equilibrium temperature from holography*, *Physical Review D* **88** (2013) 126003 [1309.4089].

[134] J. Erdmenger, Z. Guralnik and I. Kirsch, *Four-dimensional superconformal theories with interacting boundaries or defects*, *Phys. Rev. D* **66** (2002) 025020 [hep-th/0203020].

[135] K. Skenderis and M. Taylor, *Branes in AdS and pp-wave spacetimes*, *Journal of High Energy Physics* **2002** (2002) 025 [hep-th/0204054].

[136] J. Mas, J.P. Shock and J. Tarrio, *Holographic Spectral Functions in Metallic AdS/CFT*, *arXiv e-prints* (2009) arXiv:0904.3905 [0904.3905].

[137] K.-Y. Kim, J.P. Shock and J. Tarrío, *The open string membrane paradigm with external electromagnetic fields*, *Journal of High Energy Physics* **2011** (2011) 17 [1103.4581].

[138] N. Seiberg and E. Witten, *String theory and noncommutative geometry*, *Journal of High Energy Physics* **1999** (1999) 032 [hep-th/9908142].

[139] D. Areán and A.V. Ramallo, *Open string modes at brane intersections*, *Journal of High Energy Physics* **2006** (2006) 037 [hep-th/0602174].

[140] T. Ishii and K. Murata, *Floquet superconductor in holography*, *Phyisical Review D* **98** (2018) 126005 [1804.06785].

[141] A. Kundu, *Steady states, thermal physics, and holography*, *Advances in High Energy Physics* **2019** (2019) .

[142] A. Karch, A. O'Bannon and E. Thompson, *The stress-energy tensor of flavor fields from AdS/CFT*, *Journal of High Energy Physics* **2009** (2009) 021 [0812.3629].

[143] S.A. Hartnoll, P.K. Kovtun, M. Müller and S. Sachdev, *Theory of the Nernst effect near quantum phase transitions in condensed matter and in dyonic black holes*, *Physical Review B* **76** (2007) 144502 [0706.3215].

[144] T. Morimoto, Y. Hatsugai and H. Aoki, *Optical Hall conductivity in 2DEG and graphene QHE systems*, *Physica E Low-Dimensional Systems and Nanostructures* **42** (2010) 751 [0911.0253].

[145] Y. Ikebe, T. Morimoto, R. Masutomi, T. Okamoto, H. Aoki and R. Shimano, *Optical Hall Effect in the Integer Quantum Hall Regime*, *Physical Review Letters* **104** (2010) 256802 [1004.0308].

[146] A. Kumar, A. Nemilentsau, K.H. Fung, G. Hanson, N.X. Fang and T. Low, *Chiral plasmon in gapped Dirac systems*, *Physical Review B* **93** (2016) 041413 [1509.00790].

[147] J.W. McIver, B. Schulte, F.U. Stein, T. Matsuyama, G. Jotzu, G. Meier et al., *Light-induced anomalous Hall effect in graphene*, *Nature Physics* **16** (2020) 38 [1811.03522].

[148] T. Oka and H. Aoki, *All Optical Measurement Proposed for the Photovoltaic Hall Effect*, in *Journal of Physics Conference Series*, vol. 334 of *Journal of Physics Conference Series*, p. 012060, Dec., 2011, DOI [1007.5399].

[149] H. Dehghani and A. Mitra, *Optical Hall conductivity of a Floquet topological insulator*, *Physical Review B* **92** (2015) 165111 [1506.08687].

[150] T. Oka and L. Bucciantini, *Heterodyne Hall effect in a two-dimensional electron gas*, *Physical Review B* **94** (2016) 155133 [1607.01041].

[151] W. Kohn, *Periodic thermodynamics*, *Journal of Statistical Physics* **103** (2001) 417.

[152] H.-J. Schmidt, J. Schnack and M. Holthaus, *Periodic thermodynamics of the rabi model with circular polarization for arbitrary spin quantum numbers*, *Phys. Rev. E* **100** (2019) 042141.

[153] O. Aharony, O. Bergman, D.L. Jafferis and J. Maldacena, *Script N = 6 superconformal Chern-Simons-matter theories, M2-branes and their gravity duals*, *Journal of High Energy Physics* **2008** (2008) 091 [0806.1218].

[154] S. Hohenegger and I. Kirsch, *A note on the holography of Chern-Simons matter theories with flavour*, *Journal of High Energy Physics* **2009** (2009) 129 [0903.1730].

[155] D. Gaiotto and D.L. Jafferis, *Notes on adding D6 branes wrapping RP^3 in $AdS_4\times CP^3$*, *Journal of High Energy Physics* **2012** (2012) 15 [0903.2175].

[156] N. Jokela, J. Mas, A.V. Ramallo and D. Zoakos, *Thermodynamics of the brane in Chern-Simons matter theories with flavor*, *Journal of High Energy Physics* **2013** (2013) 144 [1211.0630].

[157] Y. Bea, N. Jokela, M. Lippert, A.V. Ramallo and D. Zoakos, *Flux and Hall states in ABJM with dynamical flavors*, *JHEP* **03** (2015) 009 [1411.3335].

USC
DE SANTIAGO

[158] S.R. Das, T. Nishioka and T. Takayanagi, *Probe branes, time-dependent couplings and thermalization in AdS/CFT*, *Journal of High Energy Physics* **2010** (2010) 71 [1005.3348].

[159] P. Glorioso, M. Crossley and H. Liu, *A prescription for holographic Schwinger-Keldysh contour in non-equilibrium systems*, *arXiv e-prints* (2018) arXiv:1812.08785 [1812.08785].

[160] C. Jana, R. Loganayagam and M. Rangamani, *Open quantum systems and Schwinger-Keldysh holograms*, *Journal of High Energy Physics* **2020** (2020) 242 [2004.02888].

[161] S.K. Domokos and A.B. Royston, *Supersymmetry of the D3/D5 Defect Field Theory*, 2207.07671.

[162] S. Kobayashi, D. Mateos, S. Matsuura, R.C. Myers and R.M. Thomson, *Holographic phase transitions at finite baryon density*, *JHEP* **02** (2007) 016 [hep-th/0611099].

[163] D. Mateos, S. Matsuura, R.C. Myers and R.M. Thomson, *Holographic phase transitions at finite chemical potential*, *JHEP* **11** (2007) 085 [0709.1225].

[164] M.M. Caldarelli, R. Emparan and B. Van Pol, *Higher-dimensional Rotating Charged Black Holes*, *JHEP* **04** (2011) 013 [1012.4517].

[165] F. Benini, *A Chiral cascade via backreacting D7-branes with flux*, *JHEP* **10** (2008) 051 [0710.0374].

[166] S.S. Gubser, *Einstein manifolds and conformal field theories*, *Phys. Rev. D* **59** (1999) 025006 [hep-th/9807164].

[167] V. Balasubramanian and P. Kraus, *A Stress tensor for Anti-de Sitter gravity*, *Commun. Math. Phys.* **208** (1999) 413 [hep-th/9902121].

[168] C. Hoyos, N. Jokela, D. Rodríguez Fernández and A. Vuorinen, *Breaking the sound barrier in AdS/CFT*, *Phys. Rev. D* **94** (2016) 106008 [1609.03480].

[169] C. Ecker, C. Hoyos, N. Jokela, D. Rodríguez Fernández and A. Vuorinen, *Stiff phases in strongly coupled gauge theories with holographic duals*, *JHEP* **11** (2017) 031 [1707.00521].

[170] C. Hoyos, N. Jokela and A. Vuorinen, *Holographic approach to compact stars and their binary mergers*, *Prog. Part. Nucl. Phys.* **126** (2022) 103972 [2112.08422].

[171] M. Natsuume, *Causal hydrodynamics and the membrane paradigm*, *Phys. Rev. D* **78** (2008) 066010 [0807.1392].

[172] J.M. Maldacena, *Wilson loops in large N field theories*, *Phys. Rev. Lett.* **80** (1998) 4859 [hep-th/9803002].

USC DE SANTIAGO

[173] S.-J. Rey and J.-T. Yee, *Macroscopic strings as heavy quarks in large N gauge theory and anti-de Sitter supergravity*, *Eur. Phys. J. C* **22** (2001) 379 [hep-th/9803001].

[174] S. Ryu and T. Takayanagi, *Holographic derivation of entanglement entropy from AdS/CFT*, *Phys. Rev. Lett.* **96** (2006) 181602 [hep-th/0603001].

[175] S. Ryu and T. Takayanagi, *Aspects of Holographic Entanglement Entropy*, *JHEP* **08** (2006) 045 [hep-th/0605073].

[176] W. Fischler, A. Kundu and S. Kundu, *Holographic Mutual Information at Finite Temperature*, *Phys. Rev. D* **87** (2013) 126012 [1212.4764].

[177] J. Erdmenger and N. Miekley, *Non-local observables at finite temperature in AdS/CFT*, *JHEP* **03** (2018) 034 [1709.07016].

[178] N. Jokela and A. Pönni, *Notes on entanglement wedge cross sections*, *JHEP* **07** (2019) 087 [1904.09582].

[179] N. Jokela and A. Pönni, *Towards precision holography*, *Phys. Rev. D* **103** (2021) 026010 [2007.00010].

[180] M.M. Wolf, F. Verstraete, M.B. Hastings and J.I. Cirac, *Area Laws in Quantum Systems: Mutual Information and Correlations*, *Phys. Rev. Lett.* **100** (2008) 070502 [0704.3906].

[181] M. Headrick, *Entanglement Renyi entropies in holographic theories*, *Phys. Rev. D* **82** (2010) 126010 [1006.0047].

[182] S.A. Hartnoll and P. Petrov, *Electron star birth: A continuous phase transition at nonzero density*, *Phys. Rev. Lett.* **106** (2011) 121601 [1011.6469].

[183] V.G.M. Puletti, S. Nowling, L. Thorlacius and T. Zingg, *Holographic metals at finite temperature*, *JHEP* **01** (2011) 117 [1011.6261].

[184] O. Bergman, N. Jokela, G. Lifschytz and M. Lippert, *Quantum Hall Effect in a Holographic Model*, *JHEP* **10** (2010) 063 [1003.4965].

[185] N. Jokela, M. Järvinen and M. Lippert, *A holographic quantum Hall model at integer filling*, *JHEP* **05** (2011) 101 [1101.3329].

[186] B.S. DiNunno, N. Jokela, J.F. Pedraza and A. Pönni, *Quantum information probes of charge fractionalization in large-N gauge theories*, *JHEP* **05** (2021) 149 [2101.11636].

[187] A.F. Faedo, D. Mateos and J. Tarrío, *Three-dimensional super Yang-Mills with unquenched flavor*, *JHEP* **07** (2015) 056 [1505.00210].

[188] N. Jokela, J.M. Penín and K.C.S. Rigatos, *Gravity duals for defect quivers in the Veneziano limit*, 2112.14677.

USC
DE SANTIAGO
DE COMPOSTELA

USC
UNIVERSIDADE
DE SANTIAGO
DE COMPOSTELA





Since the holographic duality was proposed by Maldacena in 1997 it has been generalised in order to study a wide range of problems. One prominent example among the variety of extensions of the duality is the addition of flavor degrees of freedom as a result of the inclusion of supplementary D-branes on the initial system. The main goal of this thesis is the application of the correspondence in two particular situations where fields transforming in the fundamental representation of the gauge group are taken into account. In order to do so, we will study a system of intersecting D3 and D5 branes. In the first part, we will try to gain some insight into periodically driven systems, while the second part will be devoted to the construction of a holographic dual that realises anistropy, as well as a finite baryon density.